Geochemical and mineralogical investigation of the Merensky Reef and its noritic hangingwall at Two Rivers Platinum Mine and Eerste Geluk, Eastern Bushveld, with special reference to the PGE distribution and cryptic variation of the mineral chemistry

By

JARLEN JOCELYN BEUKES

DISSERTATION

Submitted in the fulfilment of the requirements for the degree

of

MAGISTER SCIENTIAE

in

Geology

in the

Faculty of Science

at the

University of the Free State, South Africa

Supervisor: C.D.K Gauert

December 2014

Declaration

I, Jarlen Jocelyn Beukes, hereby state that all work contained in this dissertation is the original work of the author, except where referenced or specific acknowledgements is made to the work of others. I further declare that no part of this thesis has been, or is concurrently being submitted for a degree or other qualification at any other university or educational institution.

Signed:  Date: 09/12/ 2014 Place: Stellenbosch

Abstract

This research study focuses on the unusual occurrence of noritic lenses (termed “brown sugar norite” by mine geologists), within the pyroxenite of the Merensky Reef as well as its hanging wall at Two Rivers Platinum Mine, situated on the southern sector of the eastern limb of the Bushveld Complex. The primary purpose of this study is to determine the origin of these noritic lenses (hereafter referred to as BSN) and their influence on PGE distribution within the Merensky Reef. This study will also attempt to characterise the cumulate rocks associated with the Merensky Reef unit through geochemistry and mineralogy. Furthermore, a comparison with similar rock types of different genetic facies types of the same stratigraphy north of the Steelpoort fault at Eerste Geluk will be performed.

The BSN is a fine-grained mela-gabbronorite and only occurs where the upper chromite stringer of the Merensky Reef unit is present. Orthopyroxene is the dominant cumulate phase in both the BSN and pyroxenite of the MR followed by interstitial plagioclase. Clinopyroxene occurs mostly as an exsolved lamellae phase within orthopyroxene and as intermittent rims around orthopyroxene. This can be attributed to exsolution of the Ca end member during decrease in temperature and compositional change of the melt during cooling. Some of the chromite crystals present in the pyroxenite are well-rounded possibly indicating magmatic erosion.

Textural features of minerals from the different rock types such as plagioclase inclusions within orthopyroxenes as well as triple junctions of orthopyroxene crystals suggest disequilibrium and recrystallization of mineral phases respectively. The dominant mineral phases control most of the chemical composition of the rocks in accordance with their mineral proportions as they concentrate most of the lithophile elements.

The main difference between the Merensky reef at Two Rivers Platinum and the Merensky reef north of the area at the farm Eerste Geluk is the absence of brown sugar norite at the latter. Also, the minerals of the Eerste Geluk Merensky lithologies display a higher degree of alteration or deformation and a higher concentration of hydrous minerals. Eerste Geluk is situated proximal to the Steelpoort fault which suggests that the rocks in the area were affected by faulting and late hydrothermal fluids which resulted in the alteration of minerals. Strontium isotope analyses of five representative samples of the Merensky interval at TRP yielded $^{87}Sr/^{86}Sr$ ratios typical of Critical Zone magma. Though both the pyroxenite and BSN have $^{87}Sr/^{86}Sr$ ratios representative of Critical Zone magma, the BSN has a lower ratio relative to pyroxenite. This suggests that it formed from a more primitive magma. Whole rock MgO content is higher in the BSN, ranging between 24-28 wt. % compared to the 21-23 wt. % MgO

found within the surrounding Merensky reef pyroxenite. This provides some evidence suggesting that the BSN formed from a more primitive magma.

EPMA results show cryptic vertical variation of En content, Al2O3, TiO2 and MnO in orthopyroxene and An content variation in plagioclase. This indicates fractionation and replenishment of magma.

Base metal sulphides and associated PGMs occur disseminated throughout the Merensky pyroxenite interval. The PGMs analysed by EPMA are relatively enriched in Pt but are poor in Pd and Rh. These findings are consistent with the ICP-MS study done on the base metal sulphides. Textural features such as zonation of these PGMs suggest the action of late stage magmatic processes. The occurrence of the BSN has not influenced the content of the PGE mineralisation. It contains relatively little if any base metal sulphides and PGMs. It is therefore suggested that the BMS and PGM saturation was not affected during crystallization of BSN.

With regards to emplacement, it is suggested that the BSN formed prior to the MR and that a magmatic erosion caused by the injection of the new MR magma may have disturbed the previously formed BSN layer. It thus resulted in isolated lenses of relict and primitive BSN. The BSN is not laterally consistent in the TRP area and may be attributed to this phenomena. The absence of BSN in other mines of the Bushveld may be due to this reason, or the occurrence of the BSN has been overlooked due to its similarities to MR pyroxenite.

Table of Contents

List of abbreviations

Amp	Amphibole
An	Anorthite
%An	An content= Cation ratio of 100*Ca/ (Ca +Na+K)
b.d.l	below detection limit
BIC	Bushveld Igneous Complex
BSE	Backscattered electron images
BSN	Brown Sugar Norite
BMS	Base metal sulphides
Chl	Chlorite
Chr	Chromite
Cp	Chalcopyrite
Cpx	Clinopyroxene
CLZ	Lower Critical Zone
CUZ	Upper Critical Zone
En	Enstatite
%En	content= Cation ratio of 100*Mg/ (Mg+Fe) in pyroxene
EST	Eerste Geluk
Fs	Ferrosilite
GU	University of Graz
LN	Leuconorite
MAn	Mottled Anorthosite
MCU	Merensky Cyclic Unit
MLN	Melanorite
MPXT	Merensky Pyroxenite
MPPXT	Merensky Pegmatoidal Pyroxenite
Mg#	Cation ratio of 100*Mg/ (Mg+Fe) in chromite
MR	Merensky Reef
MsN	Mesonorite
MSS	Monosulphide Solid Solution
Opx	Orthopyroxene
PGE	Platinum Group Elements
PGM	Platinum Group Minerals
Plag	Plagioclase
Pn	Pentlandite
Po	Pyrrhotite
PPXT	Pegmatoidal Pyroxenite
PXF	Feldspathic Pyroxenite
PXT	Pyroxenite
Py	Pyrite
SAn	Spotted Anorthosite
SEM- EDSWDS	Scanning Electron Microscopy-Energy Dispersive Spectrometry
Sulph	Sulphide
TRP	Two Rivers Platinum Mine
UFS	University of the Free State
UG-2	Upper Group 2
Wo	Wollastonite
XRF	X-ray Fluorescence Spectroscopy

List of figures

List of tables

Chapter 1: Introduction

This chapter gives a general review of the location of the study area, a brief mining history, local and the regional geology as well as a literature review of former studies done on the Bushveld Igneous complex (BIC).

The “Bushveld” is a term used to describe mafic and ultramafic rocks of the BIC; however, according to the South African Commission for Stratigraphy (SACS, 1980) the basal part of the complex is referred to as the Rustenburg Layered Suite. It has been established that the BIC is the world’s largest layered intrusion, with a large size of 65000km² and an approximate thickness of 8km (Cawthorn, 1996; Cawthorn & Ashwal, 2009). It is approximately 2060Ma old and being the largest host of PGMs, Chromium and Vanadium (Viljoen & Schürmann, 1998) it comes as no surprise why South Africa in particular is one of the leading producers of platinum.

Two Rivers Platinum Mine (TRP), a joint venture between African Rainbow Minerals (ARM) and Impala Platinum, is a relatively young mine as the development of the mine only started in 2005 (Cowell M. , 2011). TRP is located on the southern part of the Eastern Limb of the BIC, in the Mpumalanga Province, South Africa (as seen in figure 1). It is located on the farm Dwarsriver 372 KT (also the location of the Dwarsriver geological monument), a mountainous area with the Dwarsriver running through it (figure 2). Currently only the UG2 layer is mined whilst the development of the Merensky Reef has ceased for the time being.

This study is based on the Merensky Reef which crops out in the TRP area with special reference to the occurrence of an apparent noritic unit, the brown sugar norite (BSN). Four Merensky Reef facies have been identified in the area based on the grade distribution of PGEs in the MR and the thickness of the reef. The MR in this area is characterised as a pyroxenite bounded by two chromitite stringers, however, the top stringer is absent in some MR intersections (Rose, 2010) and is overlain by norite, anorthosite or pyroxenite to a lesser extend as hanging wall and has a mottled or spotted anorthositic footwall. Distortion of the typical Merensky Cyclic Unit is observed where the BSN is present. These norites have been identified within the Merensky pyroxenite as well as hanging wall. Samples were taken at two locations underground. Drill core samples of the MR interval at the farm Eerste Geluk north of the Steelpoort fault (see figure 1b) were also taken for comparison of geochemistry and mineralogy.

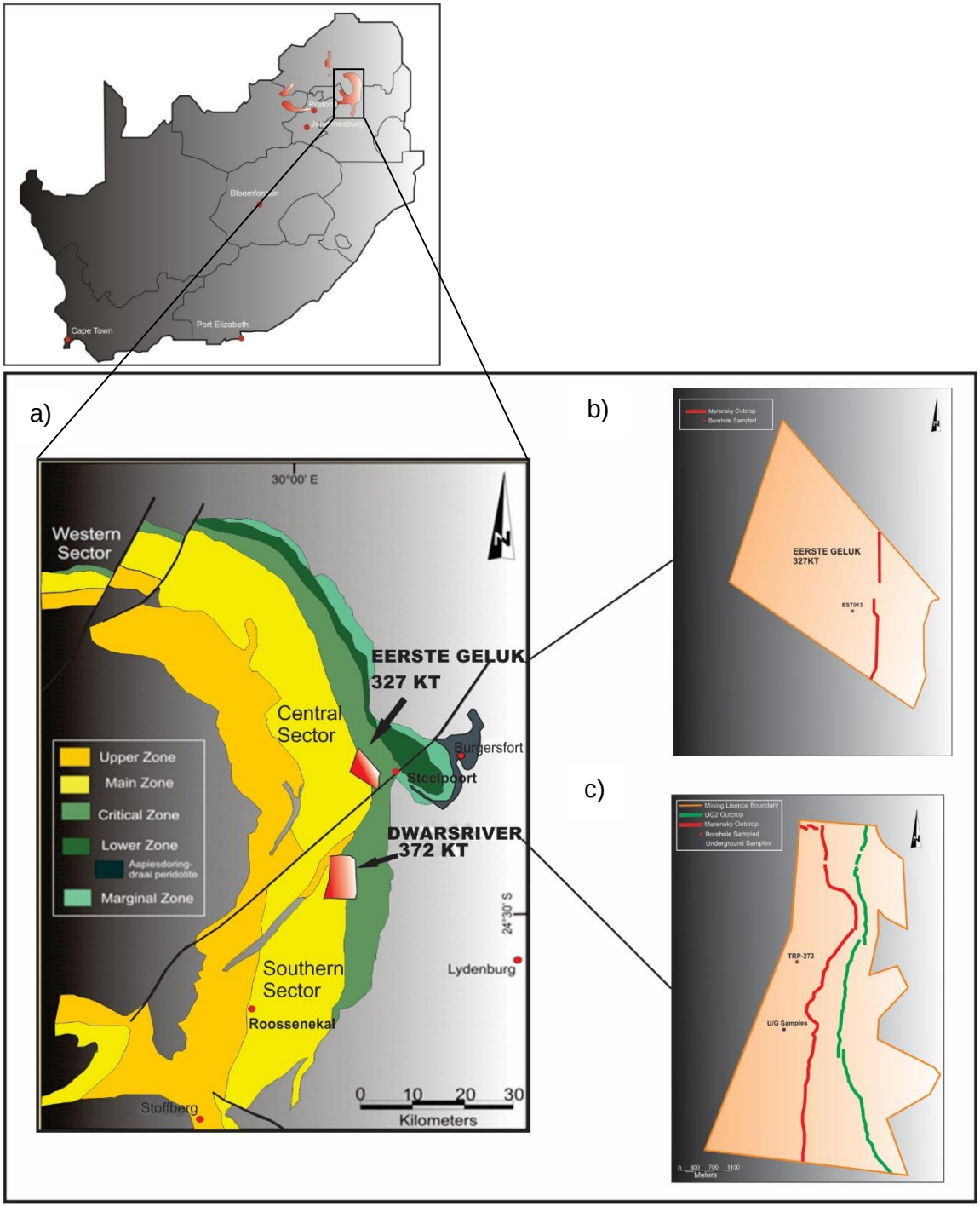

Figure 1: a) Generalised geological map of the Eastern limb of the Bushveld Igneous Complex (Modified after Cameron & Abendroth, 1957; Sharpe & Chadwick, 1982; Clarke, et al., 2005). The farms Dwarsriver 372 KT and Eerste Geluk 327 KT are indicated by the red areas. b) and c) indicates drillcore and sample sites as well as MR and UG2 outcrops in the farm areas.

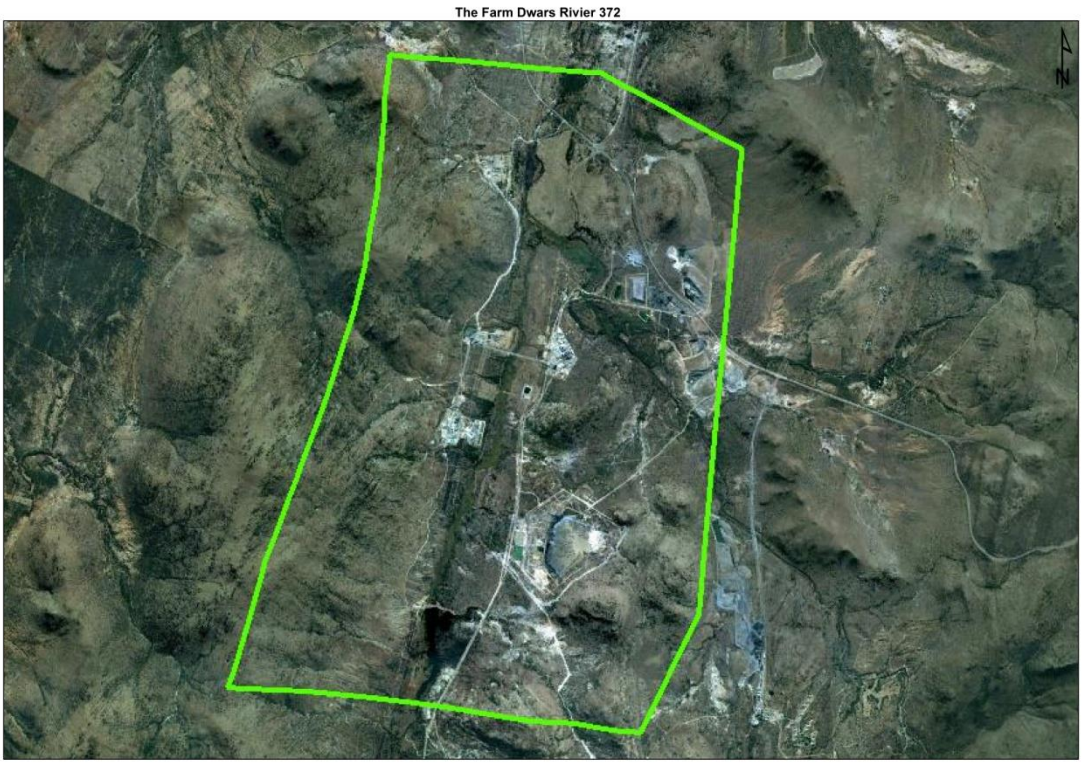

Figure 2: Satellite Image of the farm Dwarsriver 372 KT, (Google images, June 2011)

1.1 General Geology of the BIC

The BIC intruded the Transvaal Supergroup and outcrops as four distinct limbs, namely the western, far western, northern and eastern limb.

Previous studies by Cawthorn & Webb (2001) suggest that the eastern and western limbs are connected at depth and have formed within a single lopolithic intrusion as their mafic sequences are significantly similar and such a similarity could not petrographically be accounted for by two totally discrete bodies. The northern limb differs slightly from the eastern and western limbs (Seabrook et al., 2005; Cawthorn & Ashwal, 2009).

This BIC consists of four distinctive igneous suites. The first suite would be early mafic sills followed by the Rooiberg group comprising of felsites which basically marks the end of the Transvaal Supergoup and the beginning of the Rustenburg Layered Suite (RLS). The third suite, RLS, comprises of mafic and ultramafic rocks formed from repetitive influxes of magma. The Lebowa Granite Suite is the final suite of the Bushveld event and has intruded through the centre of the mafic/ultramafic rocks (Naldrett et al., 2008).

The layered mafic rocks (i.e. RLS) of the BIC are derived from three magmatic lineages namely, a lower part containing the Lower and Critical Zones which is believed to have crystallized from high-Mg and-Si parent liquids, Lower Main Zone which formed from more

evolved aluminous tholeiitic liquids and the Upper Zone above the Pyroxenite Marker originating from the mixing of the residua of the prior liquids with a final major injection of tholeiitic liquid (Kruger, 1994). Marginal Zone is believed to represent variable cumulus enrichment into a number of chemically different magma based on its mineralogy and thickness ((Eales & Cawthorn, 1996).

Various possible theories exist for the emplacement of the BIC as simplified in (Eales, 2001) however the most favoured theory thus far is seemingly that of Eales & Cawthorn (1996) who propose that the emplacement of the BIC occurred by multiple injections of magma varying in volume. This theory is supported by the overall occurrence of distinct breaks in the initial Sr isotope ratios which points out resorption of former crystallising phases more specifically seen in the increase of $^{87}Sr/^{86}Sr$ close to the boundary between CZ and MZ, see figure 3 (Eales, 2001; Kruger, 1994; Kruger & Marsh, 1982).

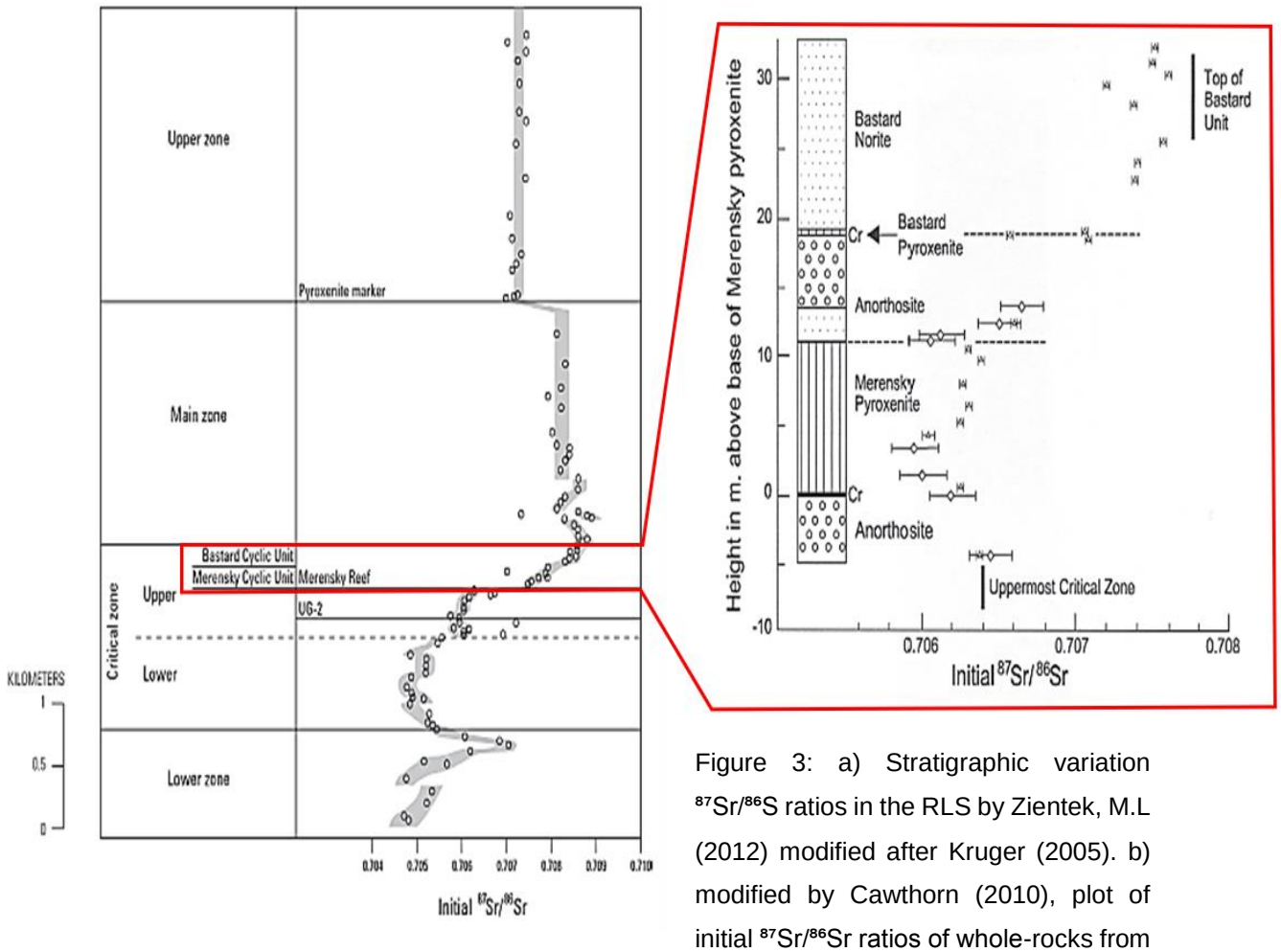

Figure 3: a) Stratigraphic variation $^{87}Sr/^{86}S$ ratios in the RLS by Zientek, M.L (2012) modified after Kruger (2005). b) modified by Cawthorn (2010), plot of initial $^{87}Sr/^{86}Sr$ ratios of whole-rocks from a section from thick Merensky package on Western platinum mines indicated by triangles (Shelembe, 2006). Typical values obtained for thin Merensky package from Kruger and Marsh (1982) is included as diamond symbols for comparison. Typical Upper Critical Zone and Main Zone ratios, from Kruger (1994), are included as thick vertical bars.

The RLS consists of a Marginal, Lower, Critical, Main and Upper Zone (SACS, 1980) but for the purpose of this study the focus will be on the uppermost Critical and lowermost Main Zone.

1.1.1 Critical Zone

Figure 4: Figure 4: Layering of UG in anorthosite at the Dwarsriver monument, eastern Bushveld Complex.

The Critical Zone display magnificent layering (figure 4). The Merensky reef and UG2 layers which are rich in PGE mineralisation and chromite occurs in this zone. Due to the presence of these layers the CZ is the economically most important zone of the BIC.

The exact boundary between the CZ and Main Zone (MZ) is still vague; however, the major break in Sr isotope ratio and unconformity at the bottom of the Merensky Cyclic Unit (MCU) influenced Kruger (1992) to make the boundary between CZ and MZ at the base of the MCU. The CZ is subdivided into a Lower, Middle Group and Upper Critical Zone. The lower part of the Critical Zone is made up of ultramafic rocks (harzburgite and pyroxenite) and the Upper Critical Zone consists of pyroxenite layers, norite and anorthosite (Wilson & Chunnett, 2006).

The Lower Critical Zone (C_LZ) is also known to have up to 7 layers of chromitite layers whereas the Upper Critical Zone (C_UZ) has up to 5 substantial chromitite layers (Cawthorn R.G, 2007). In the C_LZ, Lower Group chromitite layers (LG 1-7) and the Middle Group chromitite layer (MG1) has higher PGE values (30-800 ppb range for Pt and Pd) than the surrounding silicate rocks. The MG3-MG4 and the Upper Group chromitite layer (UG1 and 3) have higher PGE concentrations (200 to 4000ppb of Pt and Pd) than the chromitite layers of C_LZ (Barnes & Maier, 2002b).

Rocks of the C_UZ have incompatible element ratios, Pb isotope, initial Sr, Nd and Os compositions transitional between C_LZ and MZ (Kruger., 1994; Harmer et al., 1995; Barnes & Maier, 1999; Schoenberg et al., 1999 and Maier et al., 2000). It is believed that these rocks represent the result of the mixing of the two magmas that formed the RLS (Barnes & Maier, 2002b).

1.1.2 Main Zone

The MZ overlies the CZ. It is the thickest of all four zones of the BIC [up to about 3.1km in thickness (Ashwal et al., 2005); however, when compared to the mineral deposits of the other zones, the MZ is quite barren (Harney & von Gruenewaldt, 1995) .

The base of the MZ varies stratigraphically depending on the criteria used. It is generally believed that the base of the MZ be taken from the top of the Giant Mottled Anorthosite which overlies the Bastard Cyclic Unit of the C_UZ (Cawthorn, 1996).

The main zone rocks consist of plagioclase, Ca-poor and Ca-rich pyroxene as cumulus minerals (Cawthorn and Ashwal, 2008). Von Gruenewaldt (1973) and von Gruenewaldt & Strydom (1985) have subdivided the MZ based on the lithological variations, namely Subzone A, B and C. Overlying the CZ is Subzone A which comprises of norites, gabbros, anorthosites and pyroxenite. Subzone B is made up almost completely of gabbronorites. Subzone C consists of norites, gabbros, gabbronorites and anorthosites. The Pyroxenite Marker forms the base of Subzone C.

1.1.3 Merensky Reef

The Merensky Reef (MR) has been studied intensely over the years as its discovery has sparked both economic and scientific interest.

"The term 'Reef' refers to the economically important zone contained largely within a medium- to coarse grained plagioclase-pyroxenite and is specifically the mining zone of payable metal values" Wilson and Chunnett, 2006. The "Merensky Reef" is a mining term for these rocks (Lee, 1996). However, Cawthorn and Boerst (2006) defines the MR as cumulate rocks, regardless of their lithology, that consists of possible extractable PGE mineralisation.

The MR broadly refers to the package of rocks located at the top of the Critical Zone that contains PGE mineralisation of economic grade (Viljoen M. J., 1999). In general, there are two types of MR, as described by Barnes and Maier (2002), namely a normal reef and a potholed reef where the normal reef shows the least degree of transgression of the silicate stratigraphy and conformably overlies the anorthositic footwall. Where the MR does not rest conformably on its footwall and much of the stratigraphy between the MR and the UG2 Reef is missing, the reef is referred to as "potholed" reef (Barnes & Maier, 2002b). It is believed that the potholes of the MR formed as a result of an event whereby the MR abruptly transgressed the footwall cumulates (Lee, 1996).

Both the MCU and Bastard Cyclic Unit (BCU) consist of cycles of chromitite, pyroxenite, norite and anorthosite (Seabrook et al., 2005). The MR is basically found at the bottom of the MCU.

The hanging wall of the MR is generally norite which grades to anorthosite of the BCU. The footwall is anorthositic (either 'mottled' or 'spotted' anorthosite) and rarely pyroxenite. The Bastard Cyclic Unit overlies the MCU. The Bastard unit is so called because of its physical similarity to the MCU however it is poor in PGE content (Vermaak, 1995).

The MR is generally composed of texturally heterogeneous pegmatoidal feldspathic pyroxenite, partially pegmatoidal feldspathic pyroxenite or feldspathic pyroxenite (Lee, 1996). The absence of pegmatitic pyroxenite does not affect the PGE grade of the reef (Cawthorn & Boerst, 2006). The MR is bounded by two chromitite stringers though the top stringer is not always present. Up to 4 chromitite seams may be present in a section (thickness varying from less than 1 to 10cm), which are sequentially overlain by pegmatoidal feldspathic pyroxenite (Barnes & Maier, 2002a). The highest grade of PGE mineralisation is associated with the upper and basal chromitite stringers (Lee, 1996).

The MR has been referred to in previous studies as having 70% cumulus pyroxene and 30% intercumulus plagioclase (Vermaak, 1976; Lee, 1996) but Cawthorn & Boerst (2006) reckons that by using the terminology and model by Wagner (1960) such a report would be flawed. They suggest that the MR should rather be described as having 50% cumulus pyroxene and 20% and 30% of intercumulus pyroxene and plagioclase, respectively.

The thickness, composition as well as the position of mineralisation of the MR varies along strike in both the Western and Eastern Limbs (Schouwstra et al., 2000).This variation of the reef is referred to as facies (Rose, 2010). The MR can be as thin as 4cm and can be up to 4m thick, however, it is usually about 1m thick and normally the MR has an inward slope of about 7° to 49° toward the centre of the BIC though in contained areas it may dip up to 65° (Lee, 1996).

The MR holds an almost steady grade of PGEs ranging between 5 -8g/t over a thickness of between 40-120cm over distances of more than 100kms in both the Eastern and Western limbs (Wagner, 1929; Vermaak, 1976; Lee, 1996; Barnes & Maier, 2002a; Cawthorn et al., 2002a). Seabrook et al. (2005) have reported PGE grades up to 10g/t, usually associated with about 3% base metal sulphides and related platinum group metals (PGM). The distribution of PGE with height depends on the thickness of the reef; where the reef is relatively thin or only one chromitite layer is present, substantial PGE mineralisation is found in the footwall below the pyroxenite and chromitite layer; where the reef is relatively thick PGE mineralisation occurs progressively higher in the succession and is more likely follow the upper chromitite layer (Cawthorn, 2010).

1.2 Previous work

1.2.1 Models of formation

The BIC have been studied intensively over the years, however, the exact genetic process or processes responsible for the geochemical and petrographical nature of this intrusion as well as the number, kind, volume and source of the possible magma types involved are still debated. With this said, it is clear that extensive data exists for the BIC, several processes have been suggested (though not all are plausible), theories have been formulated and tested. Godel et al., (2007) proposes that any model for the formation of the MR needs to consider, firstly, the connection between PGE & PGM and the BMS; secondly, the preferential distribution of BMS; and lastly, the enrichment of IPGEs and Pt relative to Si, Nd, Pd and Au in the chromitite layers. An overview of some of the major models of formation will hereafter be discussed.

Hydrothermal magmatic formation

Accessory phase minerals (apatite, phlogopite and amphiboles) connected to the ore zones of the Bushveld and Stillwater Complexes are more Cl-rich than the same minerals in other parts of these intrusions and other layered intrusions (Boudreau et al., 1986). These authors envisioned that crystallization of an interstitial melt would result in extremely Cl-rich fluid being exsolved which can dissolve and transport metals, REE and the alkalis as it move up through the crystal pile; based on the Holland (1972) that proposes that 'dry' magmas such as the parent magmas of the BIC may exsolve efficient metal-transporting hydrothermal fluids nearly post solidification. Volatile phases is suggested to have concentrated PGE as it percolated upwards through the hot possibly partially molten crystal pile (Boudreau & McCallum, 1989 and 1992) though it is difficult to support these theories geochemically (Mathez, 1995).
Pyroxenite of the MR are highly evolved in REE and poorly evolved in major elements due to metasomatism which is believed to have implicated 1) the upward percolation of hydrated silicate melt and 2) its reaction with the cumulate pile (Mathez, 1995). Mathez 1995 suggested that the PGEs found within the MR pyroxenite were metasomatically redistributed.

Hydrothermal models for the deposition of PGEs argue that PGEs were deposited after the cumulus processes, implying that the source for mineralisation came from the underlying rocks, therefore FW rocks are expected to be depleted in PGE. However this is not plausible in some cases such as at the Impala mine in the Western BIC (Barnes & Maier, 2002a) where it is observed that underlying rocks of the reef were not depleted in PGE thus making intercumulus fluid percolation from below unlikely.

Magma Mixing

It has been proposed by previous workers that the C_UZ did not crystallize by in situ crystallization but rather that it formed as a result of the mixing of magmas after an addition of magma to the chamber (Irvine, 1977; Eales et al., 1991; Mondal & Mathez, 2007; Godel et al., 2007). It is believed that this model accounts for the PGE concentration and base metal sulphides in the MCU. These authors basically propose that a plagioclase and trapped liquid crystal pile which underlain fractionated silicate magma formed; an influx of Mg rich magma was then introduced into the chamber which mixed with the resident magma bringing orthopyroxene, plagioclase and PGE alloys onto the liquidus.

A product of magma mixing is a magma composition enriched in chromite (chromite saturated magma, as proposed by Irvine, 1977) within the stable chromite stability field leading to concise crystallization of chromite only. This, as well as the density of the chromite crystals causing them to sink, accounts for the monomineralic chromite layer forming at the floor of the chamber. (Robb, 2005)

Orthopyroxene crystals from the pegmatitic pyroxenite in the MCU is believed to have grown by reaction between the small primary crystals of the initial pyroxenite and superheated liquid suggested to have been added magma due to the pressure reduction following lateral expansion of the chamber (Cawthorn & Boerst, 2006).

Mixing of Minerals

From isotopic data, such as that of Kruger & Marsh (1982), it can be seen that both the MZ and CZ have distinct signatures. By the use of Cr/MgO and Sr isotope data Seabrook et al. (2005) postulates that the MCU and BCU have magmatic signatures of either CZ or MZ. Based on the mixture of Sr isotope values of both zones, the Merensky pyroxenite is referred to as a "Transitional Zone" (Kruger F. J., 1992). It was observed that pyroxenite of the MCU comprises orthopyroxene that have compositions typical of CZ though in the overlying parts of the MCU plagioclase compositions are strongly typical MZ and orthopyroxene that of CZ (Seabrook et al., 2005). Sr isotope values of Bastard pyroxenite are transitional between CZ and MZ whereas the orthopyroxene remain typical CZ (Prevec et al., 2005; Seabrook et al., 2005). The authors (Seabrook et al., 2005) further suggest that MZ magma was injected at the base of the MCU which resulted in the CZ being displaced upwards; however these magmas did not mix but mingled. The suggested model for the formation of the MR however does not account for the reversal to abundant orthopyroxene crystallization that formed the pyroxenite of the MR with a typical CZ signature; it is therefore proposed that a further influx of CZ

occurred (Wilson & Chunnett, 2006). Schűrmann (1993) proposed that displacement was the result of B1 magma (CZ magma), though higher in liquidus temperature, being less dense than the intruding magmas which in turn crystallized orthopyroxene. These orthopyroxenes were denser and therefore sunk and slumped through the B2/B3 magma (possibly MZ and a later influx of CZ magma) producing the feldspathic pyroxenite of the UG1, UG2, Merensky and Bastard units and the Boulder Bed (Schűrmann, 1993).

CZ emplacement, followed MZ magma injection into the chamber describes the assorted chemical composition and strong thermal gradients of the MCU. The MZ had a cooling effect on the resident CZ magma (believed to have been close to sulphide saturation and rich in PGE, as indicated by compositions of marginal sills by Davies & Tredoux ,1985) resulting in the precipitation of immiscible sulphide leading to the formation of the MR. (Wilson and Chunnett, 2006)

1.3 Geology of study area

The Steelpoort fault zone is located about seven kilometres north of the study area. Neighbouring farms of Dwarsriver 372 KT are Tweefontein 360 KT in the north, De Grootboom 373 KT in the east, Thorncliffe 374 KT in the southeast, Richmond 370 KT to the south and Kalkfontein 367 KT west of the farm. Tectonism is evident in the farm by faulting as a result of the Steelpoort fault zone nearby. Dolerite dykes which are fine-to-medium grained are related to the Steelpoort fault and trend parallel to it in a NNE direction.

It has been observed from some exploration drill core that there are certain cases where these dolerite dykes partially or completely replace the MR or UG-2. The presence of the Steelpoort fault affects the lithologies as it can be seen that the succession occurring in the southern sector are rather different to those of the central sector (Cowell M. , 2003).

The RLS occurs in the study area and comprises of the Critical Zone and the Main Zone, specifically the CUZ and the Lower Main Zone. Both the Merensky Reef and the UG-2 chromitite horizons sub-crop on surface in Dwarsriver 372 KT. PGE mineralisation are associated with the MR as well as UG-2. The Merensky pyroxenite sub-crops along a north-south strike on the western slopes of the Small Dwarsriver valley. The MR dips 7 to 10 degrees to the west (Cowell M. , 2003).

The MR in Dwarsriver 372 KT is divided into four facies types based on the PGE distribution and the thickness of the unit (Cowell M. , 2003), see figure 5. As mentioned previously, the erratic occurrence of BSN in the MCU disrupts the normal layering of the MCU. The BSN

however occurs in confined areas of the mine and was found within facies 1. The four facies types are:

- Facies 1: The PGE mineralisation is associated with the upper and basal chromitite stringers which are approximately 2.4m thick. This facies type is similar to the 'Western Platinum Facies of the Western BIC.
- Facies 2: PGE mineralisation occurs throughout the pyroxenite and is not intimately associated with chromite mineralisation. The MR of this facies type has thicknesses of approximately 2.7m thick on average and is the dominant facies type at TRP.
- Facies 3: This facies is known as "thick reef". The thickness of the Merensky pyroxenite of this reef is usually greater than 3m but averages 4.85 m. This facies type is limited to the southern portion of the TRP lease area. Three distinct peaks of PGE mineralisation observed; two peaks are associated with the upper and basal chromite stringers and one with the Merensky pyroxenite only.
- Facies 4: This facies is also known as "thin reef". The Merensky pyroxenite of this type is usually less than 1m thick (0.9 m on average). The upper chromite stringer and its associated mineralisation are normally absent. This facies type is limited to the central portion of Dwarsriver 372 KT.

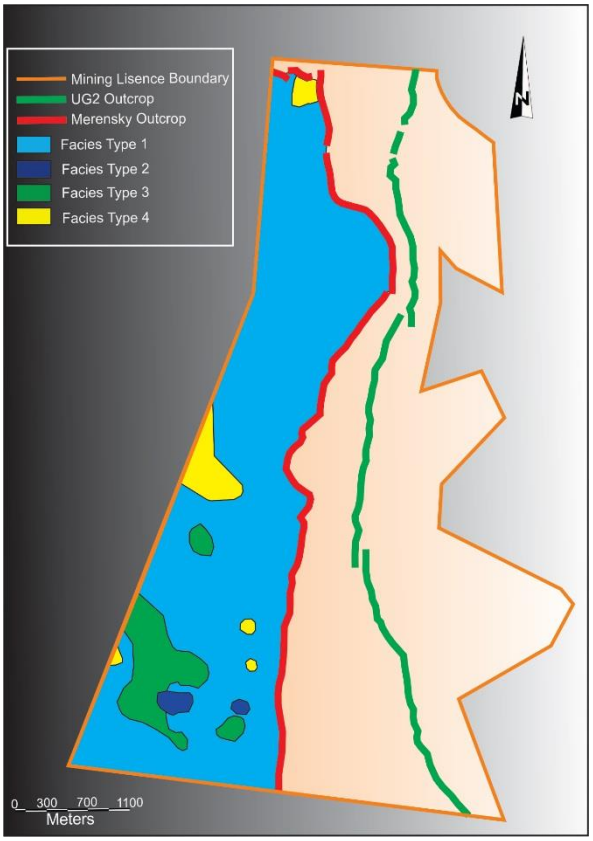

Figure 5: Overview of the different facies type of MR in the study area as well as the Merensky Reef and UG2 outcrop in the farm area (Modified after Management TRP PDF-PowerPoint presentation, 2011)

1.4 Mining history of Two Rivers Platinum

In 1920 exploration and limited mining of the MR in the Dwarsriver area took place. Most work was done on the Western BC because of its better infrastructure and the great depression in the 1930s which led to the end of mining activity on the Eastern Limb. Goldfields bought surface and mineral rights to prospect the LG6, UG2 and Merensky Layers for chrome and PGEs.

In 1998, Associated Manganese Mines of South Africa Limited (ASSMANG) bought the farm mainly to mine the LG6. After AVMIN obtained PGE rights of the farm from ASSMANG, it formed a joint venture with Impala Platinum where a pre-feasibility study known as the Puma Project was assessed in 2001. ARM and Impala Platinum formed a joint venture in 2005; this resulted in the formation of the Two Rivers Platinum Mine. In 2006 the plant was formally commissioned (ARM), 2007). The source of PGE and chromium mining at the TRP was from the UG-2 until recently due to lack of a refined geometallurgical model for the MR in the study area.

1.5 Objectives of study

- Determine how the ‘brown sugar norite’ differs from the pyroxenite and norite at TRP as well as north of the Steelpoort fault at Eerste Geluk in its modal mineral composition.
- Characterise the cumulate rocks associated with the Merensky Reef unit by the use of geochemistry and mineralogy.
- Understand the magmatic processes such as magma replenishment, melt emplacement, crystallization history mineralization and post-magmatic modification involved during MR formation.
- Determine the origin of the ‘brown sugar norite’ lenses and their influence on the PGE distribution within the Merensky Reef.
- Understand how the emplacement of the MR at selected positions of TRP and EST took place, subsequently understanding the crystallization history resulting in an improved emplacement model. This would allow for a better exploration techniques and mining model.

Chapter 2: Petrography

2.1 Introduction

This chapter deals with the macroscopic and microscopic investigation of the main Merensky Reef rock types at TRP (see figure 5 and appendix A1-1 for location of MR u/g samples) which are pyroxenite, anorthosite and norite. The rock units of the Merensky Reef north of the Steelpoort fault on the farm Eerste Geluk will also be described in this chapter, highlighting similarities or differences.

2.2 Macroscopic description of main rock types

2.2.1 Hanging Wall

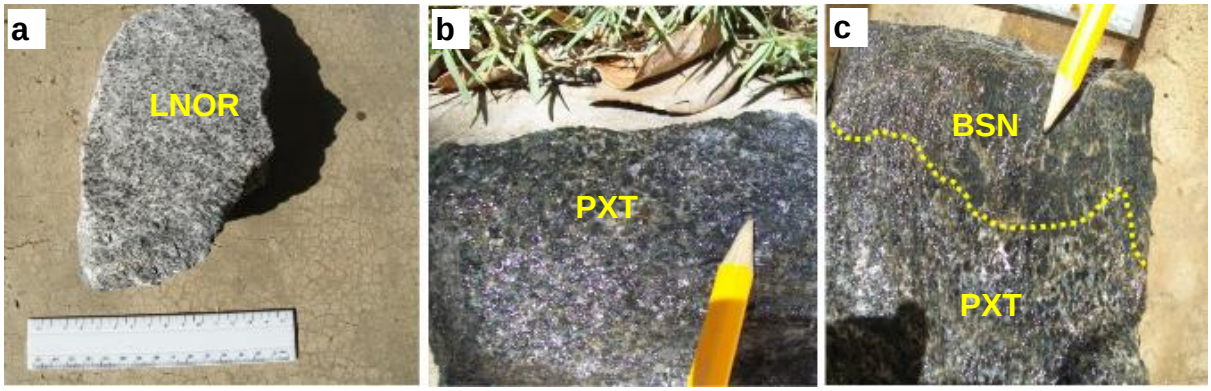

Figure 6: Hanging wall a) leuconorite, b) pyroxenite and c) brown sugar norite vs. pyroxenite

Underground samples of the MR show that the immediate hanging wall consists of spotted anorthosite (SAn) which gradually grades to leucocratic norite and in certain areas of the mine, such as location N and S, the anorthosite is replaced by pyroxenite and BSN (figure 6). Anorthosite is a leucocratic igneous rock consisting primarily of cumulus plagioclase (90-100%) and minimal pyroxene (mainly orthopyroxene of between 5-10%). “Spotted anorthosite” is derived from the presence of pyroxene as “spots” or “specks” within the anorthosite. The SAn thus has a creamy white colour due to the dominant presence of plagioclase with black/dark brown spots of pyroxene. The rock is medium to coarse grained with pyroxene crystals of approximately 2mm of size.

The pyroxenite that replaces the hanging wall anorthosite is medium to coarse grained. Pyroxenite is a mafic igneous rock consisting mainly of pyroxene (90 to 100%) and of minimal plagioclase. The hanging wall pyroxenite differs from the MR pyroxenite in that it contains minimal amounts of sulphides (except for in areas in close proximity to the upper chromitite stringer) and appears, macroscopically, to have more visible interstitial plagioclase.

The common hanging wall norites of the MR are namely leucocratic norite and melanorite. Typical leucocratic norite consists of pyroxene and plagioclase (in a 50:50 ratio). The IUGS classified the norm sample SARM-7 [a composite sample of the MR at 5 mines in the south Western limb, (Steele et al., 1975) consisting of 60% orthopyroxene, 25% plagioclase, 6% clinopyroxene, 6% chromite, 1% sulphides] as a coarse grained to very coarse melanorite and not a pyroxenite (Barnes & Maier, 2002b); hence some authors refer to the MR pyroxenite as melanorite depending on the modal proportions of the rock. The MR pyroxenite at TRP contains >90% pyroxene and is therefore not referred to as melanorite.

The BSN is more similar to mela-gabbronorite, in that it consists of approximately 60% orthopyroxene and up to 10% clinopyroxene. These rocks have an outer brown “sugary” appearance in some cases with a fine to medium grain size. The BSN are finer grained than the pyroxenite, making it difficult to identify the minerals (especially plagioclase) macroscopically. BSN colour varies from brown (where sugary textured on the outside) to a fine grained dark brown to dark grey colour.

2.2.2 Merensky Pyroxenite

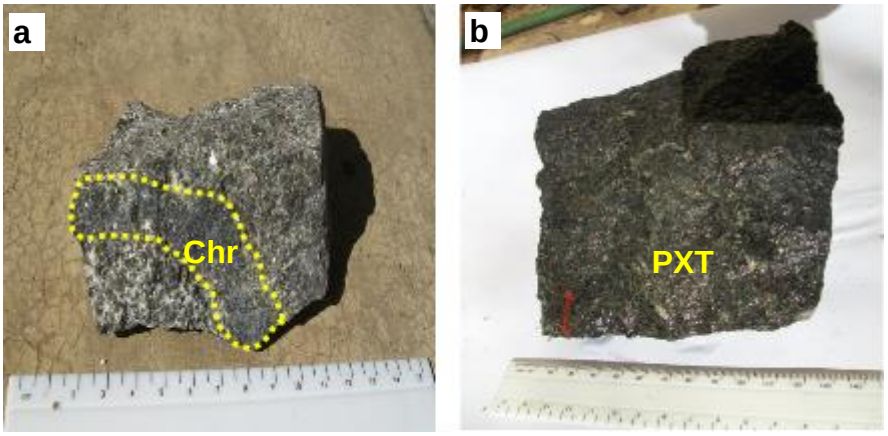

Figure 7: a) Merensky Pyroxenite with chromitite stringer and b) Merensky pyroxenite

The MR pyroxenite generally consists chiefly of orthopyroxene (over 90%). The pyroxenite of the MR at TRP can be classified as “normal” pyroxenite (as defined by Cawthorn & Boerst, 2006) however where in close proximity to the BSN it appears to be more feldspathic as a higher intercumulus plagioclase content is observed macroscopically (figure 7). The pyroxenite is coarse grained with varying grain sizes (approximately 3mm) and has a dark green appearance. Base metal sulphides (BMS) occur disseminated throughout the MR pyroxenite however a higher amount of BMS mineralisation is found in close proximity to the chromitite stringers.

The thickness of the MR pyroxenite depends on the facies type which in this case is facies 1 characterised by a pyroxenite bounded by an upper and basal chromitite stringer. These stringers mark the upper and lower limits of the primary PGE mineralisation of the reef (Viljoen & Schürmann, 1998). The chromitite stringers in the samples are relatively thin ranging from approximately 4 to 10mm. Due to the thickness of the chromitite layers in the MR chromite is regarded as an accessory phase of the entire mineralised reef (Teigler & Eales, 1993). The chromitite is fine grained with a black glittery appearance.

2.2.3 Merensky Pegmatoidal Pyroxenite

The pegmatoidal pyroxenite is a term used in this study to describe a coarser grained pyroxenite. The grain sizes ranges between about 1 and 2.5cm. The pegmatoidal pyroxenite is located below the MR pyroxenite and it may also occur near the upper limits of the MR pyroxenite. As with the pyroxenite, the pegmatoidal pyroxenite has a dark green appearance with interstitial plagioclase that is more prominent. It also contains larger sulphide “blebs”. The occurrence of pegmatoidal pyroxenite is limited in the MR profiles at TRP hence not focused on in this study.

2.2.4 Brown Sugar Norite

The BSN occurs as lenses within the MR pyroxenite and hanging wall pyroxenite. It appears that these BSN lenses are not laterally consistent as it has not been observed in previous studies done on exporational boreholes in the TRP area (Rose, 2010), but are however observed in underground exposures. It seems that BSN are only observed where the top chromitite stringer is present. As described in 2.2.1, the BSN is more similar to the mela-gabbronorite. These BSN lenses are approximately between 7cm to 16 cm in thickness as seen in figures 8 and 10 a to c. It has also been noted that the BSN is usually associated with pegmatoidal or relatively more plagioclase rich pyroxenite (as seen in figure 8). The BSN lenses may also be characterised by a feldspathic rim (figures 10 a and b) which may be attributed to a reaction between the MR pyroxenite melt and BSN. The transition of BSN into the pyroxenite varies between gradual to sharp. On one of the sites visited underground (N1G, line 5), the BSN has been observed to occur as a layer. It is suggested that while parts of the BSN layer was eroded leaving relicts of BSN lenses behind, other parts of the BSN layer may have been displaced by the HW pyroxenite during possible magmatic erosion. X Ray Computed Tomography of the two rock types at contact makes it possible to view the distribution of the minerals in 3D (figures 9a-d). The defect analysis function allows for the representation of defects such as voids, cracks or pores in the BSN and MR pyroxenite (figure 9d). It can be seen that the BSN is finer grained with a less sulphides present (figure 9a-c).

The BSN evidently has a larger volume of voids or pores relative to the adjacent MR pyroxenite.

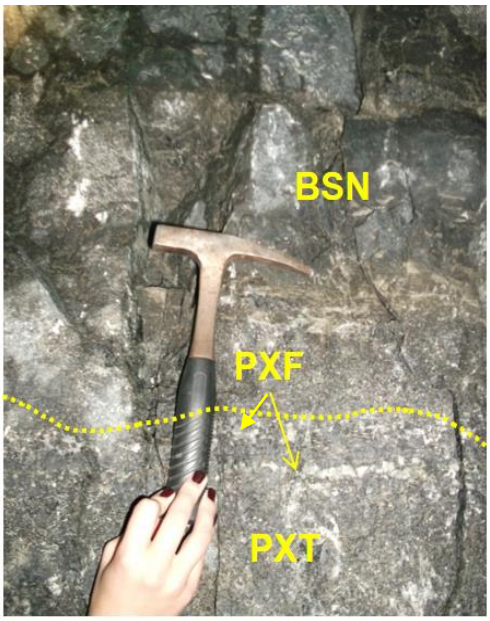

Figure 8: Merensky reef profile where BSN is intersected underground at location N1E, line 5E. (Picture by E. v. /d. Westhuizen, 2012)

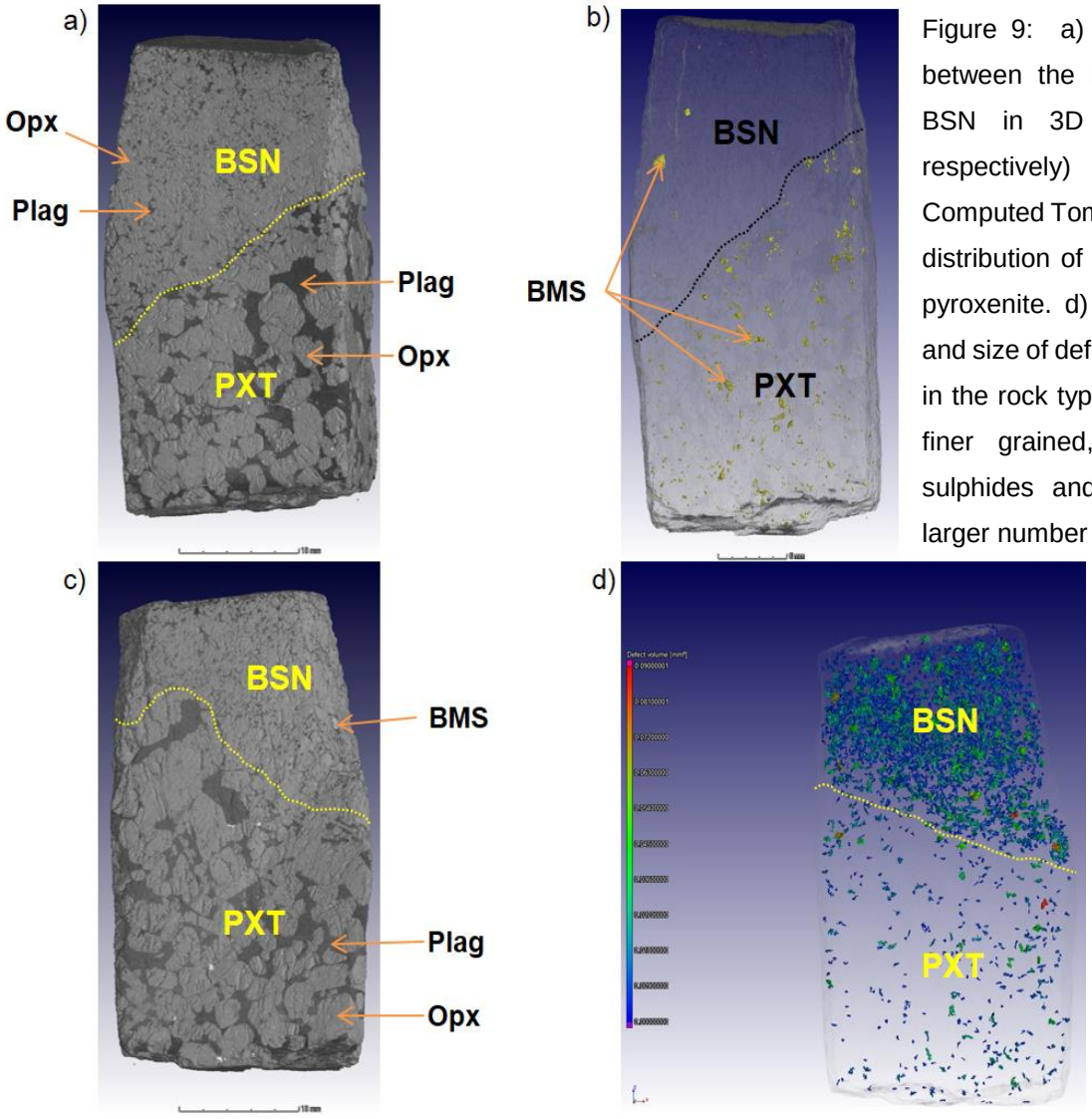

Figure 9: a) and c) show the contact between the Merensky pyroxenite and BSN in 3D (front and back view respectively) by the use of X-Ray Computed Tomography. b) illustrates the distribution of sulphides in the BSN and pyroxenite. d) illustrates the distribution and size of defects (mainly voids) present in the rock types. Note that the BSN are finer grained, contain relatively less sulphides and plagioclase and has a larger number of voids.

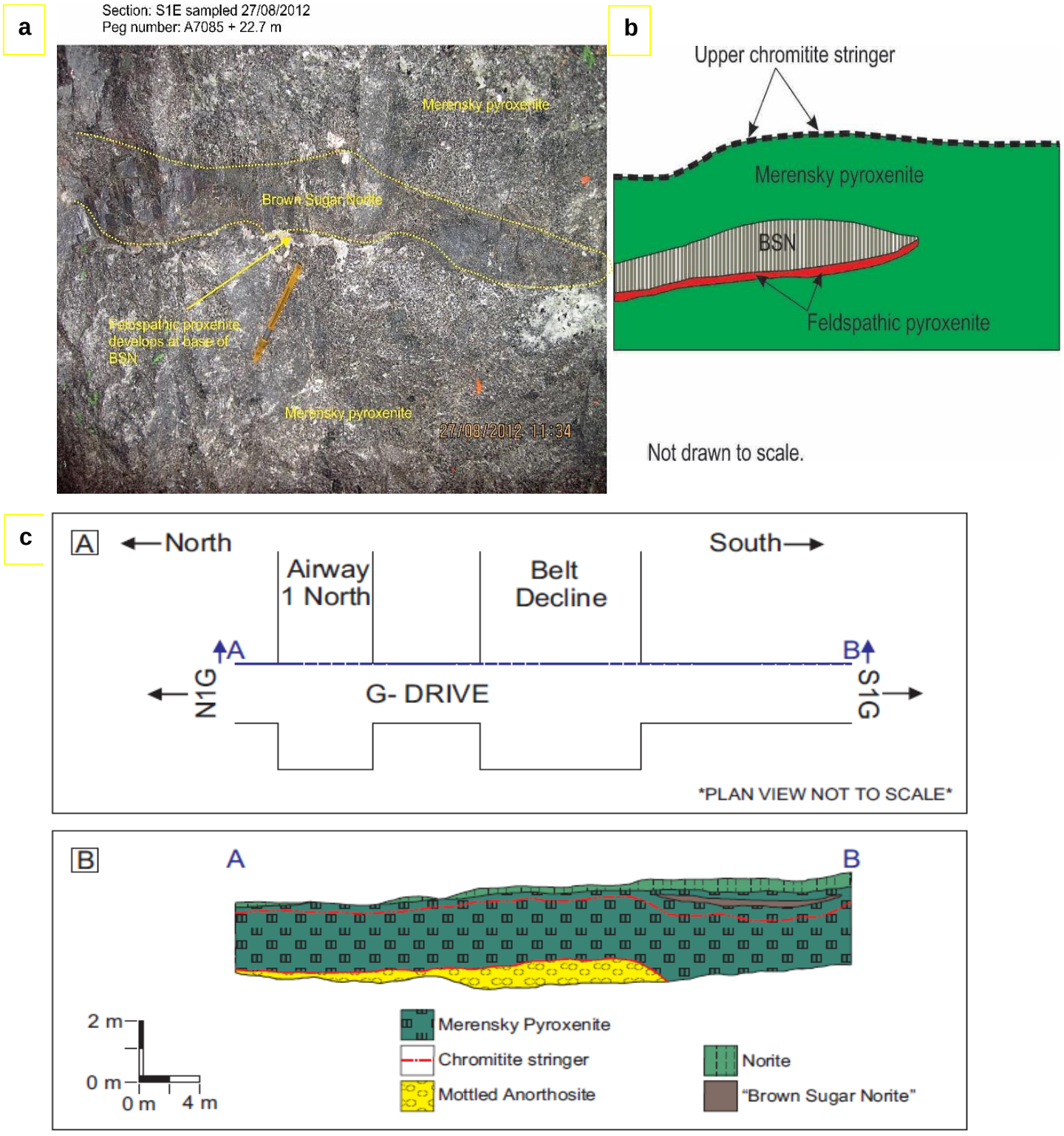

Figure 10: a) photograph and captions by D. Rose accompanied by, b), a cartoon he made depicting his interpretation of BSN lenses within MR pyroxenite after doing underground mapping in location S1E at TRP in 2012. c) a drive mapping by D. Rose of an exposure where a BSN lense occurs above the upper chromitite stringer at TRP.

2.2.5 Footwall

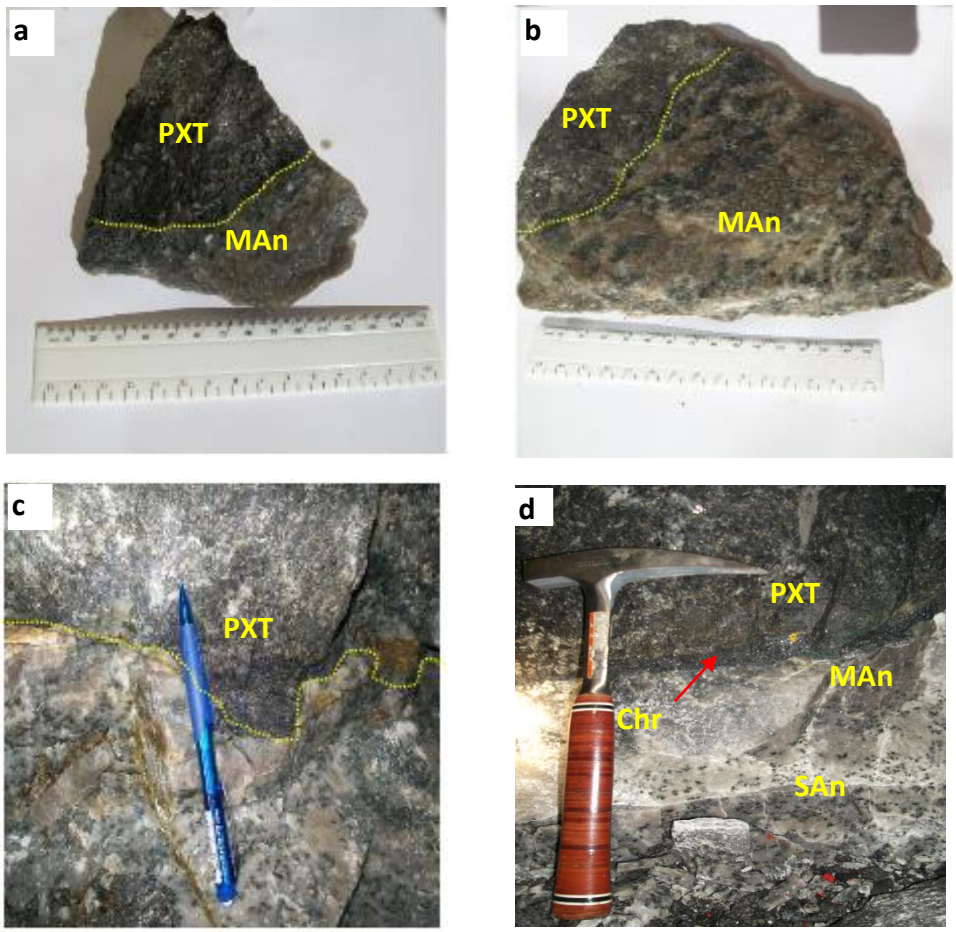

Figure 11 a to c) Footwall lithology comprising of pyroxenite, basal chromitite stringer and mottled anorthosite (MAn). As seen in c) and d) a transition from mottled to spotted anorthosite may occur.

The footwall of the MR consists mainly of mottled anorthosite (MAn) which may grade to spotted anorthosite as seen in figure 11c) and d) where BSN has been found present in the MR profile. The name, “mottled” anorthosite, is derived from the occurrence of pyroxenes as “mottles” or clusters ranging from approximately 1cm to over 4cm within the anorthosite. A sharp contact exists between the lower chromitite seam (at the bottom of the MR pyroxenite) and the anorthositic footwall. MAn has similar mineral composition as the SAn in that it is predominantly made up of plagioclase (approximately 90%) with minimal amounts of pyroxene. It is a medium to coarse grained rock with an overall pinkish white appearance with green to brownish black “mottles” of pyroxene.

2.3 Microscopic description of main rock units

2.3.1 Anorthosite

Spotted anorthosite found in the hanging wall has similar mineralogical features to that occasionally found in the footwall. The same is true for footwall mottled anorthosite. As

mentioned before, anorthosite primarily consists of plagioclase (>90%). Spotted anorthosite contains anhedral to interstitial orthopyroxene and to a lesser extend clinopyroxene crystals (figure 12). These crystals are mostly isolated and intergranular. In mottled anorthosite poikilitic clinopyroxene and, less abundantly, orthopyroxene occur in the cumulus plagioclase giving rise to the “mottled” appearance of the pyroxenes as seen in figure 11. The plagioclase displays no preferred orientation. Where in close proximity to either upper or basal chromitite stringers sulphides may be present (see figure 13D).

2.3.1.1 Spotted Anorthosite

Spotted anorthosite is the most dominant rock type in the MR hanging wall and consists primarily of anhedral to interstitial pyroxene (mostly orthopyroxene) in cumulus plagioclase.

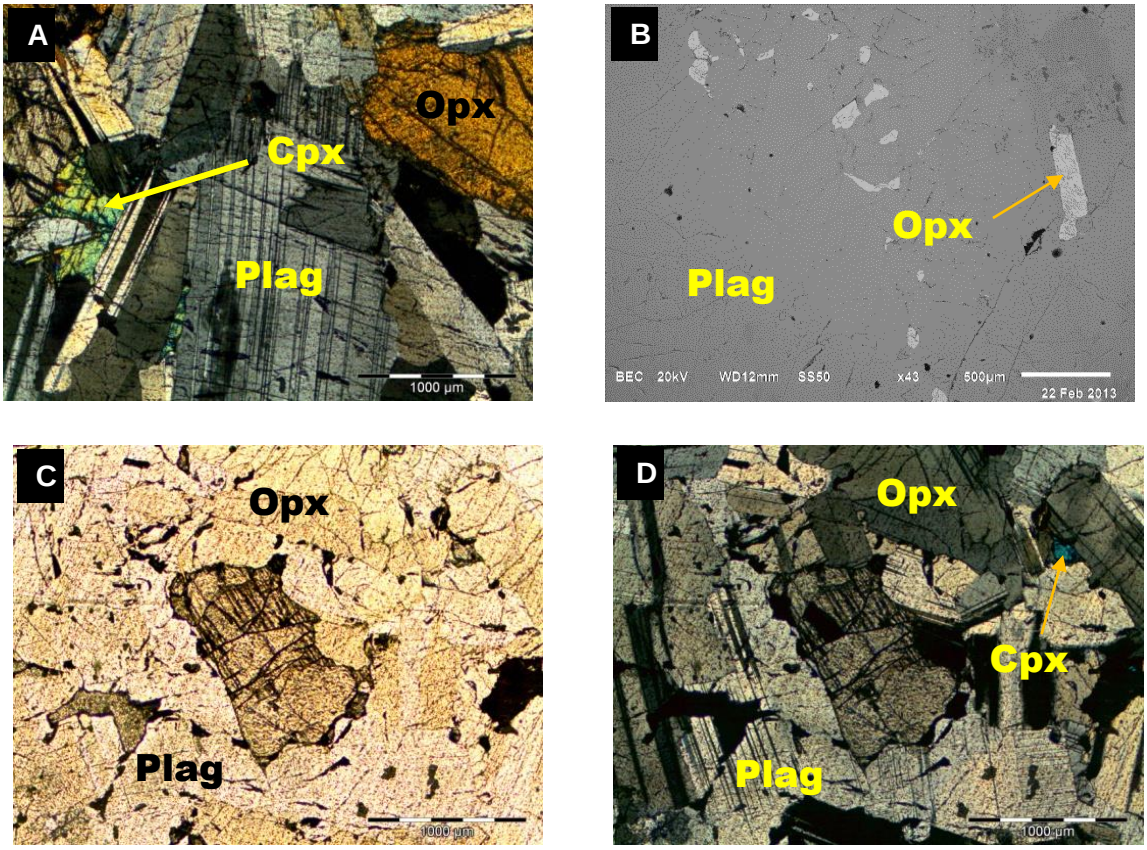

Figure 12: Photomicrographs (A, C and D) under PPL (plane polarised light) and XPL (crossed polarised light) and Backscatter electron (BSE) image (B) of the spotted anorthosite hanging wall illustrating some of the main petrographic features. A) Cumulus plagioclase (plag) with intercumulus clinopyroxene (cpx) and orthopyroxene (opx). B) Backscatter image of opx in intercumulus plagioclase. C) and D) opx surrounded by cumulus plagioclase under PPL and XPL respectively. Note the alteration of the central orthopyroxene at the rims.

2.3.1.2 Mottled Anorthosite

The footwall of the MR at TRP and consists of interstitial pyroxene (mostly clinopyroxene) set in cumulus plagioclase.

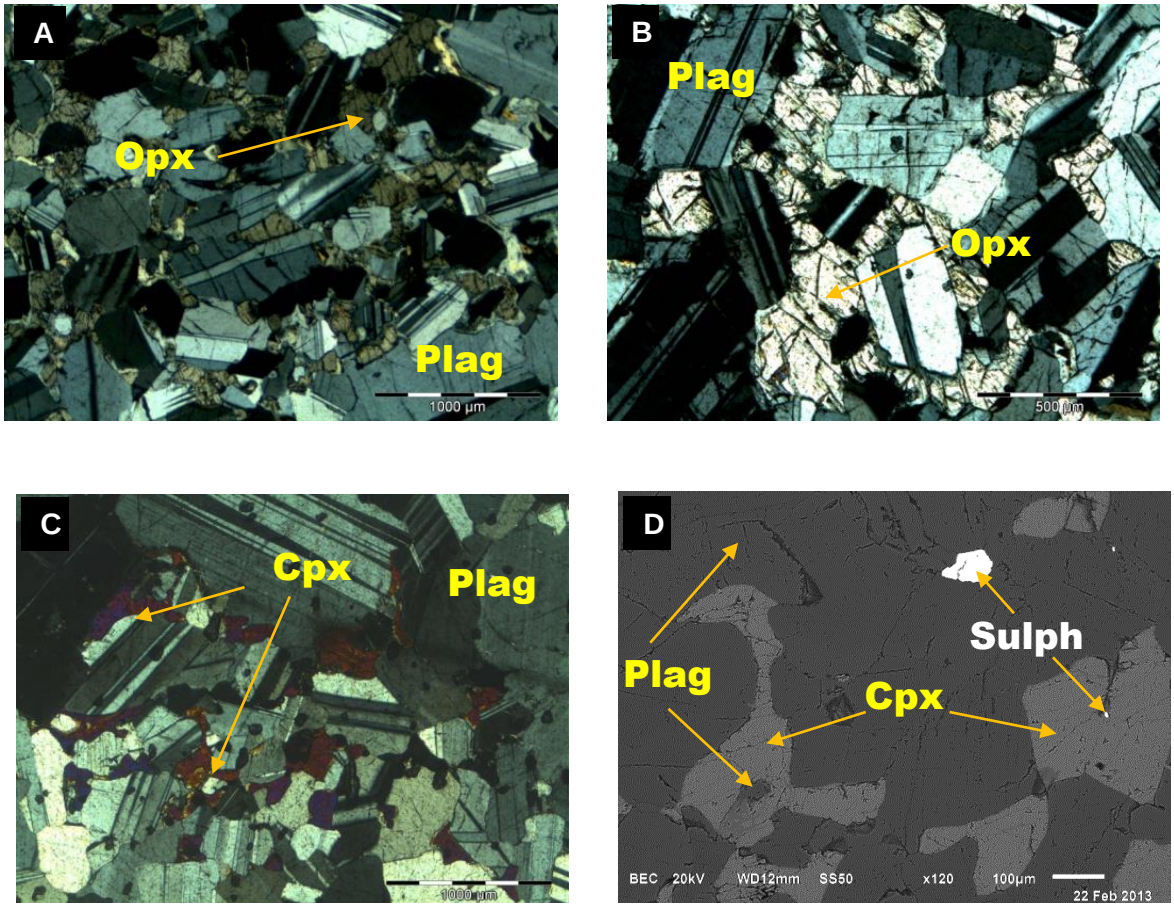

Figure 13: Photomicrographs (A, B and C) under PPL (plane polarised light) and XPL (crossed polarised light) and backscattered electron (BSE) image (D) of the mottled anorthosite footwall illustrating some of the main petrographic features. A, B and C illustrate typical mottled anorthosite features whereby clinopyroxene and/or orthopyroxene occur as “mottles” in cumulus plagioclase. D) Interstitial clinopyroxene in cumulus plagioclase with sulphides occurring (in close proximity to basal chromitite stringer). Plagioclase may also be enclosed within clinopyroxene as seen in the BSE image.

2.3.2 Merensky Pyroxenite

The Merensky pyroxenite consists mainly of cumulus orthopyroxene followed by interstitial plagioclase and minor phases of clinopyroxene, biotite and amphibole and occasional chromite and sulphides as reflected by its estimated modal mineralogy (figure 19). *Olivine* has not been noted in the TRP samples.

The *orthopyroxene* occur as coarse grained euhedral, subhedral to anhedral crystals as seen in figure 14A to H. Most of the orthopyroxene crystals have “cracks” and display a prominent cleavage. Rounded pyroxene crystals may occur as inclusions within plagioclase (figures 14E and F). Interesting textures exist between orthopyroxene and plagioclase as seen in figure 14H which may have been caused by the reheating of minerals by the injection of new magma. Olivine has not been observed in the TRP samples.

Plagioclase mostly occurs as an interstitial phase within the pyroxenite as seen in figures 14A to H. Other plagioclase textures which are less common are zoned tabular plagioclase crystals as well as rounded plagioclase inclusions within orthopyroxene.

Clinopyroxene is less abundant than orthopyroxene. One of the major textures observed for clinopyroxene in this study is the occurrence of clinopyroxene as discontinuous rims at the borders of orthopyroxene (figures 14B and E). Another prominent texture are exsolution lamellae of clinopyroxene which are strongly related to orthopyroxene from which it exsolved (the orthopyroxene may unlikely be replaced). These clinopyroxene lamellae appear as thin high birefringence streaks within the orthopyroxene crystals (figure 14G).

Amphiboles present in pyroxenite are alteration phases of orthopyroxene. Plagioclase may alter to sericite and biotite. Euhedral to rounded chromite crystals and irregular shaped sulphides occur disseminated throughout the pyroxenite. Closer to the bounding chromitite stringers an increase in occurrence of the chromite and sulphides (namely, in order of most abundant, pyrrhotite, pentlandite, chalcopyrite and pyrite) is common. The sulphides are thus associated with the chromitite stringers.

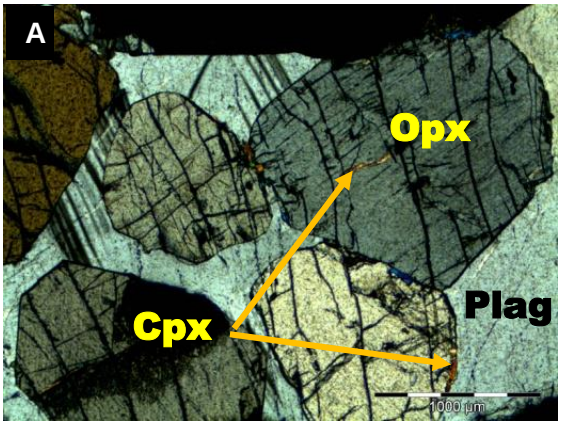

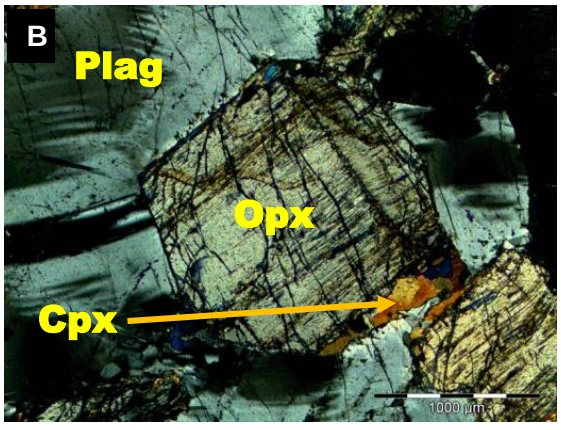

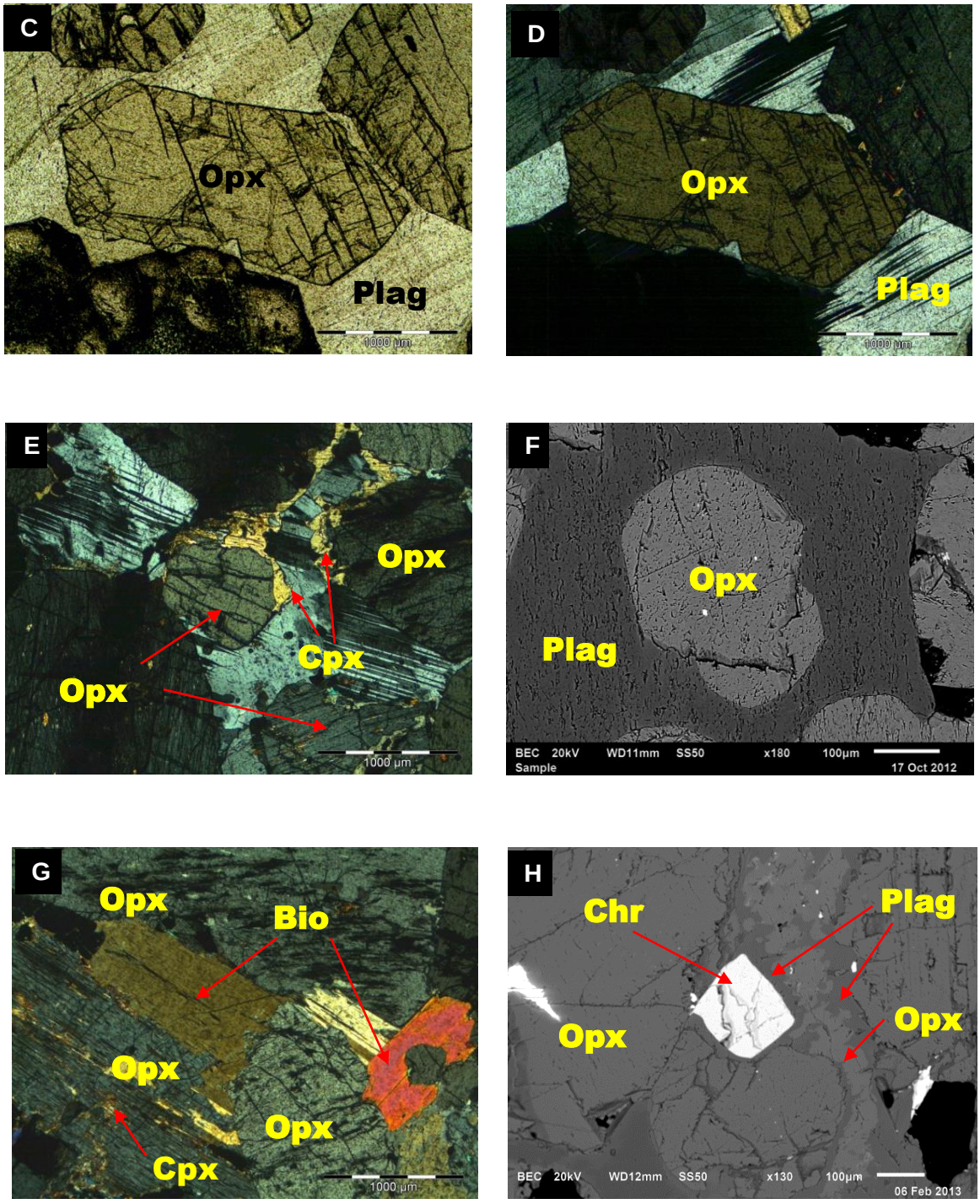

Figure 14: Photomicrographs (A – E, F and G) under PPL (plane polarized light) and XPL (crossed polarised light) and Backscattered electron (BSE) image (F and H) of the MR pyroxenite (PXT) showing the chief prominent petrographic features. A) Primary texture for the pyroxenite is cumulus orthopyroxene (opx) in plagioclase. B) Photomicrograph showing discontinuous rim of clinopyroxene (cpx) around opx crystals. C) and D) Euhedral opx under PPL and XPL; note the prominent ~90° cleavage and "cracked" appearance. E) Rounded anhedral opx crystals in plag, note the discontinuous rim of at the border of the opx crystals. F) BSE of rounded anhedral Opx inclusion within plag which is another typical texture of opx in the MR PXT. G) Photomicrograph depicting biotite (possibly the last

mineral to have crystallized from the volatile rich late stage melt) and the exsolution lamella of cpx from altered opx. H) BSE showing the occurrence of chromitite in PXT; an unusual texture of the interstitial plag and opx is noted as opx is commonly observed as a cumulus phase with interstial plagioclase in pyroxenite. This unfamiliar texture may have resulted from reheating by new magma

2.3.3 Merensky Pegmatoidal Pyroxenite

The Merensky pegmatoidal pyroxenite (PPXT) is coarser grained than the MR pyroxenite (PXT). It therefore has a similar mineral assemblage as that of MR pyroxenite with larger crystals of cumulus orthopyroxene and intercumulus plagioclase with minor abundances of clinopyroxene, amphibole, biotite, occasional chromite and sulphides [figure 15A-D]. It appears that the PPXT shows a distinct poikilitic texture than the PXT. Large oikocrysts of either orthopyroxene or clinopyroxene are present with inclusions of chromites as seen in figures 13B and C. Plagioclase may be interstitial or occur as rounded inclusions within orthopyroxene (figure 15D). Clinopyroxene discontinuous rims are associated with the clinopyroxene exsolution lamellae as seen in figures 15B and C where clinopyroxene exsolved from orthopyroxene and was accumulated at the rims.

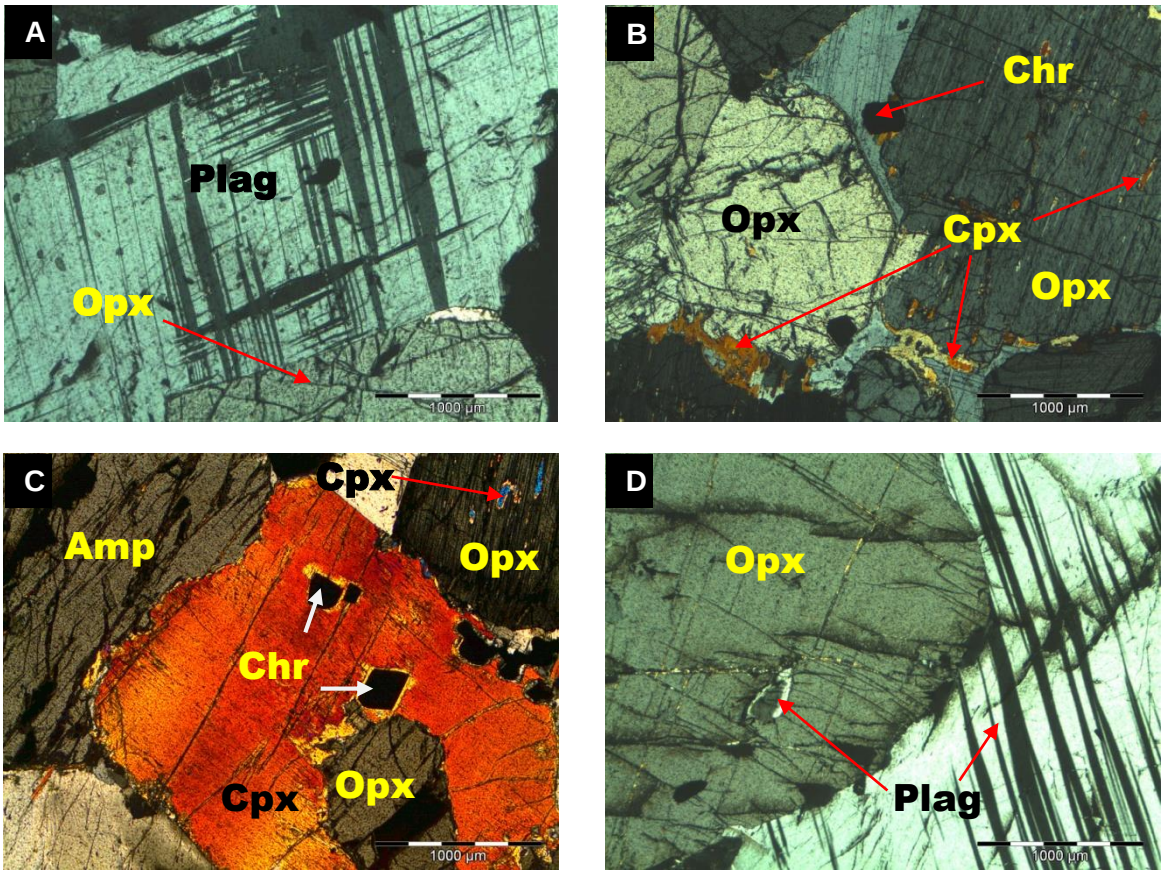

Figure 15: Photomicrographs (A to D) under XPL (cross polarised light) of the MR pegmatoidal pyroxenite of the main petrographic features observed. A) Photomicrograph showing larger crystals of Pl depicting a rather mosaic twinning pattern. B) Variety of opx crystals with interstitial Pl. Exsolved Cpx occurs at the borders of opx; subhedral chr crystals present. C) Large cpx oikocryst with inclusions of

opx and euhedral to subhedral chr. D) Photomicrograph of a subhedral opx crystal with resorbed plag inclusion.

2.3.4 Brown Sugar Norite

The brown sugar norite (BSN) is mainly comprised of rounded fine grained orthopyroxene (figure 16A-E). Von Gruenewaldt (1989) states that in most gabbros and norites the plagioclase predominates the pyroxene. It is clear from the estimated modal mineral abundance (figure 19) that the BSN is more enriched in pyroxene relative to plagioclase (about 65% pyroxene and 20% plagioclase) thus making it more likely to be a melanorite. Plagioclase occurs as an interstitial phase. Where there is a juxtaposition of orthopyroxene crystals triple junctions formed as seen in figure 16B. These triple junctions are evidence of recrystallization of BSN and suggests that the minerals of BSN may have been recrystallized by a heating event such as the intrusion of MR magma. The impingement of orthopyroxene crystal boundaries, as seen in figure 16A, may form pockets of interstitial plagioclase. Clinopyroxene mainly occurs as oikocrysts enclosing the fine grained orthopyroxene crystals as well as plagioclase (figure 16F). The clinopyroxene may occur as cumulus rounded crystals and in some cases, it may have rounded inclusions of orthopyroxene as seen in figure 16D. As seen in figure 16C, rounded inclusions of orthopyroxene are also found within plagioclase. The BSN contains a relatively high concentration of alteration phases such as biotite (as a subsolidus alteration of opx), amphibole, sericite and chlorite (figure 16G). Figure 16G also illustrates deformation of orthopyroxene crystals. Disseminated chromite and sulphides are less common than in the MR PXT.

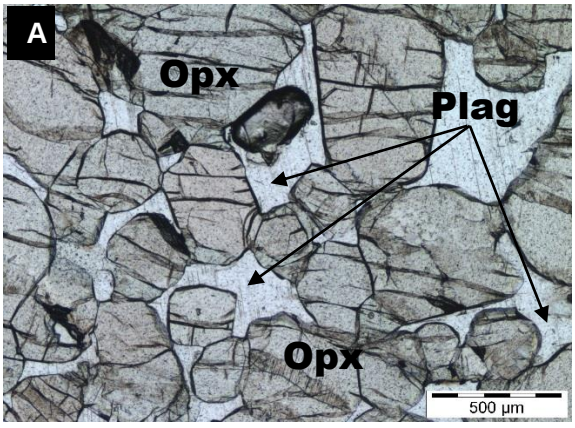

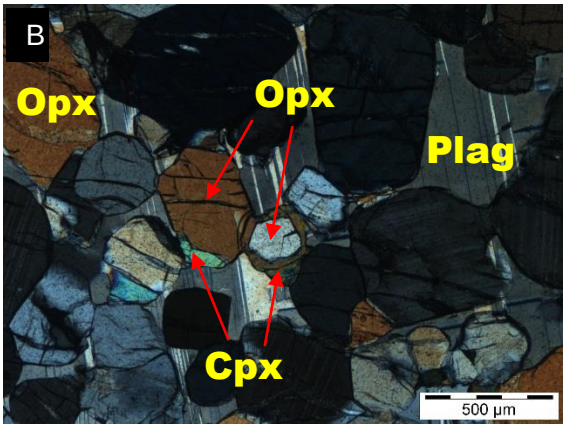

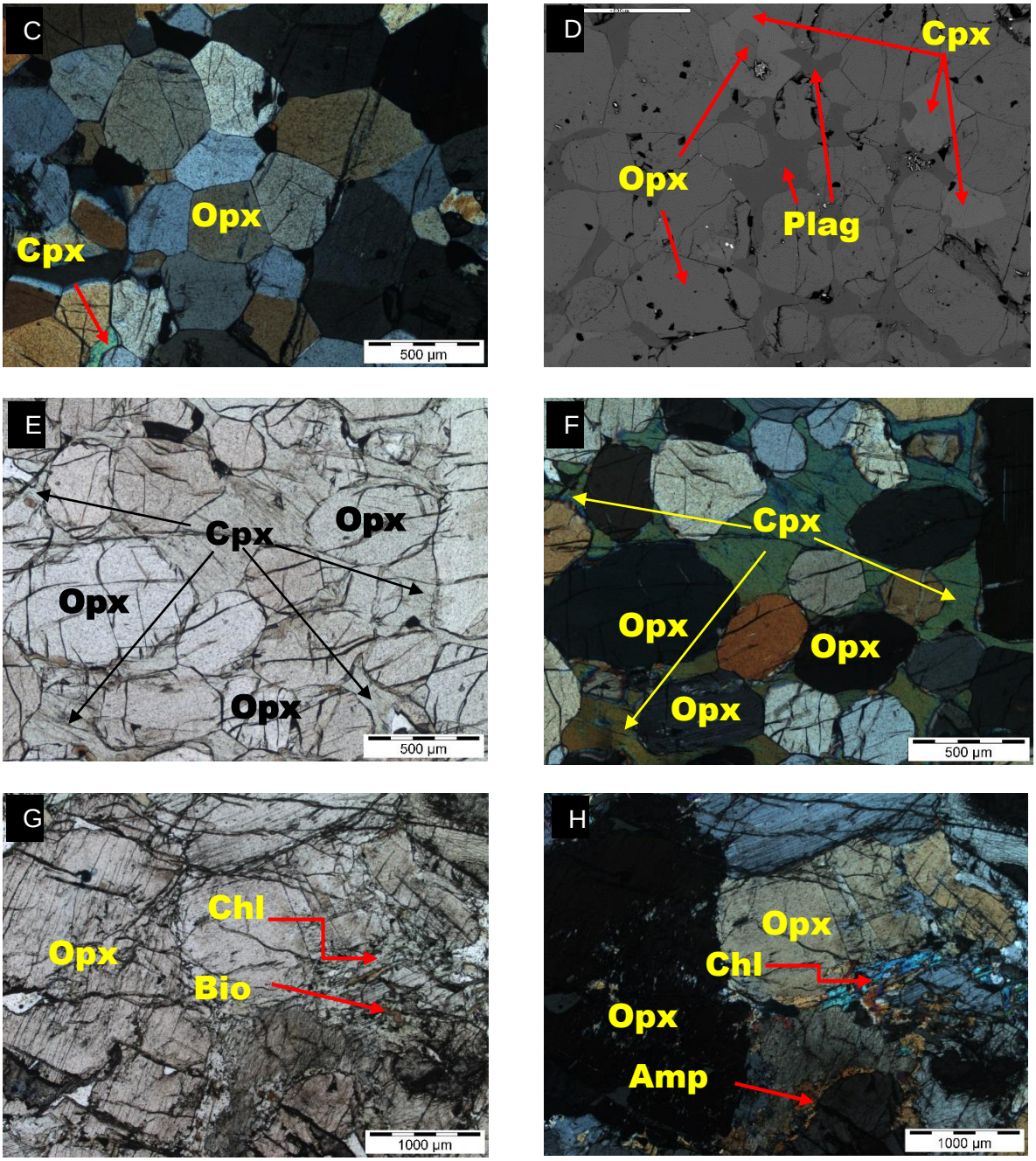

Figure 16: Photomicrographs (A to C & E to H) under XPL (cross polarised light) and back scattered electron (BSE) image (D) of the BSN found within pyroxenite and hanging wall of the MR, focusing on the main petrographic features observed. A and B) Photomicrograph showing fine to medium crystals of opx with interstitial plagioclase. Note cpx at rim as well as enclosing opx crystal under PPL and XPL. C) Impingement of opx crystals, forming triple junctions (under XPL). D) BSE image of BSN with primary cpx crystals. E) and F) Photomicrographs under PPL and XPL depicting Cpx oikocrysts enclosing medium to fine crystalline opx resulting in a poikilitic texture. G) Illustrates alteration of biotite to chlorite in a BSN lense found within the MR pyroxenite, near the bottom chromitite stringer. Note the deformation of opx crystal, depicted by the “kinks” in the crystal.

2.3.5 Chromite

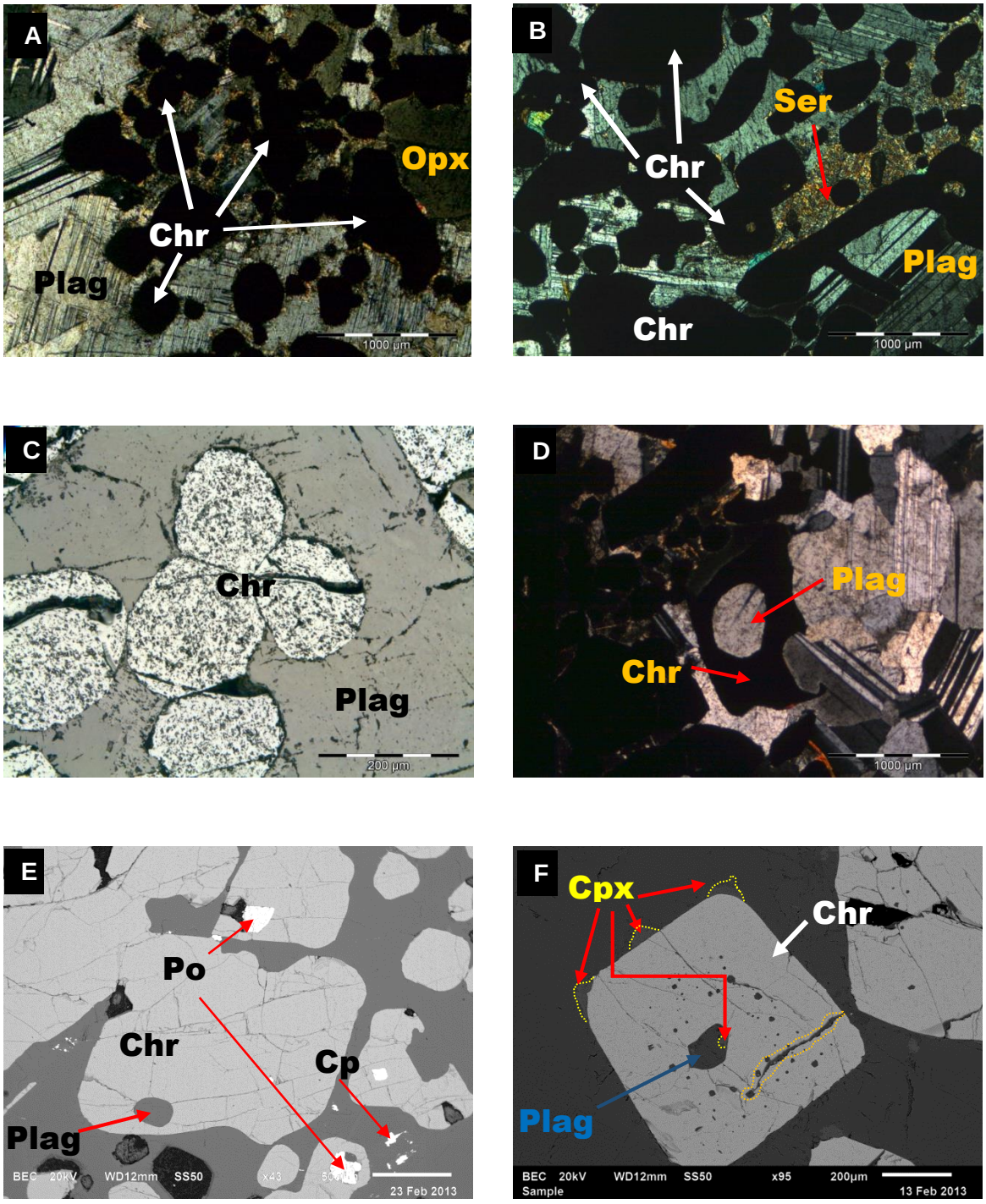

Figure 17: Photomicrographs (A-D) under XPL (cross polarised light) and back scattered electron (BSE) image (E & F) of the chromites (Chr) associated with the MR pyroxenite focusing on the main petrographic features observed. A) and B) Photomicrographs showing common appearance of the chr in the chromitite stringers; note the variance in crystal shapes and the annealing textures of some the crystals. C) Triple junction of rounded chr crystals. D) Rounded plag enclosed within chr. E) BSE image of Po (pyrrhotite) and plagioclase inclusions within various chr crystals. Cp (chalcopyrite) has also been noted F) BSE image of chr with rounded plag inclusions and vein.

Chromite crystals occur as disseminated crystals throughout the pyroxenite and as coalescent and sub-coalescent crystals at the chromitite stringers. Chromitite crystals are mostly euhedral /subhedral to round however as seen in figure 17B these also occur as irregularly shaped crystals (anhedral). Triple junctions are formed where the chromite crystals were impinged (figure 17C). Clinopyroxene reaction rims may occur around the chromites (17A&F). The chromitite crystals may enclose other mineral phases such as plagioclase, orthopyroxene and sulphides (17B, D-F). Chromite crystals tend to anneal resulting in a large mass of chromite (figure 17A).

2.3.6 Base Metal Sulphides

Base Metal Sulphides (BMS) observed in the underground samples of the MR pyroxenite are namely pyrrhotite (Po), pentlandite (Pn), chalcopyrite (Cp) and seldom pyrite (Py). BMS also occur in the hanging wall and footwall lithology of the MR to a lesser extent. Though the BMS is found in various concentrations throughout the MCU, the BMS appear to be related to the chromitite stringers. The BMS occur primarily as interstitial phases as it filled the pore spaces between the cumulus minerals of the pyroxenite (figures 18A-F). Inclusions of BMS are present within the other mineral phases as seen in figure 18G. BMS which has been observed as veins within in the silicate minerals (with special reference to chalcopyrite) as well as an association between BMS and biotite in some cases (figure 18F and H) indicates that possible late hydrothermal processes were involved. Intergrowths of Pn with Cp are found associated with Po and Py as seen in figures 18C&D.

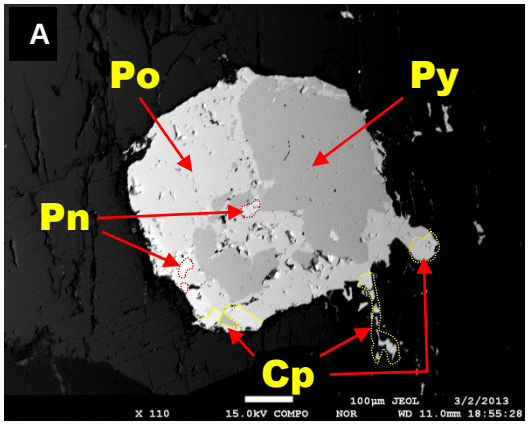

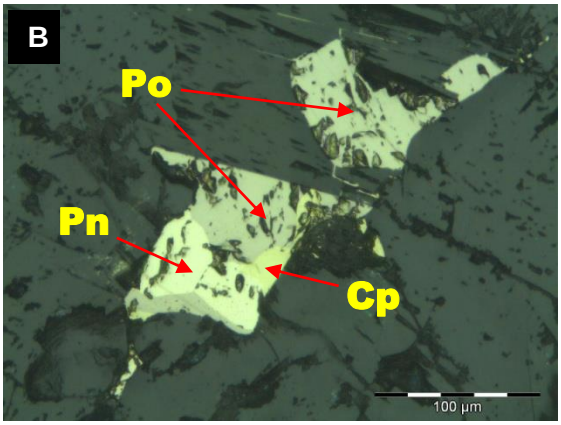

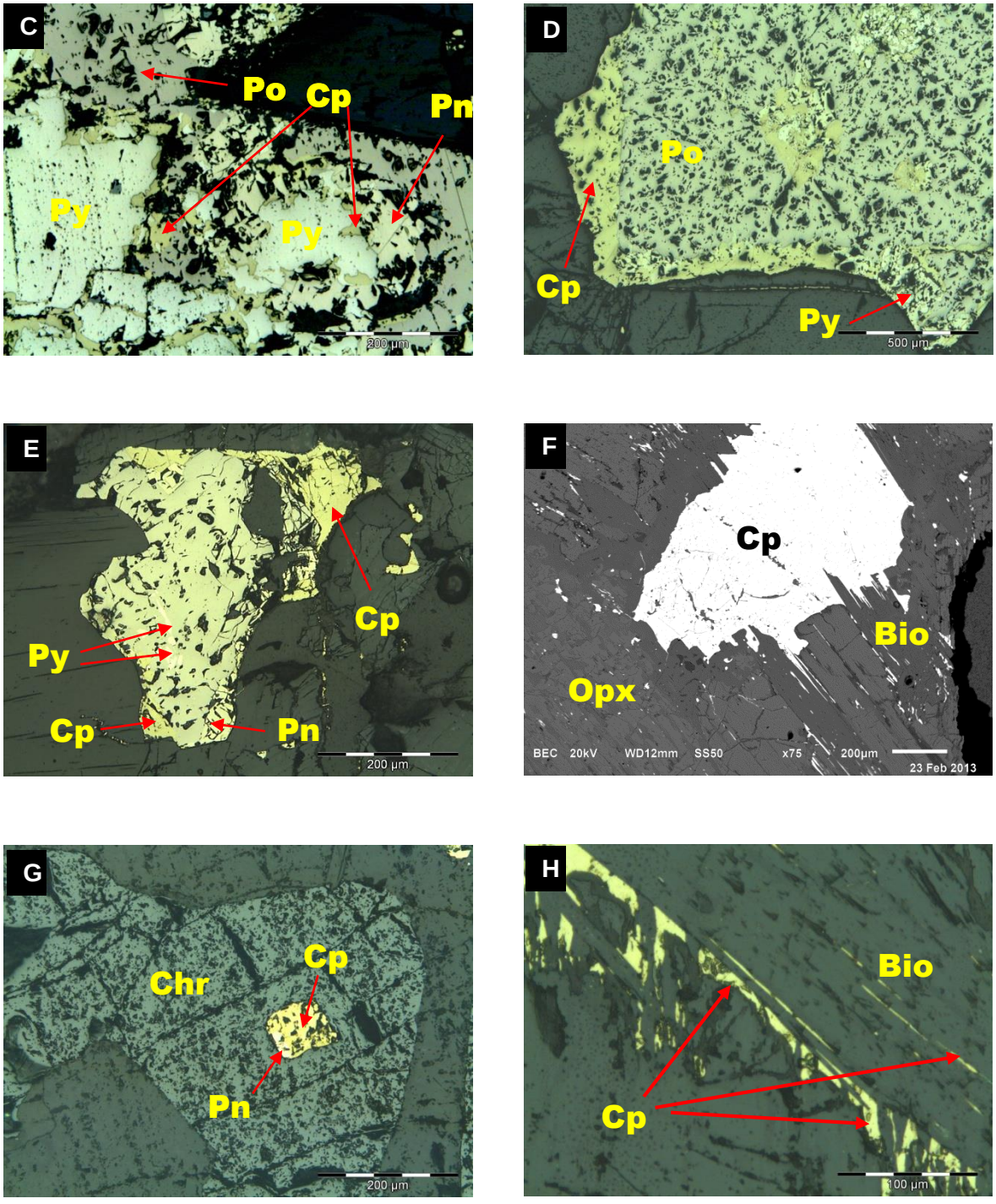

Figure 18: Photomicrographs (B-E, G &H) under XPL (cross polarised light) and back scattered electron (BSE) image (A & F) of the BMS associated with the MR pyroxenite showing the main petrographic features. A) BSE image showing main BMS assemblage present in pyroxenite with exsolution flames of pentlandite. B) Photomicrograph depicting dominant Po phase. C) & D) Photomicrographs showing Pn intergrowth patterns or "flames" associated with Po and Py. E) Typical interstitial BMS, which is comprised chiefly of Po, giving rise to a "bleb"-like appearance. F) & H) Chalcopyrite associated with biotite indicating possible remobilisation. G) Cp crystal enclosed in Chr.

2.3.7 Estimated modal mineral abundance of underground samples of MR profile where BSN is present

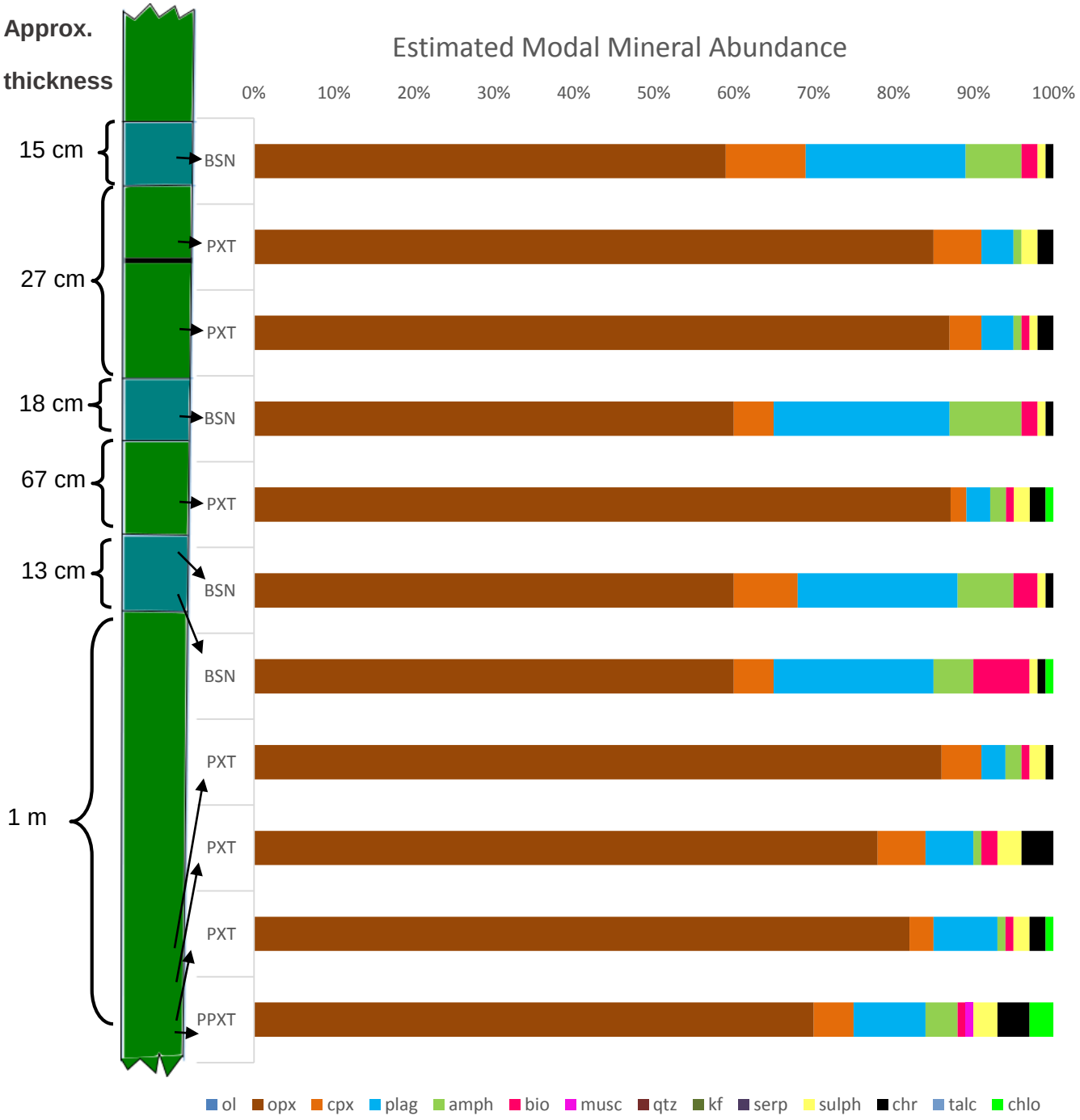

Figure 19: Figure illustrating the estimated modal mineral abundance of a MR underground section where BSN lenses are presented here as a vertical sequence in order from the HW at the top to lower pyroxenite of the MR at location S1D, line 5, TRP. (note, the BSN is not necessarily a stacked unit. The BSN lenses occur within the HW and MR pyroxenite as seen in figure 65.)

2.4 Description of rock units of the Merensky Cycle north of study area; Eerste Geluk 327 KT

Figure 20: Photograph of the EST013 drill core of the Merensky Unit north of the Steelpoort Fault. (Picture taken by Schanoor, Free University of Berlin).

The Merensky units of the farm Eerste Geluk appear to be macroscopically similar to those found at TRP, however, there is an absence of the BSN and the first meter of the immediate hanging wall of the MR consists of mesonorite followed by a transition of anorthosite to leuconorite. This is not the case at TRP where the immediate hanging wall is usually composed of spotted/mottled anorthosite (which may grade into leuconorite) or to a lesser extend pyroxenite (figure 20).

2.4.1 Norite

Two types of norites are present in the HW of Eerste Geluk farm, namely leuconorite and mesonorite. The norite of the MCU consists predominantly of plagioclase and orthopyroxene, with plagioclase being the most abundant (figure 24). No sulphides or chromites were observed except for the mesonorite in close proximity to the chromite stringer. The norites display a mesocumulate to adcumulate texture. A widespread occurrence of plagioclase inclusions within various pyroxene crystals is observed along with the alteration of orthopyroxenes to amphiboles or the replacement of orthopyroxene by clinopyroxene, as seen in figures 21. These textures suggest primary crystallization along opx-plag cotectic where

plagioclase crystallization occurs only after the orthopyroxene component was exhausted in the melt. Clinopyroxene forms in the interstitial space when Na is exhausted by the massive crystallization of plagioclase.

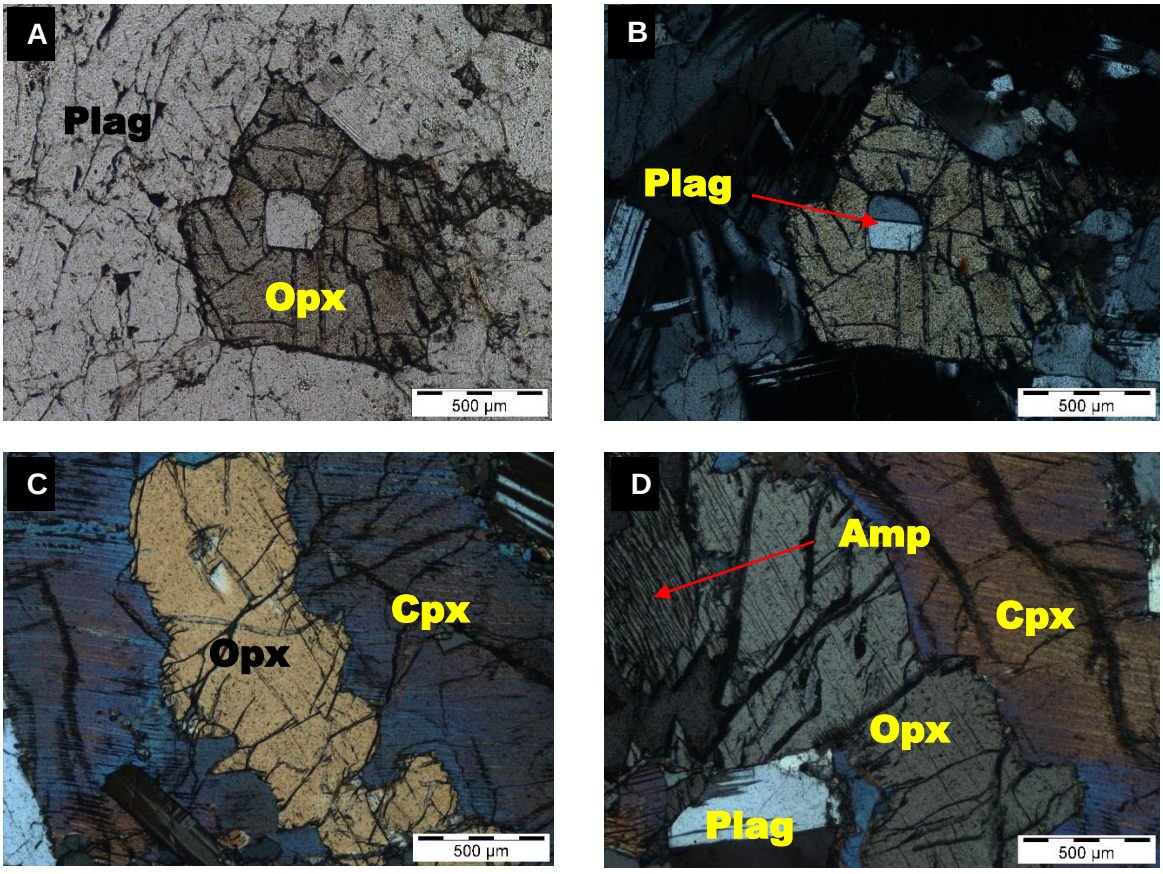

Figure 21: Photomicrographs depicting the main petrographic features of the noritic HW of drill core EST013 under PPL and XPL. A) and B) shows a leuconorite where an orthopyroxene with a plagioclase inclusion occurs with surrounding cumulus plagioclase as seen under PPL and XPL respectively. C) and D) Alteration of orthopyroxene, where orthopyroxene occurs within clinopyroxene (with orthopyroxene exsolution lamellae) along with plagioclase which may have been included later in mesonorite; note amphiboles replacing orthopyroxene as seen in D).

2.4.2 Pyroxenite

The EST “feldspathic pyroxenite”, which is a mine term, consists primarily of cumulus orthopyroxene with interstitial plagioclase as seen in figure 22. According to IUGS classification this rocktype is a melanorite because the plagioclase is greater than 10%. Feldspathic pyroxenite is not an appropriate IUGS term. Clinopyroxene is the third most dominant silicate phase dominating amphibole, biotite and other minor phases such as sulphide and oxide which consist mostly of chromites. The pyroxene grain size ranges from medium to coarse with grain shapes varying from euhedral to anhedral. The melanorite

becomes coarser near the footwall as it comprises of larger crystals, it is then referred to as “pegmatoidal pyroxenite”. Though orthopyroxene occurs as a cumulus phase, clinopyroxene mostly occurs as an interstitial phase in Eerste Geluk melanorite. A high amount of orthopyroxene crystals with clinopyroxene exsolution lamellae is present. It appears that the Ca content within orthopyroxene crystals varies. A Ca content of between 0,4 to 0,9 wt.% is observed for orthopyroxene with exsolution lamellae whereas subhedral to anhedral orthopyroxene crystals where no exsolution is present have 1.3 to 1.7wt% Ca. Certain euhedral crystals have been observed to have Ca concentration ranging between 2 to 3.3%.

In comparison to the MR at the TRP, the Eerste Geluk MR melanorite is observed to be highly altered. Alteration may be associated with late hydrothermal fluids as suggested by the increase of hydrous minerals such as amphibole and tardive biotite (as seen in figure 22 E and F). Deformation of orthopyroxene crystals is also indicated by “kinks” in the orthopyroxene crystals with exsolution lamellae as seen in figure 22 G and H. These orthopyroxenes may represent xenocrystals as the kink bands could only form in sub-solidus conditions. In addition, zonation of plagioclase has also been observed in the lower melanorite and footwall of EST which has not been identified in TRP samples suggesting that the minerals at EST have been modified by later processes.

At TRP, little or no olivine was observed in the pyroxenite, however at Eerste Geluk, olivine occurs in the FW melanorite (approximately 1m below the bottom chromitite stringer) accompanied by iddingsite (figure 22 I and J). Its presence indicates that mafic minerals such as olivine and orthopyroxene have been replaced by later iron rich minerals. Some of the olivine crystals have orthopyroxene inclusions creating a poikilitic texture.

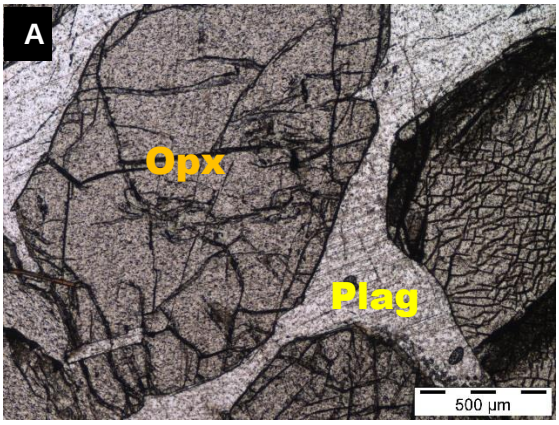

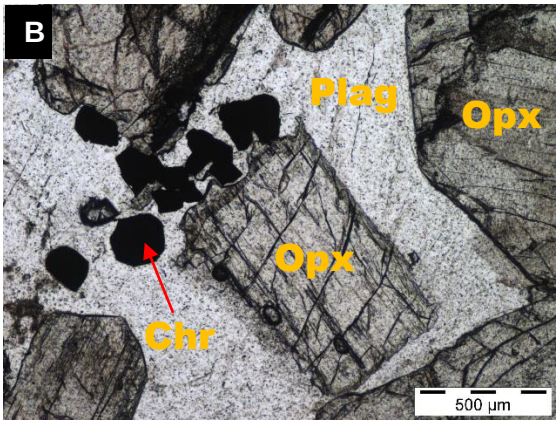

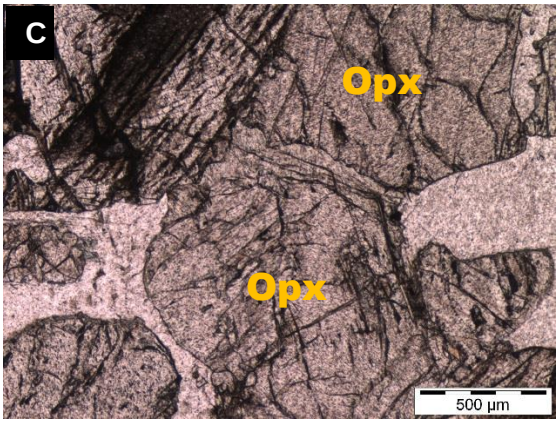
C
Opx
Opx
500 µm

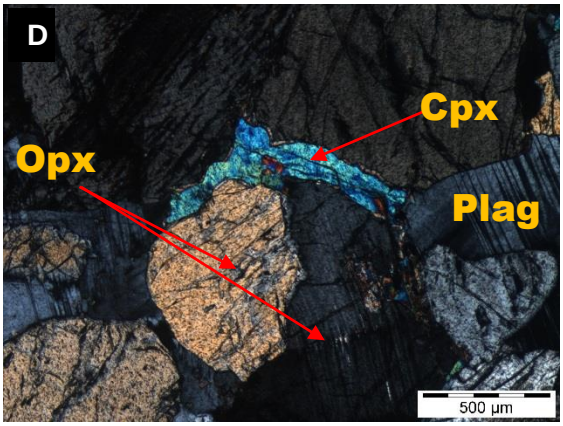
D
Cpx
Opx
Plag
500 µm

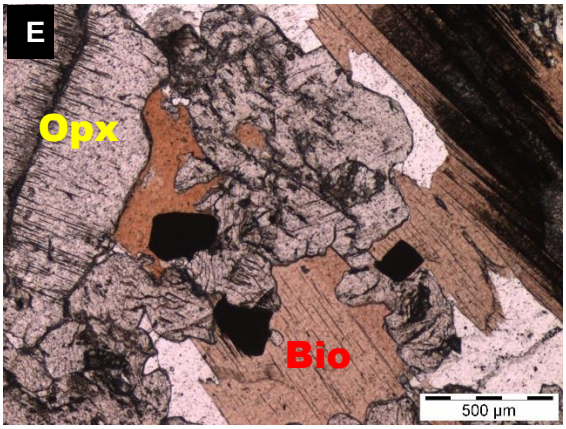
E
Opx
Bio
500 µm

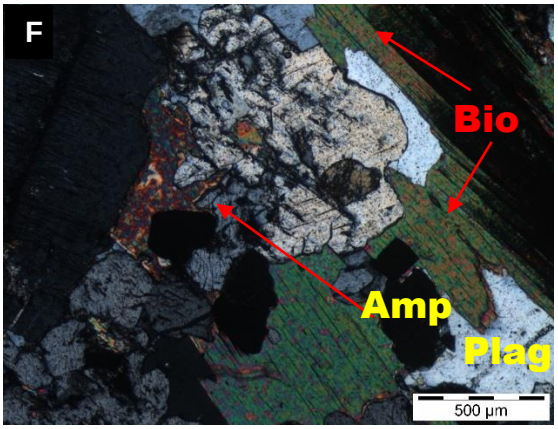
F
Bio
Amp
Plag
500 µm

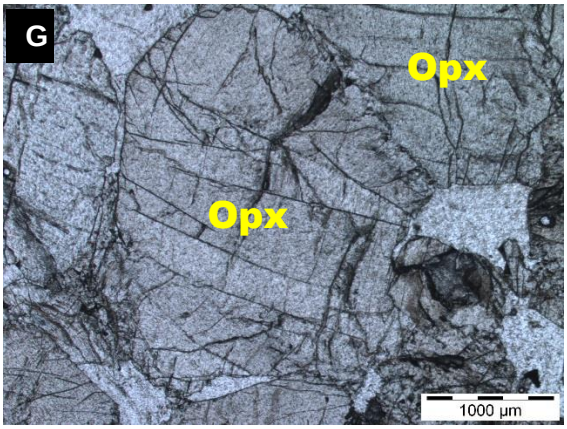
G
Opx
Opx
1000 µm

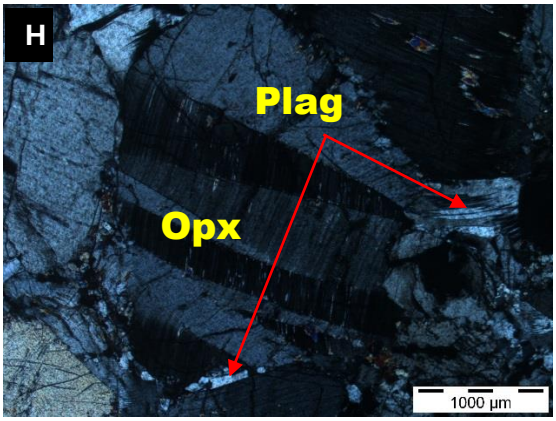
H
Plag
Opx
1000 µm

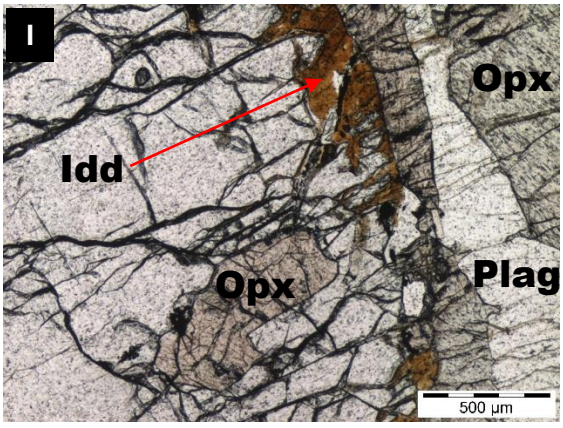
I
Opx
Idd
Opx
Plag
500 µm

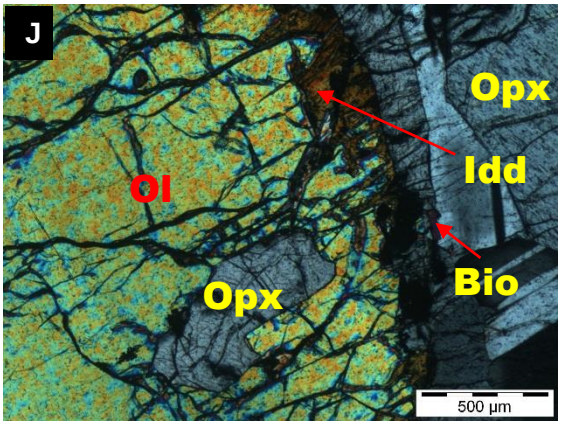
J
Opx
Idd
Ol
Opx
Bio
500 µm

Figure 22: Photomicrographs of melanorite of Eerste Geluk, representing the main petrographic features observed under PPL and XPL. A) Shows a subhedral orthopyroxene crystal with interstitial plagioclase under PPL. B) Occurrence of chromite crystals within the pyroxenite; the crystal boundary of the orthopyroxene is distorted as a result of the chromite crystals under PPL. C) and D) shows amalgamation of two orthopyroxene crystals with a discontinuous rim of clinopyroxene derivative of possible recrystallization (under PPL and XPL respectively). E) and F) Shows a general alteration of pyroxenes to amphiboles; late phase biotite and associated with sulphide occurrence under PPL and XPL. G) and H) Photomicrographs under PPL and XPL of orthopyroxene with "kinks" and curved orientations indicating possible deformation of crystals. I) and J) Photomicrographs under PPL and XPL of olivine with iddingsite alteration and orthopyroxene inclusion. Minor biotite also present.

2.4.3 Anorthosite

The anorthosite at Eerste Geluk consists mainly of plagioclase with an average content of 65%, followed by minor phases of orthopyroxene, clinopyroxene and biotite. Various shapes of plagioclase are present ranging from large elongated to small rounded crystals. Where pyroxene, predominantly clinopyroxene, encloses plagioclase crystals a poikilitic texture is creating resulting in the so-called "mottled" anorthosite. A large amount of these clinopyroxene has orthopyroxene exsolution lamellae represented in figure 23 A&B. Euhedral to subhedral orthopyroxene may also occur within the surrounding plagioclase where the anorthosite is referred to as "spotted" (figure 23 C&D). Biotite present is mostly an alteration phase of the pyroxenes.

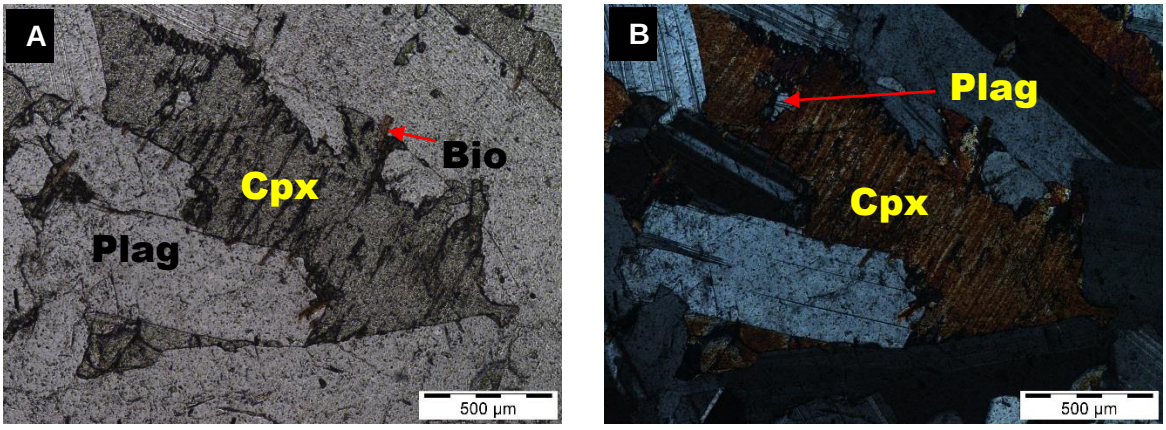

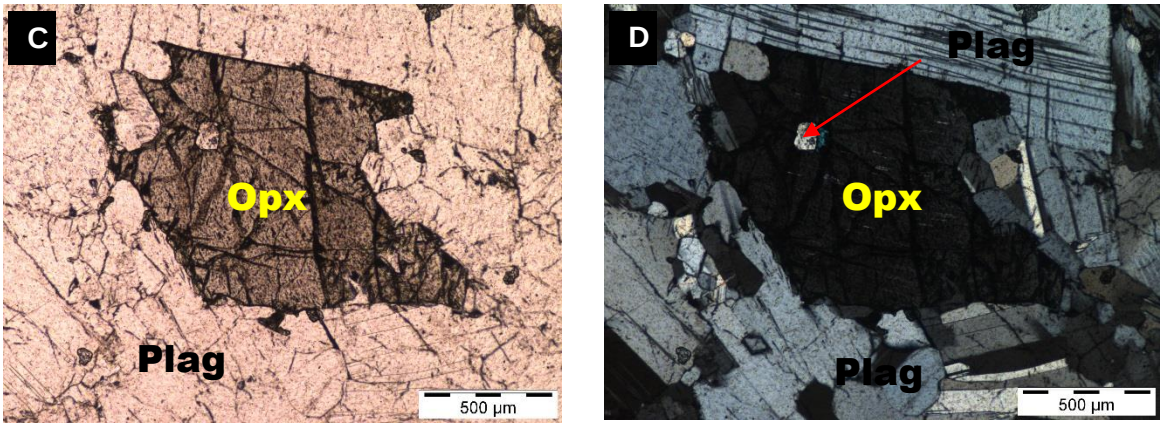

Figure 23: Photomicrographs of HW mottled and spotted anorthosite of Eerste Geluk, illustrating the dominant petrographic textures. A) and B) Photomicrographs under PPL and XPL of a clinopyroxene oikocryst with orthopyroxene lamellae with surrounding plagioclase. C) and D) shows subhedral orthopyroxene containing a plagioclase inclusion. Note the clinopyroxene discontinuous rim of the included plagioclase.

2.4.4 Estimated Modal Mineral Abundance

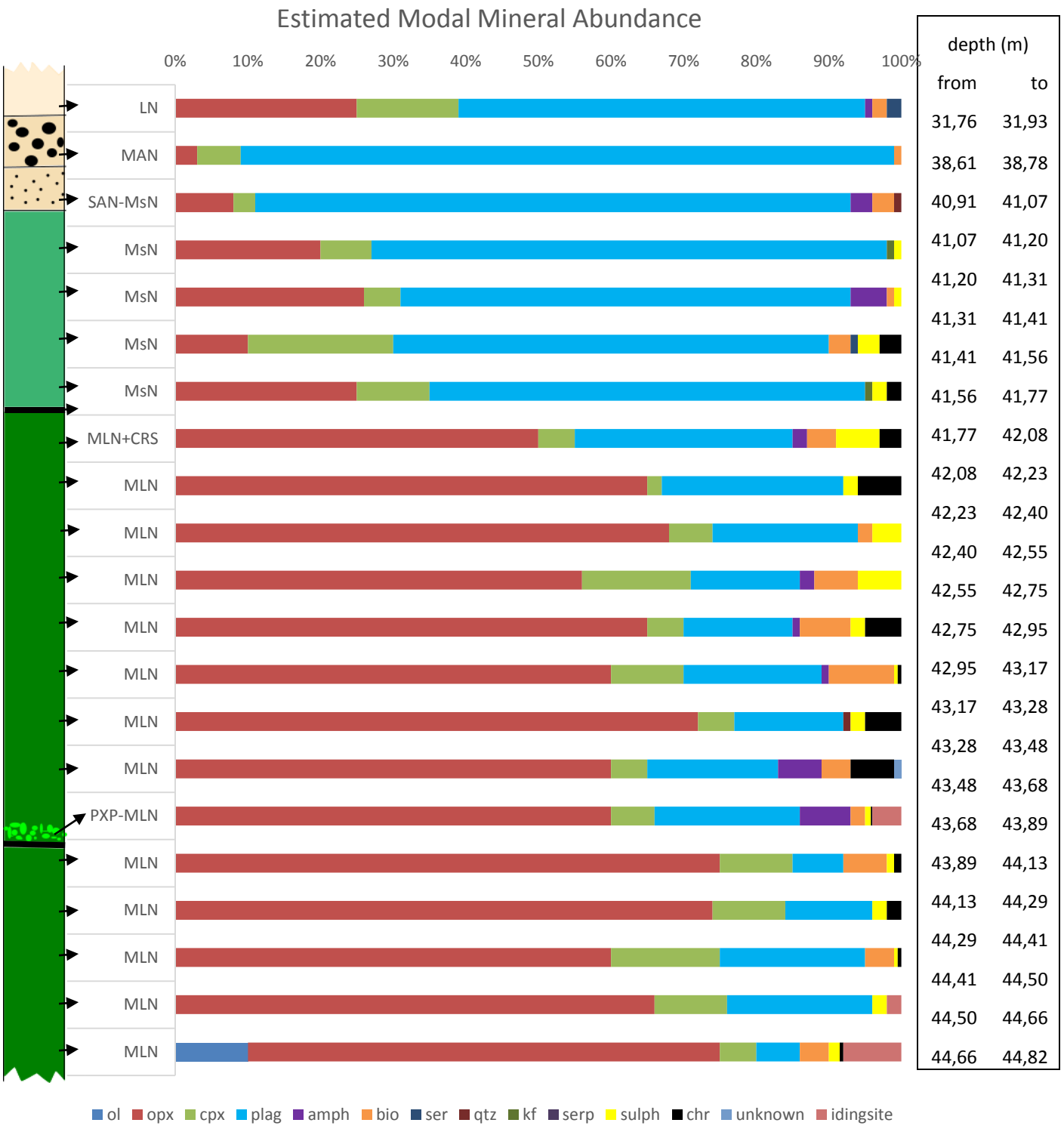

depth (m)	
from	to
31,76	31,93
38,61	38,78
40,91	41,07
41,07	41,20
41,20	41,31
41,31	41,41
41,41	41,56
41,56	41,77
41,77	42,08
42,08	42,23
42,23	42,40
42,40	42,55
42,55	42,75
42,75	42,95
42,95	43,17
43,17	43,28
43,28	43,48
43,48	43,68
43,68	43,89
43,89	44,13
44,13	44,29
44,29	44,41
44,41	44,50
44,50	44,66
44,66	44,82

Figure 24: Estimated modal mineral abundance of drill core EST013 from the farm Eerste Geluk.

2.5 Summary of main rock types

2.5.1 Anorthosite

The plagioclase content in the anorthosite is commonly over 60% to nearly 100%. An estimated mineralogy is given for EST drill core samples from the Eerste Geluk farm (as seen in figure 24) where it can be seen that the highest plagioclase content is found in the HW mesonorite, leuconorite, spotted and mottled anorthosite. Spotted and mottled anorthosite have similar mineral compositions comprising dominantly of intercumulus pyroxene with a modal abundance of between 5% and 10 % and plagioclase with a modal abundance of greater than 90%. A “spotted” appearance of anorthosite is created where orthopyroxene crystals occur interstitially within surrounding plagioclase. Where clinopyroxene crystals are clustered separated by plagioclase, a “mottled” variety of anorthosite is formed. Both spotted and mottled anorthosite display similar textural features. These textural features are mostly ophitic/poikilitic where pyroxene oikocrysts enclose plagioclase crystals partially or completely (as seen in figure 12A and figure 13 A, B and C). These textures are the same in both hanging wall and footwall.

2.5.2 Pyroxenite

This rock unit comprise largely of orthopyroxene followed by plagioclase as can be seen in estimated modal mineral abundance percentages of underground TRP samples (as seen in figures 19). The orthopyroxene crystals vary from euhedral to subhedral to slightly anhedral. Triple junctions of orthopyroxene crystals suggest recrystallization has taken place. The subordinate clinopyroxene occurs largely as discontinuous rims around orthopyroxene crystals and to a lesser extend as large crystals. Certain orthopyroxene crystals exhibit exsolution lamellar of clinopyroxene. The exsolved clinopyroxene tends to concentrate at the edges of orthopyroxene forming discontinuous rims in part. Everitt (2012) suggests that exsolution lamellae of clinopyroxene along with the occurrence of discontinuous rims indicate disequilibrium reactions in the crystal mush. As illustrated in figures 14 A to E orthopyroxene crystals may be cemented together by means of intergranular necking of clinopyroxene at orthopyroxene boundaries. The plagioclase in this rock type appears to be mostly interstitial and continuous. Plagioclase may also occur as inclusions within pyroxene or as recrystallized coarser crystals on a minor scale. Seabrook (2005) proposes that inclusions of plagioclase in poikilitic pyroxene may represent crystals that have not been recrystallized, i.e., early cumulus plagioclase crystals (also Eales et al., 1991). The poikilitic orthopyroxene thus suggest entrainment and partial resorption of plagioclase as proposed by Mitchell et al. (1998). Amphiboles may replace orthopyroxene in certain instances. Poikilitic and ophitic textures are the most common textures in the pyroxenite.

Chromite crystals are mainly euhedral to subhedral and occur sparsely scattered within the pyroxenite and increase in abundance in close proximity to either the top or basal chromitite stringer. Rounded chromite in poikilitic plagioclase (such as in figure 17C) may suggest that chromite existed before plagioclase crystallization. Chromite crystals may also be well preserved as euhedral crystals enclosed within poikilitic pyroxene as seen in pegmatoidal pyroxenite in figure 15C. When not disseminated, chromite crystals tend to anneal, resulting in the joining of recrystallized chromite crystals, forming large masses of chromite or joined strings of chromite crystals. Sintering and annealing indicated by subhedral to euhedral and composite shapes of chromite suggest reheating of chromite crystals.

The base metal sulphides (BMS) are disseminated throughout the MR pyroxenite as well as the footwall and hanging wall units. These sulphides are pyrrhotite, pentlandite, chalcopyrite and very seldom pyrite. The sulphides may replace interstitial mineral phases such as orthopyroxene and plagioclase or occur as inclusions within the silicates and also oxides (chromite). The base metal sulphides present in the pyroxenite may be associated with the chromitite stringers. These sulphides increase in abundance close to the upper and bottom stringer displaying occasional “net” or “spider web textures” macroscopically as the sulphides replaced the interstitial silicates. An association of BMS (especially chalcopyrite) with secondary minerals such as biotite (see figures 18 F and H) may be related to late hydrothermal processes.

Pyroxenite and pegmatoidal pyroxenite display similar mineralogical composition and textural features though the pegmatoidal pyroxenite has larger crystals. The pegmatoidal pyroxenite in this study has relatively more secondary minerals, indicating that additional alteration might have occurred. Clinopyroxene oikocrysts encloses other mineral phases such as chromite, orthopyroxene and/or plagioclase. Plagioclase crystals may also occur as inclusions within orthopyroxene.

The MR melanorite rocks of drill core EST013 display similar petrographic features as TRP. However, the EST samples appear to be more altered than the TRP pyroxenite. The EST melanorite samples have a higher concentration of hydrous minerals. Orthopyroxene crystals seem to have undergone deformation as suggested by kink bands present in certain orthopyroxene crystals. These kink bands are sharply defined zones where deformation within the crystal occurred through gliding (Starkey, 1968), suggesting plastic flow deformation processes was present. These crystals may represent xenocrystals as the kink bands could only form in sub-solidus conditions. In footwall pyroxenite olivine has been observed to have altered to iddingsite alongside orthopyroxene. Orthopyroxene inclusions within olivine (figure 22 I & J) may suggest a crystallization at higher pressure than the Bushveld chamber (Eales

and Costin, 2012) where orthopyroxene forms before olivine. Another possibility would be that the two minerals formed along the olivine-orthopyroxene co-tectic. These petrographic features may indicate that late processes such as hydrothermal processes brought about alteration of minerals. This is plausible as the Eerste Geluk farm is located in close proximity to the Steelpoort Fault, a potential feeder zone (Cawthorn et al., 2002b). Faulting and late-stage hydrothermal fluid may have resulted in alteration of minerals in the rock units as seen in the petrology of the EST samples. The availability of fluids would thus also favour brittle deformation by means of fracturing of crystals. Most sulphide rich samples of the EST013 drill core have been removed prior to this study, therefore a comparison between TRP and EST samples in this regard was not possible.

2.5.3 Brown sugar norite

Compared to pyroxenite, the BSN is finer crystalline. The orthopyroxene appears to be better rounded than the orthopyroxene found in the pyroxenite. Triple junctions are common in the BSN where orthopyroxene crystal boundaries impose on adjacent orthopyroxene crystal boundaries. This may suggest subsolidus recrystallization of these crystals during a heating event. Exsolution lamellae of clinopyroxene from orthopyroxene crystals have been observed. A gabbroic texture is usually observed whereby large oikocrysts of clinopyroxene or plagioclase enclose numerous rounded orthopyroxene. Clinopyroxene also occurs along the rims of the orthopyroxene crystals and instances have also been noted where orthopyroxene inclusions are found within rounded clinopyroxene crystals. Plagioclase appears mostly as an intercumulus continuous mineral phase. According to the textural and modal description the BSN should be a melanorite. Secondary phase minerals such as biotite, chlorite and amphiboles are present. These minerals are indicative of late alteration processes. Deformation of orthopyroxene (indicated by “kinks” in the orthopyroxene as seen in figure 16G) suggest that the orthopyroxene may have been present as crystals during the emplacement of BSN. Sub-solidus recrystallization of BSN (evident by triple junctions of minerals as seen in figure 16B) suggests that the BSN may have been heated possibly by the intrusion of MR magma. The occurrence of base metal sulphide and/or disseminated chromite crystals is less common in BSN than in pyroxenite. This could suggest that the BSN is a potential dilutant for the MR ore where depleted BSN would dilute the MR pyroxenite which is more enriched in BMS and PGM. The lower Sr isotope ratio and higher MgO concentration in BSN compared to MR pyroxenite (as described in the following geochemistry and mineral chemistry chapters) evidently suggest that the BSN formed from a more primitive magma. It is therefore more probable that the BMS and PGMs were depleted in the BSN by the heating of the BSN during replenishment by MR magma.

Chapter 3: Whole rock geochemistry

3.1 Introduction

In this chapter the whole rock geochemistry of all rock types, determined by XRF, is displayed in various format. XRF analyses were carried out on underground samples taken from the Two Rivers Platinum mine as well as from drill core from the farm Eerste Geluk farm No.EST-013. Major and trace element compositions are given in tables 1 and 2. The dominant silicate phases, orthopyroxene and plagioclase, control most of the chemical composition of the rocks according to their modal proportions as it concentrates most of the lithophile elements. The occurrence of silicate phases, whether major or minor, determines the nature of the cumulate rocks. Elements other than SiO_2, MgO, FeO, CaO, Na_2O and Al_2O_3 are controlled by minor phases such as clinopyroxene, amphibole, mica, chromite, sulphide, quartz and other accessory minerals such as chlorite, iddingsite and sericite. The geochemical data are plotted in vertical geochemical profiles to observe variations between the MR at TRP and of Eerste Geluk. Harker diagrams plotted against MgO are shown to display the chemical variation of the various cumulus rock types. Table 1 and 2 summarizes the major element and trace element XRF data of TRP and EST found in appendices A2-1 & A2-3 and A2-2 & A2-4 respectively.

3.2 Major elements

MgO vs. FeO, TiO_2, MnO, Al_2O_3, CaO, Na_2O and K_2O results respectively for the same stratigraphic intervals of TRP and EST are opposed to each other, as seen in Figure 25 a) to n). Pyroxenite and brown sugar norite (BSN) appear to have the highest MgO and FeO concentrations and anorthosite the lowest. BSN display a higher MgO concentration (24-28 wt. %) than pyroxenite (21-23wt. % MgO) at TRP. When compared to the pyroxenite of Eerste Geluk, the FeO content at TRP is relatively higher with concentrations varying between approximately 11-15wt. percent compared to the 11-12wt. % FeO in EST samples. TiO_2 and MnO content for both TRP and EST are low ranging from 0,01-0,19wt.% TiO_2 and 0,06-0,2wt.% MnO and 0,16-0,3wt.% TiO_2 and 0,15-0,2wt.% MnO for TRP and EST respectively.

Al_2O_3, CaO, Na_2O and K_2O display a negative correlation with MgO as seen Figures 25g) to n). The occurrence of plagioclase and orthopyroxene influence the major element oxides within the different rock types. Anorthosite comprises of lesser amounts FeO and MgO as it contains the least amount of mafic minerals. Al_2O_3, CaO, Na_2O and K_2O are much higher in anorthosite and mesonorite than the MR pyroxenite due to the presence of plagioclase. The concentrations of K_2O in all rock types are low. The MR pyroxenite from both areas has an average of approximately 5wt. % Al_2O_3 compared to the 27wt. % Al_2O_3 in anorthosite and 24wt. % Al_2O_3 in mesonorite. In figure 25i) and j) it can be seen that the anorthosite,

mesonorite and leuconorite have the highest CaO values. Anorthosite with an approximate 14wt. %, pyroxenite 4wt. %, mesonorite 14wt% and leuconorite 11wt. % CaO on average is observed.

Table 1: Overview of major element concentrations (wt. %) in rock types and LLD (average) of Two Rivers Platinum mine underground samples and drill core, EST013, samples from the farm Eerste Geluk 327KT.

Location	Rocktype		SiO2	Al_2O_3	CaO	Cr_2O_3	Fe_2O_3	K_2O	MgO	MnO	P_2O_5	TiO_2	Na_2O
TRP	**Pyroxenite**	Average	50.96	5.48	4.14	0.64	13.56	0.02	22.57	0.09	0.01	0.09	0.05
	n=15	Min.	46.09	3.81	3.32	0.37	11.42	0.00	21.07	0.06	b.l.d	0.01	0.01
		Max.	53.96	7.36	4.81	1.38	16.62	0.15	24.55	0.23	0.05	0.28	0.71
	LLD (ppm)		Not calc.	84	26	208	20	20	102	22	14	52	266
	Brown sugar norite	Average	53.48	4.40	3.42	0.42	12.77	0.01	26.34	0.14	0.01	0.13	0.01
	n=5	Min.	51.98	3.01	2.56	0.40	11.15	0.00	24.12	0.09	0.00	0.04	0.01
		Max.	54.84	5.87	4.25	0.44	14.76	0.05	28.17	0.22	0.02	0.21	0.01
	LLD (ppm)		Not calc.	84	26	206	20	20	103	22	14	52	267
	Mottled Anorthosite	Average	48.21	31.01	15.26	0.41	1.71	0.08	0.82	0.01	0.01	0.03	1.72
	n=3	Min.	47.24	29.25	15.06	0.00	0.71	0.06	0.08	0.00	0.00	b.l.d	1.30
		Max.	49.31	32.58	15.46	1.24	3.58	0. 14	2.06	0.02	0.01	0.07	2.37
	LLD (ppm)		Not calc.	86	28	205	20	20	102	21	14	53	257
	Spotted Anorthosite		51.63	22.70	10.91	0.09	4.60	0.17	6.68	0.00	0.00	0.00	1.51
	LLD (ppm)		Not calc.	86	28	205	20	20	102	21	14	53	260
	Pegmatoidal Pyroxenite		50.32	5.54	4.25	0.33	14.05	0.00	21.25	0.09	0.00	0.04	0.01
	LLD (ppm)		Not calc.	84	27	208	20	20	102	22	14	52	266
	Spotted Anorthosite to Leuconorite		51.45	22.36	11.07	0.11	5.63	0.06	7.94	0.00	0.00	0.00	1.09
	LLD (ppm)		Not calc.	86	28	205	20	20	102	21	14	53	260
EST	**Melanorite**	Average	52.82	5.60	4.24	0.46	12.26	0.16	23.20	0.19	0.02	0.23	0.42
	n=9	Min.	50.47	3.70	3.31	0.32	11.02	0.03	21.14	0.15	0.01	0.15	0.15
		Max.	55.44	6.76	4.96	0.81	13.68	0.17	24.56	0.21	0.07	0.41	1.15
	LLD (ppm)		119	93	45	183	22	30	96	25	22	54	419
	Mesonorite	Average	49.83	24.18	13.58	0.07	4.23	0.11	5.98	0.07	0.01	0.08	1.55
	n=3	Min.	49.34	20.84	13.15	0.03	2.85	0.09	3.39	0.05	0.01	0.06	1.26
		Max.	50.28	27.57	14.29	0.11	5.50	0.13	8.31	0.10	0.01	0.09	1.73
	LLD (ppm)		117	160	74	175	20	29	92	21	22	53	415
	Foot wall Melanorite	Average	52.65	4.52	4.09	0.23	12.61	0.09	24.93	0.22	0.01	0.23	0.09
	n=9	Min.	50.52	2.25	2.64	0.15	11.85	0.04	23.03	0.20	0.01	0.18	0.00
		Max.	54.08	5.44	5.14	0.27	13.64	0.14	26.94	0.23	0.03	0.30	0.20
	LLD (ppm)		119	88	45	183	22	29	97	23	22	54	420
	Pegmatoidal Pyroxenite		53.47	4.00	3.38	0.24	13.03	0.07	25.71	0.22	0.04	0.25	0.53
	LLD (ppm)		119	86	42	184	22	28	98	24	22	54	420
	Mottled Anorthosite		48.17	29.91	15.51	0.02	1.31	0.17	1.33	0.03	0.01	0.05	2.25
	LLD (ppm)		117	176	78	174	19	30	91	21	22	53	413
	Spotted Anorhosite to Mesonorite		49.66	25.22	12.74	0.04	4.25	0.12	5.81	0.07	0.01	0.07	1.63
	LLD (ppm)		118	163	71	176	20	29	93	21	22	53	415

Table 2: Overview of certain trace element concentrations (ppm) in rock types and LLD (average) of Two Rivers Platinum mine underground samples and drill core, EST013, samples from the farm Eerste Geluk 327KT.

Location	Rocktype		Ti	V	Cr	Rb	Sr	Y	Zr	Ba	Zn	Ni	Cu	Co
TRP	**Pyroxenite**	Average	2647	134	4388	4	74	5	15	43	70	3519	1333	149
	n=14	Min	1592	99	2742	1	48	3	5	20	58	554	93	93
		Max	3418	164	9063	7	107	6	27	81	80	13881	5193	309
	LLD (ppm)		9	4	8	5	4	6	Not calc.	2	1	1	1	1
	Brown sugar norite	Average	2503	116	2954	2	55	4	10	28	73	762	289	107
	n=5	Min.	1775	103	2749	1	34	3	4	b.l.d	65	481	39	98
		Max.	4132	141	3151	7	79	7	31	63	92	1246	697	119
	LLD (ppm)		8	4	7	4	4	6	Not calc.	2	1	1	1	1
	Mottled Anorthosite	Average	447	9	96	3	439	1	3	148	0	112	58	6
	n=3	Min.	358	4	8	3	421	1	3	139	b.l.d	29	9	3
		Max.	584	17	222	3	449	2	4	154	0	262	137	12
	LLD (ppm)		12	4	8	4	3	6	Not calc.	1	1	1	1	1
	Spotted Anorthosite		1501	43	717	5	373	4	21	140	17	692	607	40
	LLD (ppm)		10	4	8	4	3	6	Not calc.	1	1	1	1	1
	Pegmatoidal Pyroxenite		2392	125	2650	3	75	5	13	46	73	3818	1969	139
	LLD (ppm)		9	4	8	5	4	6	Not calc.	2	1	1	1	1
	Spotted Anorthosite to Leuconorite		1167	49	736	2	327	3	5	128	20	878	620	48
	LLD (ppm)		10	4	8	4	3	6	Not calc.	1	1	1	1	1
EST	**Melanorite**	Average	11358	667	20137	31	335	21	76	234	327	392	3053	473
	n=9	Min.	7016	516	13175	3	203	13	31	40	279	194	2644	443
		Max.	11382	955	33903	181	452	35	178	405	380	895	4012	497
	LLD (ppm)		8	4	6	4	2	1	Not calc.	3	1	1	1	Not calc.
	Mesonorite	Average	779	51	639	3	331	2	4	139	14	182	348	33
	n=3	Min.	620	31	322	2	286	2	4	114	6	95	249	22
		Max.	935	73	970	3	370	3	4	163	20	290	458	44
	LLD (ppm)		8	4	3	1	1	1	1	3	1	1	1	Not calc.
	Foot wall Melanorite	Average	10384	552	9429	16	246	20	60	179	300	183	2982	471
	n=9	Min.	2409	137	1893	5	67	5	14	20	69	30	579	99
		Max.	14597	660	12238	27	350	28	92	345	362	626	5202	630
	LLD (ppm)		7	4	4	1	1	1	1	3	1	2	1	Not calc.
	Pegmatoidal Pyroxenite		11677	573	11065	10	256	25	54	169	341	212	3290	518
	LLD (ppm)		7	4	7	5	2	2	Not calc.	3	1	1	2	Not calc.
	Mottled Anorthosite		2782	117	835	13	1851	8	87	691	b.d.l	289	434	32
	LLD (ppm)		12	4	8	4	3	6	Not calc.	2	1	1	1	Not calc.
	Spotted Anorhosite to Mesonorite		744	37	466	3	352	1	4	130	17	124	273	32
	LLD (ppm)		8	4	3	1	1	1	1	3	1	1	1	Not calc.

a)

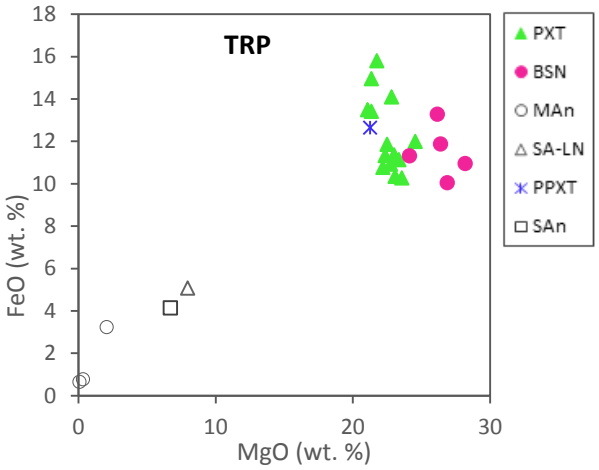
TRP
FeO (wt. %)
MgO (wt. %)
PXT
BSN
MAn
SA-LN
PPXT
SAn

b)

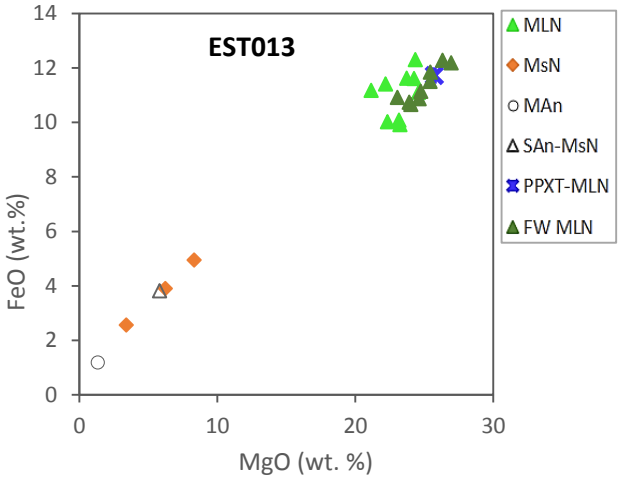
EST013
FeO (wt.%)
MgO (wt. %)
MLN
MsN
MAn
SAn-MsN
PPXT-MLN
FW MLN

c)

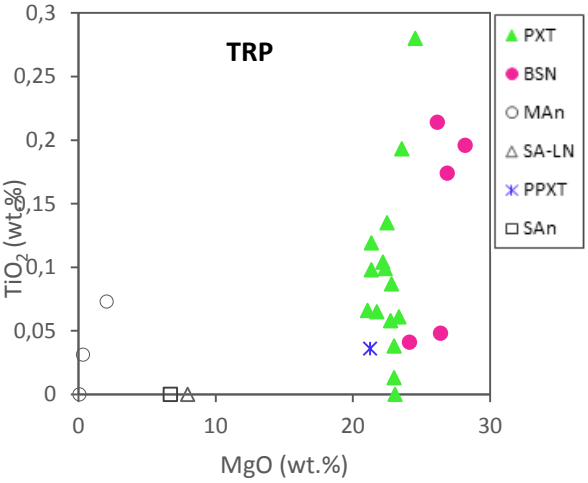
TRP
TiO2 (wt.%)
MgO (wt.%)
PXT
BSN
MAn
SA-LN
PPXT
SAn

d)

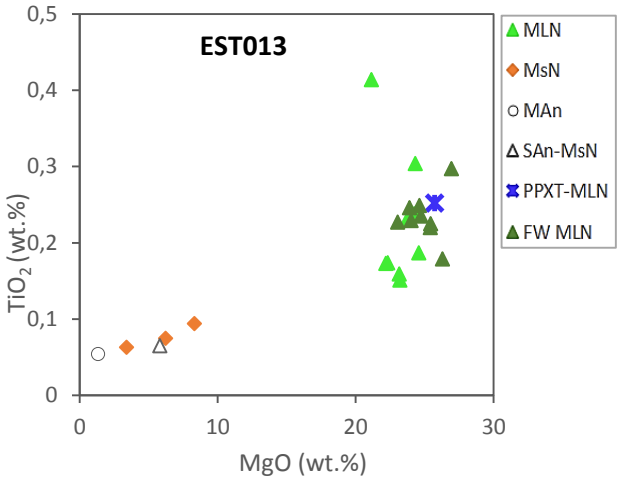
EST013
TiO2 (wt.%)
MgO (wt.%)
MLN
MsN
MAn
SAn-MsN
PPXT-MLN
FW MLN

e)

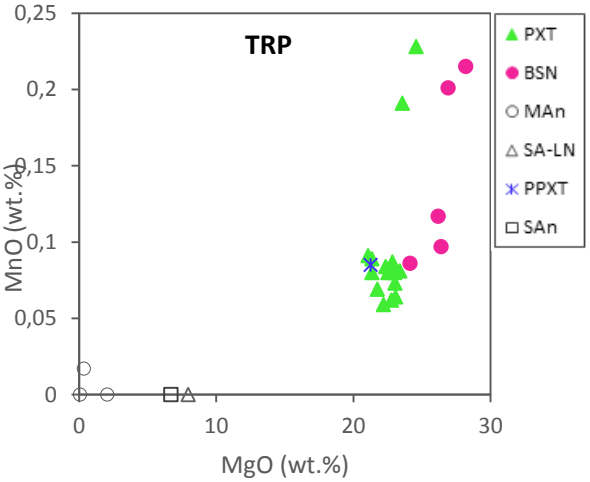
TRP
MnO (wt.%)
MgO (wt.%)
PXT
BSN
MAn
SA-LN
PPXT
SAn

f)

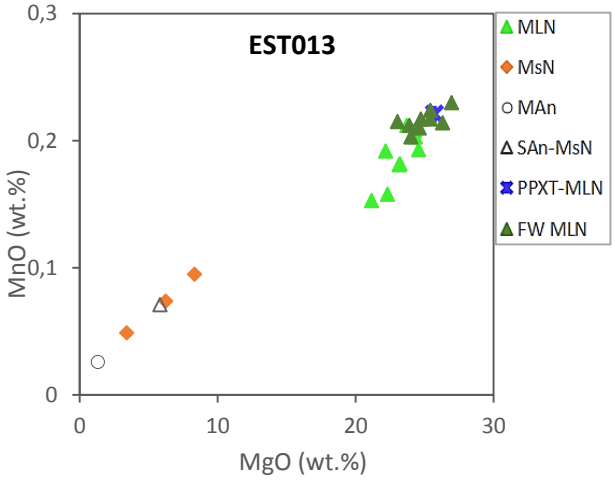
EST013
MnO (wt.%)
MgO (wt.%)
MLN
MsN
MAn
SAn-MsN
PPXT-MLN
FW MLN

g)

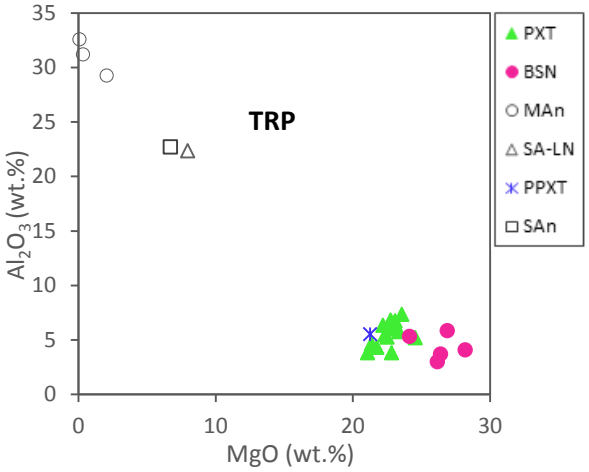
TRP
PXT
BSN
MAn
SA-LN
PPXT
SAn
Al2O3 (wt.%)
MgO (wt.%)

h)

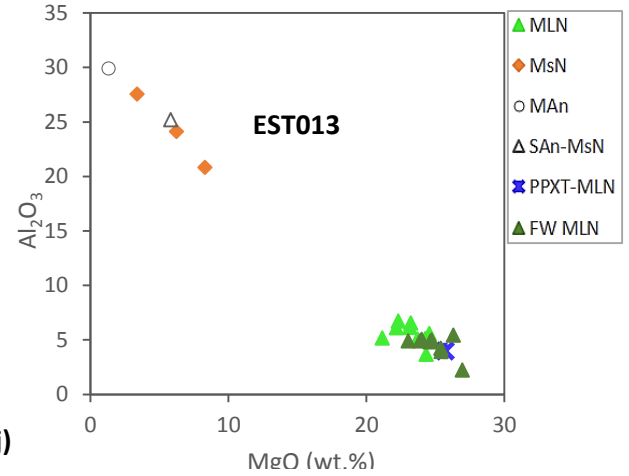
EST013
MLN
MsN
MAn
SAn-MsN
PPXT-MLN
FW MLN
Al2O3
MgO (wt.%)

i)

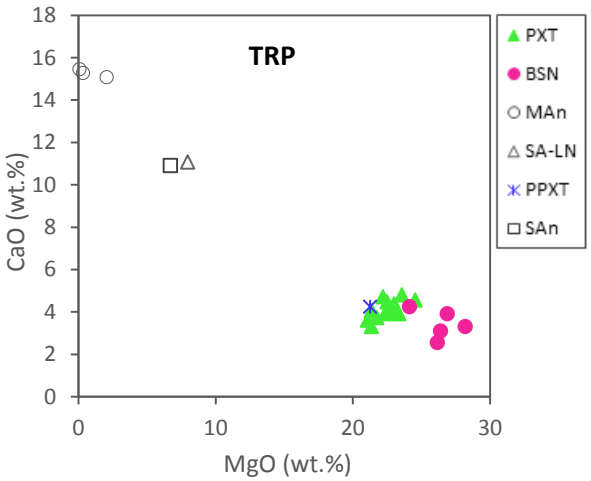
TRP
PXT
BSN
MAn
SA-LN
PPXT
SAn
CaO (wt.%)
MgO (wt.%)

j)

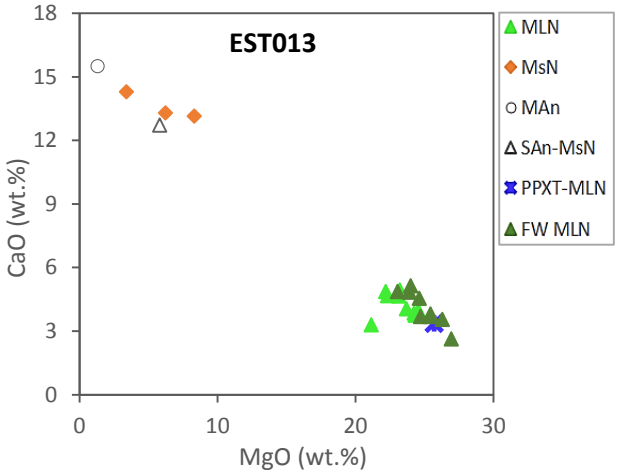
EST013
MLN
MsN
MAn
SAn-MsN
PPXT-MLN
FW MLN
CaO (wt.%)
MgO (wt.%)

k)

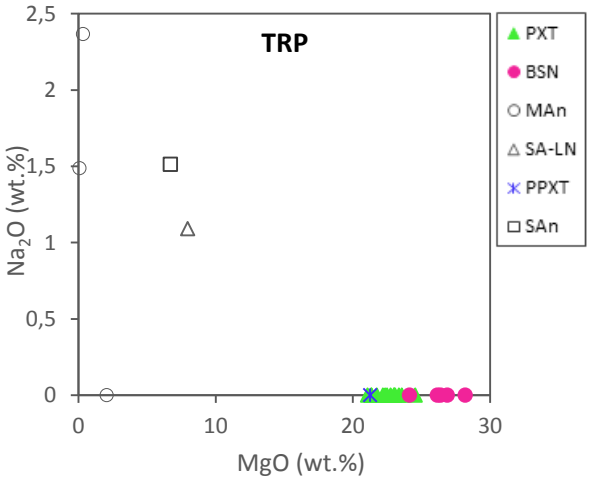
TRP
PXT
BSN
MAn
SA-LN
PPXT
SAn
Na2O (wt.%)
MgO (wt.%)

l)

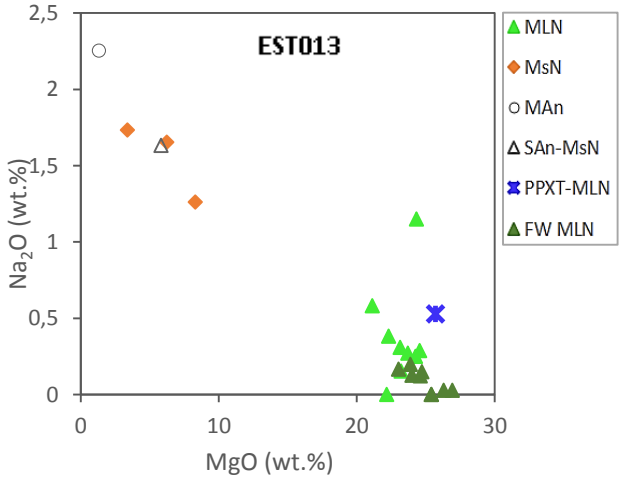
EST013
MLN
MsN
MAn
SAn-MsN
PPXT-MLN
FW MLN
Na2O (wt.%)
MgO (wt.%)

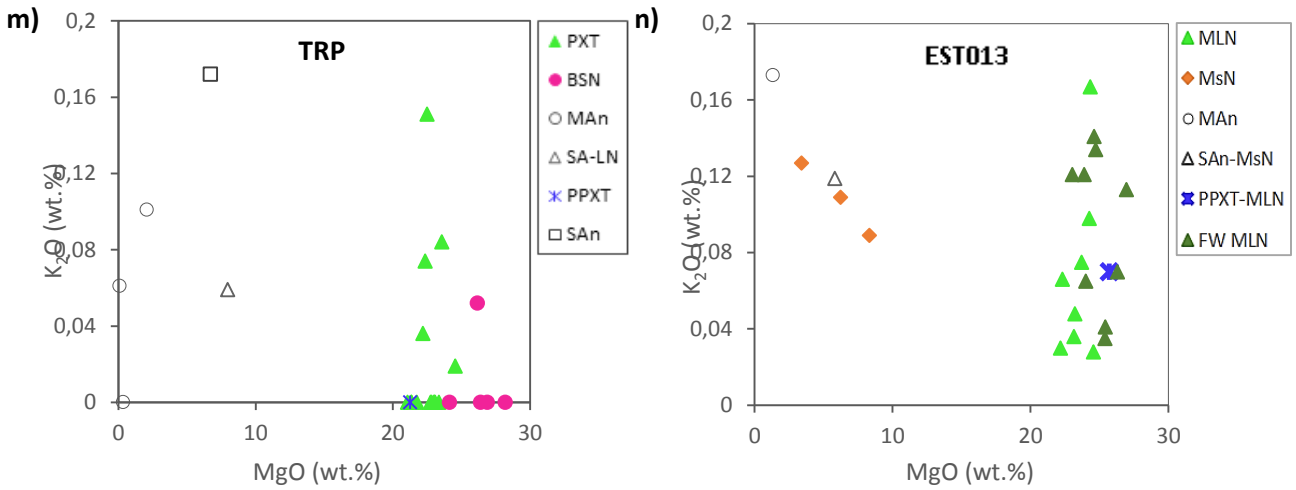

Figure 25: Harker diagrams of major element oxides FeO, TiO_2, MnO, Al_2O_3, CaO, Na_2O and K_2O plotted against MgO for underground TRP samples and Eerste Geluk drill core samples

3.3 Trace elements

Trace element ratios are good indicators of magmatic conditions as processes such as fractionation, magma differentiation or magma replenishment are usually reflected by the presence or absence of trace elements within different rock types. The abundance of trace elements is largely controlled by the different minerals present in the rock because of the partitioning of the elements into these minerals. Trace elements such as Cr, V and Zn are compatible in silicate phases such as orthopyroxene and particularly into chromite whereas Rb, which partitions into biotite/phlogopite, Y and Zr are incompatible in the major silicate and oxide phases. Cr/V is an indication of fractionation and is controlled by the early stage Cr-partitioning into chromite and V into late stage magnetite. A positive correlation is observed for Cr/V plotted against Mg# as seen in figures 26a) and b) where pyroxenite has a higher Cr/V content than the other rock types. A negative trend can be distinguished for Zr/Y when plotted against Mg # for anorthosite in figure 26c) and mesonorite in figure 26d). The pyroxenite (and anorthosite to a certain extend) at TRP shows variable Zr/Y (figure 26c) pointing to a mixture of source magmas whereas at EST the Zr/Y ratio for all rock types are very homogeneous (figure 26d). Ti/Zr displays positive trends in the different rock types when plotted against Mg# as seen in figures 26e) and f). At TRP the pyroxenite and BSN display highly variable Ti/Zr ratio (figure 26e) and at EST similarly both melanorite and mesonorite display variable Ti/Zr ratio indicating a different magma lineage. Relatively high Ti/Zr ratios are observed for BSN in figure 26e). In figures 26g) and h) positive trends are observed for Rb/Zr versus Mg# for pyroxenite and BSN whereas a negative trend is observed for anorthosite and mesonorite. The highest values of Rb/Zr are found in the anorthosite at TRP (average of 0.740 Rb/Zr) due to the concentration of plagioclase. As seen in figure 26g the Rb/Zr ratio is mostly

homogenous in all rock types at TRP whereas at EST (figure 26 g) the Rb/Zr ratio is variable in all rock types indicating a different magma lineage.

Linear relationships are observed for most major and trace elements against MgO and Mg# respectively. These results correspond to those of Maier (1991) who suggested that the linear relationships show possible repeated injections of magma during the deposition of the rocks.

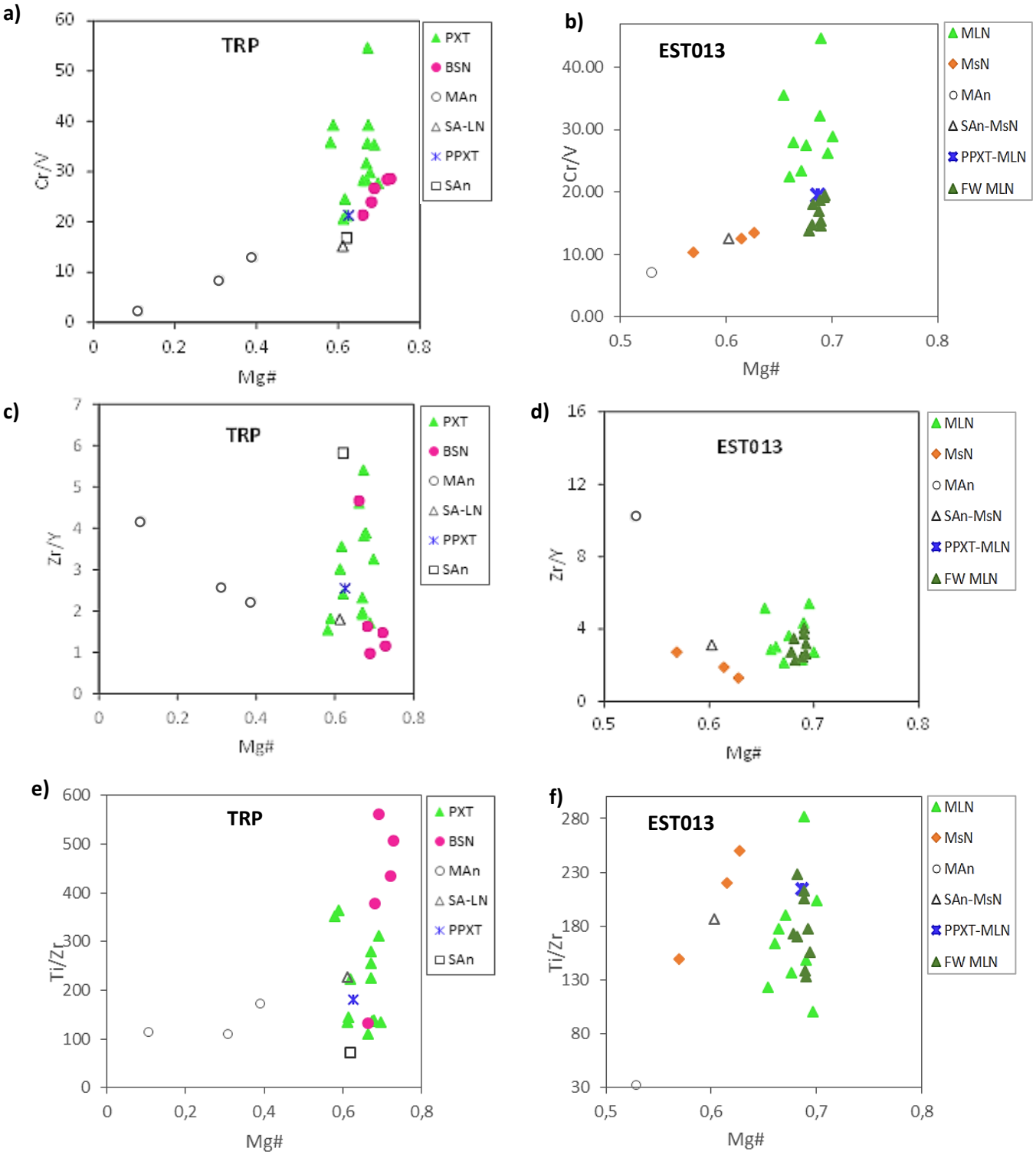

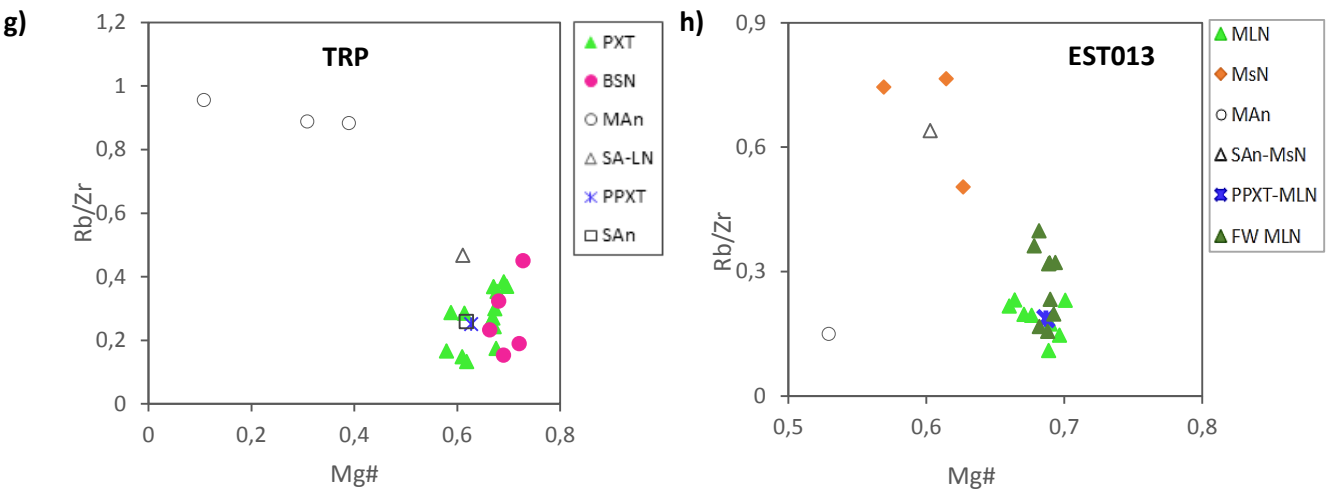

Figure 26: Harker diagrams of trace element concentration ratios Cr/V, Zr/Y, Ti/Zr and Rb/Zr for TRP underground samples (figures a, c, e and g) and EST drill core (figures b, d, f and h) of MR profile in ppm.

Trace element and trace element ratios of rocks against stratigraphic height is used as a test for multiple injection of magma and post cumulus migration of residual magma (Cawthorn & McCarthy, 1985). Mg# [MgO/ (MgO+FeO)], which is influenced by the presence of chromium, is used to indicate magma fractionation. Due to the fact that orthopyroxene is the only (dominant) mafic phase present in these rocks, it can be assumed that Mg# versus height of the whole rock would mirror the changes in orthopyroxene through this interval (Cawthorn, 1996). Variations in Mg# and Cr# are largely attributed to the varying ratio of plagioclase to orthopyroxene in the different rock types. In the stratigraphic profiles of Mg# in figure 27a) and c) a negative trend is distinguished as the Mg# decreases with an increase in height due to change to more feldspar-rich rocks. In close proximity to the chromitite stringers the Mg# increases and may be due to the incorporation of Mg into chromite and exchange of Mg and Fe in the orthopyroxene. The opposite is true for Cr content (wt. %) where an increase in Cr wt. % with an increase in height is observed (figure 27b and d) especially in the chromite rich lithologies. Chromium has a high compatibility in orthopyroxene. MR pyroxenite has a higher Cr wt. % than BSN and chromite occur disseminated in anorthosites near chromitite stringer at TRP therefore #Cr increases with height. *Note that BSN in statigraphic figures (figures 27 to 31) for TRP where BSN lenses are presented as a vertical sequence in order from the HW at the top to lower pyroxenite of the MR the BSN is not necessarily a stacked unit nor are they layers. The BSN lenses occur within the HW and MR pyroxenite as seen in figure 65 and are presented in the stratigraphic figure as a vertical sequence for visualization and betterunderstanding of geochemical variation with height.*

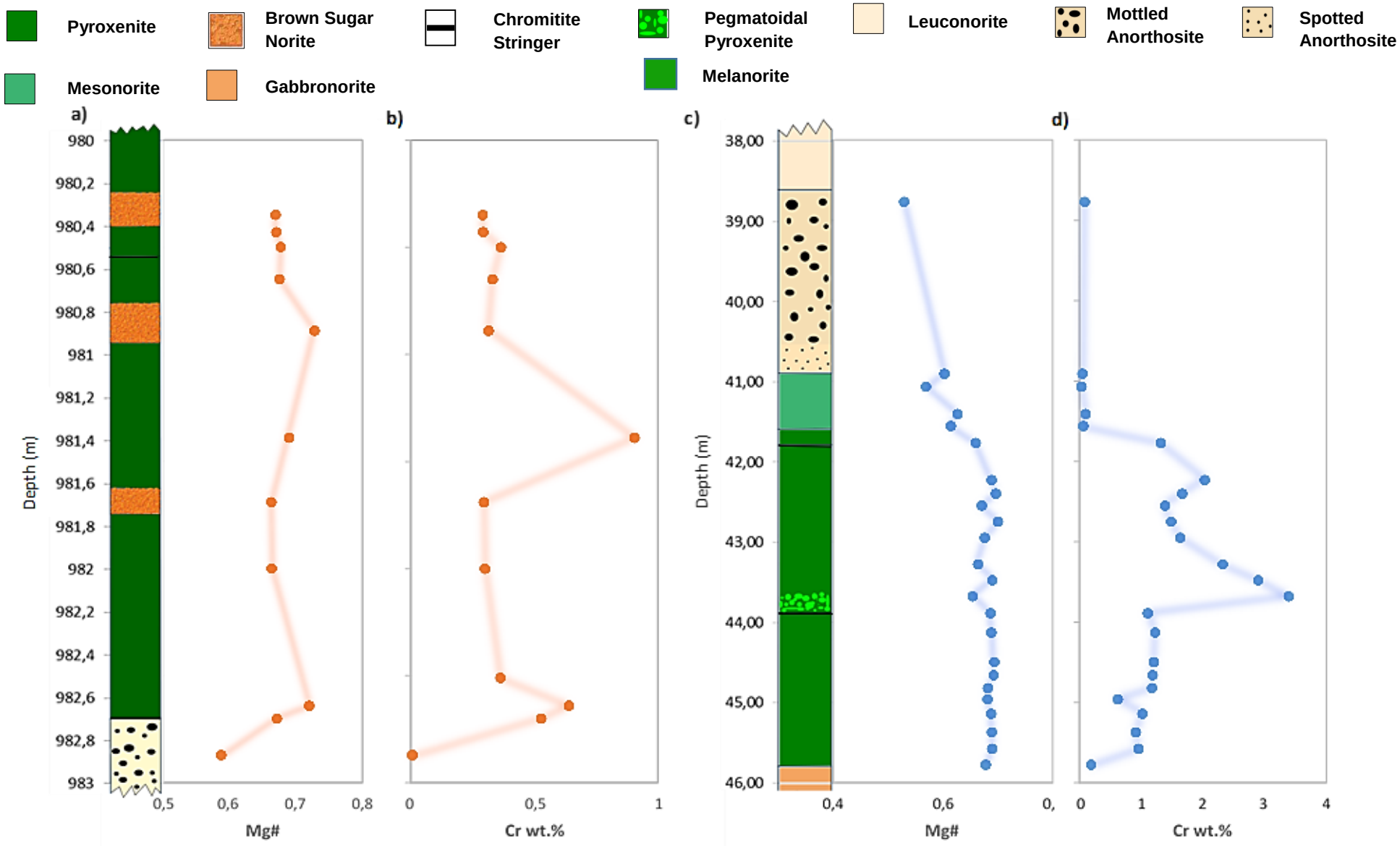

Figure 27: Variation in Mg# and Cr wt. % with stratigraphic height respectively in TRP (a and b) and in Eerste Geluk (c and d)

Trace element ratios are useful as it enables one to identify fractionation of two trace elements aiding in the determination of possible magma replenishment or different magma lineages. A “zigzag” pattern is observed for trace element ratios against stratigraphic height as concentration varies with elevation (figures 28 and 29). Different magma pulses and/or magma fractionation may have been responsible for this pattern. The incompatible trace elements plotted against stratigraphic height also reflect the presence of variable amounts of interstitial liquid during rock formation.

It can be seen in figures 28 to 31 and table 2 that the compatibility of trace element ratios in the various rock types differs. As mentioned earlier, elements such as Cr, V and Zn are more compatible in silicate phases such as orthopyroxene as well as in oxides such as chromite, hence concentration of these trace elements are higher in the pyroxenite than in the hanging wall or footwall anorthosite where it is more depleted, as seen more clearly in figure 29a), Eerste Geluk samples. The Cr/V trace element ratio shows the enrichment of Cr over V. Cr is mostly concentrated in chromite. Cr/V content in pyroxenite and melanorite samples at TRP and EST respectively changes with stratigraphic height due to the varying amount of chromite crystals present throughout the profile (see figure 28 and 29). Trace element concentrations are therefore greatly influenced by the modal proportions of the various minerals present. Chromitite stringers were not analysed (not enough sample material).

Sr has a high partitioning coefficient for plagioclase as it substitutes easily for Ca and K because of its ionic radius (1.18Å) (Maier, 1991). Rock units with a dominant plagioclase phase therefore have a higher Sr concentration average as seen in anorthosite and mesonorite (Table 1 and 2).

The elements Rb, Zr, Y, and Nb are a function of fractionation processes in part but predominantly a reflection of the proportion of intercumulus minerals representing trapped residual liquid (Maier, 1991). A spike in these elements as observed for Rb and Zr in close proximity to the bottom chromitite stringer (figure 31 a and b). Higher Rb and Zr (spikes) in the interstitial liquid may have resulted from accumulation of incompatible elements in a low fraction of evolved liquid during batch crystallization. It thus indicates the presence of evolved trapped liquid which is residual after batch crystallization of a pool of magma. Cumulus minerals have low Zr concentration due to the insignificant partitioning of Zr into the cumulates. The element is thus concentrated in the intercumulus liquid (Maier, 1991). The highest concentrations of Zr and Rb are found in the pyroxenite. The TRP pyroxenite samples have an average of about 4 ppm Rb and 15 ppm Zr, whereas a much higher concentration of 31 ppm Rb and 76 ppm Zr on average is observed for melanorite of the EST drill core (see table2).

Relatively high concentrations of immobile trace element ratios such as Zr/Y would reflect the presence of liquid phases or crustal contamination during the crystallization of minerals.

The elements Cu, Ni, Co and Zn partition into sulphides. As noted by Seabrook (2005) because elements such as Ni are compatible in orthopyroxenes they are a less reliable measure for sulphide content; however Cu is a more reliable measure of the sulphide present in the various rock types. An increase in Cu concentrations in figure 31 a) and b) would thus indicate sulphide enrichment. At EST it can be seen that the MR melanorite interval is significantly enriched in Zr, V, Sr, Rb, Ba, Ni, Cu, Cr, Co and Zn (figures 30 b and 31 b) relative to TRP (figures 30a and 31a). As mentioned previously, Rb and Zr represent trapped liquid and the significant increase of these elements in the MR melanorite at EST therefore indicates higher amounts of trapped liquid at EST. The Zn, Cu, and Ni enrichment reflects increased concentration of sulphides within the pyroxene interval relative to the adjacent felsic hanging wall and foot wall at EST. Co partitions preferentially into sulphides as well as spinel and olivine (Rajamani & Naldrett, 1978). In early magmatic processes Co substitutes for Fe and Mg which are similar in charge and ionic radius, Co is generally enriched in mafic rocks relative to felsic igneous rocks. Co therefore preferentially substitutes for Mg in olivine and orthopyroxene and its high concentrations depends on the modal proportion of olivine and orthopyroxene (Gauert, 1998). However, because pentlandite is the second most abundant sulphide present in the analysed pyroxenites the significant Co enrichment reflects the presence of pentlandite. Increase in Co also correlates to increase in Ni and Cu (figure 31 a & b). The Co enrichment is therefore correlated to sulphides rather than to mafic minerals only.

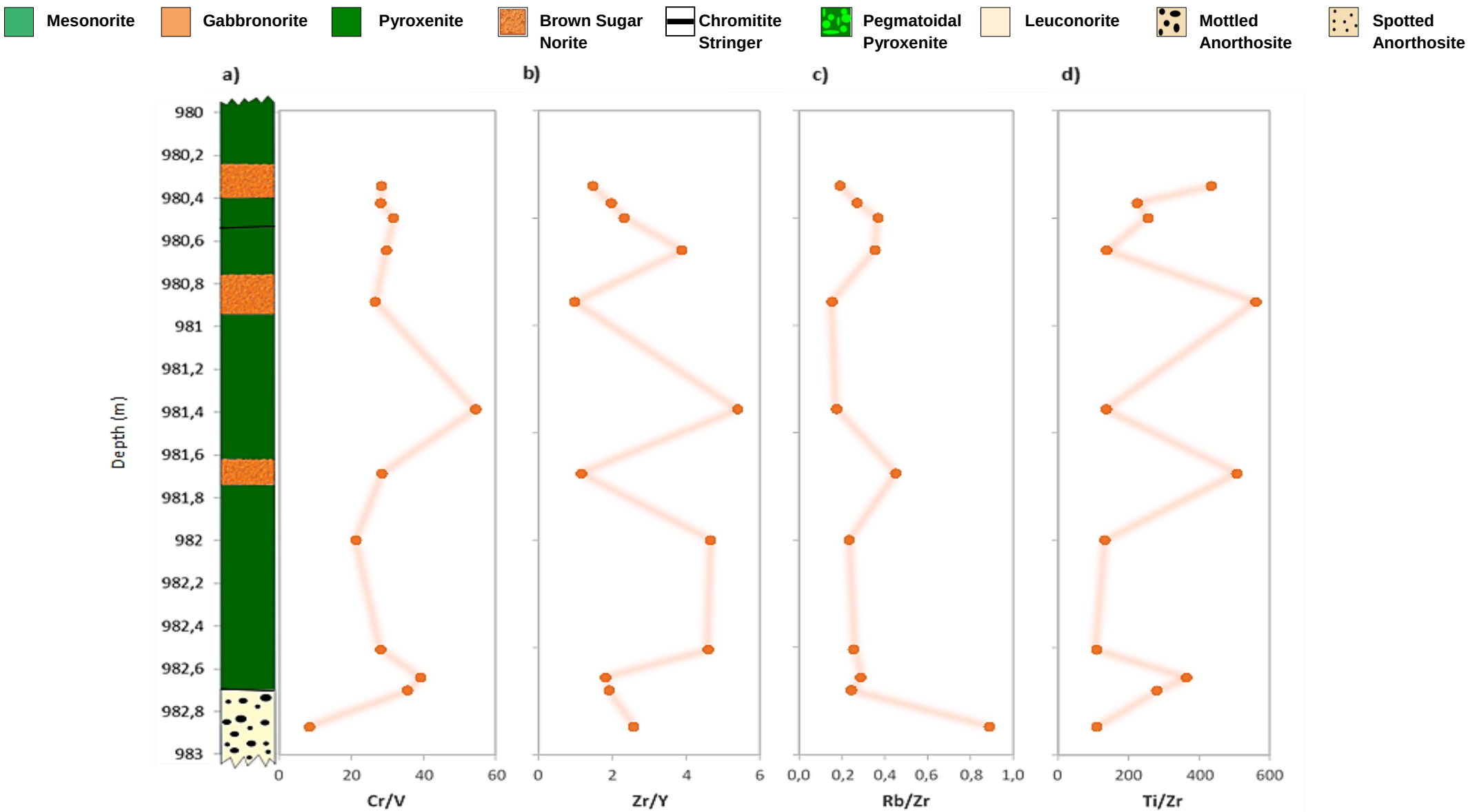

Figure 28: Variation of trace element ratios Cr/V, Zr/Y, Rb/Zr and Ti/Zr wt. % in rock types with stratigraphic height at TRP.

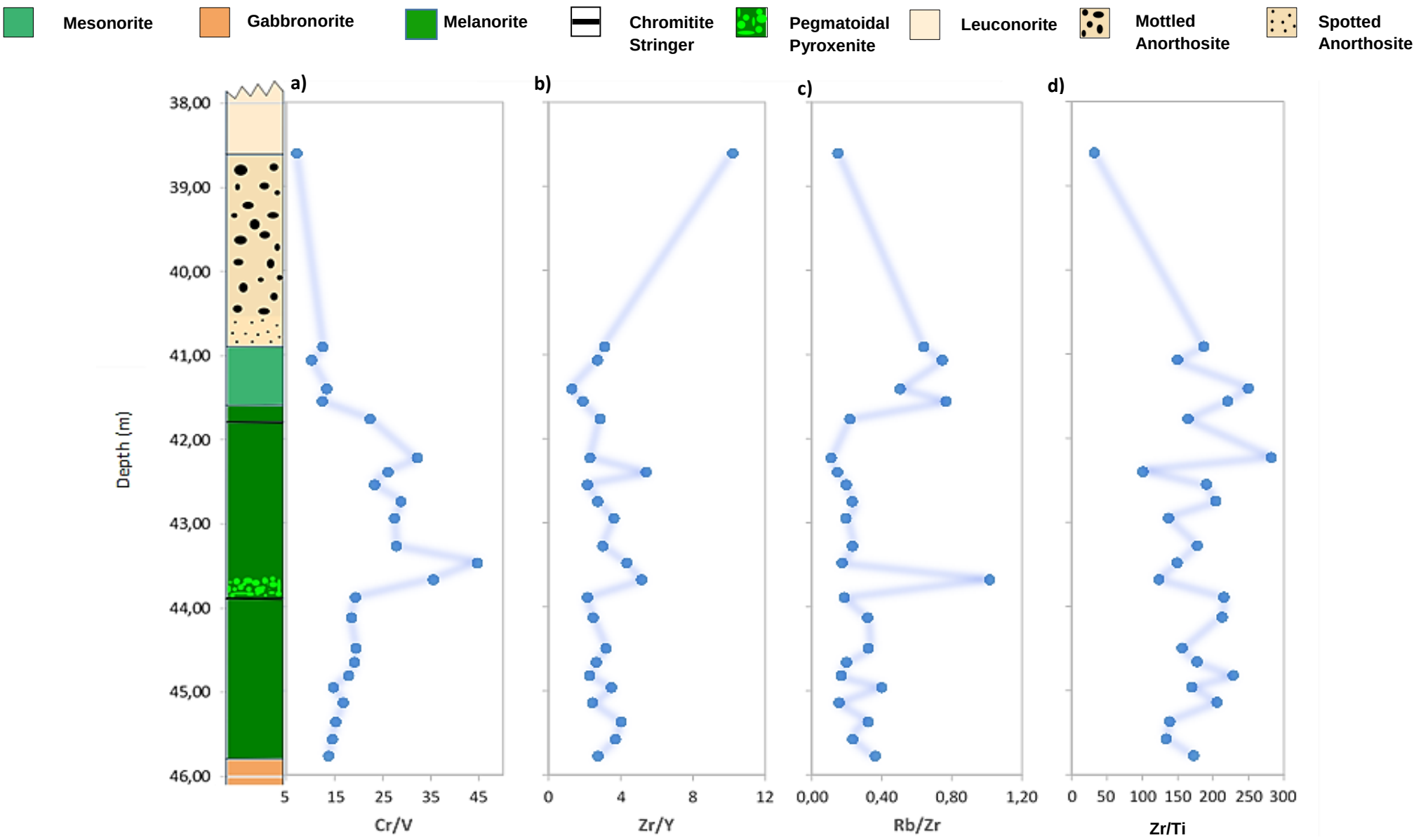

Figure 29: Variation of trace element ratios Cr/V, Zr/Y, Rb/Zr and Ti/Zr wt. % in rock types with stratigraphic height at Eerste Geluk.

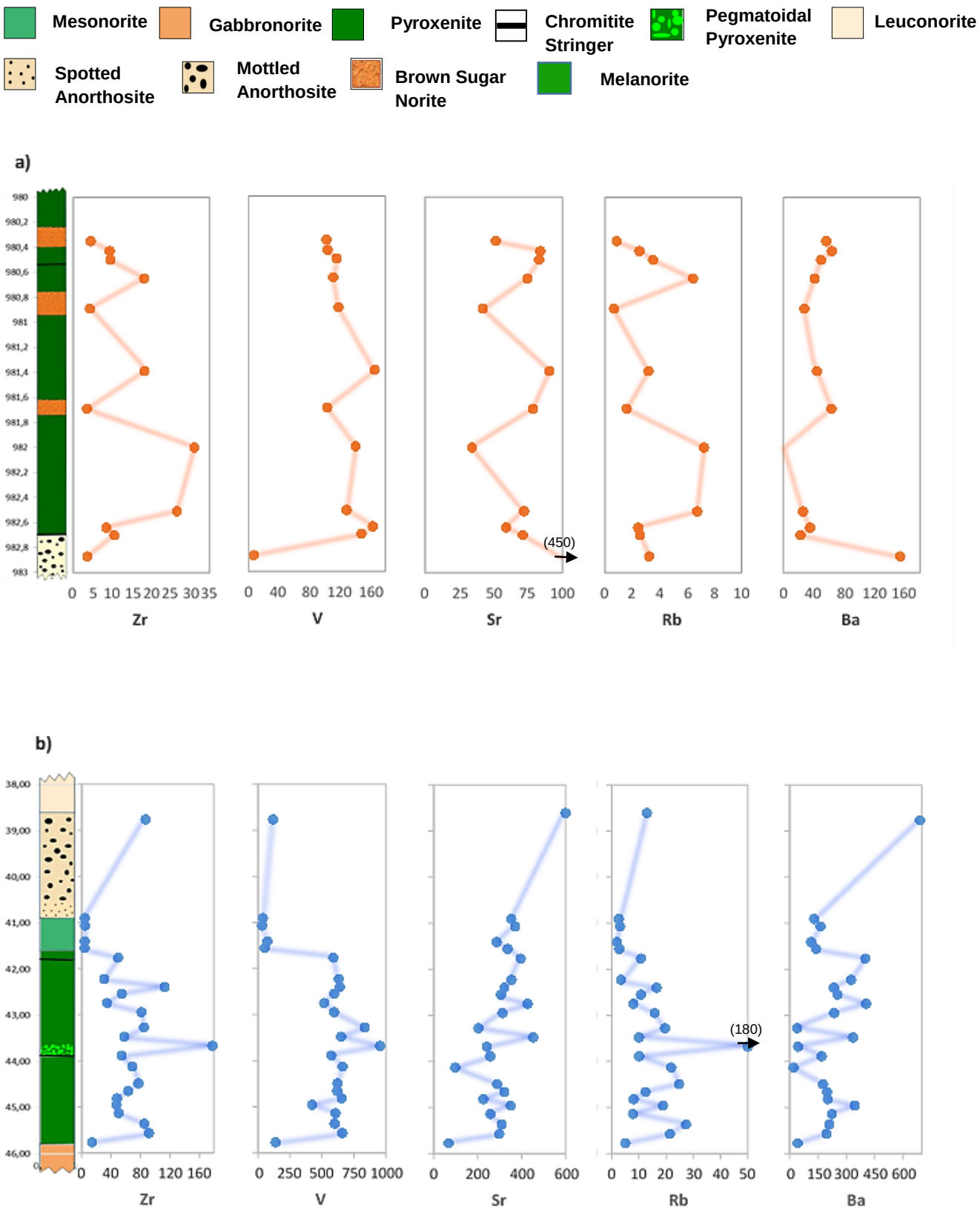

Figure 30: Trace element concentrations plotted against stratigraphic height for a) underground samples of the MR at TRP and b) drill core EST013 samples of the farm Eerste Geluk.

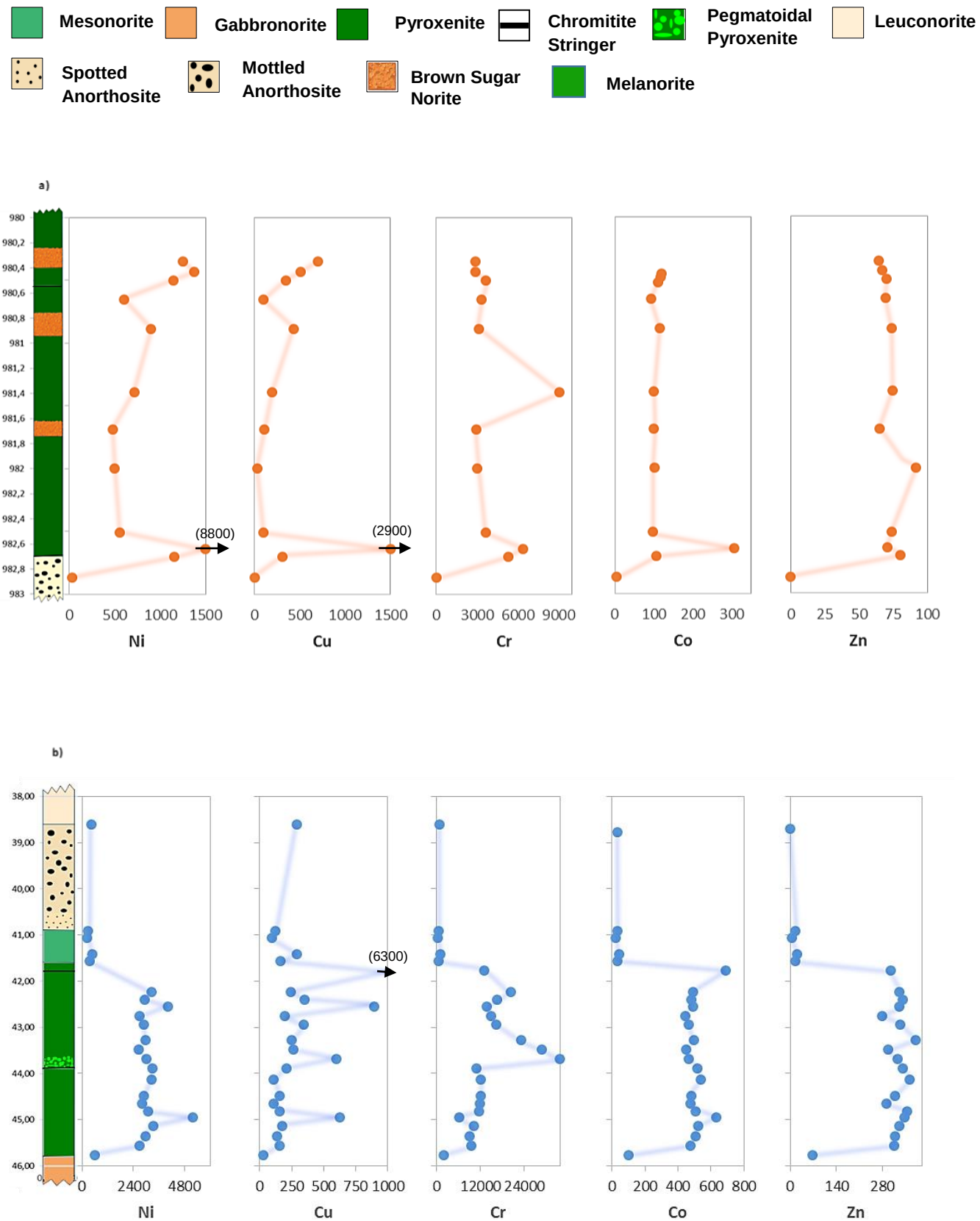

Figure 31: Trace element concentrations plotted against stratigraphic height for a) underground samples of the MR at TRP and b) drill core EST013 samples of the farm Eerste Geluk.

Chapter 4: Mineral and Isotope Chemistry

This chapter characterises the mineral chemistry of orthopyroxene, clinopyroxene and plagioclase as well as chromite and sulphides found within the rock types associated with the MR at TRP. These rock types are mainly pyroxenite and anorthosite along with the erratic occurrence of BSN from underground samples taken at TRP. The mineral chemistry of EST013 drill core samples of farm Eerste Geluk 327 north of the Steelpoort fault have also been documented. EPMA and SEM-EDX/WDX analyses have been carried out on these samples and their compositions are displayed in this chapter. The motivation behind these analyses is to locate cryptic variation indicating fractional crystallization, replenishment or retainment processes. An overview of EPMA and SEM data in appendices A3-1 to A3-10 for silicates, oxides and BMS are given in tables 3,4,5,7 and 8.

4.1 Orthopyroxene and Clinopyroxene

Table 3: An overview of mineral compositions of orthopyroxene in the various rock types at TRP and EST. *TRP_PXT= TRP MR pyroxenite, TRP_PPXT= TRP pegmatoidal pyroxenite, TRP_BSN= TRP_ brown sugar norite, TRP272_PXT= pyroxenite from the borehole TRP272, EST_MsN= EST mesonorite and EST_MLN=EST MR melanorite. B.d.l= below detection limit*

		Orthopyroxene										
Rocktype		**SiO_2**	**CaO**	**K_2O**	**MgO**	**Al_2O_3**	**FeO**	**MnO**	**TiO_2**	**Na_2O**	**$Cr2O_3$**	**Total**
TRP_PXT	Average	54.78	1.24	0.02	28.6	1.23	12.47	0.09	0.07	0.02	0.42	98.94
per 6 oxygens	Cations	1.97	0.05	0.00	1.53	0.05	0.38	0.00	0.00	0.00	0.01	4.00
n=52	Std	1.16	0.79	0.04	1.62	0.44	1.59	0.11	0.17	0.02	0.13	
	Max	58.84	3.67	0.29	33.89	3.89	15.36	0.34	1.12	0.13	0.86	
	Min	50.19	0.26	b.d.l	23.79	0.69	8.1	b.d.l	b.d.l	b.d.l	0.14	
TRP_PPXT	Average	54.88	1.27	0.01	27.7	0.95	13.79	0.27	0.22	0.01	0.4	99.50
per 6 oxygens	Cations	1.98	0.05	0.00	1.49	0.04	0.42	0.01	0.01	0.00	0.01	3.99
n=7	Std	0.31	1.5	0.02	1.25	0.31	0.73	0.06	0.08	0.02	0.11	
	Max	55.43	4.67	0.04	28.57	1.51	14.49	0.34	0.35	0.04	0.54	
	Min	54.53	0.62	b.d.l	25.00	0.55	12.23	0.18	0.1	b.d.l	0.23	
TRP_BSN	Average	55.48	0.82	0.02	29.7	1.09	12.17	0.14	0.1	0.02	0.48	100.02
per 6 oxygens	Cations	1.97	0.03	0.00	1.57	0.05	0.36	0.00	0.00	0.00	0.01	4.00
n=69	Std	0.81	0.37	0.06	0.94	0.24	0.93	0.11	0.1	0.03	0.11	
	Max	59.16	2.09	0.45	31.71	1.48	14.64	0.34	0.31	0.22	0.66	
	Min	53.77	0.06	b.d.l	24.92	0.13	9.51	b.d.l	b.d.l	b.d.l	0.01	
TRP272_PXT	Average	54.71	0.78	0.02	25.85	0.97	14.93	0.05	0.02	0.02	0.25	97.60
per 6 oxygens	Cations	2.01	0.03	0.00	1.41	0.04	0.46	0.00	0.00	0.00	0.01	3.97
n=16	Std	1.36	0.52	0.01	1.43	0.25	2.08	0.02	0.01	0.03	0.12	
	Max	57.94	2.06	0.04	29.1	1.52	19.26	0.09	0.04	0.11	0.49	
	Min	53.43	0.32	b.d.l	25.33	0.68	12.4	0.02	b.d.l	b.d.l	b.d.l	
EST_MsN	Average	56.11	1.28	0.03	27.32	0.98	15.06	0.05	0.01	0.02	0.31	101.17
per 6 oxygens	Cations	1.99	0.05	0.00	1.44	0.04	0.45	0.00	0.00	0.00	0.01	3.99
n=11	Std	0.89	1.29	0.07	0.67	0.13	0.78	0.03	0.01	0.02	0.05	
	Max	58.81	4.94	0.27	28.1	1.17	16.16	0.08	0.03	0.06	0.4	
	Min	55.39	0.37	b.d.l	25.6	0.69	13.12	b.d.l	0,00	b.d.l	0.2	
EST_MLN	Average	55.66	1.22	0.01	29.88	0.98	13.29	0.26	0.19	0.01	0.36	101.86
per 6 oxygens	Cations	1.95	0.05	0.00	1.56	0.04	0.39	0.01	0.01	0.00	0.01	4.02
n=43	Std	0.58	1.17	0.01	1.05	0.33	0.97	0.05	0.06	0.03	0.12	
	Max	56.5	6.17	0.04	31.52	1.76	14.65	0.36	0.3	0.17	0.57	
	Min	54.39	0.43	b.d.l	25.82	0.37	10.86	0.15	0.05	b.d.l	0.12	

Table 4: An overview of mineral compositions of clinopyroxene in the various rock types at TRP and EST. *TRP_PXT= TRP MR pyroxenite, TRP_PPXT= TRP pegmatoidal pyroxenite, TRP_BSN= TRP brown sugar norite, TRP272_PXT= pyroxenite from the borehole TRP272, EST_MsN= EST mesonorite and EST_MLN=EST MR melanorite. B.d.l= below detection limit*

		Clinopyroxene										
Rocktype		**SiO_2**	**CaO**	**K_2O**	**MgO**	**Al_2O_3**	**FeO**	**MnO**	**TiO_2**	**Na_2O**	**$Cr2O_3$**	**Total**
TRP_PXT	Average	52.96	22.62	0.01	15.5	1.65	4.61	0.05	0.23	0.24	0.75	98.62
per 6 oxygens	Cations	1.97	0.90	0.00	0.86	0.07	0.14	0.00	0.01	0.02	0.02	3.99
n=19	Std	0.44	1.20	0.01	0.63	0.49	0.73	0.04	0.21	0.16	0.37	
	Max	53.56	24.41	0.02	16.33	2.82	5.96	0.14	0.59	0.42	1.31	
	Min	52.29	20.23	b.d.l	14.25	1.01	3.09	b.d.l	b.d.l	b.d.l	b.d.l	
TRP_PPXT	Average	52.71	21.48	b.d.l	15.53	1.75	5.09	0.13	0.49	0.33	0.75	98.26
per 6 oxygens	Cations	1.96	0.86		0.86	0.08	0.16	0.00	0.01	0.02	0.02	3.98
n=6	Std	0.56	0.30	not calc	0.48	0.49	0.35	0.04	0.10	0.07	0.16	
	Max	53.56	22.01	b.d.l	15.96	2.52	5.57	0.18	0.61	0.46	0.86	
	Min	51.9	21.18	b.d.l	14.91	1,00	4.67	0.05	0.33	0.28	0.44	
TRP_BSN	Average	53.37	22.21	0.01	16.19	1.57	4.16	0.1	0.3	0.37	0.87	99.15
per 6 oxygens	Cations	1.97	0.88	0.00	0.89	0.07	0.13	0.00	0.01	0.03	0.03	3.99
n=43	Std	0.71	1.24	0.02	0.81	0.32	0.73	0.06	0.18	0.06	0.12	
	Max	54.79	23.84	0.14	20.24	2.44	11.35	0.21	0.63	0.5	1.02	
	Min	52.19	15.04	b.d.l	15.12	0.73	3.06	b.d.l	b.d.l	0.28	0.52	
TRP272_PXT	Average	52.86	22.43	0.05	14.73	2.27	5.24	0.15	0.41	0.08	0.63	98.85
per 6 oxygens	Cations	1.96	0.89	0.00	0.81	0.10	0.16	0.00	0.01	0.01	0.02	3.97
n=7	Std	1.16	4.62	0.13	1.30	2.12	1.15	0.16	0.19	0.21	0.28	
	Max	50.38	12.07	0.34	17.5	7.04	7.79	0.01	0.08	0.55	1.03	
	Min	52.6	22.83	b.d.l	13.64	0.98	4.42	b.d.l	0.27	b.d.l	0.23	
EST_MsN	Average	54.55	23.62	0.02	15.86	1.25	4.87	0.04	0.04	0.27	0.34	100.86
per 6 oxygens	Cations	1.98	0.92	0.00	0.86	0.05	0.15	0.00	0.00	0.02	0.01	3.99
n=5	Std	0.44	0.34	0.01	0.32	0.26	0.29	0.03	0.01	0.03	0.08	
	Max	55.17	23.94	0.03	16.28	1.51	5.29	0.07	0.06	0.31	0.45	
	Min	53.96	23.12	0.01	15.45	0.86	4.51	b.d.l	0.02	0.24	0.23	
EST_MLN	Average	53.5	21.6	b.d.l	16.87	1.62	4.7	0.13	0.4	0.36	0.69	99.87
per 6 oxygens	Cations	1.96	0.85		0.92	0.07	0.14	0.00	0.01	0.03	0.02	4.00
n=28	Std	0.91	1.89	0.03	1.37	0.34	0.35	0.03	0.14	0.09	0.22	
	Max	57.68	22.57	0.07	23.55	2.21	5.23	0.2	0.63	0.49	1.08	
	Min	52.53	12.12	b.d.l	15.97	0.82	3.8	0.05	0.11	0.12	0.12	

In table 3 it can be seen that the major element composition of orthopyroxene in the various rock types at TRP and EST do not show significant variation. FeO content in Opx at EST, however, are relatively higher with averages of 15,1% in EST mesonorite and 13.3% in EST melanorite compared to the average 12,5% and 12,2% FeO in TRP pyroxenite and BSN respectively. A maximum of 19.3% and an average of 14.9% FeO are observed for Opx in the pyroxenite of borehole TRP272. The average compositions of major elements in clinopyroxene of the different rock types at both TRP and EST are fairly similar (table 4). Clinopyroxene in EST mesonorite which has an average of 23.6% CaO is slightly more enriched in CaO than in the EST melanorite (average 21.6%).

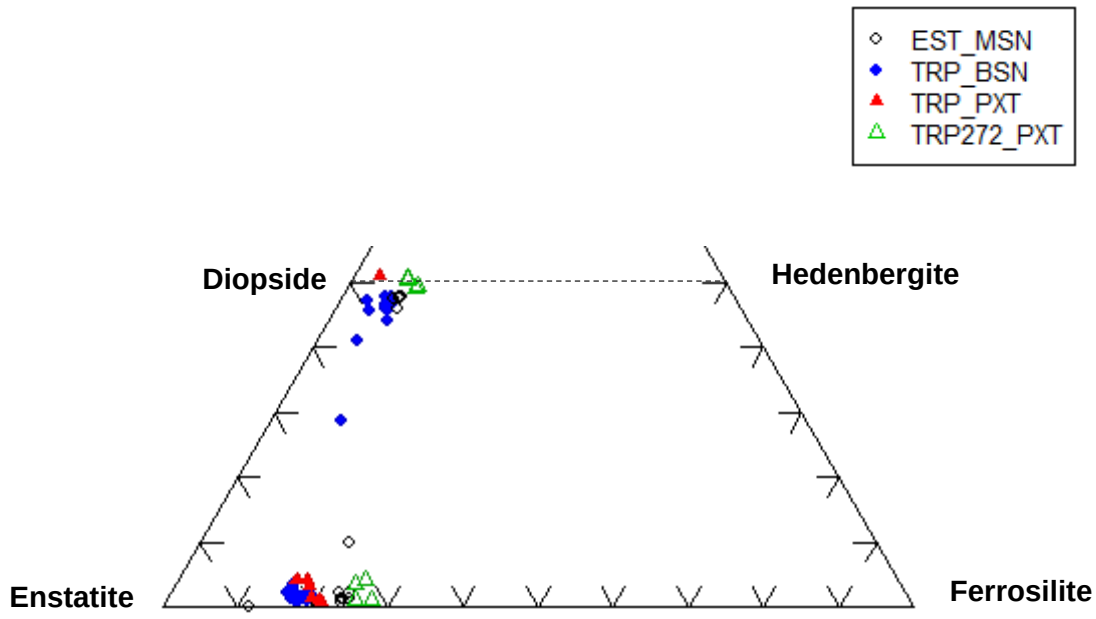

Figure 32: Ternary diagram of Opx and Cpx crystals within the HW rock units of the TRP MR underground samples (where BSN is present in profile) and the HW drill core samples of EST013 MR.

Figure 32 illustrates the difference in composition of Opx and Cpx crystals found within the HW rock units of the TRP MR as well as that of the EST013. These crystals are medium to fine crystalline. The Opx data plot within the enstatite field, however the various compositions cluster together so that three distinct trends or groups can be observed. An overview of end member compositions as calculated by NORM is given in appendices A3-2 and A3-4. Opx crystals of the TRP HW pyroxenite have a compositional range of En_{78-80} whereas the overlying BSN Opx crystals have a slightly higher composition of $En_{80-82.}$ The EST013 HW Opx has a much lower En composition of $En_{70-76,}$ except for the two outliers, one with a composition of En_{88} where the Fe content of the Opx is relatively low and the other outlier a composition of En_{70} where the Opx has a relatively higher Ca content of 4% (figure 32). The small rounded as well as the Opx crystals with Ca exsolution lamella appear to have a slightly higher En content than the surrounding Opx. Further north from where underground samples were taken borehole TRP 272's Opx within in the pyroxenite have the lowest En content ranging between En_{71} and En_{74}.

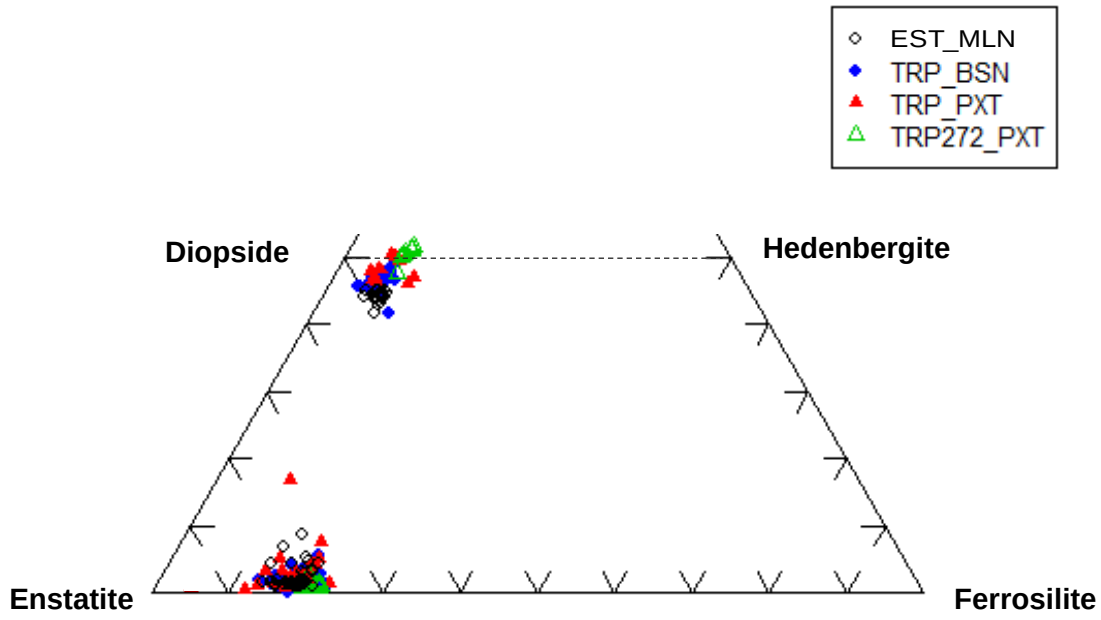

Figure 33: Ternary diagram for Opx and Cpx, representing the composition of Opx within the pyroxenite of the MR of TRP as well as the MR melanorite of EST013 found north of the Steelpoort Fault (farm Eerste Geluk).

In the enstatite field within figure 33 an overlap of orthopyroxene composition is seen. The %En of Opx crystals within the TRP MR pyroxenite ranges from En_{74-88} with the pyroxenite near the top chromitite stringer having higher %En (En_{79-83}) while the pyroxenite near the bottom stringer have relatively lower %En (En_{76-79}). The anomalous En_{95} Opx crystal has a Fe content of less than 3% and a low total composition, therefore disregarded. The BSN lenses within the MR pyroxenite display slightly similar En values as that of the surrounding pyroxenite (En_{76-85}) where Opx crystals from the BSN lense in the upper pyroxenite have a higher En content (En_{81-85}) compared to the lower range of %En (En_{76-83}) of the BSN in the pyroxenite above the bottom chromitite stringer. %En of orthopyroxenes adjacent to the chromitite stringers (figure 17 A) or enclosed within the chromite crystals have higher En content (reaching up to En_{89}) compared to Opx found in pyroxenite at a greater distance from the chromitite stringers. The relatively high En content of orthopyroxene near the chromitite stringer may be attributed to the effect of re-equilibration during the cooling of orthopyroxene and chromite. The composition of the EST013 MR pyroxenite ranges from En_{76-85} hence the overlap of Opx data.

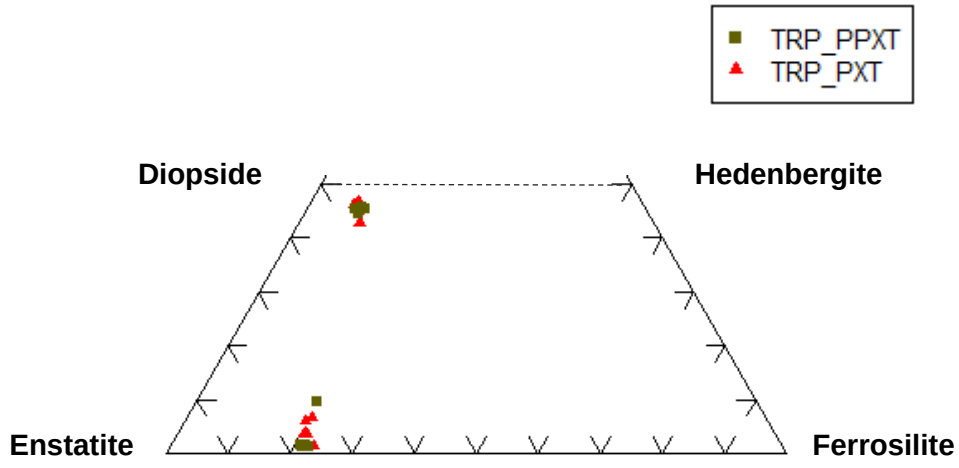

Figure 34: Ternary plot displaying the composition of Opx and Cpx of MR pegmatoidal pyroxenite and the adjacent MR pyroxenite at TRP.

The Opx crystals within the pegmatoidal pyroxenite may be larger than those found within the normal pyroxenite but display similar mineral chemistry as Opx crystals in the normal pyroxenite found in close proximity to the bottom chromitite stringer. As seen in figure 34, the Opx data plots within the enstatite field at concentrations similar to that found in the rest of the MR pyroxenite. The composition of the pegmatoidal Opx crystals has a minimum of En_{71} and a maximum of En_{78}.

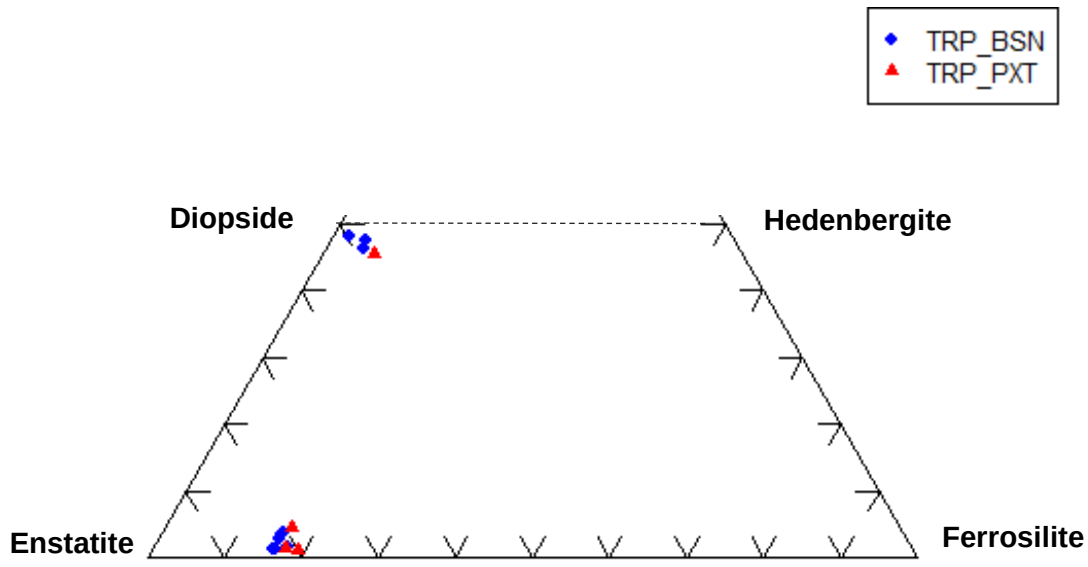

Figure 35: Ternary diagram for Opx and Cpx where there is a sharp change from MR pyroxenite to BSN at one of the MR underground exposures.

The BSN does not only occur as lenses within the pyroxenite, in one of the MR underground exposures where BSN is present, the BSN is found as a thick layer (approximately 1m thick) in sharp contact with underlying pyroxenite (N1G line 5) which is a rare occurrence. Figure 35

illustrates that the Opx compositions in the BSN are slightly higher than the composition of Opx crystals in the pyroxenite. BSN has an average Opx composition of En_{82} and the MR pyroxenite an average of $En_{80.}$

Figure 36a shows the En content plotted against stratigraphic height for the MR and the BSN profile. It can be seen that the En content decreases with an increase of height. The Opx compositional variation trend in MR pyroxenite in this study corresponds with Opx compositional variations in MR by various authors (Cawthorn, 1996; Eales and Cawthorn, 1996; Eales, 2001; Naldrett et al., 2008; Rose, 2010). This En in Opx trend displays normal fractionation which is likely for the MR where a high En content is observed adjacent to the footwall which decreases with increasing height. The Opx from pyroxenite near the top chromitite stringer has an average of En_{81} and the pyroxenite near the bottom chromitite stringer an average of En_{79}. The difference in composition of BSN and pyroxenite at the different heights results in a 'saw-tooth' pattern. Higher En content in Opx crystals in pyroxenite in the upper and lower extremes of the MR is associated with the presence of the chromitite stringers.

MnO concentrations in Opx of both the pyroxenite and BSN vary makes it difficult to positively identify a trend (figure 36b). The normal trend of MnO in Opx of the MR is a decrease with an increase in stratigraphic height. Though this trend has been observed in TRP drill core in other studies (such as Rose, 2010, Giebel, 2013) it is not the case where BSN is present in the MR profile. An opposite trend however is observed because the MnO content of Opx is higher in the upper parts of the MR profile compared to the bottom.

Al_2O_3 in Opx is relatively low in the MR rock units (figure 36c). A decrease in of Al_2O_3 in Opx is seen with an increase in height however two peaks or "jumps" occur in this trend where there is a sudden increase in Al_2O_3 content; one in the lower BSN lense, and the other in the pyroxenite below the top chromitite stringer. Opx in the hanging wall pyroxenite and BSN have an average Al_2O_3 content of 1.12% and 1.23% respectively. The average Al_2O_3 content in the MR pyroxenite is 1.20% while the BSN lenses occurring in this pyroxenite have an average of 1.08%.

Opx within both the pyroxenite as well as the BSN contain very little TiO_2 with concentrations of less than 0.1 % (figure 36d). The hanging wall pyroxenite and BSN as well as the BSN below the top chromitite stringer have the highest TiO_2 concentration of more than 0.02% on average. There is a consecutive increase and decrease of TiO_2 with increase in elevation resulting in a "saw tooth" pattern. The variation in TiO_2 content of Opx depicts fractionation of magma.

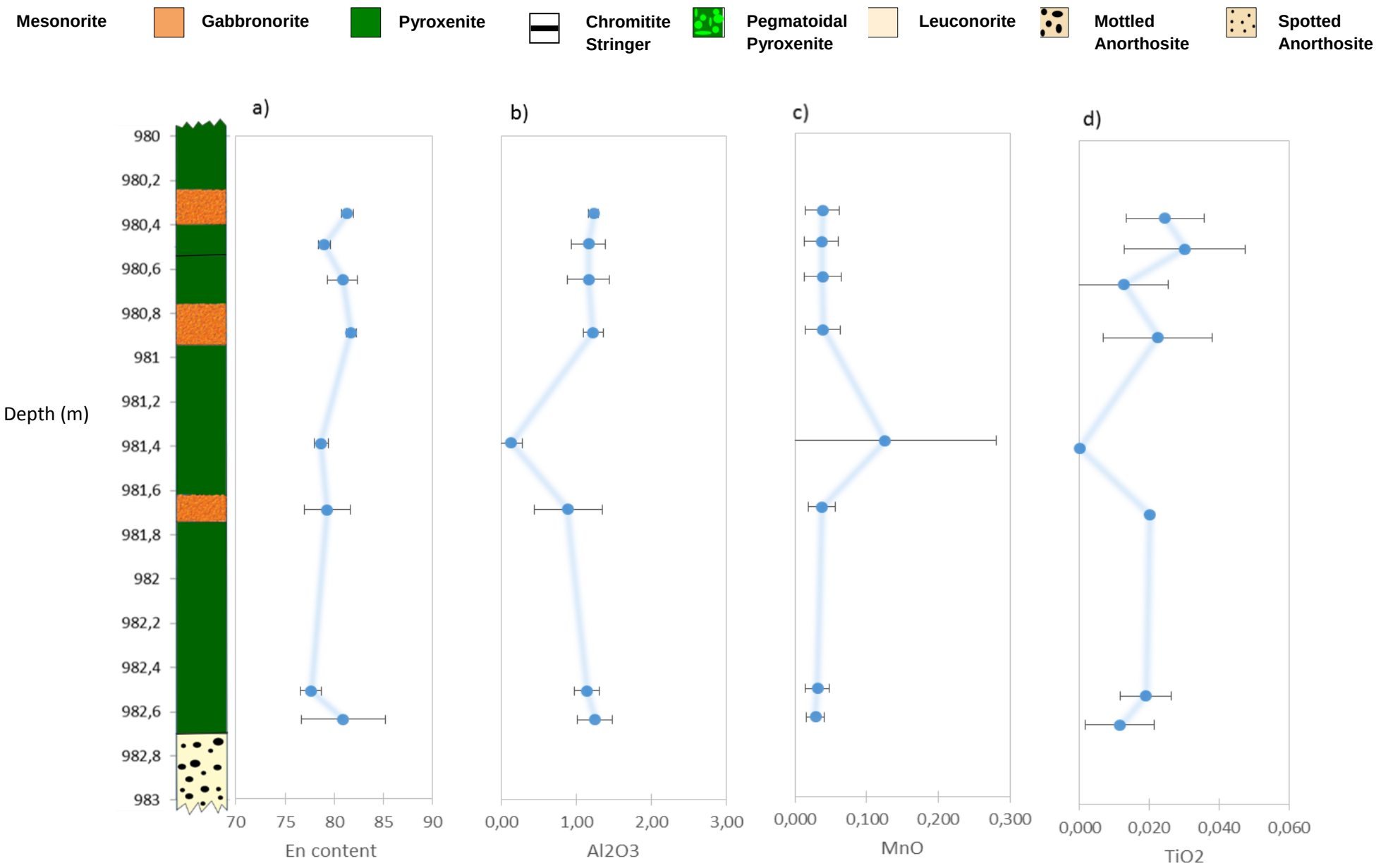

Figure 36: Vertical variation of the average and standard deviation of a) En content b) MnO, c) Al_2O_3, and d) TiO_2 in orthopyroxene found in underground samples of MR pyroxenite and BSN at TRP plotted against stratigraphic height.

The composition of Cpx within the rock types associated with the MR is plotted along with Opx in ternary diagrams, as seen in figures 32 to 35. Cpx is not as dominant as Opx within the samples. Cpx occur mostly as discontinuous rims around or as exsolved lamella from Opx crystals. In the HW (see figure 32), as with Opx, Cpx can be delineated into groups. The Cpx composition plots within the diopside and augite fields. HW MR pyroxenite and BSN have an average %Wo of 44% and 48% respectively. The HW mesonorite of EST013 has an average %Wo composition an average of 47%. Cpx compositions of the MR pyroxenite in both TRP and EST overlap within the augite field making it difficult to define Cpx trends of the various rock types (figure 33). Cpx from the MR pyroxenite contains between Wo_{46} and Wo_{50} and between Wo_{42} and Wo_{49} has been recorded for BSN. The EST MR melanorite has Cpx with a lower %Wo ranging between Wo_{42} and Wo_{45}. Cpx at TRP-272 MR pyroxenite reaches up to Wo_{49} with an average of Wo_{51} which is significantly higher than what is found in the other rock types. Cpx compositions of TRP MR pyroxenite adjacent to pegmatoidal pyroxenite are similar with an average of Wo_{45} each.

4.2 Plagioclase

Table 5: An overview of mineral compositions of plagioclase in the various rock types at TRP and EST. *TRP_PXT= TRP MR pyroxenite, TRP_PPXT= TRP pegmatoidal pyroxenite, TRP_BSN= TRP brown sugar norite, TRP272_PXT= pyroxenite from the borehole TRP272, EST_MsN= EST mesonorite and EST_PXF=EST MR melanorite. B.d.l= below detection limit*

		Plagioclase										
Rocktype		**SiO_2**	**CaO**	**K_2O**	**MgO**	**Al_2O_3**	**FeO**	**MnO**	**TiO_2**	**Na_2O**	**$Cr2O_3$**	**Total**
TRP_PXT	Average	50.22	14.32	0.09	0.02	31.23	0.11	b.d.l	0.01	3.8	0.02	99.82
per 8 oxygens	Cations	2.30	0.70	0.01	0.00	1.68	0.00		0.00	0.34	0.00	5.03
n=46	Std	2.64	1.92	0.09	0.04	1.76	0.15	0.01	0.01	1.15	0.06	
	Max	57.66	18.04	0.38	0.24	36.07	0.71	0.06	0.08	6.57	0.3	
	Min	44.85	8.94	b.d.l	b.d.l	27.19	0,00	0,00	0,00	1.03	b.d.l	
TRP_PPXT	Average	51.22	13.42	0.21	0.05	30.95	0.31	0.03	0.03	3.51	b.d.l	99.73
per 8 oxygens	Cations	2.33	0.66	0.01	0.00	1.66	0.01	0.00	0.00	0.31		4.99
n=6	Std	0.79	0.53	0.05	0.11	0.58	0.13	0.03	0.05	0.29	b.d.l	
	Max	52.37	14.03	0.26	0.27	31.91	0.55	0.06	0.13	3.83	0.01	
	Min	50.06	12.63	0.11	b.d.l	30.09	0.17	b.d.l	b.d.l	3.06	b.d.l	
TRP_BSN	Average	50.77	13.77	0.08	0.01	31.26	0.3	0.01	0.01	3.6	0.01	99.82
per 8 oxygens	Cations	2.32	0.67	0.00	0.00	1.68	0.01	0.00	0.00	0.32	0.00	5.01
n=52	Std	1.72	0.9	0.08	0.03	1.66	0.52	0.02	0.02	0.58	0.02	
	Max	54.18	16.02	0.24	0.18	33.86	3.91	0.09	0.08	4.68	0.09	
	Min	46.94	12.16	b.d.l	b.d.l	28.06	b.d.l	b.d.l	b.d.l	2.26	b.d.l	
TRP272_PXT	Average	50.94	13.65	0.07	0.01	31.54	0.15	0.01	b.d.l	3.91	0.01	100.29
per 8 oxygens	Cations	2.31	0.66	0.00	0.00	1.69	0.01	0.00	0.00	0.34	0.00	5.02
n=9	Std	3.52	2.83	0.03	0.01	2.36	0.04	0.01	0.01	1.7	0.01	
	Max	56.26	15.7	0.1	0.02	33.45	0.22	0.03	0.01	6.32	0.03	
	Min	48.05	9.59	0.02	b.d.l	28.18	0.11	b.d.l	b.d.l	2.68	b.d.l	
EST_MsN	Average	48.46	15.75	0.13	0.01	33.26	0.2	0.01	0.01	2.64	0.01	100.48
per 8 oxygens	Cations	2.21	0.77	0.01	0.00	1.79	0.01	0.00	0.00	0.23	0.00	5.02
n=20	Std	0.39	0.34	0.03	0.01	0.26	0.08	0.01	0.01	0.17	0.01	
	Max	49.26	16.51	0.18	0.03	33.64	0.32	0.03	0.02	2.93	0.04	
	Min	47.7	15.08	0.08	b.d.l	32.67	0,00	0,00	0,00	2.29	b.d.l	
EST_MLN	Average	52.13	13.15	0.13	0.05	30.79	0.19	0.01	0.04	3.95	0.02	100.46
per 8 oxygens	Cations	2.36	0.64	0.01	0.00	1.64	0.01	0.00	0.00	0.35	0.00	5.00
n=27	Std	3.87	2.83	0.09	0.07	2.37	0.07	0.02	0.04	1.76	0.02	
	Max	60.93	18.61	0.26	0.2	35.37	0.34	0.06	0.11	8.02	0.07	
	Min	44.3	6.64	b.d.l	b.d.l	25.1	0.07	b.d.l	b.d.l	0.57	b.d.l	

In table 5 no significant differences in major element composition of plagioclase in the various rock types at TRP and EST are observed. The plagioclase in EST mesonorite appears to be more enriched in CaO relative to the other rock types and has an average of 15.8 wt.%.

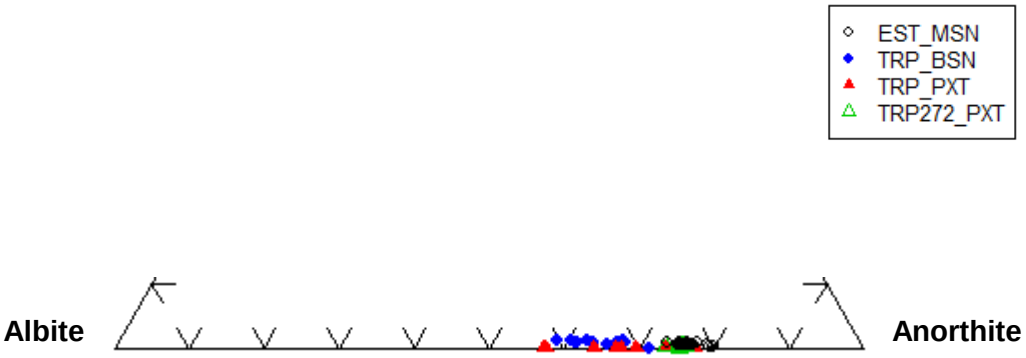

Figure 37: Ternary diagram illustrating the composition of interstitial plagioclase present in the HW of a MR profile at TRP where BSN is present compared to the plagioclase composition of HW rocks of EST013.

Interstitial plagioclase is the dominant plagioclase phase present in most of the samples. An overview of plagioclase end members of the different rock types as calculated by NORM is given in appendix A3-6. Plagioclase composition of HW units plot in different fields, as seen in figure 37. The plagioclase composition of BSN lenses in the HW plots in the labradorite field with compositions ranging from An_{59} to An_{71} with an average of $An_{71.}$ The %An in plagioclase of the TRP hanging wall pyroxenite vary between An_{57} and An_{78} and an average of An_{68} whereas in TRP-272 pyroxenite the plagioclase composition vary between An_{73} and An_{76} . The plagioclase composition of HW mesonorite of EST013 plots within the bytownite field ranging from An_{73} to $An_{80.}$ Plagioclase from HW mesonorite of the EST013 borehole therefore has the highest An composition in plagioclase.

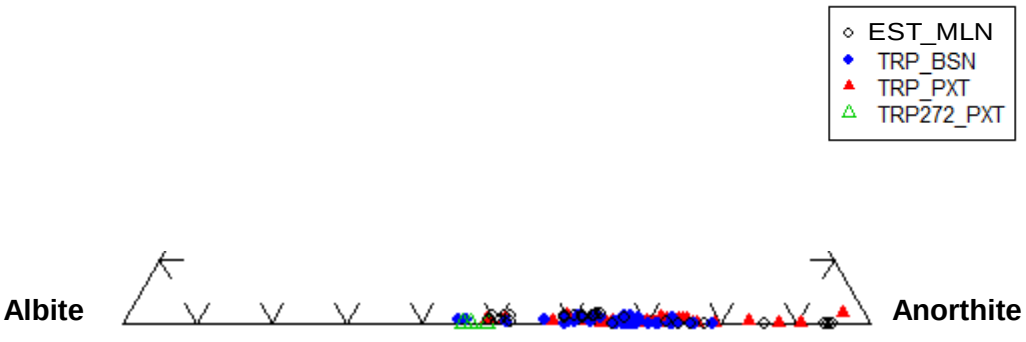

Figure 38: Ternary diagram of plagioclase compositions found within pyroxenite and BSN of MR at TRP, and that found in EST013 MR.

Figure 38 displays a large variation in the composition of plagioclase within MR pyroxenite in both TRP and EST013. The compositions plot in the field andesine, labradorite and bytownite. The plagioclase in the TRP MR pyroxenite has an average composition of An_{68} with a minimum

of An_{48} and a maximum of An_{88}. The BSN have a composition varying between An_{45} and An_{79} with an average of $An_{66.}$ MR pyroxenite of EST013 has plagioclase compositions between An_{49} and $An_{86.}$ Plagioclase enclosed within other minerals such as orthopyroxene (figure 15D) or chromite (figure 17D to F) is significantly enriched in An. These high An content may be attributed to primitive plagioclase that was rapidly enclosed in other mineral hosts such as orthopyroxene and chromite. It therefore could not react with the liquid during crystallization and cooling of the melt. The An content of enclosed plagioclase vary between $An_{75\text{-}89}$ compared to interstitial plagioclase which has an An content of about 67%.

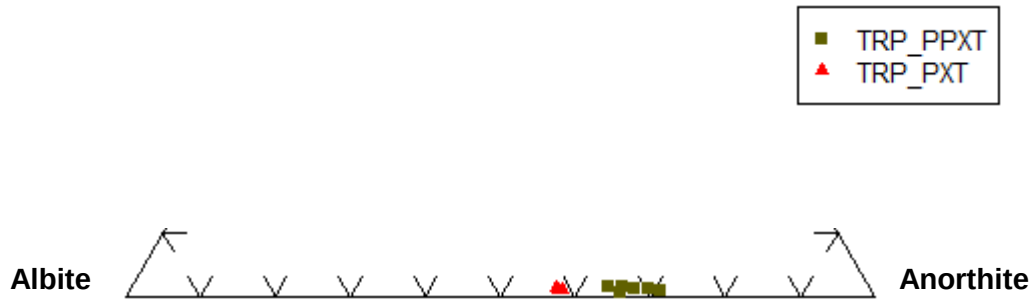

Figure 39: Ternary diagram representing the difference in composition of plagioclase found in pyroxenite in contact with pegmatoidal pyroxenite found near the lower chromitite stringer.

The composition of plagioclase found within the MR pyroxenite and pegmatoidal pyroxenite in close proximity to the basal chromitite stringer does not overlap as seen in figure 39. Plagioclase composition of the pegmatoidal pyroxenite plots largely in the labradorite field with an An content of between An_{64} and An_{71}. The composition of plagioclase in the MR pyroxenite also plot in the labradorite field but does however have a relatively lower percentage of An with an average of An_{57} and a maximum of An_{58}.

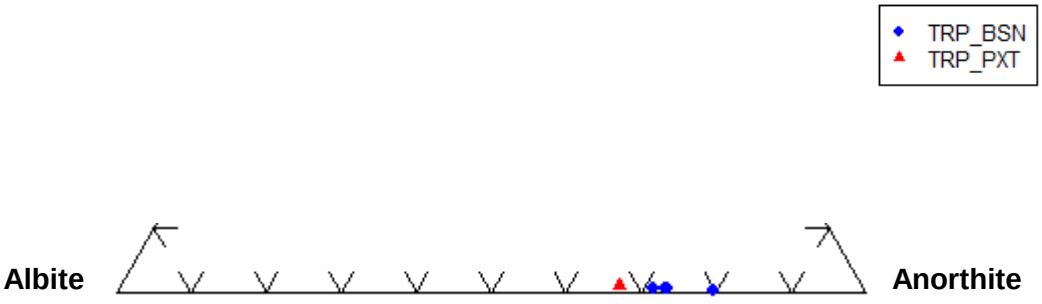

Figure 40: Ternary diagram for plagioclase compositions where there is a sharp change from pyroxenite to BSN at one of the MR profiles

It can be seen that the plagioclase composition of brown sugar norite and pyroxenite overlap. Plagioclase compositions plot within the labradorite and bytownite for both rock types as seen in figure 40. The content of the brown sugar norite has a minimum of An_{66} and maximum of An_{79}. The plagioclase composition of the pyroxenite varies between An_{67} and An_{76}. Both rock types, i.e., BSN and pyroxenite, have an analogous average plagioclase composition of An_{73}.

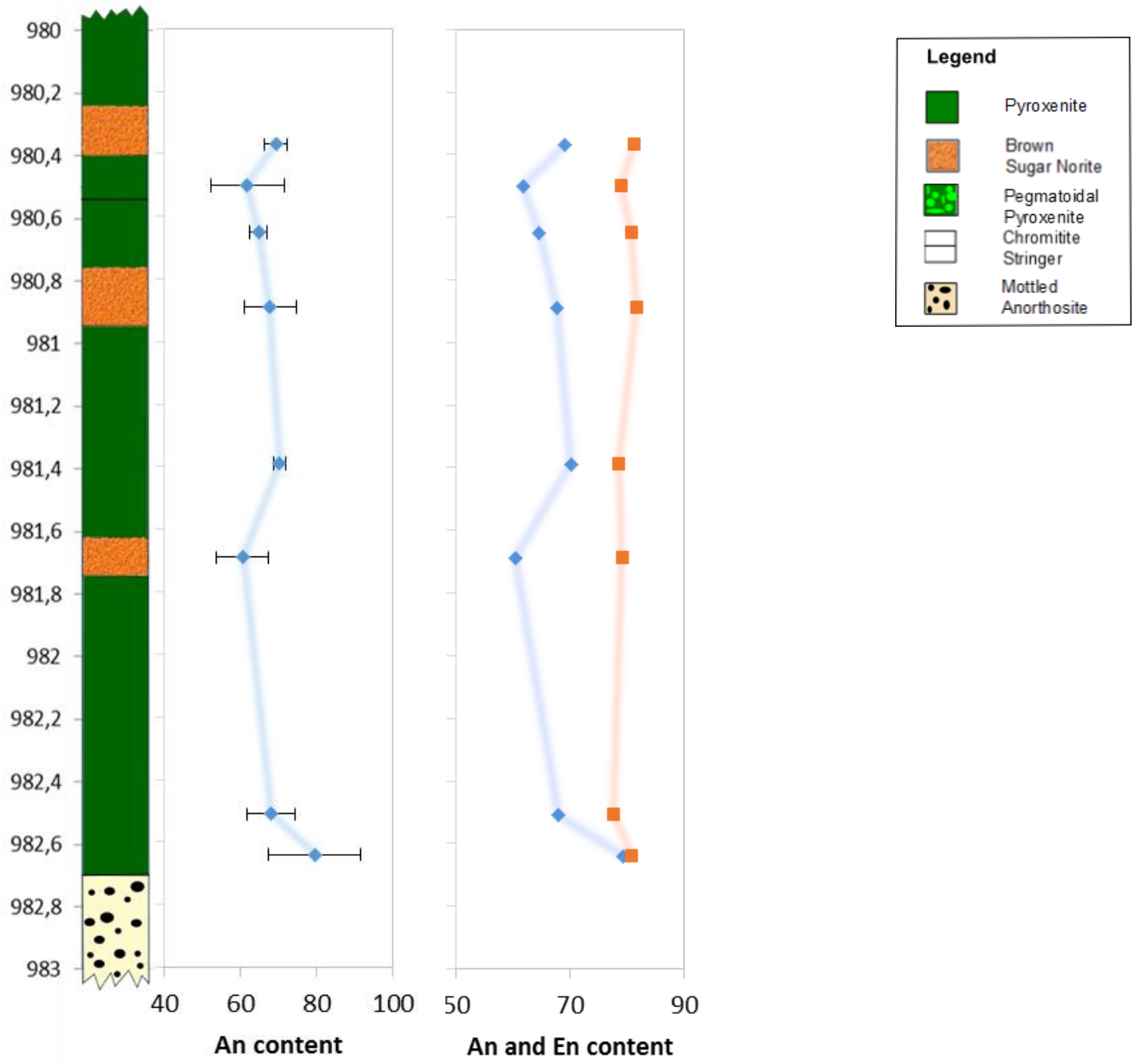

Figure 41: Compositional profile of a) average and standard deviation of An content in the plagioclase and b) average composition of An content in plagioclase and En content in orthopyroxene found in MR pyroxenite and BSN underground samples at TRP plotted against stratigraphic height.

The percentage of anorthite in plagioclase displays a cryptic variation with elevation (as seen in Figure 41). In close proximity to the basal chromitite stringer the An content is high but decreases as the stratigraphic height increases. This trend is similar to %En of orthopyroxene with elevation where the highest concentrations are found in close proximity to the binding chromitite stringers of the MR as displayed in figure 41b. The An content in plagioclase increases between 981.4 and 980.4 m depth.

4.3 Initial Sr isotopes of plagioclase separates

Table 6: Sr analyses on plagioclase separates from selected underground samples of the MR, TRP

Sample	Description	$^{87}Sr/^{86}Sr$	±2s (standard error on mean)	K_2O
NBS987	Standard	0,710246	0.000006	
JJB1	HW spotted anorthosite	**0,706480**	0.000007	0,213
JJB5	FW mottled anorthosite	**0,706476**	0.000005	0,215
JJB10	pyroxenite	**0,706644**	0.000006	0,1137
JJB11	pyroxenite	**0,706668**	0.000008	0,1195
BSN	brown sugar norite	**0,706501**	0.000009	0,1713
NBS987	Standard	0,710251	0.000006	

$^{87}Sr/^{86}Sr$ ratios are generally believed to be reliable indicators of distinct magmatic lineages, assuming that the rocks have remained closed with respect to rubidium and strontium since crystallization (Faure 1986). The above table (table 6) shows mass spectrometer analysis (from Institute Universitaire Européen de la Mer, France) for Sr which was performed on plagioclase separates of 5 underground samples from HW, FW, MR pyroxenite and BSN lense. The results illustrates that these rock types have similar $^{87}Sr/^{86}Sr$ as that characterised by the Critical Zone. The vertical profile of $^{87}Sr/^{86}Sr$ ratios in the Merensky Reef profile where brown sugar norite lenses occur vary with height as seen in figure 42. The variation in the Sr isotopic ratio suggests that there may have been an influx of new magma. The $^{87}Sr/^{86}Sr$ ratio increases from the footwall anorthosite at the pyroxenite and decreases again at the brown sugar norite. A negative trend is observed for $^{87}Sr/^{86}Sr$ versus K_2O as $^{87}Sr/^{86}Sr$ decreases with an increase in K_2O as seen in figure 43. The Merensky anorthosite has the highest K_2O content. Though both the pyroxenite and brown sugar norite have $^{87}Sr/^{86}Sr$ ratios representative of Critical Zone magma the brown sugar norite has a lower ratio relative to pyroxenite, proposing that it formed from a slightly more primitive magma.

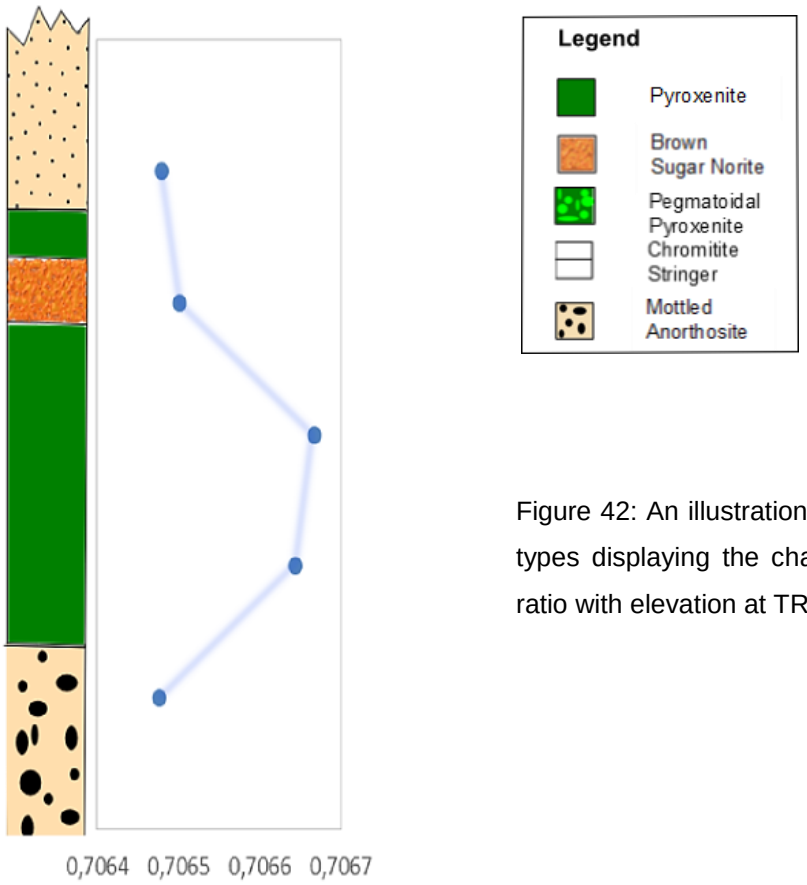

Figure 42: An illustration of different rock types displaying the change in $^{87}Sr/^{86}Sr$ ratio with elevation at TRP.

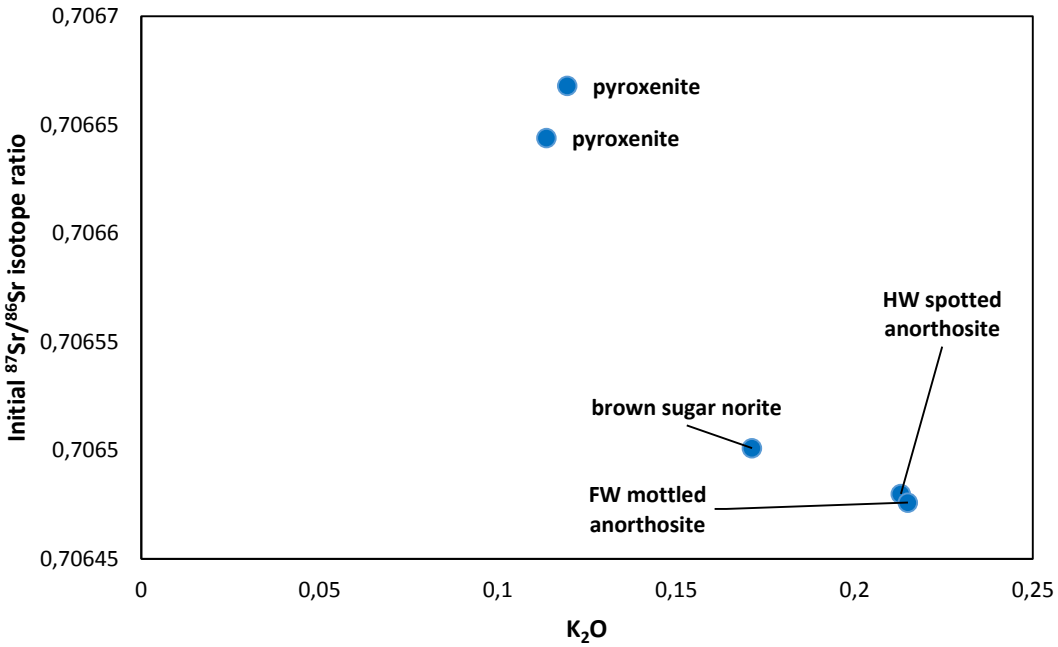

Figure 43: Binary plot of $^{87}Sr/^{86}Sr$ versus K_2O for different rock types of the Merensky Cyclic Unit.

4.4 Chromite

This section of the study focuses on the chemistry of the disseminated and massive chromite crystals occurring within the MR. In light of the erratic appearance of the BSN lenses, attention will be given to a MR profile where these BSN lenses are present in an attempt to determine possible differences in chromite chemistry between the MR pyroxenite and BSN. Chromite chemistry was thus collected for the BSN and MR pyroxenite within the MR interval directly above and below the upper and including the lower chromitite stringer along with disseminated chromite from EST. No chromitite layers from EST were investigated as these samples were removed prior to this current study.

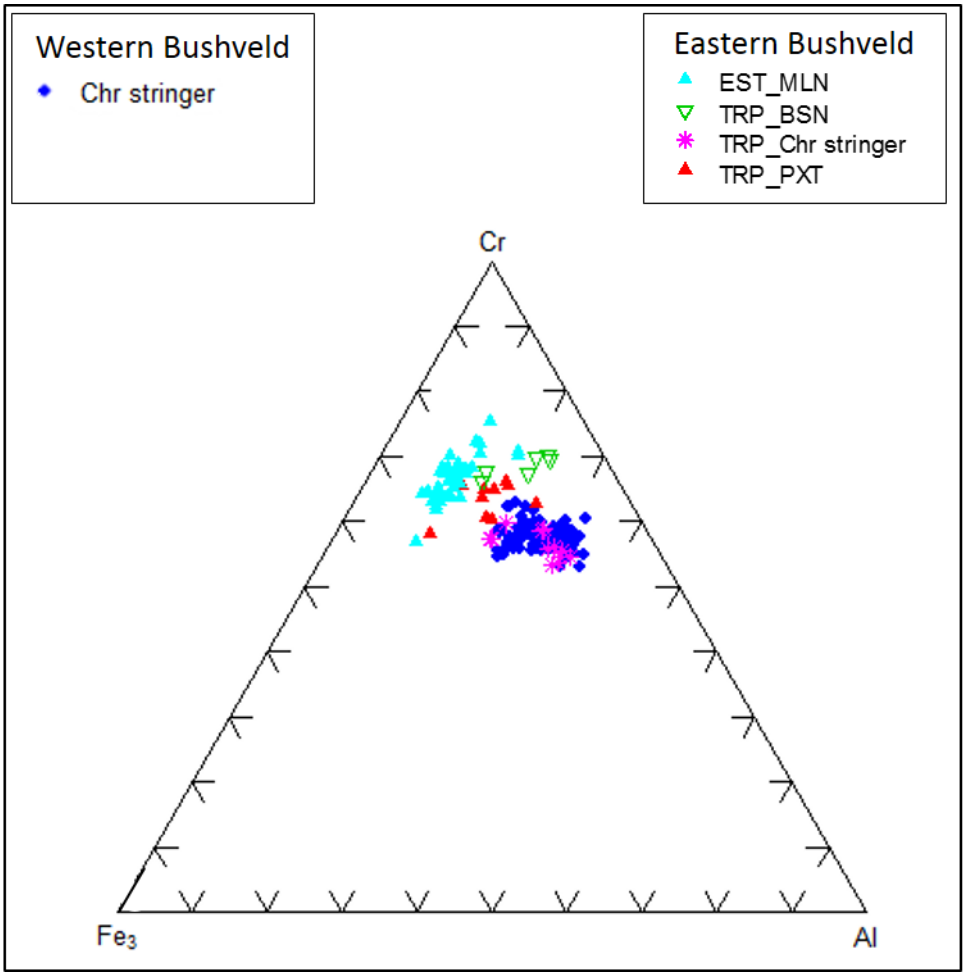

Figure 44: Cr-Fe^{3+}-Al ternary diagram of chromites found within the MR unit at TRP mine and Eerste Geluk, eastern Bushveld, in this study plotted here with chromites found within the MR unit at Lonplats' Mines in the western Bushveld (Shelembe, 2006).

Chromite compositions in this study have been plotted with chromite compositions of chromites found in the MR unit from a study done at Lonplats' Mines by Shelembe (2006) for comparison. Figure 44 illustrates a significant difference in composition of chromite from the chromitite stringers and chromite composition of disseminated chromite in pyroxenite/BSN. The TRP and EST disseminated chromite compositions are relatively lower in Al and higher in Fe than that of chromite stringers in both western and eastern BIC. Stringer chromite data from eastern and western BIC overlap (figure 44) indicating that they possibly have the same origin.

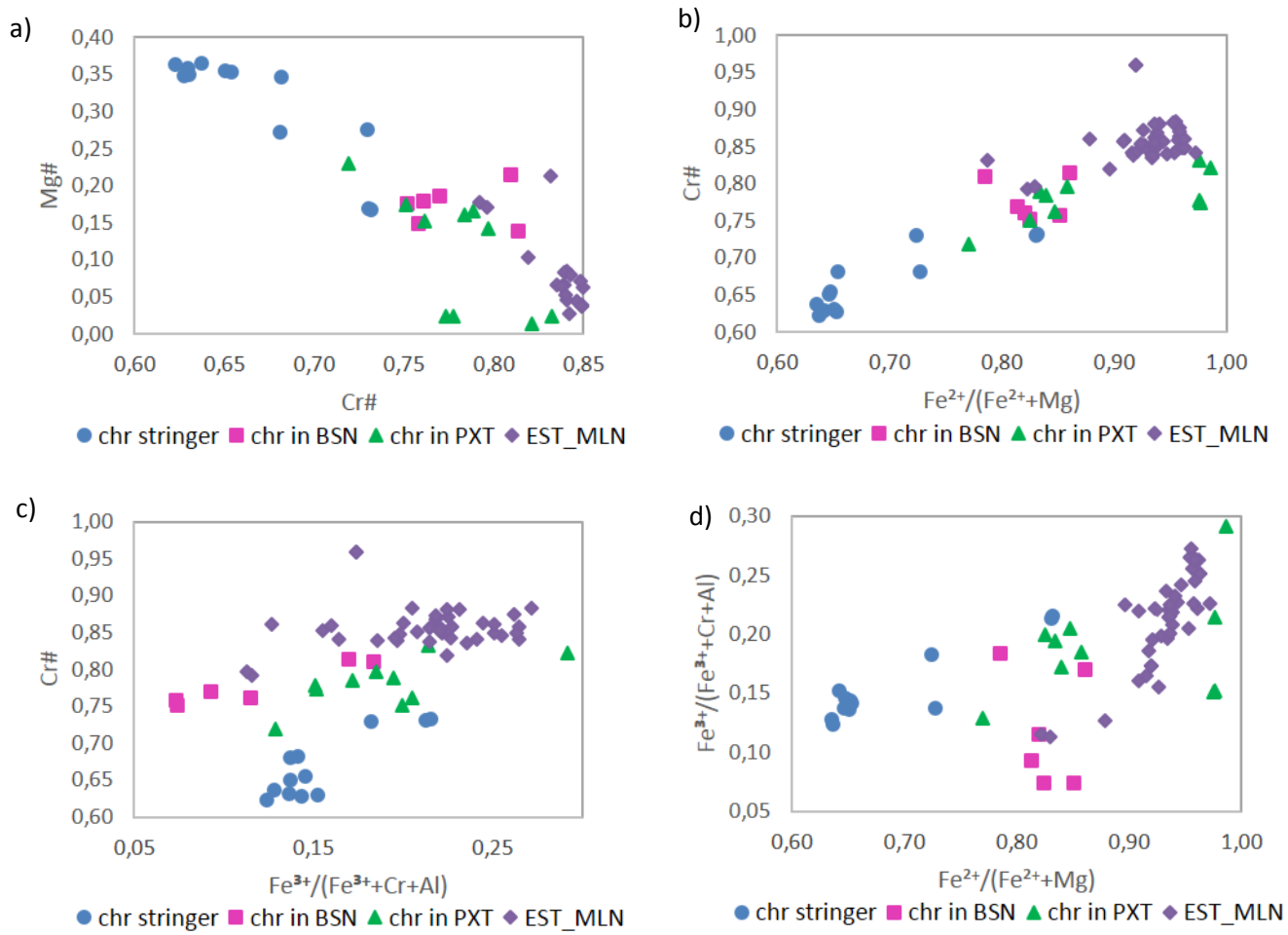

Figure 45: Binary plots of a) Cr# [Cr/ (Cr+Al)] vs. Mg# [Mg/ (Mg+Fe)], b) Cr# vs. Fe^{2+}/ (Fe^{2+}+Mg), c) Cr# vs. Fe^{3+}/ (Fe^{3+}+Cr+Al) and d) Fe^{3+}/ (Fe^{3+}+Cr+Al) vs. Fe^{2+}/ (Fe^{2+}+Mg) found within the chromitite stringer as well as disseminated chromite crystals within pyroxenite and brown sugar norite of the MR at TRP as well as in MR melanorite at EST.

Table 7: An overview of mineral compositions of chromite in the various rock types at TRP and EST. *TRP_PXT= TRP MR pyroxenite, BSN= TRP brown sugar norite, EST_MsN= EST mesonorite and EST_MLN=EST MR melanorite. B.d.l= below detection limit*

Chromite												
Rocktype		SiO_2	CaO	K_2O	MgO	Al_2O_3	FeO	MnO	TiO_2	Na_2O	$Cr2O_3$	Total
TRP_PXT	Average	0.25	0.13	0.03	2.43	7.28	39.34	0.12	1.01	b.l.d	45.16	95.75
n=27	Std	1.18	0.62	0.02	1.22	2.34	4.03	0.13	0.45	b.l.d	3.68	
	Max	6.13	3.24	0.07	4.5	11.87	49.5	0.5	1.68	0.02	56.57	
	Min	b.l.d	b.l.d	b.l.d	0.24	1.11	33.48	b.l.d	0.02	b.l.d	38.31	
TRP_CHR	Average	0.07	b.l.d	0.02	6.21	13.67	34.9	0.08	1.03	b.l.d	40.39	96.37
n=12	Std	0.11	0.01	0.01	1.58	2.63	3.72	0.02	0.71	b.l.d	1.64	
	Max	0.4	0.03	0.05	7.32	16.52	42.4	0.12	2.06	0.01	42.77	
	Min	0.01	b.l.d	0.01	3.27	9.38	31.12	0.04	0.12	b.l.d	38.05	
TRP_BSN	Average	1.05	0.06	0.01	2.36	5.92	44.35	0.17	1.49	b.l.d	39.63	95.04
n=19	Std	3.09	0.26	0.02	1.6	2.75	7.27	0.19	1.01	0.01	7.21	
	Max	13.58	1.12	0.04	7.68	10.91	55.99	0.54	3.43	0.03	49.78	
	Min	b.l.d	b.l.d	b.l.d	0.81	2.44	32.52	b.l.d	0.04	b.l.d	26.45	
EST_MLN	Average	0.14	b.l.d	b.l.d	1.66	4.89	43.6	0.12	1.02	b.l.d	42.78	94.21
n=42	Std	0.77	b.l.d	b.l.d	2.2	1.21	3.1	0.2	0.58	b.l.d	3.64	
	Max	4.97	b.l.d	b.l.d	14.79	8.22	47.88	0.72	2.05	b.l.d	51.17	
	Min	b.l.d	b.l.d	b.l.d	0.51	1.47	35.52	b.l.d	b.l.d	b.l.d	32.93	

The chromite analyses as summarized in table 7 shows that slight differences in composition do exist for chromite found within TRP chromitite stringer, TRP MR pyroxenite, BSN and EST MR pyroxenite. Chromite from the TRP chromitite stringer has relatively higher MgO and Al_2O_3 content with an average of 6.21% MgO and 13.67% Al_2O_3. Chromite found in BSN are significantly more enriched in FeO ranging between 32.52% and 55.99% FeO. Disseminated chromite in TRP MR pyroxenite has an average of 45.16% Cr_2O_3 which is relatively higher than the chromite from the other rock types.

Additional trends of disseminated and stringer chromite crystals of the MR are explored (see figure 45). A negative linear trend is observed in figure 45 a where the Cr# decreases with an increase in Mg#. This trend corresponds with “trend A” as described by Naldrett et al. (2012) where Mg/ (Mg + Fe) versus Cr/ (Cr + Al) ratio of chromite crystals from the LG-1 to the UG-2/3 of the Bushveld Complex are plotted. A “trend B” is characterised by the authors as a decrease in Mg/ (Mg + Fe) with a decrease in Cr/ (Cr + Al) in the chromite. The highest Mg# of chromite in this study is found within the TRP chromitite stringer with concentrations ranging between 0.10 and 0.15. Disseminated chromite crystals in MR melanorite at EST display relatively less variation in Mg# (0.03 average) than the disseminated chromite crystals in TRP pyroxenite (0.05 average) and BSN (0.04 average). Though the chromite crystals from EST cluster at lowest Mg# they have higher Cr# with an average of 0.92 compared to the disseminated as well as massive chromite crystals at TRP of 0.89 and 0.79 on average respectively.

In figure 45b the Cr# increases with an increase in Fe^{2+}/ (Fe^{2+}+Mg) resulting in a positive trend. The lowest Fe^{2+}/ (Fe^{2+}+Mg) in chromite is found in the TRP chromitite stringer which

has an average of 0.88 compared to the highest average concentration of 0.97 which is found in the disseminated chromite of EST MR melanorite. The compositional chemistry of the disseminated and massive chromite crystals in figures 45c and d display positive trends. Chromite found in the TRP chromitite stringer have the lowest $Fe^{3+}/ (Fe^{3+}+Cr+Al)$ content whereas the highest $Fe^{3+}/ (Fe^{3+}+Cr+Al)$ content with an average of 0.53 is found in the BSN.

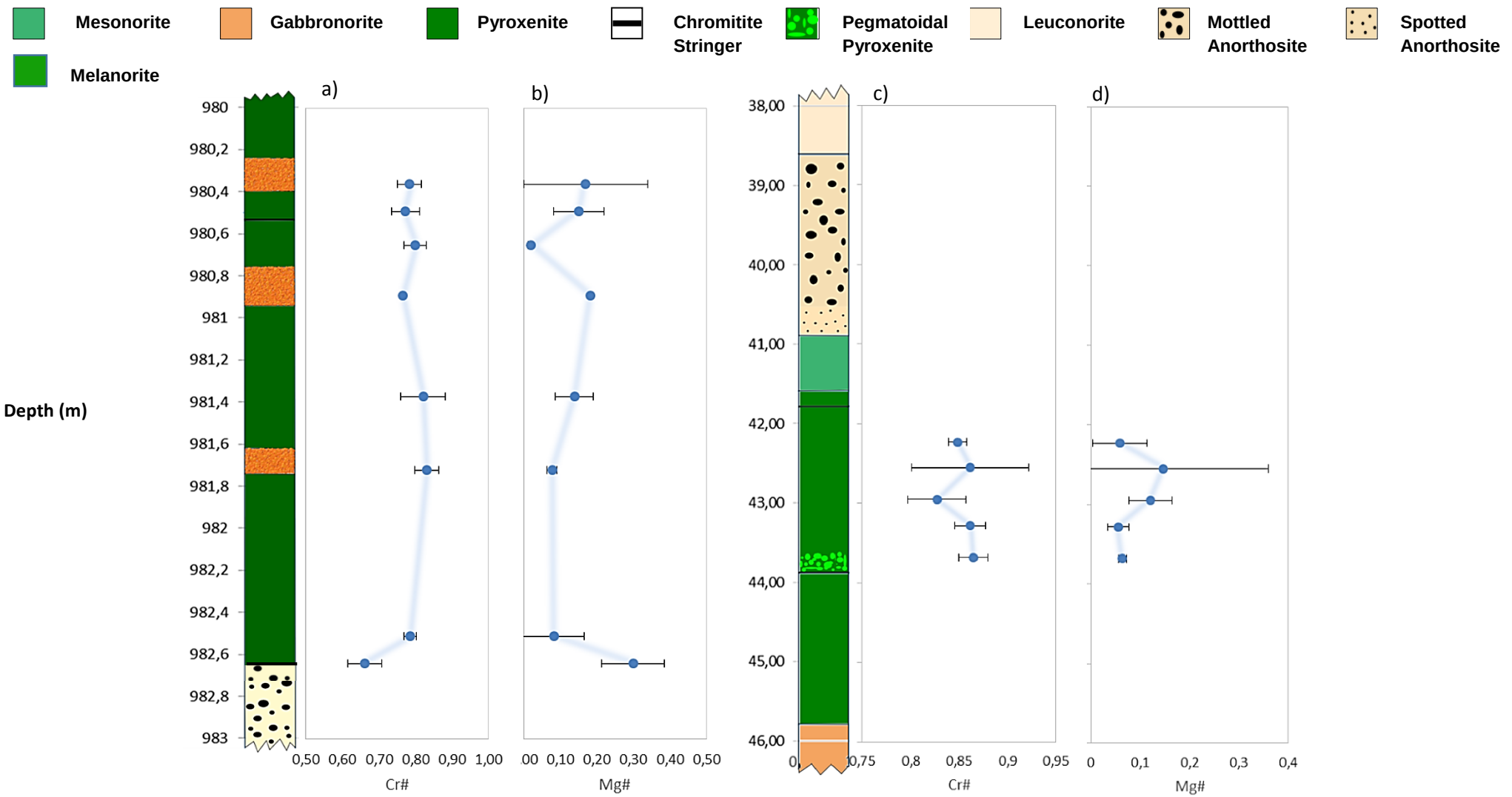

Figure 46: Cryptic variation of Cr# [Cr/ (Cr+Al)] and Mg# [Mg/ (Mg+Fe)] vs. stratigraphic height respectively at TRP (a and b) and EST (c and d). The average and standard deviation are plotted. The scale on the left indicates depth below surface.

Figure 46 displays two compositional trends in the chromite crystals found within the MR interval based on the cation ratios namely Mg/Mg+Fe and Cr/(Cr+Al) versus stratigraphic height at TRP and EST. These ratios vary systematically with height. In figure 46b it can be seen that the Mg# decreases with an increase in height in the lower part of MCU and increases again in the upper part at TRP. The concentration of Mg# is higher in the disseminated chromite crystals within the pyroxenite in close proximity to the chromitite stringer than that found in the chromite crystals of the stringer. An inverse trend is observed for the Cr# (figure 44a). An increasing trend of Cr# is observed as one move up the MR pyroxenite interval with the lowest Cr# found within the disseminated chromite crystals in the pyroxenite adjacent to the binding chromitite stringers (figure 46a).

4.5 Summary of silicates and oxide mineral chemistry

EPMA and SEM-EDX/WDX results show cryptic variation of orthopyroxene, plagioclase and chromite chemistry with elevation (see figures 36, 41 and 46). The orthopyroxene compositions plot within the enstatite field of the En-Wo-Fs ternary plot. Enstatite compositions (%En) in orthopyroxenes within the MR HW ranges from En78-80 for pyroxenite and En79-82 for BSN which is higher than that found within the HW pyroxenite of Eerste Geluk (figure 32). Orthopyroxenes within the MR pyroxenite (figure 33) have an average %En of 80 which is relatively higher than the average (En77) documented by Rose, 2012 who studied MR unit of various boreholes in the same area (TRP). It may be concluded that %En of opx in MR profiles at TRP where no BSN is present are slightly lower. An overlap in mineral chemistry exits for the opx crystals found within the pyroxenite and pegmatoidal in close proximity to the basal chromitite stringer (figure 34). The ternary plots indicate that there is a slight difference in mineral chemistry between MR pyroxenite and BSN. Whether these rocks crystalized from the same magma needs to be determined however Sr isotope data show that the MR pyroxenite and BSN have similar $^{87}Sr/^{86}Sr$ characterized by Critical Zone magma. Plagioclase separates of selected rock types of TRP MR display $^{87}Sr/^{86}Sr$ values of 0.706476 to 0.706668 (table 6). These Sr isotope values are consistent with the Sr findings by Seabrook et al., 2005, typical for Critical Zone magma. Though $^{87}Sr/^{86}Sr$ ratio of BSN and pyroxenite are similar the lower concentration of the isotope ratio by BSN suggests that the BSN lenses may have formed from a slightly more primitive magma lineage. The Sr isotope findings are supported by the correspondence with the higher En content of Opx in BSN. Plagioclase compositions plot mostly in the labradorite field and to a lesser extend in the bytownite field.

Plagioclase in the TRP MR pyroxenite has an average %An of An_{68} ranging from An_{48-88} whereas plagioclase in BSN has an average %An of 66%. EST013 plagioclase in MR pyroxenite has an average %An 62% with a minimum of An_{49} and a maximum of An_{86}. The

composition of plagioclase of the TRP MR pyroxenite and BSN are thus similar (figure 38). Additionally, as more clearly seen in figure 32, a difference in En composition is distinguished for BSN and TRP pyroxenite and in figure 37 %An in plagioclase of BSN and TRP MR pyroxenite overlap. This may suggest that the BSN lenses have slightly more primitive Opx entrained in interstitial plagioclase liquid similar to the surrounding TRP MR pyroxenite. A variation in %An of plagioclase is observed with elevation (figure 41) resulting in a "saw-tooth" pattern. A similar pattern is observed for En content in Opx versus height (figure 36 and 41b). This trend is inducive of normal fractionation; for in layered intrusions such as the BIC the An content serves as an index of differentiation (Cawthorn & Ashwal, 2009).

Mg# versus Cr# of the chromite crystals shows a negative trend as the Cr# decreases with increase in Mg# (figure 45a). Hatton & Von Gruenewaldt (1985) observed a similar trend in their analysis of BIC disseminated chromite and associated it to re-equilibration with the surrounding silicates. It is considered by Naldrett et al. (2012) that this trend may be interpreted as a result of the exchange substitution of Cr and Fe^{2+} for Mg and Al between spinel and liquid, which is affected by the Mg- Fe^{2+} spinel-liquid Kd. The opposite trends of Cr# and Mg# versus stratigraphic height (figure 46a-d) could also be accounted to the re-equilibration of chromite with the surrounding silicates. The relatively high En content of orthopyroxene near the chromitite stringer may also be attributed to the effect of re-equilibration during the cooling of orthopyroxene and chromite. The reaction Ferrosilite + Spinel = Enstatite + Hercinite explains that during cooling adjacent orthopyroxene and chromite will exchange Fe and Mg according to this reaction. Orthopyroxene is therefore more enriched in Mg and chromite in Fe as a result of cooling. Chromite crystallization is promoted by the mixing of primitive and fractionated liquid (Irvine 1977). As a result, the chemical composition of the various chromite would differ therefore chromite which formed later, for example, would have a lower Mg content than chromite which may have formed earlier. The high Mg# in chromite of the TRP and Lonplats' Mines chromitite stringers thus indicates that the chromites are more primitive than the disseminated chromite found in the other rock types.

4.6 Base Metal Sulphides and associated PGMs with EPMA

This section mainly focuses on the BMS and associated PGMs that occur within the MR pyroxenite package. EPMA analyses were carried out on 11 thin sections and 5 epoxy sections where the epoxy sections mainly include the sulphide-rich fragments of the underground MR samples. The BMS may occur disseminated throughout the pyroxenite or form 'network' or 'web-like' textures usually in close proximity to the basal chromitite stringer. The most dominant sulphide mineral observed is pyrrhotite followed by pentlandite, chalcopyrite and minor concentrations of pyrite (figure 47 A and B). Average concentrations

of selected elements present in these sulphides are illustrated in Table 8. The most dominant PGMs encountered this study are moncheite (figures 47C, 48A&B and 51D), platarsite (figure 51C and 54B) and unnamed phase that may be a Fe enriched laurite (figure 48C and D)

Table 8: Summary of the average, minimum and maximum concentrations of Cu, Fe and Ni in pyrrhotite, pentlandite and chalcopyrite.

Mineral	Cu wt% avg; range	Fe wt% avg; range	Ni wt% avg; range	S wt% avg; range
Pyrrhotite:				
TRP_PXT	**0.03**; 0.00-0.22	**60.61**; 58.62-63.16	**0.26**; 0.00-0.66	**38.53**; 35.60-40.15
TRP_BSN	**0.04**; 0.00-0.20	**60.08**; 59.23-62.58	**0.38**; 0.05-0.73	**38.71**; 38.06-39.28
EST_MLN	**0.03**; 0.00-0.15	**60.09**; 59.04-61.14	**0.82**; 0.59-1.15	**38.65**; 37.66-39.36
Pentlandite				
TRP_PXT	**0.05**; 0.00-0.24	**31.99**; 30.67-35.43	**34.59**; 32.57-35.79	**33.41**; 32.82-34.10
TRP_BSN	**0.00**; 0.00-0.00	**31.67**; 31.29-32.78	**33.61**; 33.06-34.09	**33.36**; 33.29-34.14
EST_MLN	**0.00**; 0.00-0.00	**33.59**; 30.02-37.16	**33.63**; 29.43-37.83	**33.53**; 32.52-34.55
Chalcopyrite				
TRP_PXT	**34.04**; 31.55-36.10	**30.85**; 29.65-31.81	**0.19**; 0.00-1.94	**34.62**; 33.65-35.45
TRP_BSN	**34.49**; 31.30-36.62	**30.70**; 29.78-32.22	**0.13**; 0.00-0.66	**34.78**; 34.18-36.60
EST_MLN	**33.18**; 32.96-33.39	**30.57**; 30.34-30.8	**0.05**; 0.04-0.06	**33.99**; 33.98-34.00
Pyrite				
TRP_PXT	**0.31**; 0.00-2.04	**46.76**; 45.58-47.59	**0.01**; 0.00-0.05	**52.39**; 51.38-53.22

4.6.1 BMS and PGM in pyroxenite near top chromitite stringer

Sulphides within the MR pyroxenite have been observed to increase in concentration in close proximity to the bounding chromitite stringers. An association of PGMs with BMS at the crystal boundaries or enclosed within BMS may be related to exsolution of PGMs from monosulphide solid solution (Penberthy & Merkle, 1999). Moncheite is the most dominant PGM observed in this study.

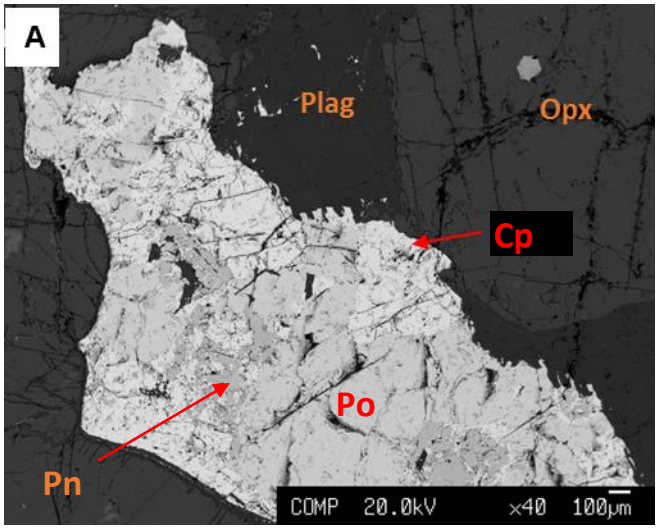

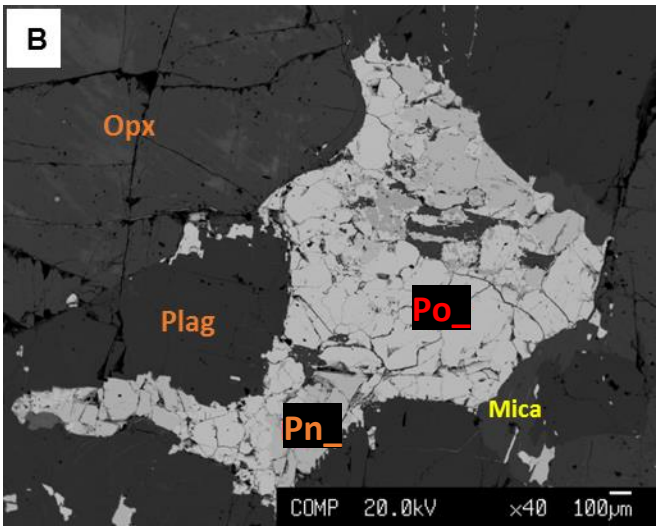

C **Moncheite:**

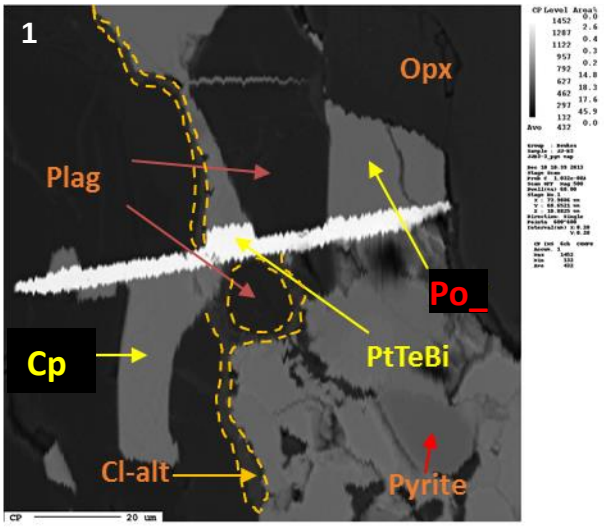

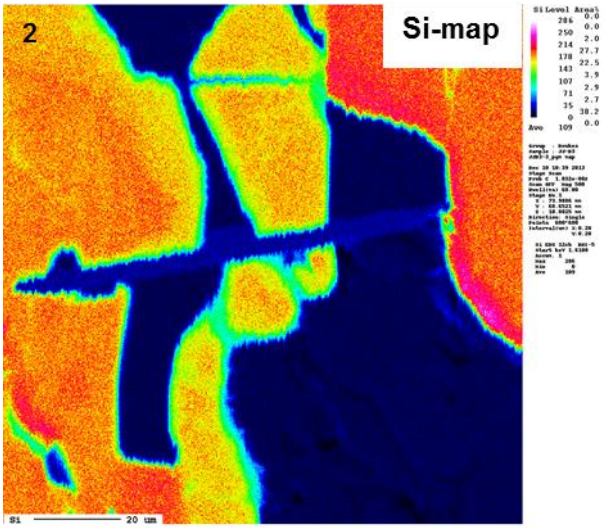

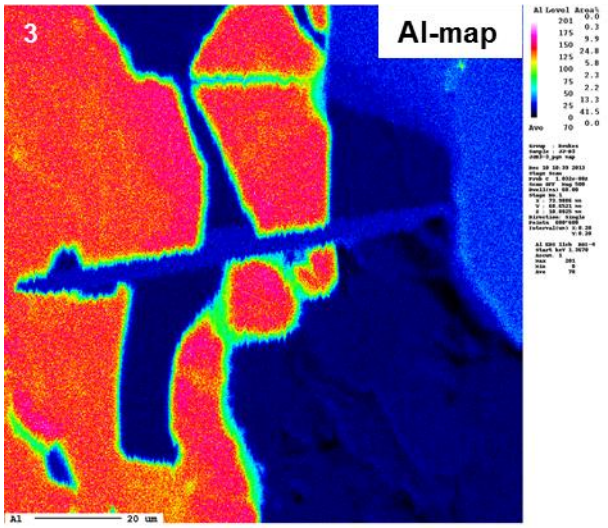
3
Al-map
Al
20 um

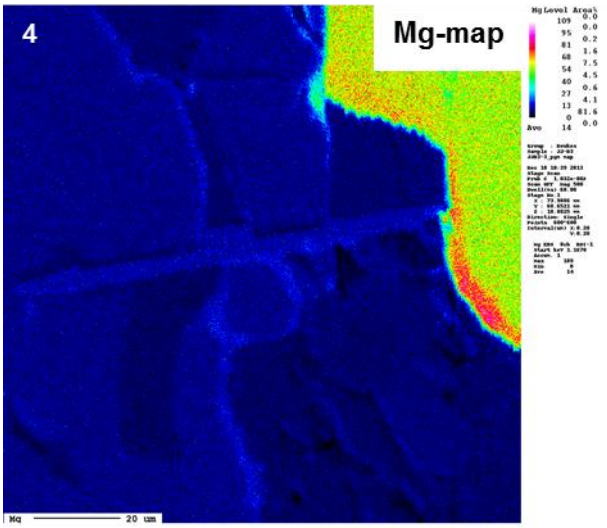
4
Mg-map
Mg
20 um

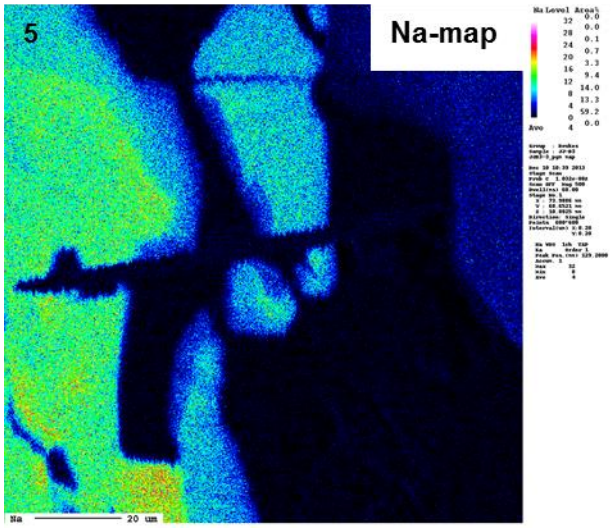
5
Na-map
Na
20 um

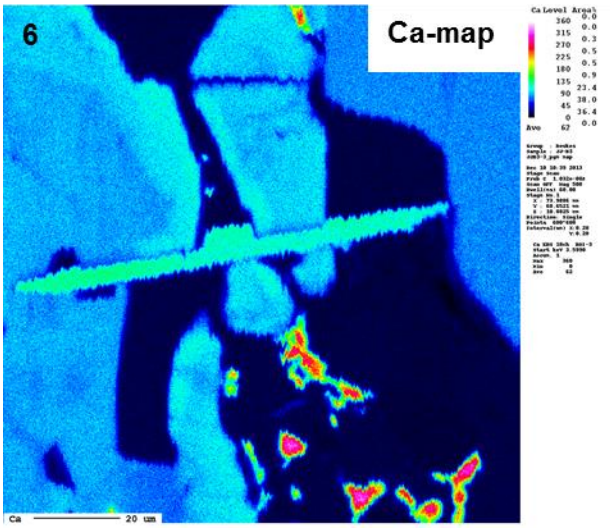
6
Ca-map
Ca
20 um

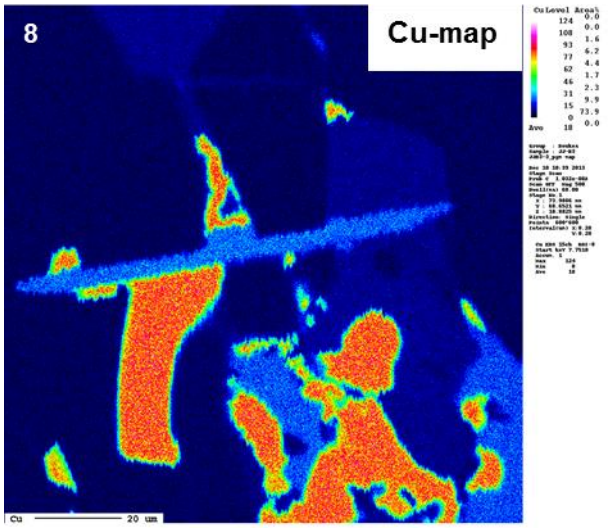
8
Cu-map
Cu
20 um

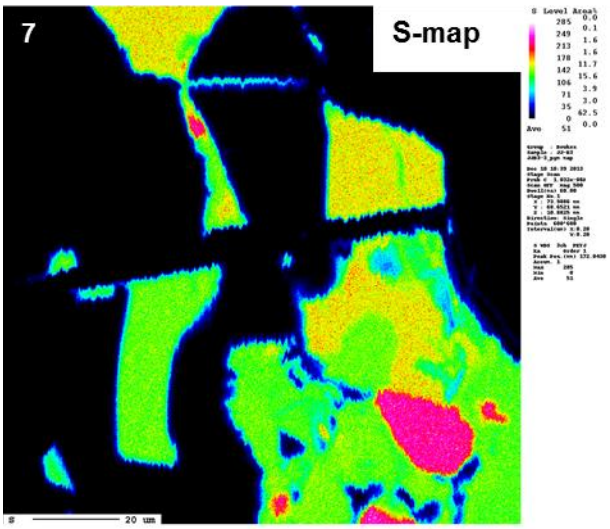
7
S-map
S
20 um

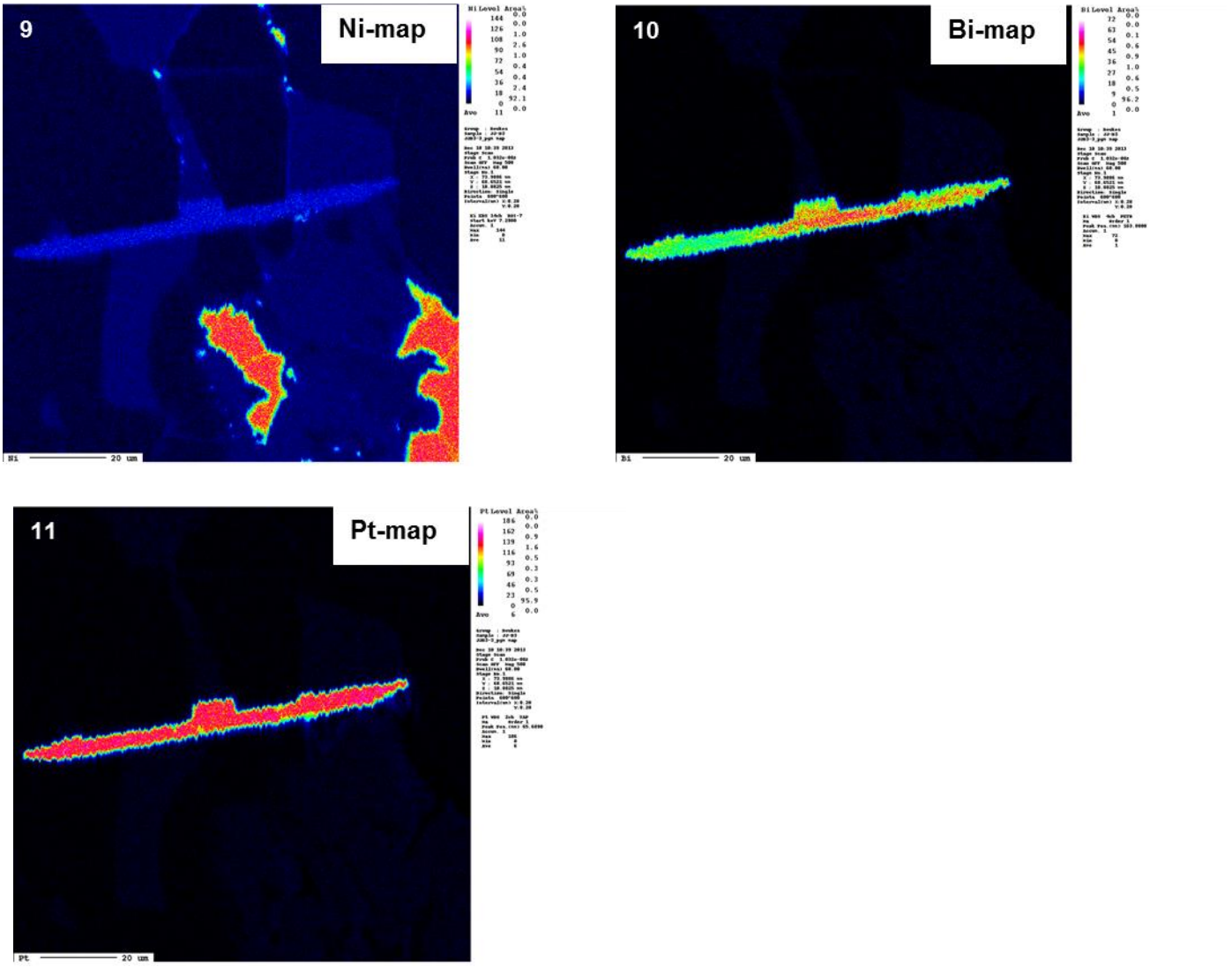

Figure 47: A and B) are common sulphides occurring within the TRP MR pyroxenite in close proximity to the upper chromitite stringer. Note the reaction rims/ sulphide "flames" at the edges in contact with surrounding silicates. C) C1 to 11 shows the occurrence of moncheite cutting through pyrrhotite. It may be that the sulphides got displaced. Note the chlorite alteration along plagioclase-BMS-PGM boundaries as seen in C1 (chlorite confirmed by EPMA measurement, however not recorded). In C10 it can be seen that the Bi is enriched more along the centre of the PGM whereas in C11 the Pt distribution is more homogeneous.

4.6.2 BMS and PGM in pyroxenite near bottom chromitite stringer

PGM found in association with BMS are usually extremely small with grain sizes less than 20 µm and can therefore be difficult to locate and measure using an electron microprobe. The following BSE images 48 A to C illustrate relatively larger PGM making it possible to observe features such as zonation. The "worm-like" shape of moncheite (such as in figure 48 A) is a common observation in samples close to a chromitite stringer.

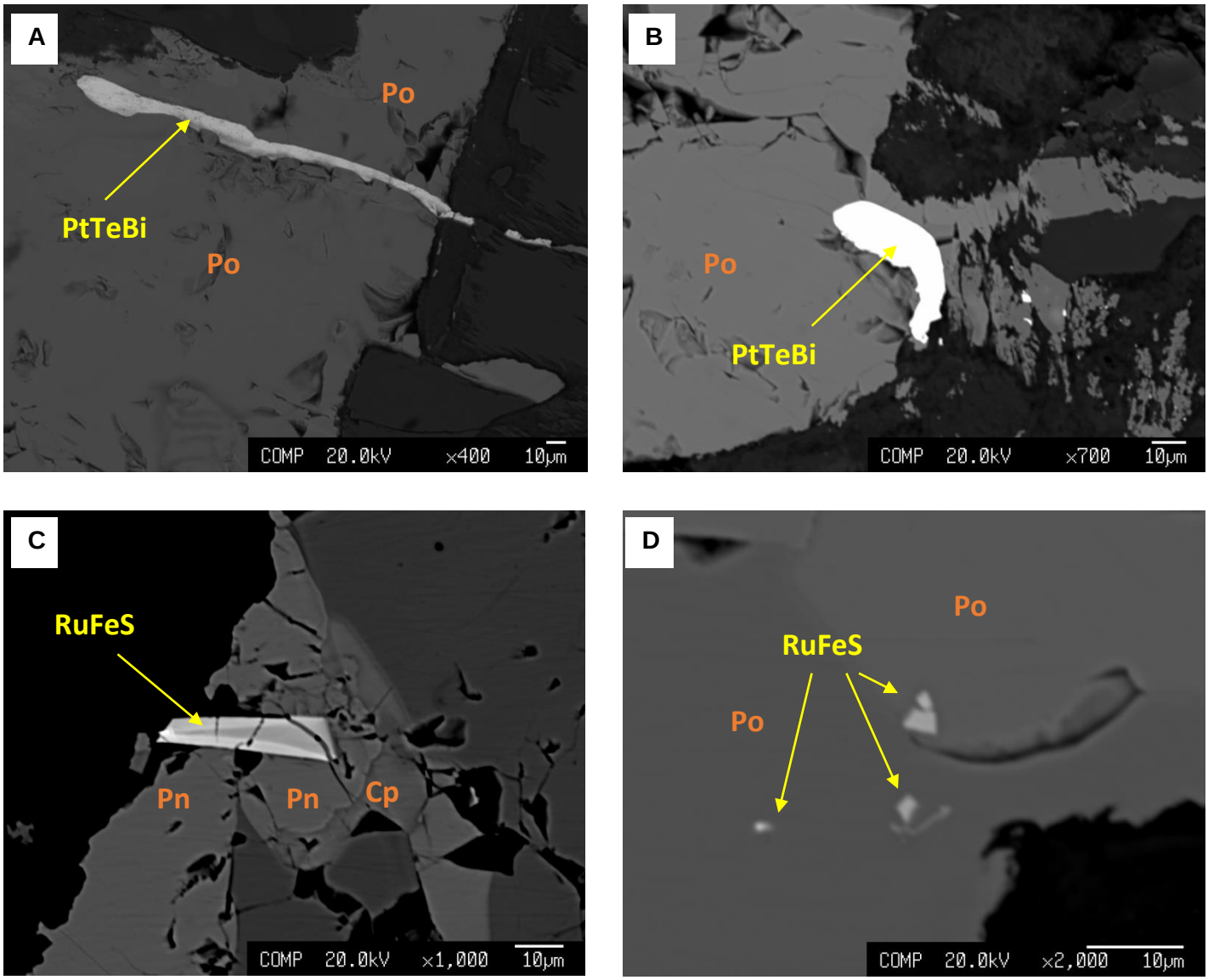

Figure 48: A to D) BSE images of PGMs found within sulphides (mainly pyrrhotite) of the pyroxenite found close to the bottom chromitite stringer. A) shows "worm" shaped moncheite which have flowed/intruded into the pyrrhotite. B) this moncheite appears to be more primary than secondary (like the PGM seen in A). C and D) depicts a unnamed phase (possibly Fe enriched laurite) found at the edge or within pentlandite. Note the zonation of laurite in C).

A

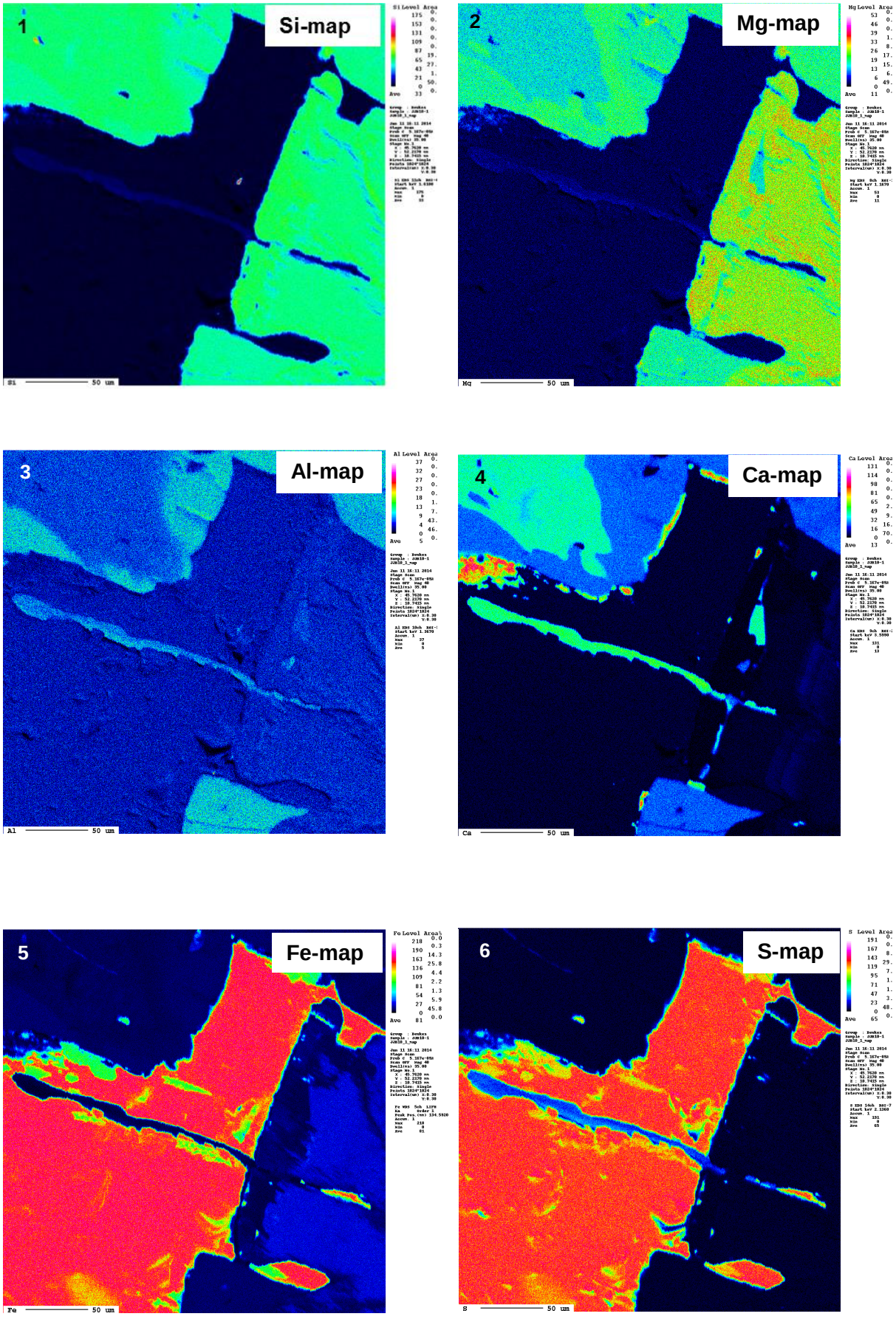

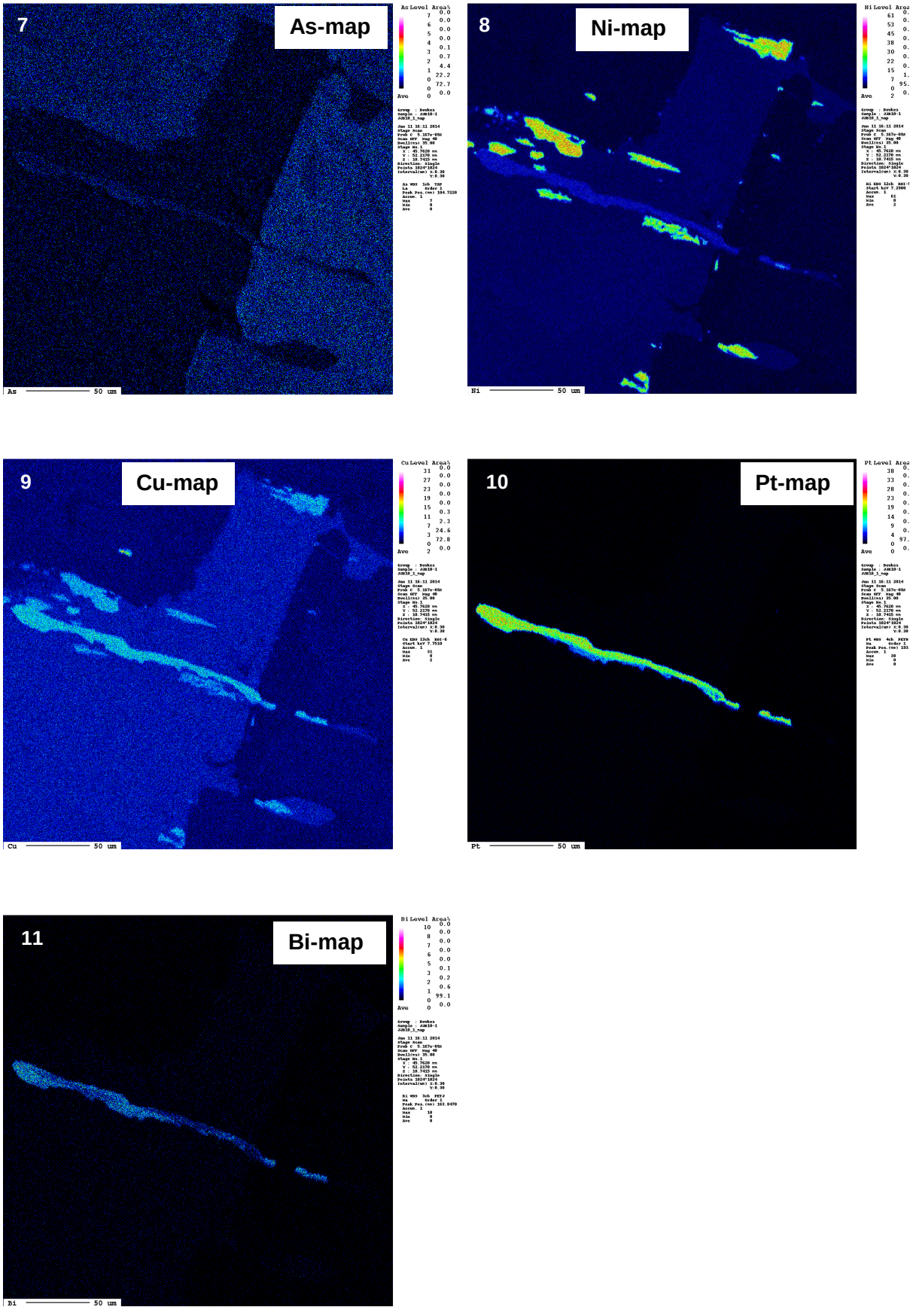

Figure 49: Images A1-11 depicts the element distribution of the area in figure 48A).

C

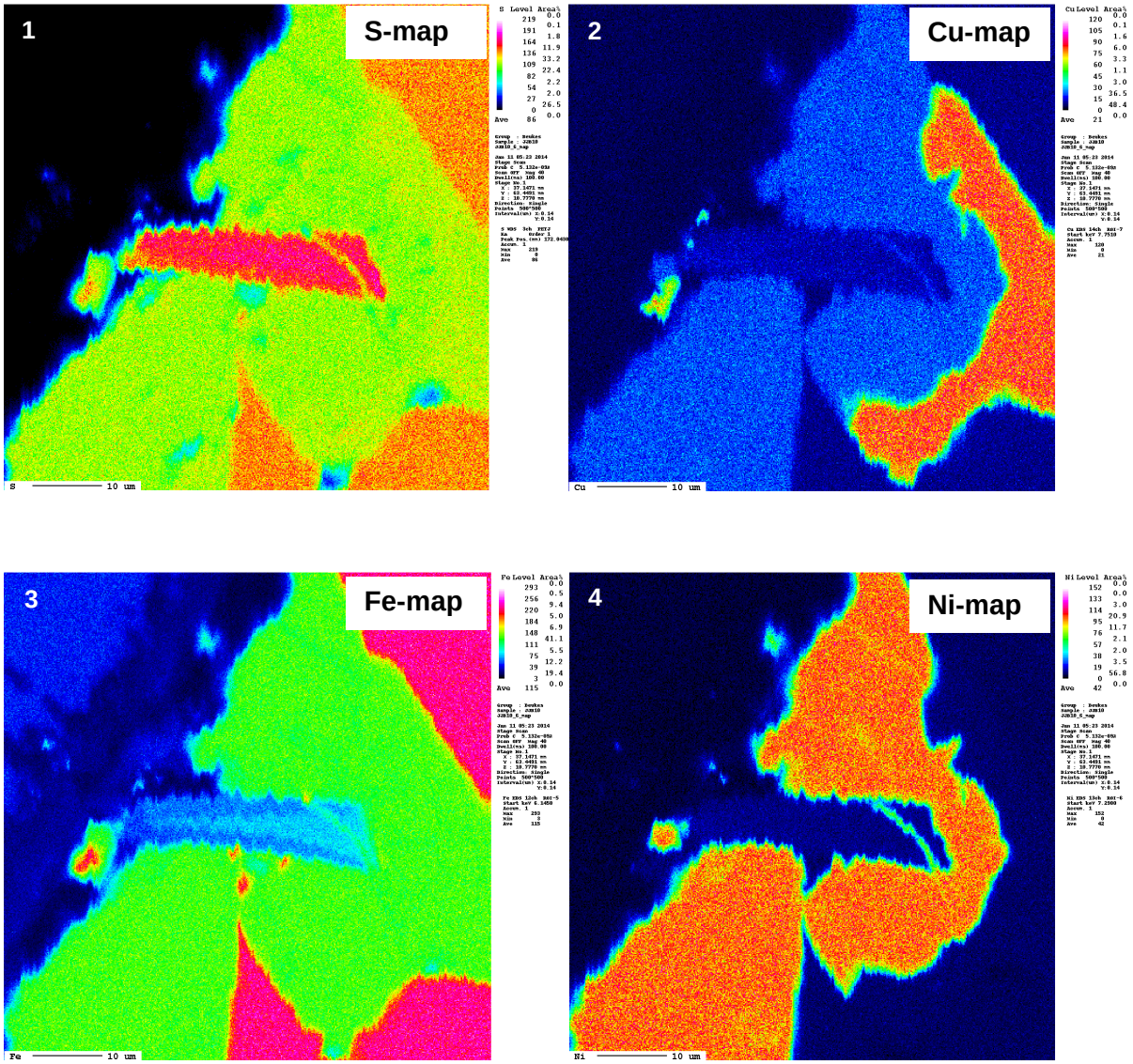

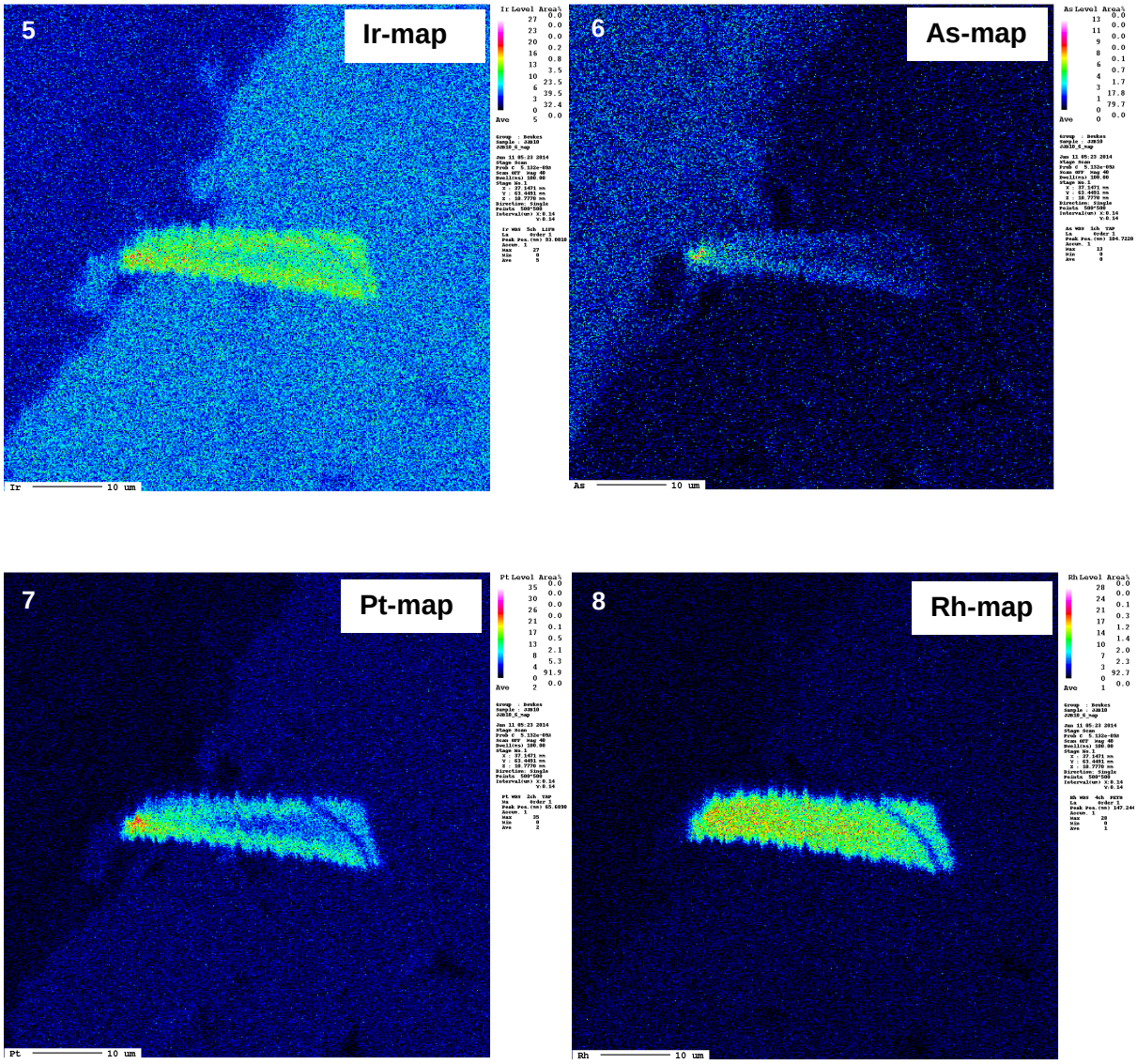

Figure 50: The above images (C1-8) are various element distribution maps of unnamed phase (possible Fe rich laurite) in figure 48C. Note the Pt and As enriched tip in C7. The Fe (C3), Ir (C5) and Pt (C7) distribution within the PGM is zoned.

Figure 51 A and B display poikilitic texture of BMS enclosing or partially enclosing chromite. It is a familiar textural feature where BMS is associated with chromite. BMS may also be enclosed by chromite as illustrated in figures 17 E and 18 G.

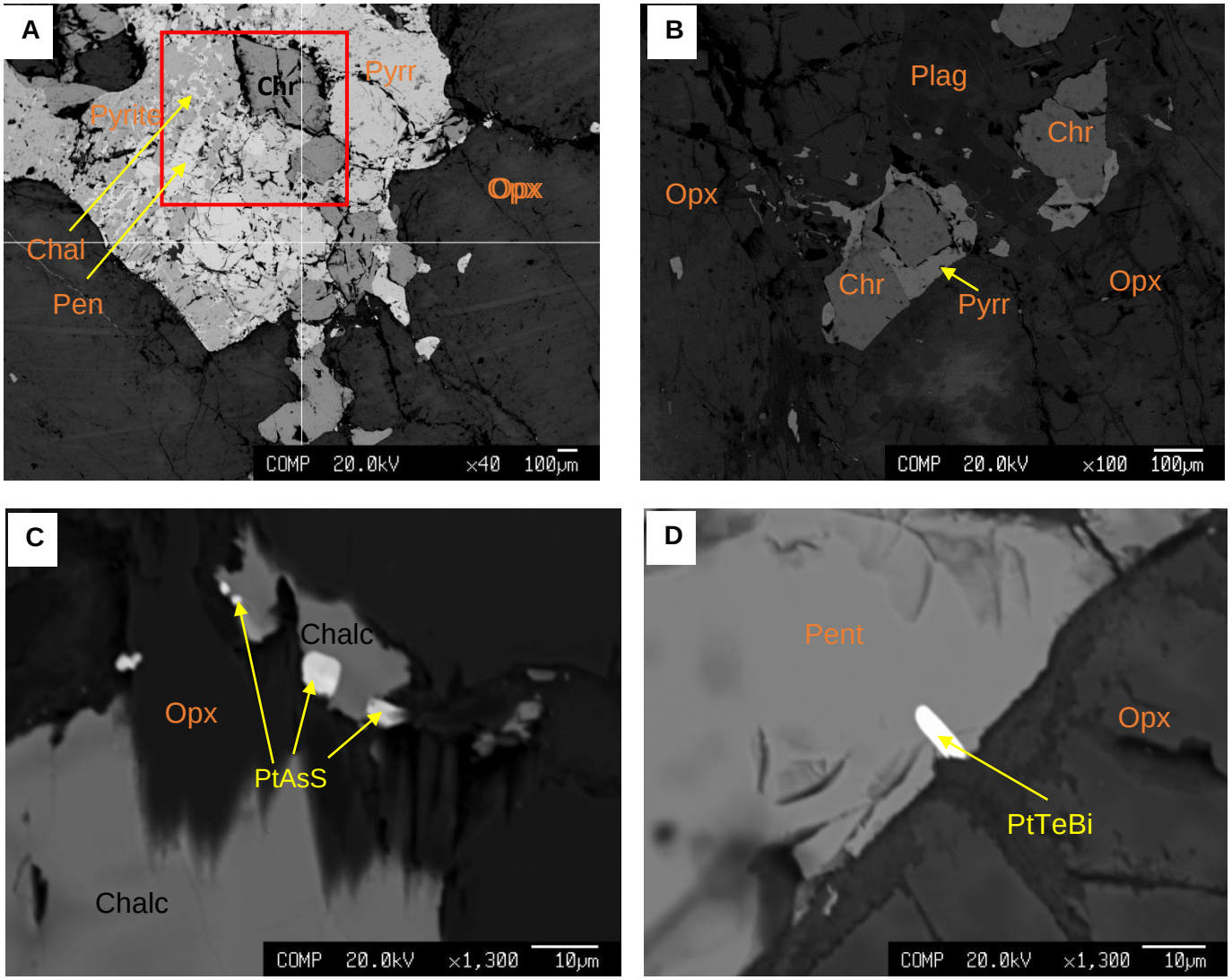

Figure 51: A and B) BSE images illustrating the association of BMS with oxides, mainly chromitite. C) BSE image showing the occurrence of platarsite found at the borders of chalcopyrite. D) BSE image of moncheite found typically at the borders of sulphides, pentlandite in this case.

A

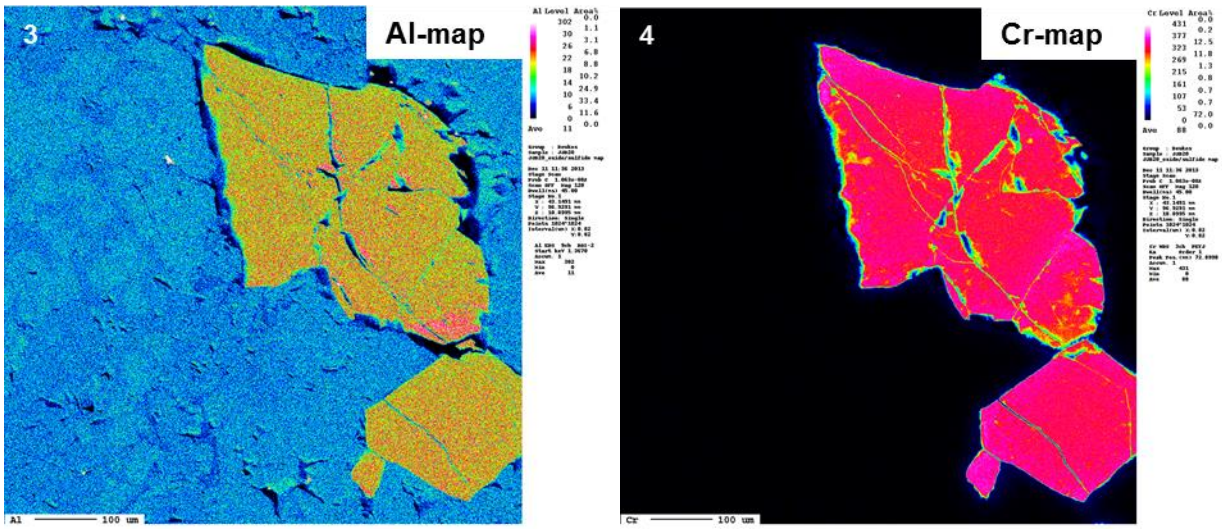

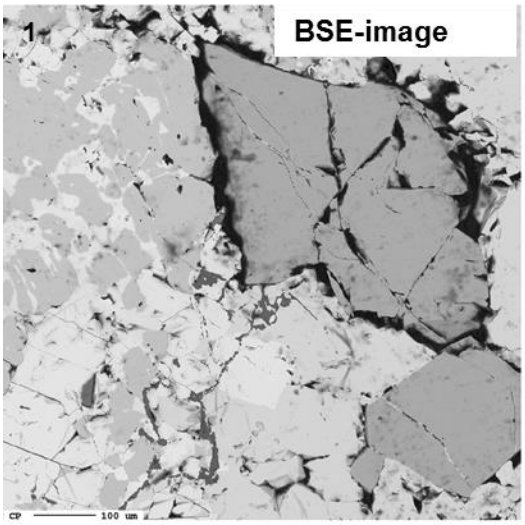
1
BSE-image
100 um

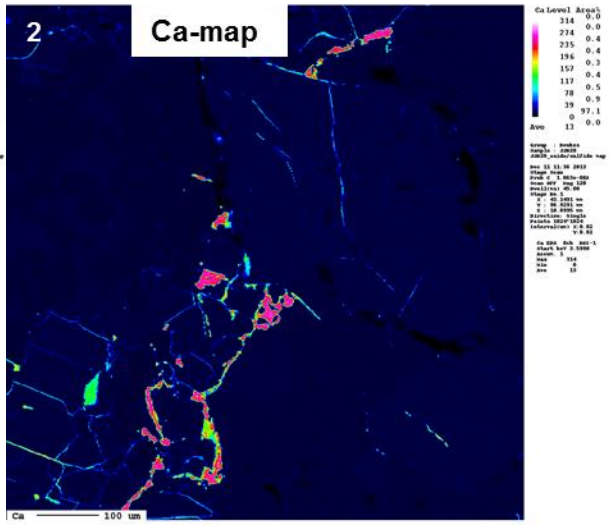
2
Ca-map
100 um

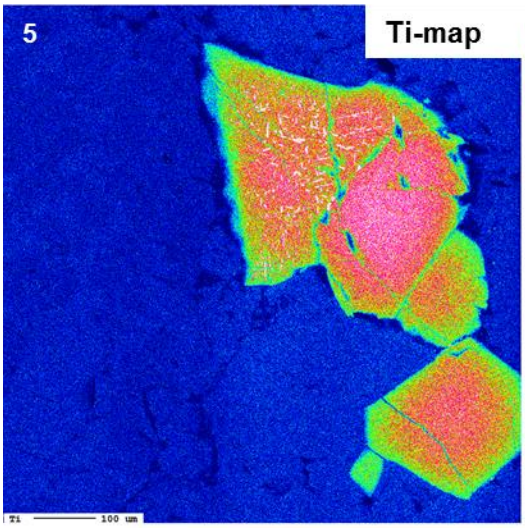
5
Ti-map
100 um

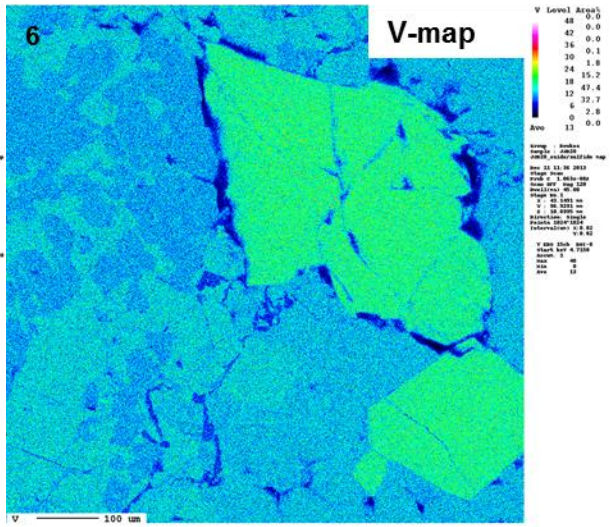
6
V-map
100 um

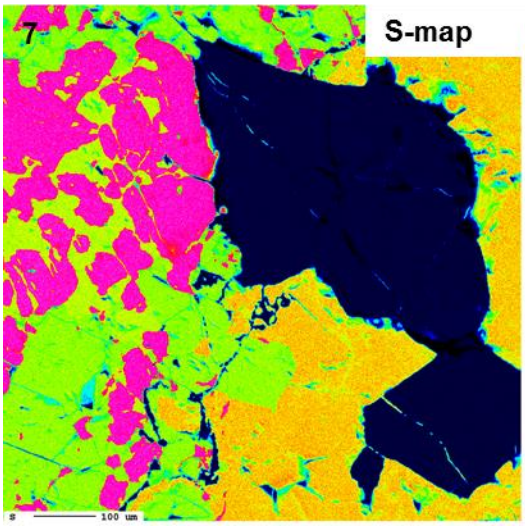
7
S-map
100 um

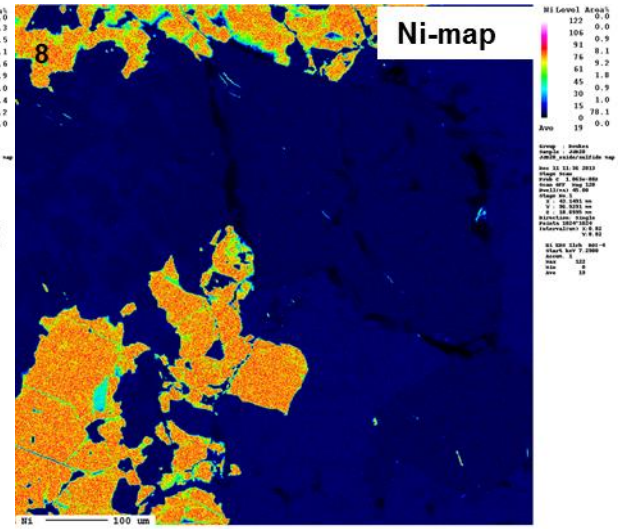
8
Ni-map
100 um

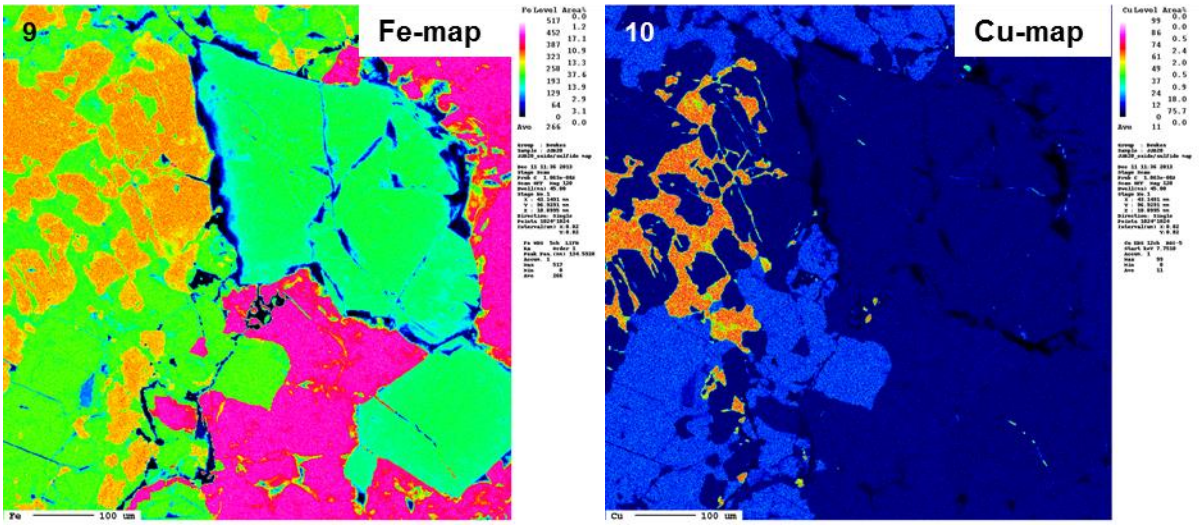

Figure 52: The above images are element distribution maps of the zoomed portion (red box in figure 51 A). Please note the the Ca-veins present in A-2 as well as the exsolution of titanium from the surface of the chromite in A-5. Chalcopyrite and pentlandite tend to display “sieve” or “net” like textures as they exsolved from pyrrhotite.

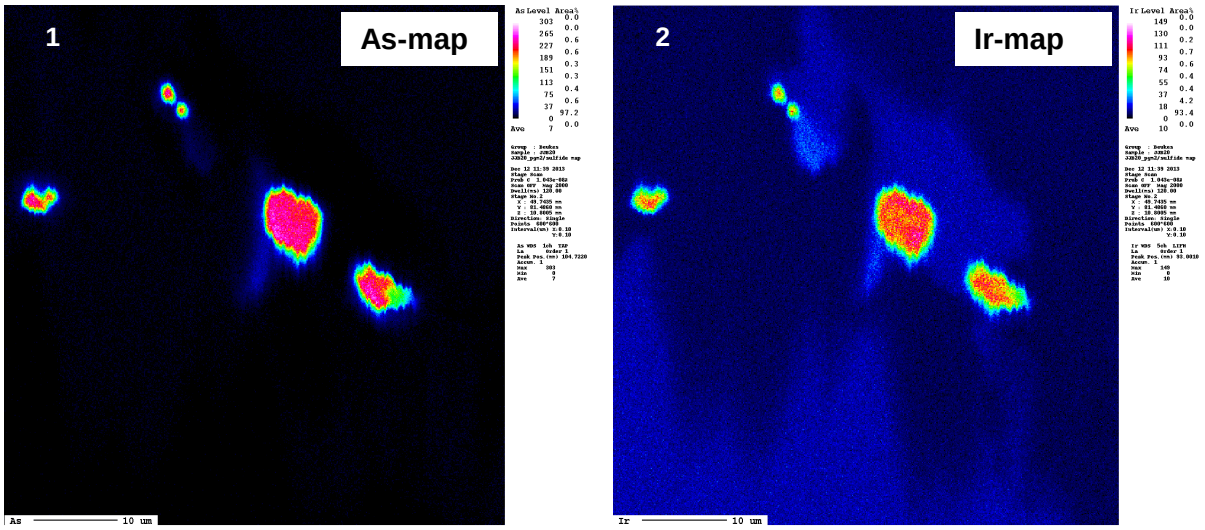

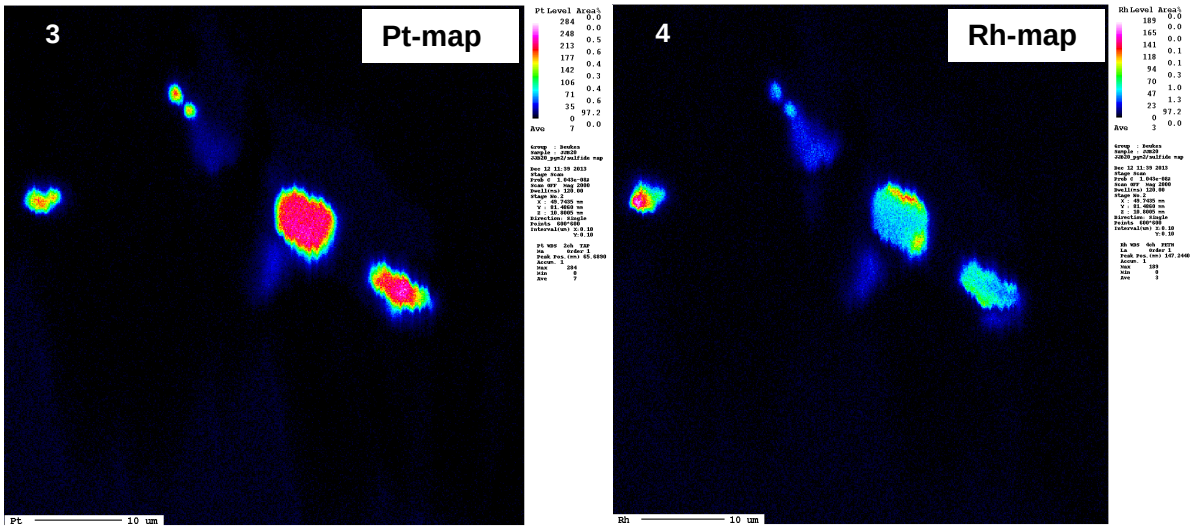

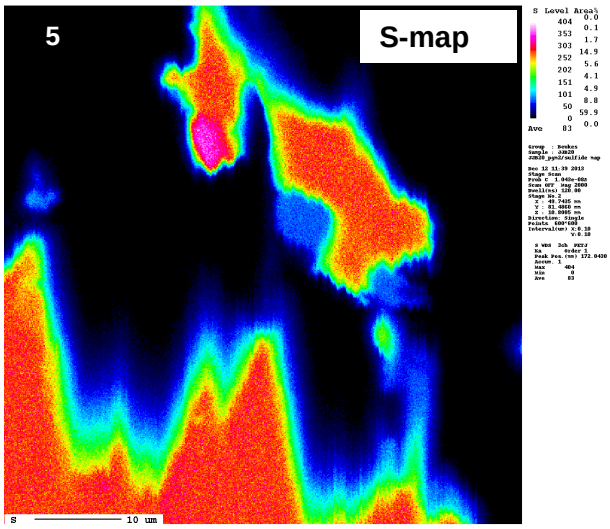

Figure 53: The above images (C1-5) are element distribution maps of platarsite in figure 51C. The elements As (C1), Ir (C2) and Pt (C3) are distributed evenly throughout the PGM. Rh appears to be enriched in only certain spots of the PGM.

4.6.3 BMS and PGM in BSN

The CT scanner image in figure 9b as well as the modal mineralogy in figure 19 shows that the BSN contains fewer sulphides than the TRP pyroxenite. Similarly relatively less if any PGM are present. Sulphides present in the BSN are mostly fine grained.

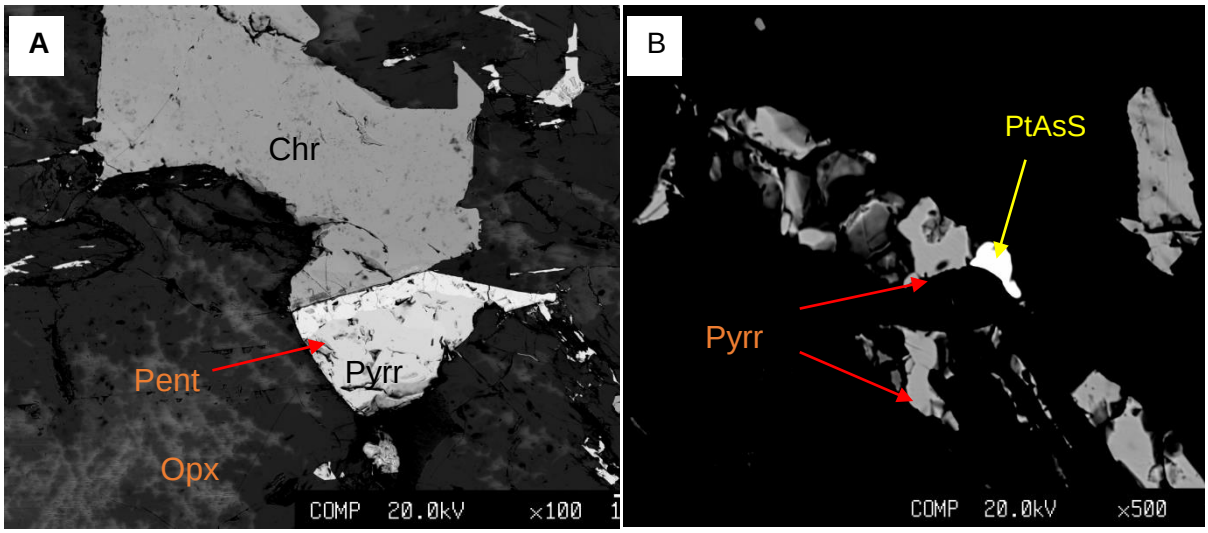

Figure 54: A) BSE image showing common occurrence of sulphides within the BSN. B) BSE image indicating platarsite associated here with pyrrhotite and chalcopyrite. The BSN may contain some BMS but it is relatively poor in PGMs or contains rather small PGM crystals making it difficult to analyse PGMs within the BSN.

4.6.4 Summary of BMS and PGMs

The dominant base metal sulphides are pyrrhotite, pentlandite, chalcopyrite and, to a lesser extent, pentlandite. These sulphides occur disseminated throughout the pyroxenite however it is more concentrated in close proximity to both upper and lower chromitite stringers. There is therefore an association of BMS with the silicates and oxides present. With that being said, it has been observed that the chromitite stringers themselves contain less BMS compared to the silicates in close proximity to the stringers. Figure 51 A and B shows that the chromites may be locked within the BMS or, as seen in figure 54 A, a sharp contact may be present between BMS and chromite. The grain size of the BMS present is very variable ranging from as small as 10 microns up to 8 mm in size. Relatively less concentration of BMS were found in the BSN compared to the surrounding MR pyroxenite.

Most of the PGMs found within the pyroxenite epoxy sections of TRP mine were strongly associated with the BMS than chromite crystals present and were found at the boundaries of the BMS or less commonly enclosed within the BMS. In figure 52A-2 Ca-rich veins are observed in between sulphide boundaries indicating late hydrothermal processes involving a Ca rich fluid. Certain chromite crystals display ilmenite exsolution lamellae (figure 52A-5, Ti-map) which are consistent with findings of UG2 chromite compositions by Junge et al. (2014).

Due to the extremely small size of the PGMs detected attention is only given to the crystals approximately 10 microns or larger in size. Similarly to the study done by Junge et al. (2014) majority of the PGMs detected in the epoxy sections rarely bear any Pd and Rh and are primarily Pt bearing. The absence of Pd and Rh within the PGMs detected may be due to the fact that these PGEs are present as solid solution within sulphide minerals, pentlandite in particular (Junge et al., 2014; Holwell and Macdonald, 2010; Godel et al., 2007). This correlates to the LA ICP-MS findings of the highest concentrations of Pd (ppm) measured within pentlandite; these findings are reviewed in the following sub-chapter.

It is believed that both a 'sulphide control' and a 'chromite control' played a role in the PGE enrichment in layered intrusions such as the BIC (Junge et al., 2014). Association of PGMs with secondary silicates is thought to represent redistribution of PGMs (Rose et al., 2011).

Interesting features have been observed for some of the PGMs detected in this study. Figure 47 C1-11 illustrates a Pt-rich "submarine" shaped moncheite. It appears that this PGM cut through pre-existing BMS causing what seems to be slight displacement of the BMS. This feature may be a product of later enrichment processes that occurred within the chamber. It is also noted that the plagioclase surrounding both the PGM and BMS shows Cl-alteration at the rims (Figure 47-C1) and suggests late alteration process. The redistribution of PGMs by late fluids as suggested by Rose et al., 2011, is thus likely. In figure 48 A, the "worm-like" moncheite has 'intruded' into the pyrrhotite as is inferred from its structure. One can assume that the moncheite flowed in from a direction on the left side of the BSE image. Zonation is observed in laurite (figure 48C). Pt is enriched in the tip of the PGM as seen in figure 50-C7 of Pt element distribution map. The cutting and intruding of PGMs into BMS (mainly pyrrhotite) as well as zonation of PGMs may indicate late magmatic processes. This implies that the PGEs were not scavenged by the sulphides but rather that the PGM crystallised directly from the silicate magma to form PGMs which imposed into/through earlier BMS. This characterization agrees with the formation process of PGM as suggested by Godel et al. (2007) and Barnes & Maier (2002a). Hence some of the PGMs detected were not found at the margins or enclosed within the BMS. Zonation of PGMs may indicate recrystallization during these late magmatic events. Another possibility for moncheite formation is that because moncheite has a lower thermal stability (<300°C) which is incompatible with the melt, the PGM may have precipitated (redistributed) from a hydrothermal fluid.

4.7 Base Metal Sulphides and PGE with LA ICP-MS

The base metal sulphides (BMS), i.e. pyrrhotite, pentlandite and chalcopyrite and to a lesser extent, pyrite, occur disseminated throughout the pyroxenite of the MR. The pyroxenite of the MR at TRP has more copious BMS in close proximity to the chromitite stringers. The chromitite are considered to be sulphur-poor (von Gruenewaldt et al., 1986). Sulphide saturation was most likely responsible for the formation of BMS and the scavenging of PGE at TRP in the Merensky Reef at TRP and in the Western Limb (Teigler & Eales, 1993 and Rose et al., 2011). Sulphur saturation at the MR is also conducive of relatively high-sulphur magmas entering the chamber as the BIC evolved with time (Teigler & Eales, 1993).

4.7.1 LA ICP-MS investigation of base metal sulphides in TRP-272 drill core

Polished thick sections of three samples from borehole TRP-272 were sent to the Geochemistry lab at the University of Cardiff in Wales London for LA ICP-MS analysis of the BMS. Two of the samples, AL7909A and AL7909B, were located near the top chromitite stringer and sample AL7916 was located near the bottom chromitite stringer of the MR. In both borehole as well as other underground samples of the MR pyrrhotite is by far the most abundant sulphide mineral followed by pentlandite and chalcopyrite. The following elements S, Se, Fe, Cu, Zn, As, Cd, Sb, Te, Re, Au, Bi and the IPGEs and PPGEs were measured in the BMS of the samples. Due to isotopic interference, for quantification ^{99}Ru was used instead of ^{101}Ru and ^{106}Pd rather than ^{105}Pd or ^{108}Pd. The average PGE concentrations of the samples measured are displayed in table 9 and the detection limits in table 10.

Table 9: Average PGE concentrations in total BMS of TRP-272 drill core samples.

	Os	Ir	Ru	Rh	Pt	Pd	Au
Pentlandite	**4.39**±2.72	**4.07**±2.43	**31.13**±24.64	**22.74**±42.99	**1.31**±1.43	**206.49**±79.77	**0.08** ±0.09
n	*35*	*36*	*36*	*36*	*33*	*36*	*16*
Pyrrhotite	**2.36**±1.8	**1.77**±1.61	**12.73**±16.21	**0.41**±0.44	**0.76**±0.92	**4.32 ±5.12**	**0.03** ±0.02
n	*31*	*31*	*29*	*14*	*27*	*17*	*9*
Chalcopyrite	**2.26**±2.38	**1.43**±1.62	**4.22**±6.92	n.d	**0.14**±1.4	**12.12**±15.53	**0.43** ±0.38
n	*3*	*4*	*5*		*4*	*3*	*7*

Table 10: Detection limit for analysis of BMS by LA-ICP-MS carried out at the University of Cardiff.

	Lower limit of detection						
	Os	**Ir**	**Ru**	**Rh**	**Pt**	**Pd**	**Au**
Pentlandite	<0.02	<0.02	<0.05	<0.1	<0.02	<0.15	<0.01
Pyrrhotite	<0.02	<0.02	<0.05	<0.1	<0.02	<0.15	<0.01
Chalcopyrite	<0.02	<0.02	<0.05	<0.1	<0.02	<0.15	<0.01

LA ICP-MS measurements/analyses of BMS Pentlandite in the 3 MR samples contains the highest concentrations of PGE (the most abundant being Pd with concentrations varying from approximately 102 to 400ppm) whereas relatively low concentration of PGEs were observed for pyrrhotite and chalcopyrite (as depicted in figure 55). Pd values in pentlandite vary from less than 0.15 to more than 200ppm and less than 0.11 to 30ppm for pyrrhotite and chalcopyrite respectively. Concentrations of Pt are range from less than 0.01 to about 6ppm in pentlandite. Pyrrhotite contains from less than 0.01 to 4ppm and chalcopyrite from less than 0.01 to 3ppm Pt.

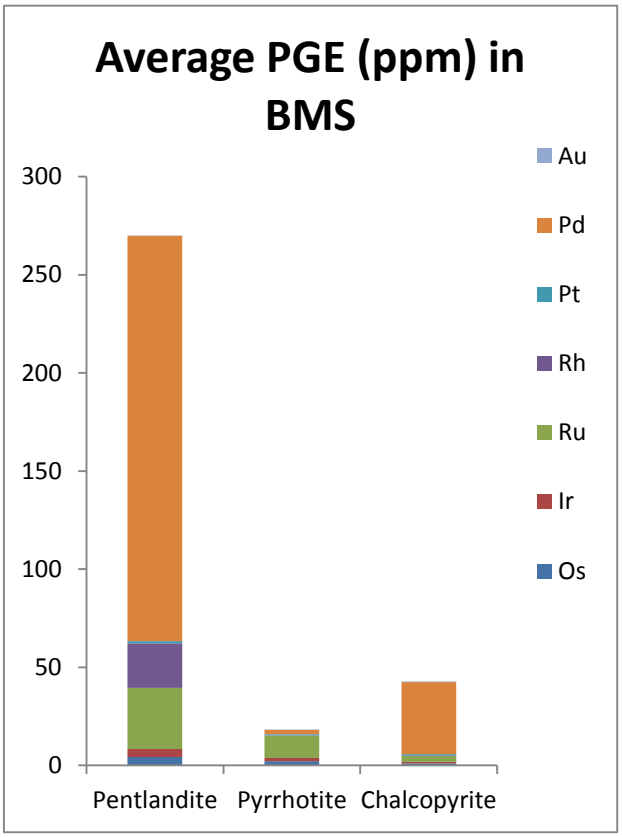

Figure 55: Average PGE (ppm) in pentlandite, pyrrhotite and chalcopyrite.

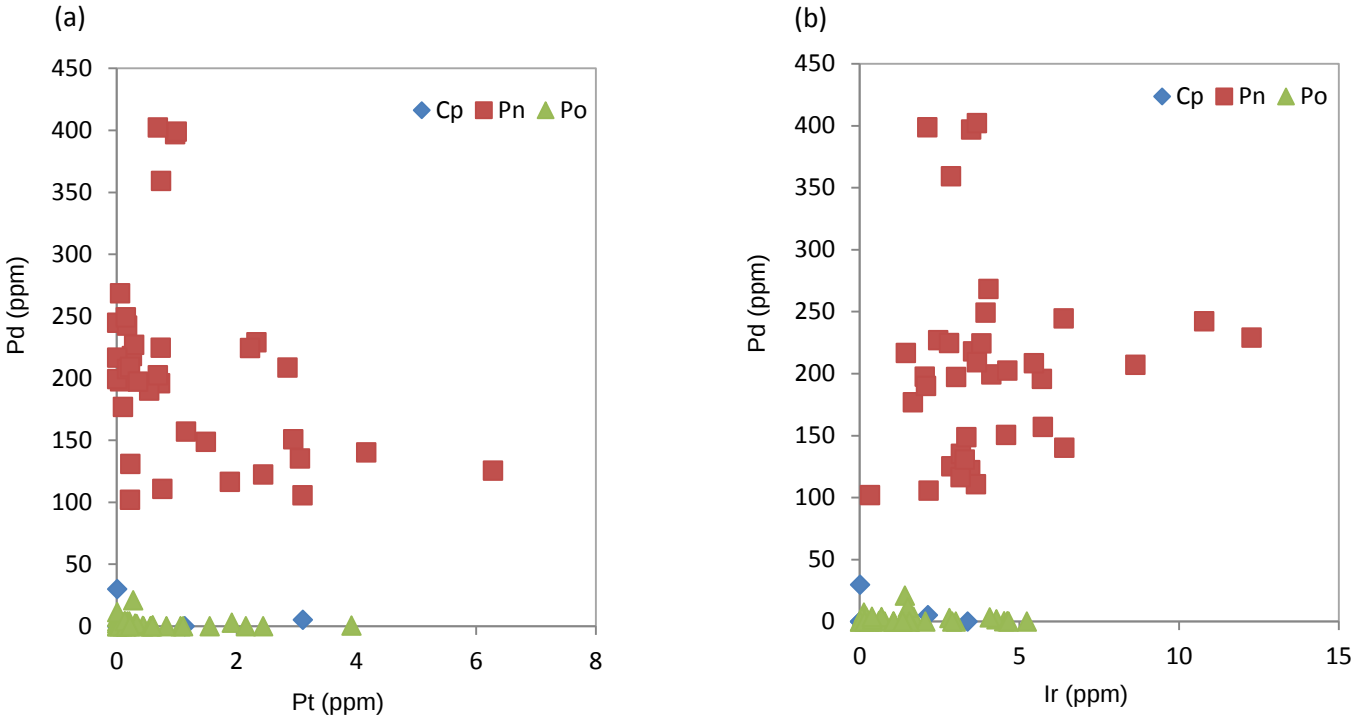

Figure 56: Binary diagrams showing a) Pd vs. Pt and b) Pd vs. Ir for chalcopyrite, pentlandite and pyrrhotite.

As seen in figure 56a no correlation exists between platinum and palladium, neither for chalcopyrite, pyrrhotite nor pentlandite. It appears that Pd is chiefly partitioned into pentlandite, whereas chalcopyrite and pyrrhotite show only minor concentrations. No correlation between Pt and other metals have been observed. Two positive trends are observed between Pd and Ir of pentlandite (figure 56b). A negative trend is observed for the same elements in chalcopyrite whereas in pyrrhotite, no trend is distinguished (figure 56b).

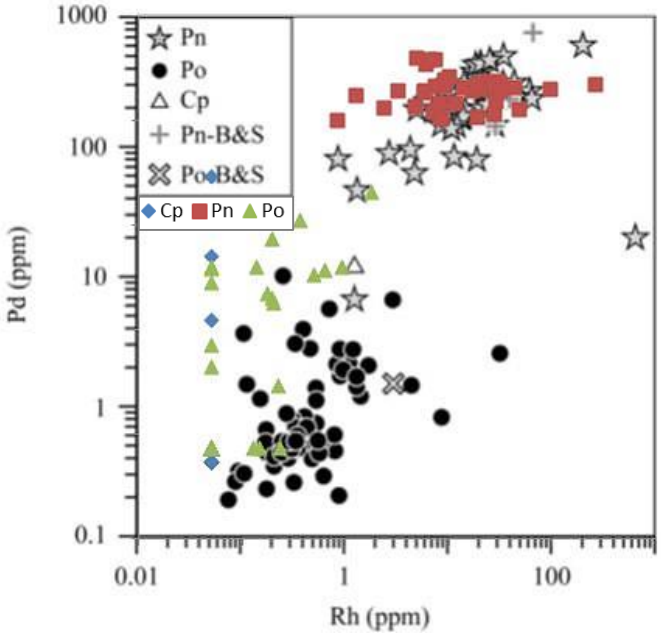

Figure 57: Binary variation diagram of Pd vs. Rh. Data compared to Godel et al.'s (2007) who added data obtained from Ballhaus & Sylvester (2000) for comparison (Pn-B&S, i.e. pentlandite analysed by Ballhaus & Sylvester and Po-B&S, i.e. pyrrhotite analysed by Ballhaus & Sylvester)

In figure 57 to 10 LA-ICP-MS BMS data of the TRP is compared to LA-ICP-MS BMS data from Godel et al. (2007) for some elements, the authors also compared their data to Ballhaus & Sylvester, 2000, ('Pn-B&S' and 'Po-B&S' for pentlandite and pyrrhotite respectively). The Rh values correspond to those of Godel et al. (2007). Rh values are highest in pentlandite varying between 0.81 to 252ppm, figure 57. In pyrrhotite they are lower varying between less than 0.1 to about 2ppm whereas in chalcopyrite only values at detection limit of Rh is observed. However, compared to the data of the other authors, TRP pyrrhotite has a higher Pd concentration than that of the Rustenburg Platinum Mine (RPM).

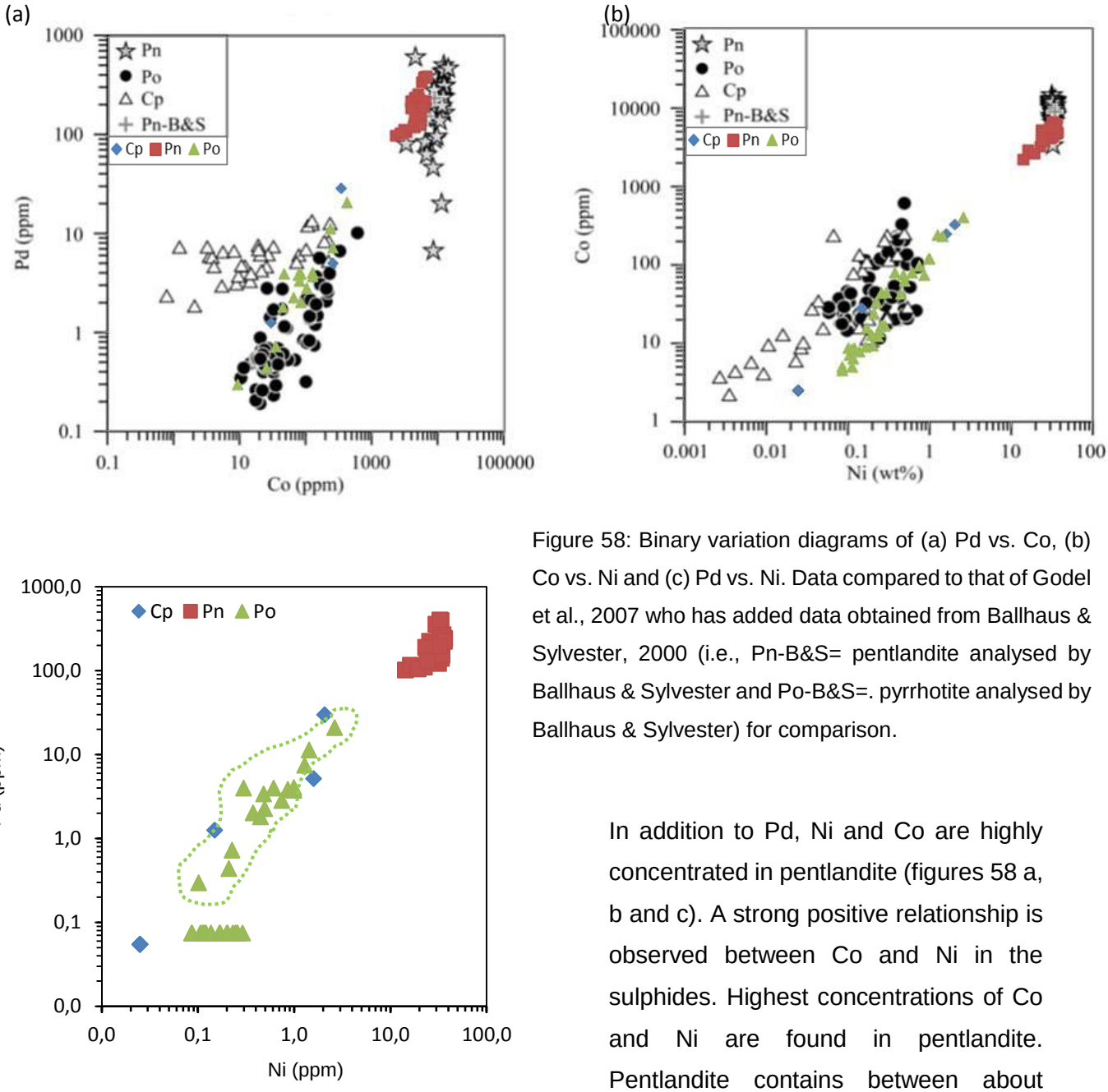

Figure 58: Binary variation diagrams of (a) Pd vs. Co, (b) Co vs. Ni and (c) Pd vs. Ni. Data compared to that of Godel et al., 2007 who has added data obtained from Ballhaus & Sylvester, 2000 (i.e., Pn-B&S= pentlandite analysed by Ballhaus & Sylvester and Po-B&S=. pyrrhotite analysed by Ballhaus & Sylvester) for comparison.

In addition to Pd, Ni and Co are highly concentrated in pentlandite (figures 58 a, b and c). A strong positive relationship is observed between Co and Ni in the sulphides. Highest concentrations of Co and Ni are found in pentlandite. Pentlandite contains between about 2200 and about 6700ppm Co and between about 14 and 37 wt. % Ni. Pyrrhotite has approximately 0.1 to 3wt. % and about 5 to 410ppm Co. Two trends are observed for pyrrhotite. The negative trend where Ni and Pd concentrations are variable is from pyrrhotite found in sulphide bearing MR pyroxenite located in close proximity to the top chromitite stringer. The other homogenous trend is associated with the below LLD concentration of Pd in pyrrhotite which is < 0.15 ppm found in MR pyroxenite located close to the bottom chromitite stringer. Chalcopyrite has the lowest concentrations of Ni and Co, with Ni varying between less than 0.05 and about 2wt. % and Co of between 5 and about 330 ppm. As seen in figure 58c, the Ni concentration increases with an increase of Pd.

Positive correlations exist for the IPGE of pentlandite and pyrrhotite (figure 59 a, b and c). Pentlandite has between less than 0.01 and about 12ppm Os. Pyrrhotite Os values vary between less than 0.01 to about 6ppm. Os values in chalcopyrite range between less than 0.01 and approximately 5ppm. Ir values in pentlandite are between about 0.32 and 12ppm, 0.01 and 5ppm in pyrrhotite and less than 0.01 and 3ppm in chalcopyrite. Pentlandite has Ru concentrations varying between 0.60 and 94ppm. Concentrations of between less than 0.06 and 48ppm and less than 0.06 and 16ppm are observed for pyrrhotite and chalcopyrite respectively. Re concentrations in the BMS are low and partitioned chiefly in pyrrhotite and pentlandite (figure 59d). Two positive trends are observed for Re or lower Ir concentrations in pyrrhotite and one positive trend or higher Ir concentrations for pentlandite. Re has a range of below detection limit (<0.02) to 0.7ppm for pentlandite and up to about 2ppm in pyrrhotite. Chalcopyrite contains concentrations lower than the detection limit which is <0.02 ppm with a maximum of 0.2ppm Re.

(a)

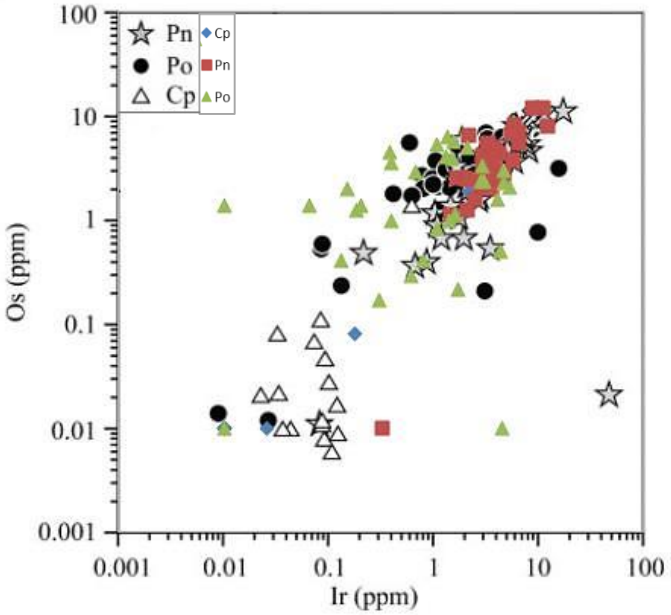

(b)

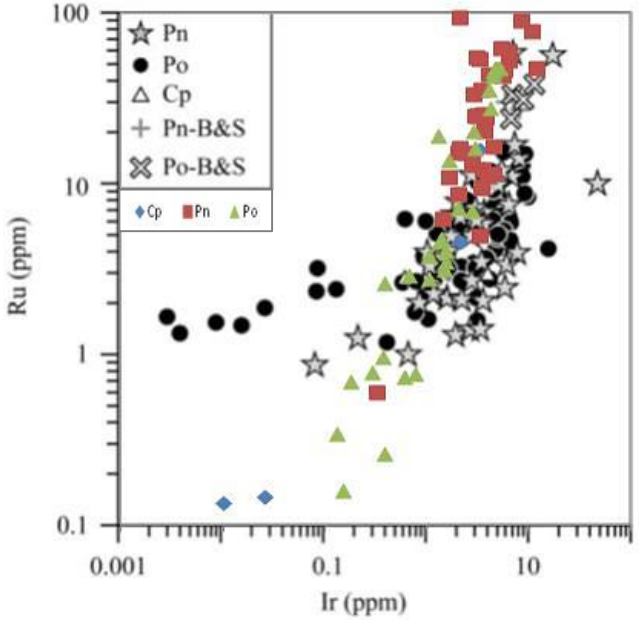

(See caption on next page)

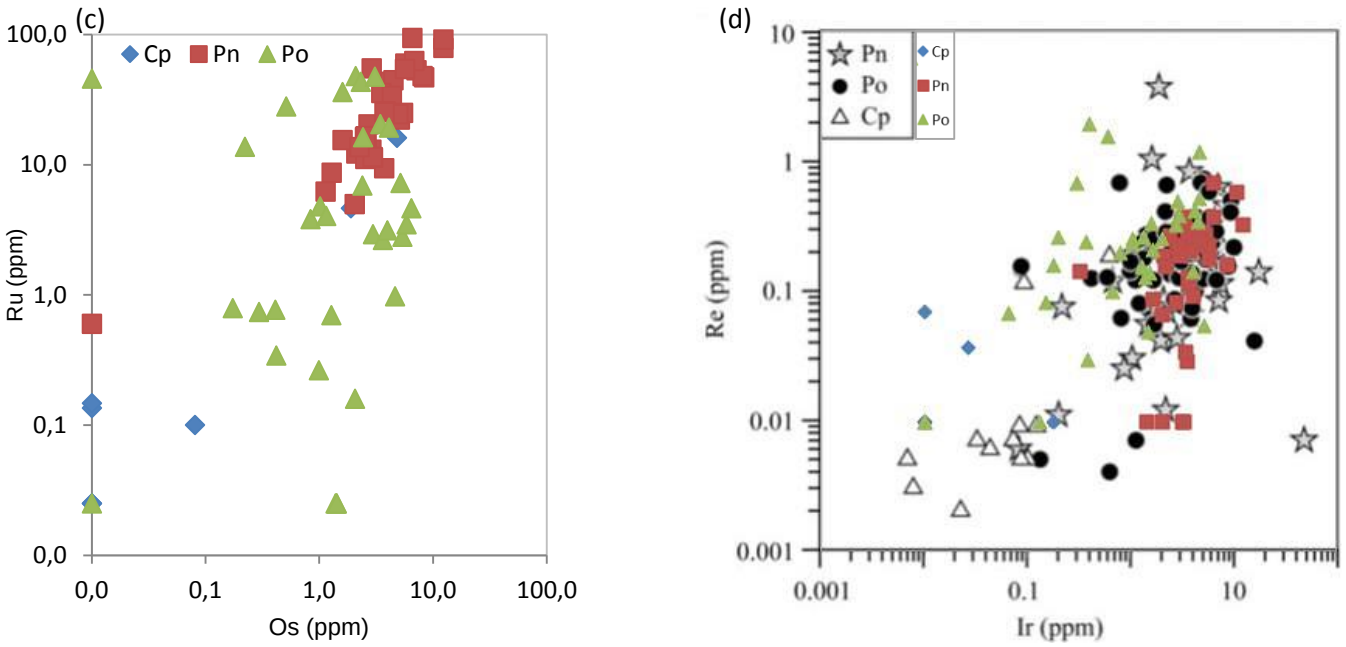

Figure 59: Binary variation diagrams of (a) Os vs. Ir, (b) Ru vs. Ir, (c) Ru vs. Os and (d) Re vs. Ir. Data obtained from Godel et al., 2007 were added for comparison (Godel et al., 2007 included data from Ballhaus and Sylvester 2000 i.e. Pn-B&S = pentlandite analysed by Ballhaus & Sylvester and Po-B&S= pyrrhotite analysed by Ballhaus & Sylvester, for comparison.)

Cu values in Figure 60 below detection limit has been replaced by half detection limit. The concentrations of Cd of the TRP BMS are much lower than that of the RPM (Godel et al., 2007) as seen in figure 60a. In figure 60b, a higher concentration of Au is found in chalcopyrite ranging between 0.04 to 1.08ppm. Au values between <0.01 to 0.35ppm and <0.01 to 0.07ppm are observed for pentlandite and pyrrhotite respectively.

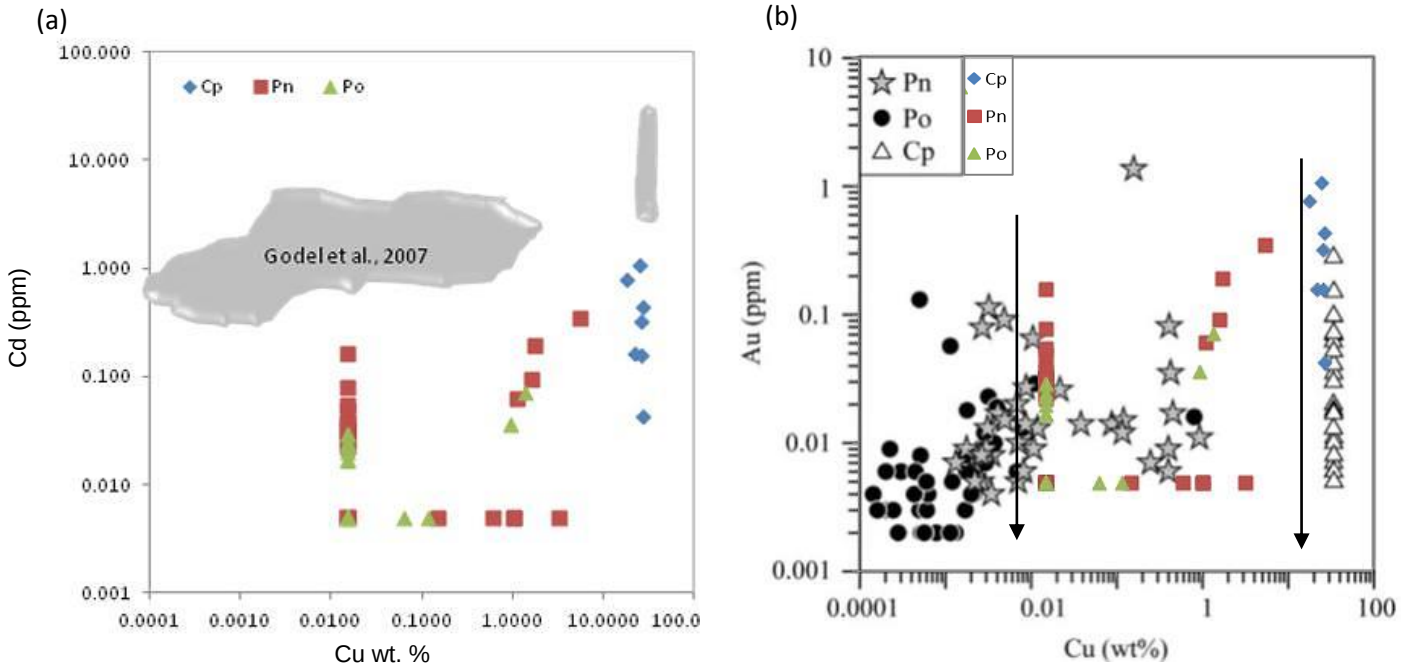

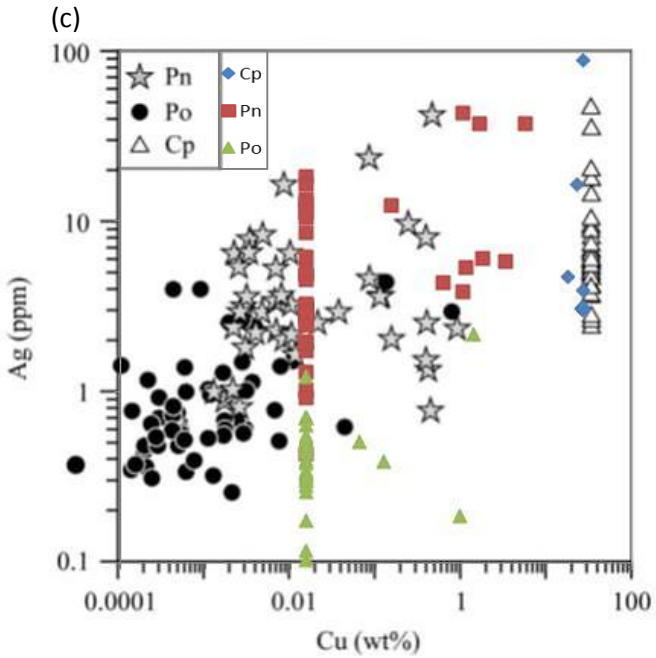

Figure 60: Binary variation diagrams of (a) Cd vs. Cu, (b) Au vs. Cu and (c) Ag vs. Cu. Data obtained from Godel et al., 2007 were added for comparison (Godel et al., 2007 included data from Ballhaus and Sylvester 2000 i.e. Pn-B&S= pentlandite analysed by Ballhaus & Sylvester and Po-B&S= pyrrhotite analysed by Ballhaus & Sylvester, for comparison.)

A similar situation can be reported for Cd with values of 2 to 12ppm in chalcopyrite, whereas a detection limit less than 0.8ppm exists for pentlandite (with an exception of 4 values) and pyrrhotite. It is difficult to identify correlations or trends between Cu and Cd, Au, and Ag due to the fact that mostly detection limit of Cu were observed in pentlandite and pyrrhotite. In figure 60c it can be seen that highest concentrations of Ag are found in chalcopyrite and pentlandite. Chalcopyrite contains Ag concentrations between approximately 3 to 88ppm. Pentlandite has about 0.4 to 43ppm Ag and pyrrhotite has less than 0.1 to about 2ppm Ag. The vertical distribution of Cu in figure 60 b and c depicts the normal concentration of Cu in chalcopyrite and below detection limit concentrations in pyrrhotite and pentlandite plotted on a log scale to display possible trends for Cu versus Au or Ag in the pyrrhotite and pentlandite.

A Fe enriched monosulphide solid solution (MSS) and a Cu enriched liquid are the products of the evolution of Fe-Ni-Cu sulphide liquid (Kullerud et al., 1969; Naldrett, 1989). Pt and Pd are incompatible in MSS (Ballhaus et al., 2001); however, concentrations of Pt and Pd in pyrrhotite have been noted in this study. The IPGE, Rh and Re are highly compatible in the Fe-rich Mss however Cu, Pt, Pd, Ag, Au, Cd and Zn were found to be highly compatible in the Cu-rich fractionated liquid (Lee, 1996; Barnes et al., 2001; Mungall et al., 2005).

The Cu-rich fractionated liquid crystallizes as intermediate solid solution (Iss) and minor Ni-rich Mss forming by exsolution chalcopyrite and cubanite whereas Mss exsolve into pyrrhotite and pentlandite at temperatures <600°C (Godel et al., 2007). At high temperatures Mss can dissolve PGE whereas at lower temperatures PGM exsolve (Makovicky et al., 1986).

It is proposed that if no redistribution of the elements occurred it is expected that Os, Ir, Ru, Rh and Re would be concentrated in the Mss products (i.e. pentlandite and pyrrhotite) and that the residual elements would therefore be enriched in chalcopyrite (Holwell and McDonald, 2007, and Godel et al., 2007). For the TRP BMS it is evident that the highest concentrations of Pt and Pd are found in pentlandite and not in chalcopyrite as is expected. It is believed that during the exsolution of pentlandite from Mss, Pd, Co and Ni partitioned into pentlandite (Godel et al., 2007). The results stated here seem to confirm this notion.

PGE inclusions within the BMS of the MR have been interpreted by Ballhaus & Sylvester (2000) as being obtained from “PGM-nuggets” that crystallized from the magma preceding sulphide saturation and which were included in the sulphide liquid once sulphide liquid saturation had been reached. Not denying the possibility of PGM being saturated in the magma prior to BMS liquid forming, Barnes et al. (2008) suggest that the inclusions formed by exsolution and that this preservation of BMS would seem unlikely given that extensive recrystallization of BMS occurred when pentlandite, pyrrhotite and chalcopyrite were exsolved.

4.7.2 LA ICP-MS analyses of base metal sulphides in EST drill core and TRP underground exposure

This subchapter focuses on LA ICP-MS analyses of BMS carried out at the Laboratory of Radiogenic Isotopes, Czech Geological Survey, Prague. The elements; Os, Ir, Ru, Rh, Pd, Pt, Au and Re were analysed in the pyroxenite of the Merensky interval at Two Rivers Platinum and Eerste Geluk.

PGE-enriched formed as an immiscible sulphide liquid that exsolved from mafic to ultramafic magma (Barnes et al., 2008; Holwell and McDonald, 2010). IPGEs (osmium, iridium and ruthenium), Rh and Ni are compatible in MSS (monosulphide solid solution) whereas palladium, platinum and gold are incompatible in the MSS (Zientek, 2012). The average PGE concentrations and standard deviations in the total BMS of the samples are given in table 11 as well as the detection limits in table 12. As with the TRP-272 samples, LA ICP-MS analyses show that the pentlandite contains a higher concentration of PGEs relative to pyrrhotite and chalcopyrite (figure 61 a & b and table 11). Pd, in particular, is the most dominant PGE present in the sulphides with concentrations ranging between 0.5 to 428 ppm. Pd concentration in pyrrhotite was below detection limit. Due to the low concentrations and peak overlaps with BMS of Ru and Rh, Ru was not calculated for pentlandite in some samples and Rh not calculated for chalcopyrite.

a)

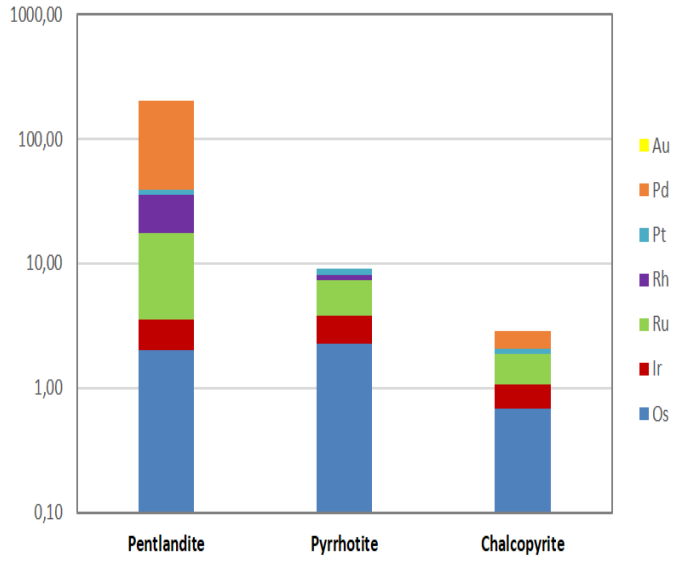

b)

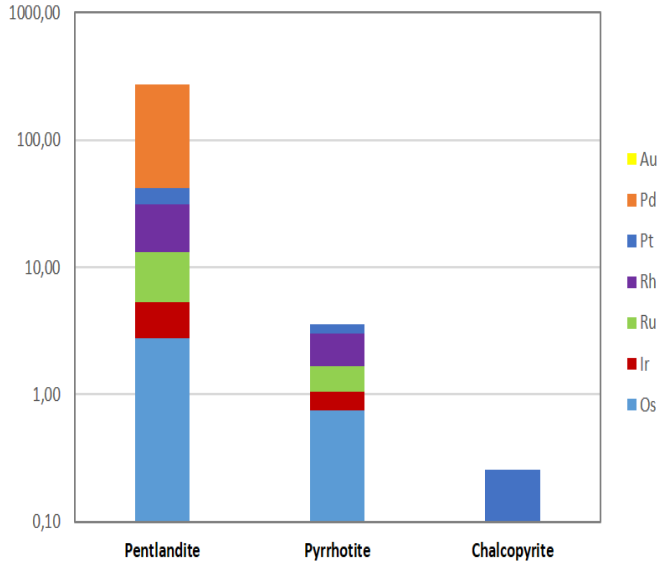

Figure 61: Average PGE concentrations in BMS from the a) TRP underground exposure samples and b) EST drill core sample,

Table11: Average PGE concentrations in the total BMS from the EST drill core sample and TRP underground exposure samples.

	Os	Ir	Ru	Rh	Pt	Pd	Au
Pentlandite	**2.14**±2.26	**1.68**±1.77	**12.65**±15.98	**18.32**±31.91	**4.69**±5.09	**175.2**±89.88	**n.d**
n	*46*	*46*	*44*	*48*	*42*	*48*	*n.d*
Pyrrhotite	**2.08**±1.92	**1.38**±1.82	**3.37**±5.94	**0.88**±1.18	**0.79**±1.33	**n.d**	**n.d**
n	*55*	*57*	*51*	*33*	*52*	*n.d*	*n.d*
Chalcopyrite	**0.68**±1.08	**0.33**±0.51	**0.82**±1.35	**n.d**	**0.18**±0.20	**0.83**±0.44	**n.d**
n	*4*	*6*	*13*	*n.d*	*20*	*2*	*n.d*

Table 12: Detection limit for the analysis of the base-metal sulphides by LA-ICP-MS.

	Lower limit of detection						
	Os	**Ir**	**Ru**	**Rh**	**Pt**	**Pd**	**Au**
Pentlandite	<0.02	<0.02	<0.05	<0.1	<0.02	<0.15	<0.01
Pyrrhotite	<0.02	<0.02	<0.05	<0.1	<0.02	<0.15	<0.01
Chalcopyrite	<0.02	<0.02	<0.05	<0.1	<0.02	<0.15	<0.01

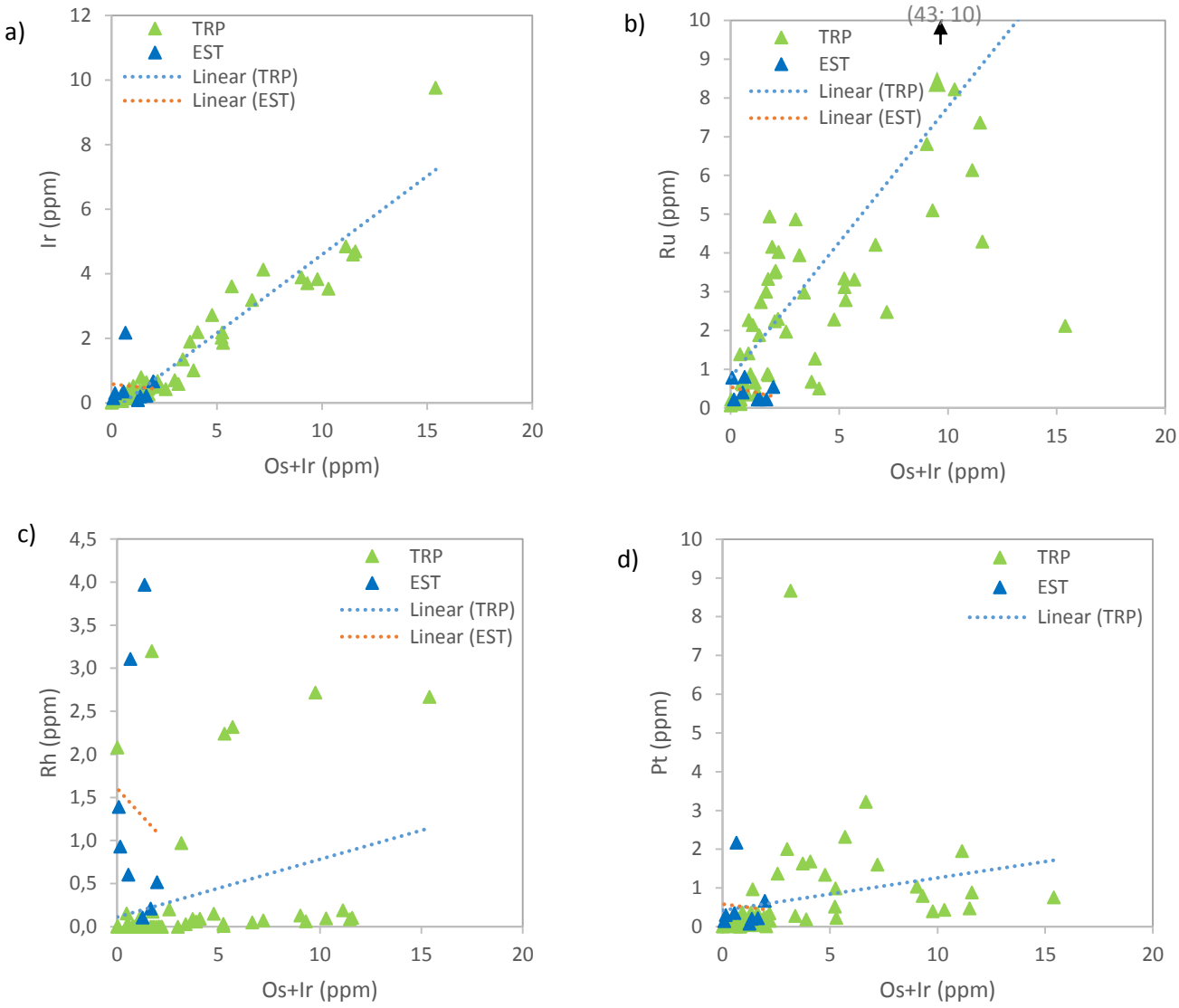

Figure 62: PGE concentrations in pyrrhotite crystals (ppm) of all samples (TRP and EST) analysed by LA ICP-MS. Note half IDL max was used to replace LLD.

In figures 62 and 63 (a & b), a positive correlation is observed for Ir and Ru vs. Os+Ir at TRP. A slightly negative linear trend is observed for EST pyrrhotite (figure 62 a and b). Ir at TRP ranges between 0.02 and 9.75 ppm in pyrrhotite and between 0.11 and 7.60 ppm in pentlandite. It can be seen that no preference for a specific sulphide is displayed by these PGE concentrations. At EST Ir ranges between 0.05 and 0.54 ppm in pyrrhotite and 0.041 and 6.25 ppm in pentlandite. Ir is therefore more enriched in pentlandite. Pyrrhotite has Ru concentrations between 0.16 and 42.7 ppm whereas Ru concentrations in pentlandite where calculated are much higher ranging between 0.95 and 58.5 ppm at TRP (figure 62b and 63b). Ru concentrations in pyrrhotite and pentlandite at EST ranges between b.d.l - 0.80 ppm and 2.27- 19.9 ppm at EST. Opposite trends

are noted for Rh in pyrrhotite of TRP & EST and a positive trend in pentlandite as an increase in Rh with an increase in Os+Ir is observed for some of the measurements in both TRP and EST (figures 62c and 63c). The Rh in pyrrhotite vary between 0.03 and 3.97 ppm and between 0.06 and 165.20 ppm in pentlandite at TRP (figures 62c and 63c). Pt display slight if any correlation with PGEs in pyrrhotite (figure 62d) and pentlandite (figure 63d). The behaviour of the IPGEs and Rh in pyrrhotite and pentlandite, which are the products of MSS, can be explained by their compatibility in MSS and incompatibility in the residual Cu-rich sulphide melt (Barnes et al., 2006, Barnes et al., 2008 and Holwell & McDonald, 2010).

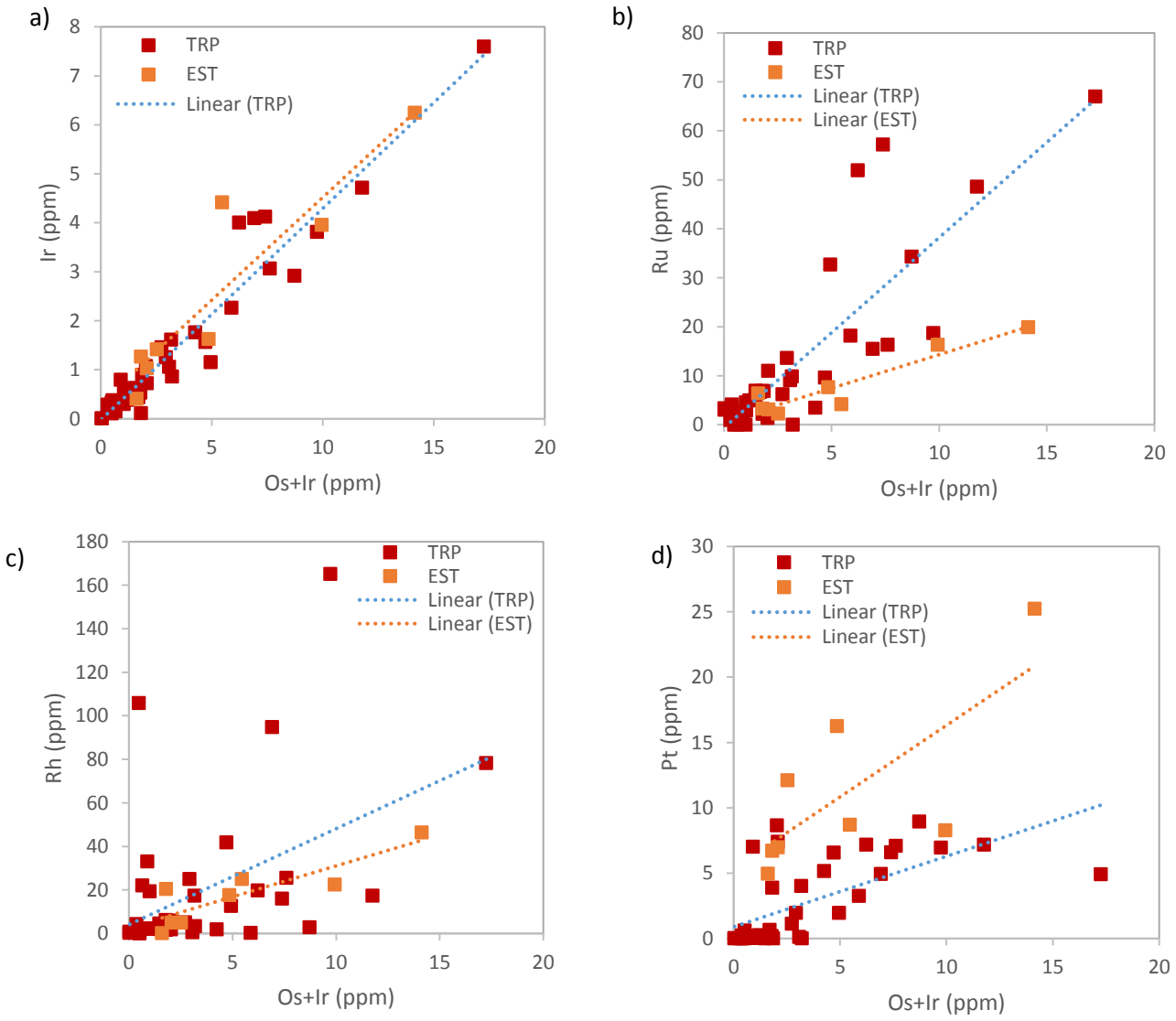

Figure 63: PGE concentrations in pentlandite (ppm) of all samples (TRP and EST) analysed by LA ICP-MS. Trend lines included. Note half IDL max was used to replace LLD.

The averages of PGE as seen in tables 13 and 14 shows that PGE concentration is higher in pentlandite than in pyrrhotite in pyroxenite, brown sugar norite as well as in the chromitite stringer. The highest Pt content in pyrrhotite is found at the chromitite stringer (JJB19.1) with a maximum concentration of 8.67 ppm. The IPGE concentrations in pyrrhotite are lower than 10 ppm however an anomalous 42.7 ppm has been reported for Ru in pyrrhotite of sample JJB 10 which is a pyroxenite in close proximity to the bottom chromitite stringer. Pd is not detected in the pyrrhotite of any of the samples. Concentrations of Rh are below detection limit for pyrrhotite of brown sugar norite and also of JJB7, a pyroxenite. In pentlandite, the highest Pt concentration is found in the pyroxenite of Eerste Geluk (sample EST013) ranging between 5 and 25.3 ppm with an average of 11.17 ppm. The highest Pd concentrations are found in the pyroxenite of sample JJB 10 with an average of 316 ppm varying between 236 and 428 ppm. Contrary to what is expected, it appears that the PGE are more enriched in the BMS found in the pyroxenite relative to the BMS found in the chromitite stringer.

Table 13: Average PGE concentrations (in ppm) in pyrrhotite of the different samples from the Merensky interval underground exposure and drill core sample, EST013_16. Rock type pxt=pyroxenite, bsn=brown sugar norite, mln=melanorite and chr=chromitite stringer

Average PGE concentrations (in ppm) in pyrrhotite					
Samlple	**JJB3**	**JJB4**	**JJB7**	**JJB10**	**JJB18a**
n	6	7	6	9	6
Rock Type	pxt	pxt	pxt	pxt	bsn
Os	**1.85** ±0.3	**0.4** ±0.1	**3.42** ±1.3	**5.54** ±1.5	**1.16** ±0.5
Ir	**1.75** ±1.7	**0.42** ±0.2	**4.33** ±1.5	**3.55** ±1.3	**0.38** ±0.2
Ru	**1.74** ±1.1	**1.6** ±0.8	**2.87** ±0.6	**9.41** ±12.7	**2.21** ±0.8
Rh	**0.09** ±0.1	**n.d**	**1.44** ±1.3	**0.63** ±1.1	**n.d**
Pt	**1.23** ±0.7	**0.35** ±0.4	**1.24** ±0.7	**0.71** ±0.6	**0.26** ±0.1
Pd	**n.d**	**n.d**	**n.d**	**n.d**	**n.d**
Samlple	**JJB18c**	**JJB19,1**	**JJB20**	**EST013_16**	
n	6	3	8	8	
Rock Type	bsn	chr	pxt	mln	
Os	**1.46** ±0.4	**1.66** ±1.2	**1.34** ±1.02	**0.75** ±0.5	
Ir	**0.57** ±0.1	**0.41** ±0.2	**0.54** ±1.07	**0.3** ±0.2	
Ru	**3.97** ±0.8	**2.96** ±1.4	**0.96** ±1.40	**0.63** ±0.2	
Rh	**n.d**	**0.59** ±0.5	**0.74** ±1.38	**1.36** ±1.4	
Pt	**0.5** ±0.7	**3.43** ±4.6	**0.49** ±1.20	**0.52** ±0.7	
Pd	**n.d**	**n.d**	**n.d**	**n.d**	

Table 14: Average PGE concentrations in pentlandite of the different samples from the Merensky interval underground exposure and drill core sample, EST013_16. Rock type pxt=pyroxenite, bsn=brown sugar norite, mln=melanorite and chr=chromitite stringer

Average PGE concentrations (in ppm) in pentlandite					
Sample	**JJB3**	**JJB4**	**JJB7**	**JJB10**	**JJB18a**
n	4	6	4	6	6
Rock Type	pxt	pxt	pxt	pxt	bsn
Os	**3.51**±2.6	**0.50**±0.4	**3.44**±1.6	**2.91**±2.2	**0.52**±0.6
Ir	**2.19**±1.7	**0.52**±0.2	**3.21**±1.1	**2.41**±1.4	**0.35**±0.2
Ru	**26.2**±18.0	**3.30**±2.3	**36.74**±24.2	**10.53**±7.6	**4.61**±1.8
Rh	**18.74**±5.2	**1.87**±1.4	**10.03**±9.0	**60.41**±59.8	**2.9**±2.4
Pt	**3.78**±2.5	**0.09**±0.1	**3.78**±1.6	**6.88**±1.2	**0.11**±0.1
Pd	**139**±39.0	**37.3**±8.4	**136**±11.0	**316**±74.8	**199**±36.5
Sample	**JJB18c**	**JJB19,1**	**JJB20**	**EST013_16**	
n	6	4	4	8	
Rock Type	bsn	chr	pxt	mln	
Os	**1.23**±0.5	**3.78**±4.2	**0.97**±0.92	**2.75**±2.8	
Ir	**0.73**±0.5	**2.58**±3.5	**0.37** ±0.39	**2.55**±2.1	
Ru	**7.09**±2.5	**22.19** ±30.9	not calculated	**7.89**±6.6	
Rh	**3.04**±2.1	**20.06**±38.8	**33.25**±49.22	**17.74**±14.8	
Pt	**1.63**±2.9	**3.18**±1.8	**0.07**±0.05	**11.17**±6.7	
Pd	**191**±12.1	**170**±53.1	**82.6**±7.04	**230**±56.3	

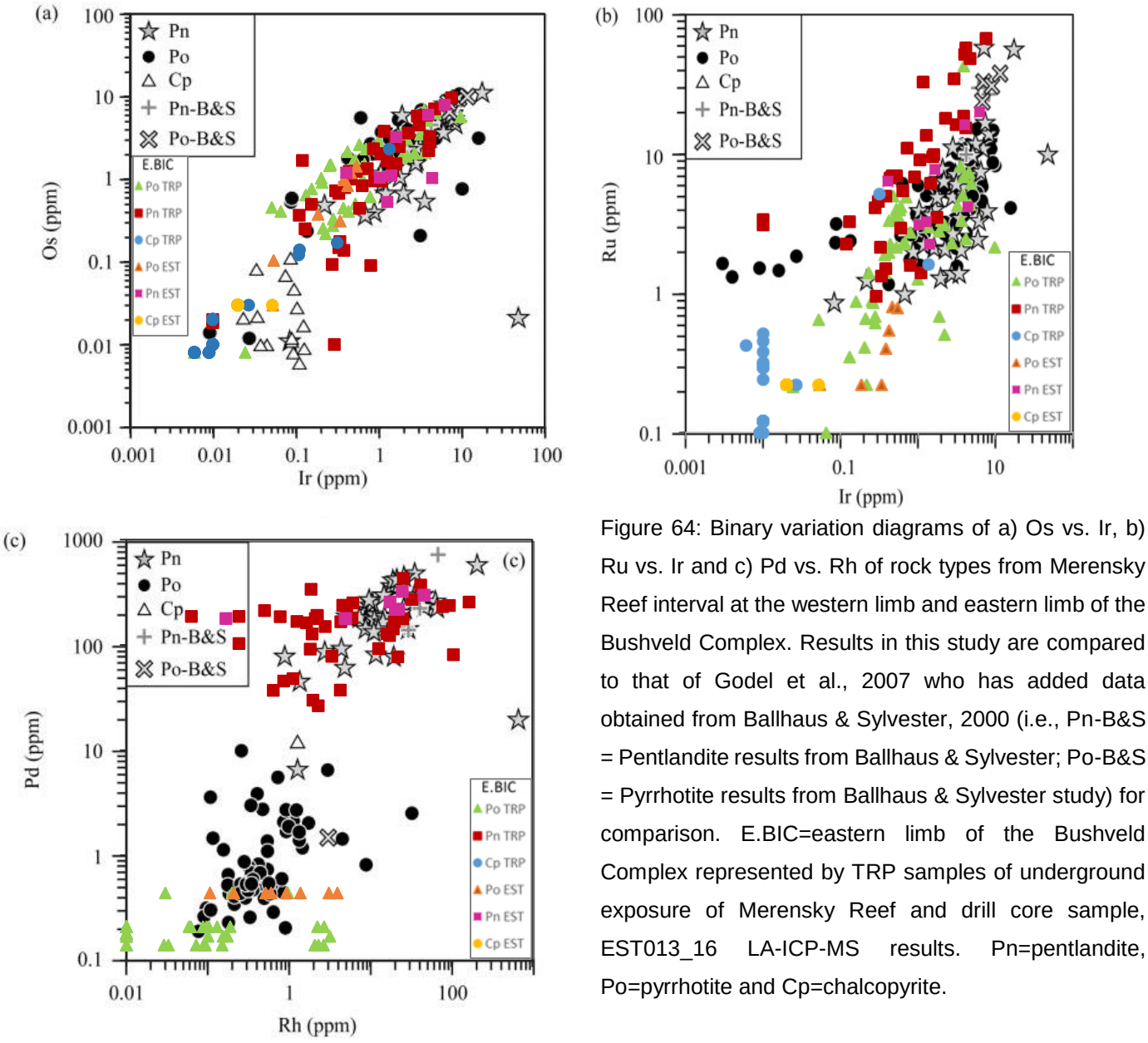

Figure 64: Binary variation diagrams of a) Os vs. Ir, b) Ru vs. Ir and c) Pd vs. Rh of rock types from Merensky Reef interval at the western limb and eastern limb of the Bushveld Complex. Results in this study are compared to that of Godel et al., 2007 who has added data obtained from Ballhaus & Sylvester, 2000 (i.e., Pn-B&S = Pentlandite results from Ballhaus & Sylvester; Po-B&S = Pyrrhotite results from Ballhaus & Sylvester study) for comparison. E.BIC=eastern limb of the Bushveld Complex represented by TRP samples of underground exposure of Merensky Reef and drill core sample, EST013_16 LA-ICP-MS results. Pn=pentlandite, Po=pyrrhotite and Cp=chalcopyrite.

Positive correlations are observed for Os and Ru versus Ir (IPGE) as well as for Pd versus Rh (PPGE) for Merensky Reef rocks from both the western and eastern limb of the BIC (see figure 64a, b and c). Analyses by Godel et al. (2007) shows Os and Ir in pyrrhotite and pentlandite of the Rustenburg Platinum Mine (RPM) range between approximately 0.1 and 15ppm (figure 64a). Os and Ir in pyrrhotite and pentlandite of Two Rivers Platinum Mine (TRP) vary between 0.02 and 9.75 ppm and between 0.05 and 6.25 ppm at Eerste Geluk. The highest concentrations of Ru in pyrrhotite and pentlandite at TRP are 42.7 and 67 ppm respectively. Ru concentrations at Eerste

Geluk reach a maximum of 0.8ppm in pyrrhotite and 20 ppm in pentlandite. Except for two values approximately 60 ppm, the highest concentrations recorded for Ru is 20 ppm in pentlandite and 15 ppm in pyrrhotite of RPM (figure 64b). Rh content in pentlandite of RPM, TRP and EST are much higher than what is found in pyrrhotite. Rh content ranges between 1 and 100 ppm, 0.06 and 165 ppm and 0.17 and 46.35 ppm in RPM, TRP and EST respectively. The Rh concentrations are below 4 ppm in pyrrhotite at TRP and EST and below 0.2 at RPM (figure 64c).

At high temperatures (higher than 600°C) Ni, Co and Cu partition coefficients into MSS are less than one and therefore a Fe rich MSS and Cu-rich sulphide liquid is formed (Barnes et al., 2008). From experimental data it is seen that with decreasing temperatures the partition coefficient of Ni increases above one and Co approaches one, hence the MSS that crystallizes from the final base metal liquid along with intermediate solid solution (ISS) is Ni rich (Peregoedova, 1999 as quoted in Makovicky, 2002). At 600°C pentlandite and pyrrhotite is exsolved from the MSS where strong depletion of Pt, Pd and Cu correlates with their incompatibility in MSS (Mungall et al., 2005, Barnes et al., 2008, Holwell & McDonald, 2010). The low and mostly below detection limit concentrations of IPGE and Rh in chalcopyrite (as seen in figures 64a to c) which is a product of ISS can be explained by the fact that these elements are compatible in the MSS and not in the residual Cu-rich sulphide melt. The ISS crystalizes from the Cu-rich sulphide liquid at lower temperatures (Godel et al., 2007) after the MSS has crystallized. The ligands for noble metals Se, As, Sb, Te and Bi are variably incompatible in MSS, partitioning strongly in the derivative melt (referred to as “semimetal liquid” by Holwell et al., 2010) and form compositionally different minerals with the PGE (Helmy et al., 2010) . If these elements were enriched in the ISS it would be reflected in the composition of chalcopyrite. If enrichment of these elements is not observed in chalcopyrite one can infer that they did not partition into the ISS but rather remained in the residual melt (i.e. “semimetal liquid”). One would therefore expect these elements (As, Te and Bi particularly), which are ligands of PGE, to form discrete minerals with derivative PGE in the residual melt, mainly Pt, which has been observed in this study. Pt and Pd are incompatible in the ISS (Peregoedova, 1998) and therefore concentrate in the residual melt which explains the low concentrations of these elements in chalcopyrite. One would also therefore expect Pt and Pd concentrations to be depleted in pyrrhotite and pentlandite. However, Pd appears to be enriched in pentlandite. Pd cannot be accommodated in the immiscible semimetal-rich melt when the Pd: semimetal ratio is sufficiently high resulting in surplus Pd which then partitions into the MSS (Holwell & McDonald, 2010). Pd is therefore observed in pentlandite. Pt in this study is below detection limit for most of the chalcopyrite and appears to be more enriched in pentlandite relative

to pyrrhotite. As seen in table 13, Pt in pyrrhotite of JJB19.1 which is a chromitite sample appear to be more enriched than the pyroxenite which corresponds to the findings of Godel et al. (2007) that BMS (pyrrhotite in this case) in the chromitite layers are slightly enriched in PGE (by a factor of 2). PGE does not only occur in the Merensky Reef as solid solutions in BMS but also as PGM. The low or rather below detection limit concentrations of Pt in chalcopyrite in this study suggest that Pt did not partition into the ISS but remained in the 'semimetal-rich' residual liquid. The Pt could thus exsolve as Pt-PGM during the exsolution of chalcopyrite or it could have crystallized as Pt-PGM from the fractionated base metal sulphide liquid (Barnes et al., 2008). Holwell & McDonald (2010) also points out that Pt and Pd will be present as discrete minerals around the margins of the sulphide blebs and in small veinlets injected into the surrounding silicates if there is a relatively high concentration of semimetals in the residual melt.

The concentrations of PGEs and metals in sulphides are influenced largely by their partition coefficients. Based on experimental data Li et al (1996) proposes that the bulk S content of the S systems from which the sulphides crystalize has a strong influence on the partition coefficients under different conditions. It appears that the amount of semimetals present in the sulphide liquid also plays an important role in determining the behaviour of Pt, Pd and Au as Pd and especially Pt and Au will partition into an immiscible semimetal liquid once all the sulphide has crystallized (Holwell &McDonald, 2010). The compatibility of Ir and Rh and the incompatibility of Pt, Pd and Cu during MSS crystallization under S saturated conditions seem to favour the theory that sulphide liquid fractionation gave rise to metal zonation (Li et al. 1996). Compositional zonation of magmatic sulphide ore deposits such as those at Sudbury, Ontario (Li et al., 1992; Li and Naldrett,1994) and Noril'sk, Siberia (Naldrett et al., 1994; Zientek et al., 1994) have been reported. It is however argued by Mungall et al. (2005) that the compatible behaviour of Ni, Ir and Rh in MSS requires equilibration of MSS and sulphide liquid at moderately high sulfur fugacity and low temperature near to the solidus of the sulphide magma and that these constraints indicate that the sulphide magma must have evolved by equilibrium crystallization rather than fractional crystallization of the MSS. Ballhaus & Sylvester (2000) suggests that the role of the sulphide melt in the Merenky Reef was to "immobilize" a pre-existing, stratiform PGE concentration in the liquid-stratified magma chamber. Barnes et al. (2008) however proposes that the PGM included and associated with BMS originates from the BMS. These aurthors agree to the possibility of the PGM having been formed prior to the base sulphide liquid but argue that present inclusions may not represent these PGM. They suggest that these PGM inclusions exsolved from the BMS they found in. Hiemstra (1979) however suggested that the PGMs were too small to have settled from

by crystal settling but rather that the PGMs crystallized as small crystals and that chromite nucleated on them therefore playing a mechanical role in crystal settling to form the Merensky Reef. This is in accordance with the Ir-Os-Ru-S inclusions in chromites. Based on the LA ICP-MS results in this study it is plausible that Pt exsolved from the residual sulphide melt to form Pt-PGM due to the relatively low Pt concentrations in the BMS. Discrete Sb-Te-Bi-PGE phases are believed to have originated from droplets of immiscible Sb-Te-Bi-enriched melts, exsolved from late-stage fractionated sulphide melt (Helmy et al., 2010). Te-Bi-PGE phases have been observed in this study (figures 47C, 48A&B and 51D) and concentrations of Te and Bi measured in the BMS being mostly below detection limit (Appendices A4-1 and A4-2). The absence of these elements (Te and Bi) in BMS is believed to be the cause of the presence of Pt and Pd in solid solution within sulphides (Holwell & McDonald, 2010). It should however also be taken into account that Pt and Pd are so big and heavy that no law of solid solution allows for these elements to replace other elements such as Fe in the sulphide lattice. Pt and Pd may be present as nano-particles of PGM in lattice defects of sulphides.

Chapter 5: Discussion

Though numerous studies were done on the Bushveld Complex MR, the eastern Bushveld has been poorly explored relative to the western Bushveld. The main aim of this study was to examine the petrology and mineral chemistry of the Merensky Reef Cyclic Unit lithologies at TRP and to compare it to rocks of similar stratigraphy from a specific area north of the Steelpoort fault. A rather erratic occurrence of 'brown sugar norite' lenses within the Merensky pyroxenite is observed in underground sections at the TRP mine. This rock type is either: 1. Not present at other mines in the Bushveld Complex or 2. It has been overlooked due to its similarities to normal Merensky pyroxenite. No BSN has been observed in the drill core, EST013, of the farm Eerste Geluk. With regards to emplacement, it is suggested that the BSN lenses may have been the product of magmatic erosion by the injection of new MR magma. Models for the genesis of the Merensky Reef have been proposed within this study, consolidated with several models from other authors. Some of these models will be discussed subsequently in light of results obtained in this study as well as other authors.

5.1 Textural features

As defined by Wager et al. (1960), the term 'cumulate' is a group term for igneous rocks formed by crystal accumulation, while the term 'orthocumulate' is a cumulate consisting essentially of one or more cumulus minerals together with the products of crystallization of the intercumulus liquid. This does not necessarily have the same composition of the contemporary magma. Lee (1996) describes the pyroxenite of the Merensky Reef as an orthocumulate of very coarse-grained subhedral to euhedral orthopyroxene constituting 70-90% and a maximum of 30% of intercumulus plagioclase. The orthopyroxenes in MR pyroxenite in this study are medium to coarse grained whereas the orthopyroxenes found in the BSN are fine grained displaying a framework of compacted orthopyroxene crystals (figures 9a and c). The grain size is largely a function of the cooling history (Williams et al., 2006). The smaller grain size of the BSN can be ascribed to faster cooling as concluded by Williams et al. (2006) since faster cooling would allow shorter time for post nucleation crystal growth and later recrystallization to occur. In some instances, these BSN lenses are associated with a rim relatively more plagioclase rich (feldspathic) or pegmatoidal pyroxenite (figures 8, 10a and b). This may be attributed to a reaction between MR pyroxenite melt and BSN, where volatiles are locally controlled at the contact between BSN and MR pyroxenite melt.

A common texture observed in cumulates of this study is the occurrence of mineral inclusions. Plagioclase inclusions within pyroxene in this study (figures 15D and 23A-D) are similar to that described by Eales et al. (1991). However, no zonation of the enclosed plagioclase has been noted. Mondal & Mathez (2007) propose that the enclosed plagioclase, i.e. chadacrysts, in pyroxene is due to postcumulus enlargement of pyroxenes and the roundness of some of the chadacrysts is due to resorption of plagioclase by the pyroxenes. The degree of resorption of chadacrysts reflects the residence time in the magma. Therefore, the rounder the chadacrysts, the further they are from their crystallization site (Mitchell et al., 1998). Plagioclase enclosed in pyroxene oikocrysts has been related to either: 1. The entrainment of plagioclase from evolved resident liquid by freshly injected magma into the chamber (Eales et al., 1991 and Maier & Eales 1994) or 2. Supercooling of fresh influxes of new magma (Mathison, 1987, Tegner & Wilson, 1995 and Krynauw & Wilson, 1995). Inclusions of pyroxene within plagioclase are more dominant than plagioclase inclusions within pyroxene in this study. The plagioclase oikocrysts may have formed by liquidus stage growth at a later stage than that of orthopyroxene (Wilson, 1992). Oikocryst crystals surrounding earlier crystallized crystals can preserve earlier crystallization textures by enclosing and isolating these crystals and limiting recrystallization (Mathison, 1987; Higgins, 1998). Included minerals (such as figures 13B&D, 15D and 17D-F) are therefore generally better representatives of original crystallization texture and mineral chemistry relative to surrounding minerals.

Clinopyroxene occurs as discontinuous rims around orthopyroxene crystals (figures 14B&E and 16B), as exsolved phases from exsolution lamellae in certain orthopyroxene crystals (figures 14G and 15B-C), and as oikocrysts enclosing plagioclase or orthopyroxene crystals (figures 15C, 16B, D, E and F) and to a lesser extent as cumulus phases within the pyroxenite (figure 16 D). A general textural feature observed for the brown sugar norite samples is the enclosing of rounded orthopyroxene crystals by clinopyroxene oikocrysts (figures 16E and F). It can be assumed that the textural history of the enclosed crystallized orthopyroxene crystals is better preserved than that of surrounding crystals that may have been subject to later processes. Evident from mineral chemistry results, slight differences in mineral chemistry exist for enclosed minerals crystals within oikocrysts relative to surrounding crystals not enclosed. Enclosed orthopyroxene in chromite have %En up to En_{89} relative to the approximate En_{80} in the normal orthopyroxene and enclosed plagioclase up to An_{83} compared to the approximate An_{67} of interstitial plagioclase, for example. Hence one can assume that the mineral crystals found within oikocryts are relatively more primitive in terms of crystallization texture and mineral chemistry. From poikilitic textures it can be

deduced that new magma was injected into the chamber mixing with the resident magma resulting in the formation of intercumulus mineral phases and subsequent oikocrysts (Mitchell et al., 1998). A common textural feature in pyroxenite of both TRP and EST is the presence of exsolved clinopyroxene in lamellae of orthopyroxene, indicating that during slow temperature decrease of the melt exsolutions occurred as seen in figure 15C, for example. Ca cations which were accommodated at higher temperatures were then too large to be accommodated in the orthopyroxene crystal lattice and were therefore exsolved as clinopyroxene. Clinopyroxene found at the rims may have been induced by the migration of the exsolved clinopyroxene to the orthopyroxene boundaries during this cooling of the magma (Prevec et al., 2005).

Pyroxenite and pegmatoidal pyroxenite are mineralogically similar. However the mineral crystals of the pegmatoidal pyroxenite are larger (up to 2 cm in size). Poikilitic textures (as seen in figure15C, for example) are more dominant in the pegmatoidal pyroxenite near the bottom chromitite stringer and are thus in accordance with the findings of Mitchell et al. (1998) that poikilitic cumulates are generally found near or at the base of a cyclic unit.

Triple junctions of minerals, mainly seen in orthopyroxene and chromite, indicate that subsolidus recrystallization of minerals occurred during a possible heating event. Chromite crystals vary from euhedral to rounded subhedral shapes. Rounded chromite within poikilitic plagioclase (figure 17C & E) suggest that chromite existed prior to plagioclase crystallization. Sintering and annealing of chromite (figures 17 a, b & 22b) may be attributed to reheating of chromite crystals. Chromite crystals within the stringer display cracks (figure 17C) and deformed shapes suggesting that deformation processes occurred. This could be due to magma mush movement or late stage consolidated rock movement. Pyroxene, plagioclase and sulphide are enclosed in chromite oikocrysts in or adjacent to the chromitite stringer as seen in figures 17 D-F and 18G. Sulphides in this study occur disseminated throughout the pyroxenite but increase in concentration near the binding chromitite stringers which act as barriers. The association of sulphides with hydrous secondary minerals such as biotite and chlorite proposes remobilization or modification by later hydrothermal processes.

Though it has similar petrographic features as TRP, EST013 drill core displays more alteration as well as a higher concentration of secondary minerals. Kink bands present in the orthopyroxenes at EST (figures 22G & H) along with those observed in BSN (figures 16 G & H) suggest that plastic flow deformation processes were active in sub-solidus conditions. In the EST footwall olivine and orthopyroxene have altered to iddingsite. Orthopyroxene inclusions within olivine (figure 22 I & J)

may suggest a crystallization at higher pressure than the Bushveld chamber (Eales and Costin, 2012) where orthopyroxene forms before olivine. Another possibility would be that the two minerals formed along the olivine-orthopyroxene co-tectic. From petrographic features it can be deduced that hydrothermal processes may have brought about alteration of minerals. This is a possibility due to the location of the Eerste Geluk farm which is in proximity to the Steelpoort Fault, a potential feeder zone (Cawthorn et al., 2002b). Faulting in the area, which displaced some compartments of rock of the BIC, may therefore have given access to late hydrothermal fluids towards already formed and cooled igneous rock of MR at EST. These late hydrothermal fluids were therefore responsible for the mineral alteration as seen in the petrology of the EST samples. The availability of fluids would thus also favour brittle deformation by means of fracturing of crystals possibly due to dissolution of crystals. Injections of new hot magma and subsequent magma mixing could possibly have triggered disequilibrium and is displayed in the textures of the minerals in the different rock types at TRP and EST. These textures as described by Everitt (2012) are exsolution lamellae of clinopyroxene along with the occurrence of discontinuous rims as well as plagioclase inclusions in orthopyroxene. Eales (1991) suggests that the plagioclase inclusions may be attributed to aberrations in the normal crystallization sequence. It is suggested that crystallization of the resident magma already started when the new magma was injected which gave rise to disequilibrium (Everitt, 2012).

5.2 Mineral chemistry variations

Analysis of petrographic textures alone is not reliable to explain the nature of rock formation processes as most of the primitive textures have been destroyed through the modification of minerals. Anomalous data in mineral chemistry is sometimes due to the polishing of thin sections where the point of measurement is too close to a crack or a crystal boundary or the thickness of the mineral of interest is too thin resulting in the mineral underneath being measured as well. Cryptic mineral chemistry variations have been observed for orthopyroxene, plagioclase and chromite at both TRP and EST (figures 36, 41 and 46 respectively). The chemical composition of orthopyroxene overlaps with the chemical composition of orthopyroxene in similar rock types at Eerste Geluk in certain instances. This indicates that these minerals may have a similar origin and thus possibly having formed from the same magma. A large variation for mineral chemistry of orthopyroxene is not observed. The mineral chemistry of orthopyroxene of the Merensky Reef pyroxenite is difficult to distinguish from that of BSN, however BSN is a bit less Wo bearing, as seen in the ternary diagram in figure 33. The data is observed to overlap within the enstatite field. The %En of TRP MR pyroxenite ranges from En_{74-88} and for the brown sugar norite, from En_{76-85}.

One might thus postulate a similar magmatic origin for the orthopyroxene crystals. If this is true then a change in temperature may have been a controlling factor for the difference in mineral size between pyroxenite and brown sugar norite. Vertical variation of En content in orthopyroxene (figure 36) displays a “jump” or increase at the BSN lenses. This suggest that though the %En in orthopyroxene of both TRP MR pyroxenite and BSN may overlap, the slight difference in composition indicates that the BSN was emplaced from another melt composition and possibly from a different magma injection. Plagioclase shows a greater variation in composition in both TRP MR pyroxenite and BSN (figure 38) which suggests the entrainment of orthopyroxene of the BSN took place in an interstitial plagioclase liquid similar to the surrounding MR pyroxenite.

The mineral chemistry of orthopyroxene and clinopyroxene of pyroxenite and pegmatoidal pyroxenite at TRP overlap (figure 34). This implies that while the grain sizes differ, the mineral chemistry is still the same. It can thus be proposed that the original small orthopyroxene crystals have been modified through enlargement. Cawthorn & Boerst, (2006) suggests that the small, primary orthopyroxene crystals have grown in reaction to the influx of superheated liquid and the primary texture have been lost in the process. Though zonation of plagioclase and orthopyroxene could not be identified in the TRP samples, zonation has been observed in pyroxenite near the bottom chromitite stringer as well as foot wall pyroxenite at EST. This indicates that the minerals have been modified through the influx of a superheated liquid. En content of orthopyroxene crystals in close proximity to the chromite stringers or enclosed within chromite crystals are higher than the surrounding orthopyroxene. This finding is similar to the study performed at TRP by Rose (2010). The high En content is ascribed to possible subsolidus re-equilibration of chromite and orthopyroxene through a continuous exchange of Fe and Mg between chromite and orthopyroxene, as explained by Eales & Reynolds (1986). An overall decrease of %En with an increase in stratigraphic height is observed for orthopyroxene. The decrease in En content may be attributed to the evolution of mineral composition (Cawthorn, 2007) due to fractionation.

An especially large variation in mineral chemistry has been observed for plagioclase. %An in plagioclase in the Merensky pyroxenite of TRP ranges between An_{48} to An_{88} with outliers of approximately An_{90} (figures 37 and 38). It has also been noted that the plagioclase crystals enclosed within pyroxene oikocrysts display higher %An compared to interstitial plagioclase. The compositional difference and %An outliers may be attributed to rapid enclosure of plagioclase formed in other mineral hosts. The plagioclase can therefore not react with the liquid during crystallization and cooling of the melt. Another possibility for compositional difference may be the injection of a superheated liquid which resulted in pyroxene enlargement as described by

Cawthorn & Boerst (2006) and resorption of plagioclase (Mondal & Mathez, 2007). There is a decrease in %An of plagioclase with an increase in stratigraphic height. This trend is typical of normal fractionation indicating that replenishment of magma occurred during crystallization.

The initial strontium content of plagioclase separates of hanging wall and footwall anorthosite along with pyroxenite and BSN are 0.706480, 0.706476, 0.70666 and 0.70650 respectively, all typical of Critical Zone values. The $^{87}Sr/^{86}Sr$ ratio is used to determine influxes of new magma in magmatic sequences (Kruger & Marsh, 1982). $^{87}Sr/^{86}Sr$ ratios in mineral separates from the Western Limb are also summarized by Kruger (1994). The pyroxenite in this study has the highest initial strontium content and is consistent with the findings of Kruger & Marsh (1982). These authors propose that the Merensky Reef and its underlying pegmatoidal pyroxenite have interstitial plagioclase with a higher Sr content relative to cumulus plagioclase of the Merensky anorthosite0. The $^{87}Sr/^{86}Sr$ ratio increases from the footwall anorthosite at the pyroxenite and decreases again at the brown sugar norite. A negative trend is observed for $^{87}Sr/^{86}Sr$ versus K_2O (figure 43) as $^{87}Sr/^{86}Sr$ decreases with an increase in K_2O indicating possible crustal contamination of the anorthositic rocks as well as the BSN. Though both the pyroxenite and brown sugar norite have $^{87}Sr/^{86}Sr$ ratios representative of Critical Zone magma, the fact that the brown sugar norite has a lower ratio closer to the mantle ratio relative to pyroxenite indicates that it formed from a magma which is line with the more primitive opx compositions in the BSN.

Where plagioclase is not a liquidus phase in early stages of crystallization, pyroxenes are enriched in Al. When plagioclase begins to crystallise, Al in pyroxene decreases, enriching it in Ti because Ti is incompatible in plagioclase (Eales et al., 1993). This phenomenon is displayed by the mineral chemistry trend of orthopyroxene with stratigraphic height (figure 36b and d showing the vertical variation of the averages of Al_2O_3 and TiO_2). Where Al decreases in orthopyroxene an increase in Ti in Opx is observed.

Chromites are the earliest phases in the mineral paragenesis and are located at the base of many cyclic units. They should therefore reflect evolutionary changes in composition of parent liquids in magma chambers (Eales et al., 1993). Numerous studies have been done on the chromite of the Merensky Reef, mainly focusing on the chromitite stringer. However, in this study greater focus has been given to the disseminated chromite crystals in order to determine any possible difference between pyroxenite and brown sugar norite. BSN contains less disseminated chromite than the surrounding TRP MR pyroxenite. No significant difference in mineral chemistry of chromite has been observed in these two rock types except that the BSN chromites contain higher

FeO. Chromite from TRP chromitite stringers has a relatively higher MgO and Al_2O_3 composition compared to the disseminated chromite crystals from TRP and EST. In figure 46b it can be seen that the Mg# decreases with an increase in height in the lower part of MCU and increases again in the upper part at TRP. The inverse is true for the Cr# 9figure 46a). However at the chromitite stringers the Cr# is much lower than that of disseminated crystals within in the pyroxenite. The opposite is true for the Mg# in chromite crystals where a decrease in Mg# with an increase of height is observed (figure 46b and d). Two distinct compositional groups of chromite can thus be distinguished, namely disseminated chromite crystals and chromitite stringers, with chromite from the TRP chromitite stringers having a higher Mg# and lower Cr# than disseminated chromite from the other rock types (figure 45). These findings are consistent with that of Rose (2010) who attributed these trends to the re-equilibration of chromite crystals with silicates (for both disseminated chromite and chromite stringers) as explained by Naldrett et al. (2012) adding that these trends may not be the primary trends. This explanation is also plausible to explain the high %En of orthopyroxene enclosed in chromite oikocrysts or in spaces between annealed chromitite crystals of the chromitite stringer respectively. The reaction Ferrosilite + Spinel = Enstatite + Hercinite explains that during cooling adjacent orthopyroxene and chromite will exchange Fe and Mg according to this reaction. Orthopyroxene is therefore more enriched in Mg and chromite in Fe as a result of cooling. Rose (2010) suggested fractionation and re-equilibration of disseminated chromite crystals as reasons for the negative Mg# trend in chromite with stratigraphic height. The exchange reaction of Mg and Fe of orthopyroxenes (and olivine) between orthopyroxene in immediate contact with chromite (Roeder et al., 1979) leads to an elevation of Mg# of the orthopyroxene (and olivine) in the immediate vicinity or in contact with dispersed crystals (Maier & Eales, 1997). The mixing of primitive and fractionated liquid promotes chromite crystallization (Irvine 1977). As a result, the chemical composition of the various chromites would differ because of the availability of certain elements such as Mg and Fe during the mixing process. This would cause chromites which have formed later to have a lower Mg content than chromites which may have formed earlier. Another possible explanation for the difference in chemistry between disseminated chromite crystals and that found in the chromitite stringer is that they did not form at the same time and in the same environment but have been entrained from different levels of the chamber. When the stringer chromite composition in this study is compared to the composition of that at Lonplats Mines in the western Bushveld no difference is observed (figure 44). The TRP and EST disseminated chromite compositions however are relatively lower in Al and higher in Fe than that of chromite stringers in both western and eastern BIC. It appears that the chromites from

the chromitite stringers are more primitive and the disseminated chromites from the other rock types are more evolved.

5.3 Whole rock major and trace element geochemistry

Whole rock geochemistry analyses are displayed by binary plots (figures 25 and 26) and vertical profiles (figures 27 to 31) of major and trace elements in chapter 4 comparing lithologies of Two Rivers Platinum to similar lithologies of Eerste Geluk. The dominant mineral phases, orthopyroxene and plagioclase, control most of the chemical composition of the rocks in accordance with their mineral proportions. This is because it concentrates most of the lithophile elements. Major elements are used to illustrate the variations of major minerals that reflect cumulus phases present in a rock because major elements partition actively into cumulus phases during fractional crystallization (Giebel, 2013). The linear relationships between major and trace elements against MgO indicate the likelihood of frequent magma influxes during the deposition of the rocks (Maier, 1991). Linear relationships between major and trace element against MgO and Mg# in this study of both Two Rivers Platinum and Eerste Geluk are analogous to geochemistry results of rocks of the Merensky reef by numerous authors (Maier, 1991, Eales et al., 1993, Cawthorn, 1996, Shelembe, 2006, Giebel, 2013). Al_2O_3 wt. % versus MgO wt. % in rocks of the Merensky reef displays a negative trend as seen in figure 25 g and h. Cawthorn (1996) attributed this trend to addition of chemically distinct magma at the Merensky Reef. Brown sugar norite displays a significantly higher MgO concentration (24-28 wt. %) than pyroxenite (21-23wt. % MgO) of the Merensky reef at Two Rivers Platinum (table 1). This indicates that the BSN is more primitive than the surrounding MR pyroxenite at TRP. Trace element and trace element ratios of rocks against stratigraphic height are used as a test for multiple injection of magma and post cumulus migration of residual magma (Cawthorn & McCarthy, 1985). Trace element ratios in the Merensky rock types at both Two Rivers Platinum and Eerste Geluk vary with stratigraphic height, displaying a saw tooth pattern (figures 28, 29, 30a-b and 31 a-b). These small scale variations in the rock types may reflect the involvement of magmas of different compositions that had not completely mixed (Wilson and Chunnett, 2006).

5.4 Sulphide mineralization and platinum group elements

This study mainly focuses on the occurrence of base metal sulphides and associated PGMs occurring disseminated throughout the Merensky pyroxenite package. The BMS is variably abundant and occurs as either anhedral crystals or most commonly as interstitial “blebs”. S and Cu are incompatible in silicates. The geochemical study by (Giebel, 2013) on the various rocks of the Merensky reef at TRP show the highest S and Cu concentrations found in the Merensky

pyroxenite, which reflects the presence of sulphides. These elements are used to understand the process of sulphide mineralization and its mutual relationship with PGE mineralization (Giebel, 2013). In Giebel's study the highest PGE concentrations were also recorded for Merensky Reef as well as UG2.

Sulphide saturation was likely one of the key factors responsible for the formation of BMS and the scavenging of PGE in the Merensky Reef at TRP and in the Western Limb (Teigler & Eales, 1993 and Rose et al., 2011). Sulphur saturation at the MR is indicative of relatively high-sulphur magmas entering the chamber as the BIC evolved with time (Teigler & Eales, 1993). According to Cawthorn (2010) PGE mineralization in thick pyroxenite occurs higher up in the succession, tracking the upper chromitite stringer, taking into account that the vertical distribution of PGE depends largely on the separation between the two chromitite stringers or the absence of one stringer. The Merensky profile from which the BSN and adjacent rocks were sampled is a facies type 1. This facies type is characterized by PGE mineralization occurring throughout the approximately 2.4m thick pyroxenite and is associated with chromite mineralisation. Though BMS and related PGMs occur throughout the pyroxenite an increase in their concentrations is noted near both top and bottom chromitite stringers.

Microprobe data of particular PGMs analysed are relatively enriched in Pt but are poor in Pd and Rh (appendix A3-9). This is consistent with the LA-ICP-MS carried out on base metal sulphides. The absence of Pd and Rh within the PGMs detected may be due to the fact that these PGEs are present as solid solution within sulphide minerals, pentlandite in particular (Junge et al., 2014; Holwell & McDonald, 2010; Godel et al., 2007). In this study a number of BMS and related PGMs are found associated with secondary silicates such as biotite and chlorite (figures 18 F&H and 47C). Rose et al. (2011) and Viljoen et al. (2011) suggest that these findings provide evidence for redistribution of PGMs by late fluids. The PGMs observed display rather interesting textures. Slight displacement in BMS caused by a PGM (moncheite) has been noted in the pyroxenite sample near the top chromitite stringer (figure 47C). In close proximity to the bottom chromitite stringer, a "worm" shaped intrusion of moncheite is seen in pyrrhotite (figure 48A). Zonation of a PGM (figure 48C) has also been observed illustrating probable recrystallization. These features indicate possible late magmatic processes. PGMs have been observed enclosed in or at the boundaries of BMS. This may be related to exsolution of PGMs from monosulphide solid solution (Penberthy & Merkle, 1999 and Holwell&McDonald, 2010). A small number of PGMs have been noted in the surrounding silicates as well as chromite. It can thus be assumed that various processes were responsible for the mineralization of PGE. The exact processes controlling PGE

mineralization has not yet been determined, however, as stated by Junge et al. (2014) both “sulphide control” and “chromitite control” played a role in the PGE enrichment of the BIC. “Chromitite control” refers to the conducive environment provided by chromitite to concentrate PGEs and “sulphide control” to PGE enrichment once sulphide precipitation began (Junge et al., 2014). Holwell & McDonald (2010) suggest that the mineralogy of Pt and Pd significantly dependent on the presence and concentrations of semimetals such as Bi and Te and that the absence of these may be the reason for the presence of Pt and Pd in solid solution within the sulphide phases.

5.5 Proposed model

Various models have been proposed by several authors over the years for the genesis of the Merensky reef with most of the comprehensive studies done on the western limb of the Bushveld Complex. The author proposes that more than one model may be applicable to the formation of the Merensky reef at subsequent stages of its formation process.

Magma chambers are irreversibly evolving systems going through phase transition by crystallization (Veksler, 2012). Veksler stresses the importance of crystallization for understanding magmatic layering and how ore deposits are formed stating that crystal settling and compositional convection are similar in the magma chamber.

Considering this, the most relevant model to explain crystal settling of the Merensky reef is by Seabrook et al (2005). These authors propose that during the formation of the Merensky reef two different magmas existed. An influx of Main Zone magma occurred at the base of the Merensky unit which displaced the Critical Zone magma upward. These two magmas however did not mix. Crystallized orthopyroxene sank through the influx of Main Zone magma due to the density contrast. These crystals collected on the crystal to form the Merensky pyroxenite (Seabrook et al., 2005). The authors suggest a mixing of crystals rather a chemical mixing of magmas.

Authors such as Wilson & Chunnett (2006), Prevec et al. (2005) support the notion that Main Zone magma was emplaced at the base of the Merensky unit displacing the Critical Zone magma upward. Wilson & Chunnett (2006) however argue that the emplacement model proposed is a simplification of the actual process.

Plagioclase separates in this study do not display a Sr-isotopic signature of the Main Zone magma; instead, the Sr-isotopic ratios are typical of Critical Zone magma. This makes it difficult to argue that orthopyroxenes crystallized in the Critical Zone and sank into the Main zone influx

or that a mixture of isotopic ratios of the plagioclase separates of the two zones exists. This may provide evidence suggesting that mixing of minerals and not magmas occurred. More in-situ high resolution isotope analyses however is needed to confirm this possibility. Alternatively, disequilibrium textures of orthopyroxene and plagioclase have been observed.

The nature of PGM is highly variable (Cawthorn et al., 2002a). Therefore, one would expect that the formation processes of the PGMs would be variable too. The cooling effect of the emplacement of the Main Zone magma on the Critical Zone magma which was close to sulphide saturation and rich in PGE could have caused the precipitation of immiscible sulphide droplets resulting in the Merensky reef (Wilson & Chunnett, 2006). These authors propose five possible processes for the origin of PGE mineralization in the Merensky Reef:

1. Collection of PGE by an immiscible sulphide liquid
2. Partitioning of the IPGE into chromite
3. Crystallization of PGM directly from the magma
4. Loss of S, Pd and base metal from the base metal sulphides in the chromitite layer
5. Redistribution of the PGE by a fluid rising from the underlying cumulate pile.

From the processes listed above, 1, 3 and 5 were observed in this study (the remaining two processes are not ruled out as the chromite has not been analysed for PGE). Collection of PGE by immiscible sulphide liquid is evident by the close association of BMS with PGE. The slight displacement of BMS by PGM and the intruding of PGM into BMS may suggest that the PGEs were not scavenged by the sulphides but rather that the PGM crystallised directly from the silicate magma to form PGMs which imposed into/through earlier BMS. Redistribution of PGE by fluids may explain the nature of the PGMs in this study, as the association of BMS and related PGMs with secondary minerals as well as the intrusive and recrystallized character of certain PGMs indicate late hydrothermal processes were present.

Whole-rock geochemistry, Sr-isotopic ratios in plagioclase separates and textural features of the various rocks in this study may indicate multiple magma injections into the chamber as suggested by Cawthorn (1996). It is thus possible for magma mixing to have taken place. Magma mixing is the most plausible mechanism for the production of chromite in the chamber as illustrated in figure 63A (Cawthorn, 1996). PGEs may have been collected by chromitite either by PGM being formed before sulphide saturation during the formation of chromite layers and/or the remaining PGE being collected by an immiscible sulphide liquid that percolated downward until it encountered the chromite layers as illustrated in figure 63A-C (Godel et al., 2007). Orthopyroxenes of the

pegmatoidal pyroxenite near the base of the Merensky reef display similar chemistry to the orthopyroxenes in the surrounding pyroxenite though their crystal size is larger (figure 34). Growth of the orthopyroxene crystals by reaction with superheated liquid (Cawthorn & Boerst, 2006) is thus a plausible explanation for the formation of the pegmatoidal pyroxenite.

The main difference between the Merensky reef at Two Rivers Platinum and the Merensky Reef north of the area at the farm Eerste Geluk is the absence of brown sugar norite at the latter locality and the fact that the minerals of the Eerste Geluk Merensky lithologies display more alteration or deformation and a higher concentration of hydrous minerals. It is in close proximity to the Steelpoort Fault making it plausible that late hydrothermal fluids gained access to already formed and cooled igneous rock of MR at EST through faulting in the area. These late hydrothermal fluids were therefore responsible for the alteration of minerals. Variable rates of cooling and crystallization could have given rise to markedly different amounts of trapped liquid in the various Merensky reef sections (Wilson & Chunnett, 2006). The BSN contains relatively little if any sulphides and PGMs. It is therefore suggested that the BMS and PGM saturation was not affected during crystallization of BSN. Though the BSN displays some similarities with the Merensky pyroxenite, its textures and crystal size suggest different magma controls such as temperature and pressure have occurred compared to the surrounding pyroxenites. As seen in the modal mineralogy bar graph in figure 19, the BSN is relatively more enriched in amphiboles and micas compared to the surrounding MR pyroxenite. It can be suggested that the composition of the BSN magma contained more fluids depressing the solidus temperature. This allows for more interstitial liquid to be collected. It is suggested that the BSN formed prior to the MR and that magmatic erosion caused by the injection of the new MR magma may have disturbed the previously formed BSN layer. It thus resulted in isolated lenses of relict and primitive BSN (figure 65D). This therefore may have caused the discontinuous appearance of BSN.

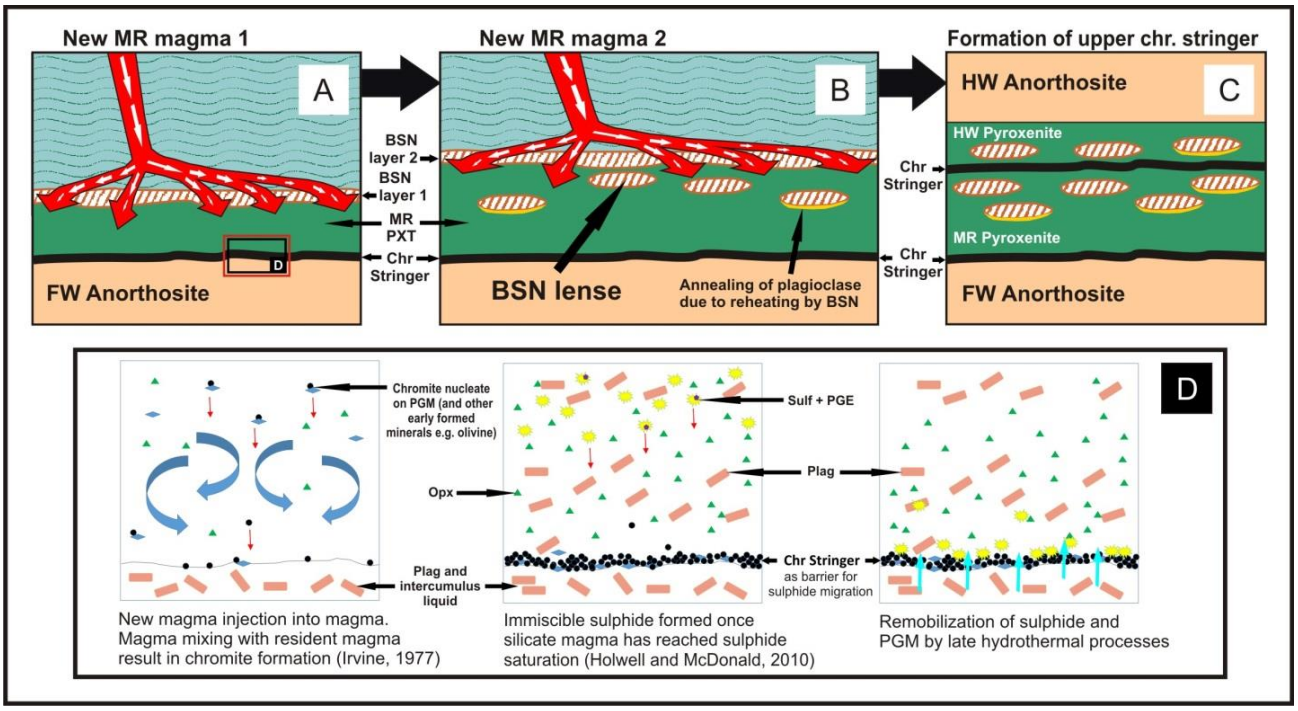

Figure 65: A simplified illustration of proposed BSN emplacement and MR formation at TRP. A - C) Proposed emplacement of BSN into MR at TRP.A) New magma injected “erodes” large parts away of pre-existing BSN layer. B) & C) As a result BSN lense relicts are found within the MR pyroxenite and HW. Feldspathic rims may also be present due to reheating by BSN. D) New magma was injected into the chamber and mixed with resident magma causing chromite to form and settle on underlying anorthosite. These chromites nucleated with PGM. Magma reached a state of sulphide saturation and immiscible sulphide formed which was denser than the silicate magma and therefore percolated downwards scavenging PGE. The chromitite stringer act as a barrier, sulphides therefore accumulated at the stringer. Late stage hydrothermal fluids redistributed sulphides and PGMs.

5.6 Conclusions

- Textural features along with complementary mineral chemistry of minerals in the various rock types, Sr analyses of plagioclase separates and whole rock geochemistry associated with the Merensky interval indicate multiple magma injections and fractionation of the magma. BSN appear to be fine grained mela-gabbronorite.
- Due to the close proximity of Eerste Geluk to the Steelpoort Fault, which is believed to run in the direction of a potential feeder to the eastern Bushveld limb, more alteration of minerals and increased presence of hydrous minerals occurs at Eerste Geluk compared to TRP as a result of faulting and associated late hydrothermal fluids in the area.
- Representative rocks of TRP show $^{87}Sr/^{86}Sr$ ratios and signatures which are typical of Critical Zone magma.
- The PGE mineralisation in rocks of this study originated possibly from a number of processes, redistribution and recrystallization of PGMs by late magmatic processes such as hydrothermal fluids being most applicable.
- The BSN is laterally inconsistent and preserved for a limited distance in the TRP area possibly due to the BSN layer being eroded by a new magma injection (MR). The apparent absence of BSN in other mines could also be attributed to magmatic erosion or the occurrence of the BSN has been overlooked due to its similarities to pyroxenite.
- The author recommends that further investigations be carried out on the occurrence of BSN throughout the entire Bushveld Igneous Complex in order to improve and better understand the emplacement models for the various rock types of the MR unit.

Acknowledgements

This study was supervised by Prof C.D.K Gauert and I would just like to express my sincere gratitude for his general advice, critical comments, patience, continuous guidance and input throughout the study.

I would also like to thank the Department of Geology at the University of the Free State for allowing me to undertake this study and to use the facilities for this study.

This study also benefited immensely from the National Research Fund (Masters Scarce Skills) for which I am very grateful.

I am indebted to the Inkaba Ye Africa organisation for their financial support throughout the study.

Mr Mike Cowell and the geology staff at Two Rivers Platinum Mine are thanked for their assistance with underground sample material of the Merensky interval.

I would like to thank Daniel Radikgomo and Jonas Choane at the Department of Geology, UFS, for producing thin polished sections and epoxy sections and the preparation of the milled samples for the XRF-analyses respectively.

The use of Jeol JXA 8230 Superprobe, instrument sponsored by NRF/NEP grant 40113 (UID 74464) is kindly acknowledged. Dr Gabi Costin and Adina at Rhodes University are greatly thanked for their willingness to assist me with everything related to the microprobe. I would also like to thank them for their hospitality and generosity during my stay in Grahamstown.

Prof Laure Dosso is thanked for mass spectrometry done on plagioclase separates at the Institut Universitaire Européen de la Mer, France.

I would also like to thank Dr I McDonald in the Geochemistry lab at the University of Cardiff, Wales for LA ICP-MS analysis done on base metal sulphides.

I am grateful for Jakub Trubac as well as Dr Ackerman for the LA ICP-MS measurements done on base metal sulphides from the Merensky pyroxenite at the Laboratory of Radiogenic Isotopes, Czech Geological Survey, Prague. Jakub's feedback and continuous assistance is greatly appreciated.

I would like to express my sincere gratitude for the Erasmus Mundus scholarship which allowed me a once in a lifetime opportunity to study in Europe.

Prof Christoph Hauzenburger and Prof Aberra Mogessi as well as the geology staff at the University of Graz is thanked for their hospitality and assistance during my stay in Graz. Special thanks to Prof Mogessi for his discussions, interest and input to my study as well as his fatherly love throughout my stay in Graz, it was highly appreciated.

I would like to heartily thank Prof Karl Ettinger at the University of Graz for his patience and assistance with the microprobe as we hunted for PGMs. Also thankful for the apples shared.

Jürgen Neubauer is also thanked for his assistance with the SEM(Eds/Wds) analyses.

I would like to thank Derek Rose for his input in this study. Always willing to answer any question I may have with regards to the TRP area, tis highly appreciated.

Emmylou Kotzè is thanked for her tremendous help in assisting with analysis as well as aiding my understanding of certain concepts when I felt clueless.

Dr Du Plessis and Stephan Le Roux at the CT Scanner Facility is thanked for allowing me to scan my sample as well as their great support throughout the last phase of my dissertation.

To the many friends and acquaintances that I made during my stay at UFS as well as the friends I made in Graz from literaly all over the world, I would like to express my gratitude. Special thanks to Lady Bridget, Lesego, Macmillan, Rorisang, Stacey, Taufeeq and Beaugan.

I would like to thank my mother, father, family and church for their love, support and encouragement in everything i have endeavoured.

Finally, above all, I would like to thank my Lord and Saviour, through whom all things are possible, Jesus Christ.

I dedicate this dissertation to my late aunt Evaline Bawa and best friend Motshidisi Rathele, may their souls rest in peace.

References

African Rainbow Minerals *(ARM)*, 2007. Annual Report.

Ashwal, L. D., Webb, S. J., & Knoper, M. W. (2005). Magmatic stratigraphy in the Bushveld northern lobe: continuous geophysical and mineralogical data from the 2950 m Bellevue drillcore. *South African Journal of Geology, 108*, 199–232.

Ballhaus, C., & Sylvester, P. (2000). Noble Metal Enrichment Processes in the Merensky Reef, Bushveld Complex. *Journal of Petrology, 41*, 545–561.

Ballhaus, C., Marian, T., & Spath, A. (2001). Magmatic Sulfide Deposits Fe-Ni-Cu-PGE-S Magmatic Sulfide Deposits Magmatic Sulfide Deposits Magmatic Sulfide Deposits. *Journal of Petrology, 42*, 1911-1926.

Barnes , S.-J., Cox, R. A., & Zientek, M. (2006). Platinum-group element gold, silver and base metal distribution in compositionally zoned sulfide droplets from the Medvezky Creek Mine, Noril'sk, Russia. *Contribution to Mineralogy and Petrology, 152*, 187–200.

Barnes, S.-J., & Maier, W. D. (1999). The fractionation of Ni, Cu and the noble metals in silicate. In R. R. Keys, C. M. Lesher, P. C. Lightfoot, & C.E.G Geological Association of Canada (Eds.), *Dynamic Processes in Magmatic Ore Deposits and their application in mineral exploration.* (Vol. Short Course Volume 13, pp. 69-106).

Barnes, S.-J., & Maier, W. D. (2002a). Platinum-group elements and microstructures of normal Merensky Reef from Impala Platinum Mines, Bushveld Complex. *Journal of Petrology, 43*, 103-128.

Barnes, S.-J., & Maier, W. D. (2002b). Platinum-group element distributions in the Rustenburg Layered Suite of the Bushveld Complex, South Africa. (C. I. Edited by L.J. Cabri, Ed.) *In The Geology, Geochemistry, Mineralogy and Mineral Beneficiation of Platinum-Group Elements, 54*, 431-458.

Barnes, S.-J., Prichard, H. M., Cox, R. A., Fisher, P. C., & Godel, B. (2008). The location of the chalcophile and siderophile elements in platinum-group element ore deposits (a textural, microbeam and whole rock geochemical study): Implications for the formation of the deposits. *Chemical Geology, 248*, 295–317.

Barnes, S.-J., van Achterbergh, E., Makovicky, E., & Li, C. (2001). Proton microprobe results for the partitioning of platinum-group elements between monosulphide solid solution and sulphide liquid. *South AfricanJournal of Geology, 104*, 275-286.

Boudreau, A. E., & McCallum, I. S. (1989). Investigations of the Stillwater Complex: Part V. Apatites as indicators of evolving fluid composition. *Contribution to Mineralogy and Petrology, 102*, 138-153.

Boudreau, A. E., & McCallum, I. S. (1992). Concentration of platinum-group elements by magmatic fluids in layered intrusions. *Economic Geology, 87*, 1830-1848.

Boudreau, A. E., Mathez, E. A., & McCallum, I. S. (1986). Halogen Geochemistry of the Stillwater and Bushveld Complexes: Evidence for Transport of the Platinum-Group Elements by Cl-Rich Fluids. *Journal of Petrology, 27*, 967-986.

Cameron, E. N., & Abendroth, H. E. (1957). Structure of Lopoliths: Discussion. *Bulletin of the Geological Society of South Africa., 79*, 3-12.

Cawthorn, R. G. (1996). Re-evaluation of magma compositions and processes in the uppermost Critical Zone of the Bushveld Complex. *Mineralogical Magazine, 60*(398), 131-148.

Cawthorn, R. G. (2007). Cr and Sr: Keys to parental magmas and processes in the Bushveld Complex, South Africa. *Lithos, 95*, 381–398.

Cawthorn, R. G. (2010). Geological interpretations from the PGE distribution in the Bushveld Merensky and UG2 chromitite reefs. *The 4th International Platinum Conference, Platinum in transition 'Boom or Bust'.*, (pp. 57-70).

Cawthorn, R. G., & Ashwal, L. D. (2009). Origin of Anorthosite and Magnetitite Layers in the Bushveld Complex, Constrained by Major Element Compositions of Plagioclase. *Journal of Petrology, 50*(9), 1607-1637.

Cawthorn, R. G., & Boerst, K. (2006). Origin of the Pegmatitic Pyroxenite in the Merensky Unit, Bushveld Complex, South Africa. *Journal of Petrology, 47*(8), 1509-1530.

Cawthorn, R. G., & McCarthy, T. S. (1985). Incompatible Trace Element Behavior in the Bushveld Complex. *Economic Geology, 80*, 1016-1026.

Cawthorn, R. G., & Webb, S. J. (2001). Connectivity between the western and eastern limbs of the Bushveld Complex. *Tectonophysics, 330*, 195–209.

Cawthorn, R. G., Lee, C. A., Schouwstra, R. P., & Mellowship, P. (2002a). Relationship between PGE and PGM in the Bushveld Complex. *The Canadian Mineralogist, 40*, 311-328.

Cawthorn, R. G., Merkle, R. K., & Viljoen, M. J. (2002b). Platinum-group element deposits in the Bushveld Complex, South Africa. In L. J. Cabri, & L. J. Cabri (Ed.), *The geology, geochemistry,mineralogy and mineral beneficiation of platinum-group elements.* (Vol. 54, pp. 389–429). Can Inst Min Metall Spec.

Clarke, B. M., Uken, R., Watkeys, M. K., & Reinhardt, J. (2005). Folding of the Rustenburg Layered Suite adjacent to the Steelpoort pericline: implications for syn-Bushveld tectonism in the eastern Bushveld Complex. *South African Journal of Geology., 108*, 397–412.

Cowell, M. (2003). *Two Rivers Platinum Mine Trial Mining Report.* Unpublished Company Report.

Cowell, M. (2011). *Two Rivers Internal Report.* Unpublished Internal Report., Two Rivers Platinum Mine.

Davies, G., & Tredoux, M. (1985). The Platinum-Group Element and Gold Contents of the Marginal Rocks and Sills of the Bushveld Complex. *Economic Geology, 80*, 838-848.

Eales, H. V. (2001). *A first introduction to the geology of the Bushveld Igneous Complex and those aspects of South African geology that relate to it.* (Vol. Popular geoscience series 2). The Council for Geoscience Geological Survey of South Africa.

Eales, H. V., & Cawthorn, R. G. (1996). Bushveld Igneous Complex. In R. G. Cawthorn (Ed.), *Layered intrusions* (Vol. 15, pp. 181-229).

Eales, H. V., & Costin, G. (2012). Crustally contaminated komatiite: primary source of the chromitites and Marginal, Lower and Critical Zone magmas in a staging chamber beneath the Bushveld Complex. *Economic Geology, 107*, 645-655.

Eales, H. V., & Reynolds, I. M. (1986). Cryptic variations within chromitites of the Upper Critical Zone, Northwestern Bushveld Complex. *Economic Geology, 81*, 1056-1066.

Eales, H. V., Maier, W. D., & Teigler, B. (1991). Corroded plagioclase feldspar inclusions in orthopyroxene and olivine of the Lower and Critical Zones, western Bushveld Complex. *Mineralogical Magazine, 55*, 479-786.

Eales, H. V., Teigler, B., & Maier, W. D. (1993). Cryptic variations of minor elements Al, Cr, Ti and Mn in Lower and Critical Zone orthopyroxenes of the Western Bushveld Complex. *Mineralogical Magazine, 57*, 257-264.

Everitt, S. J. (2012). *Evolution of the UG2 chromitite layer and its surrounding silicates: mineral composition and petrological evidence.* Master Thesis, Rhodes University. 46-47p.

Gauert, C. D. (1998). *The petrogenesis of the Uitkomst Complex, Mpumalanga Province,South Africa.* Unpublished Ph.D Thesis, University of Pretoria, Pretoria, South Africa. 315p.

Giebel, R. J. (2013). *Mineralogy, PGE, wholerock geochemistry and mineral chemistry of the upper Critical Zone (Bastard Reef, Merensky Reef, Upper Group 2 intervals) in borehole TRP 272.* Unpublished MSc thesis, University of the Free State, Bloemfontein, South Africa. 54-55, 110p.

Godel, B., Barnes, S.-J., & Maier, W. D. (2007). Platinum-Group Elements in Sulphide Minerals, Platinum-Group Minerals, andWhole-Rocks of the Merensky Reef (Bushveld Complex, South Africa): Implications for the Formation of the Reef. *Journal of Petrology, 48*, 1569-1604.

Harmer, R. E., Auret, J. M., & Eglington, B. M. (1995). Lead isotope variations within the Bushveld complex, Southern Africa: a reconnaissance study. *Journal of African Earth Sciences, 21*, 595-606.

Harney, D. M., & von Gruenewaldt, G. (1995). Ore-forming processes in the upper part of the Bushveld complex South Africa. *Journal of African Earth Sciences, 20*, 77-89.

Hatton, C. J., & Von Gruenewaldt, G. (1985). Chromite from the Swartkop Chrome Mine An Estimate of the Effects of Subsolidis Requilibration. *Economic Geology, 80*, 911-924.

Helmy, H. M., Ballhaus, C., Wohlgemuth-Ueberwasser, C., Fonseca, R. O., & Laurenz, V. (2010). Partitioning of Se, As, Te and Bi etween monosulide solution and sulfide melt - Application to magmatic sulfide deposits. *Geochimica et Cosmochimica Acta, 74*, 6174-6179.

Hiemstra, S. A. (1979). The role of collectors in the formation of the platinum deposits in the Bushveld Complex. *Canadian Mineralogist, 17*, 469-482.

Higgins, M. D. (1998). Origin of anorthosite by textural coarsening: Quantative measurements of a natural sequence of textural development. *Journal of Petrology, 39*, 1307-1325.

Holland, H. D. (1972). Granites, solutions and base metal deposits. *Economic Geology, 67*, 281-301.

Holwell, D. A., & McDonald, I. (2010). A Review of the Behaviour of Platinum Group Elements within Natural Magmatic Sulfide Ore Systems. *Platinum Metals Review, 54*, 26–36.

Irvine, T. N. (1977). Origin of chromitite layers in the Muskox intrusion and other stratiform intrusions: a new interpretation. *Geology, 5*, intrusions: a new interpretation.

Junge, M., Oberthür, T., & Melcher, F. (2014). Cryptic Variation of Chromite Chemistry, Platinum Group Element and Platinum group Mineral Distribution in the UG-2 Chromitite. *Economic Geology, 109*, 795–810.

Kruger, F. J. (1992). The origin of the Merenskt cyclic unit: Sr-isotopic and mineralogical evidence for an alternative orthomagmatic model. *Australian Journal of Earth Science, 97*, 393-398.

Kruger, F. J. (1994). The Sr-isotopic stratigraphy of the western Bushveld Complex. *South African Journal of Geology, 97*, 393-398.

Kruger, F. J. (2005). Filling the Bushveld Complex magma chamber: lateral expansion, roof and floor interaction, magmatic unconformities, and the formation of giant chromitite, PGE and Ti-V magnetite deposits. *Mineralium Deposita, 40*, 451-472.

Kruger, F. J., & Marsh, J. S. (1982). The significance of $^{87}Sr/^{86}Sr$ ratios in the Merensky cyclic unit of the Bushveld Complex. *Nature, 298*, 53-55.

Krynauw, J. R., & Wilson, A. H. (1995). Evidence for constitutional supercooling from orthopyroxene-pigeonite-plagioclase relations in the Borgmassivet suite of western Drorming Maud Land, Antarctica. *Mineralogy and Petrology, 54*, 119-36.

Kullerud, G., Yund, R. A., & Moh, G. H. (1969). Phase relations in the Cu-Fe-S, Cu-Ni-S and Fe-Ni-S systems. *Economic Geology, Monograph, 4*, 323-343.

Lee, C. A. (1996). A Review of Mineralization in the Bushveld Complex and some other Layered Mafic Intrusions. In R. G. Cawthorn (Ed.), *Layered Intrusions* (Vol. 15 Developments in Petrology, pp. 103-146). Elsevier Science.

Li, C., & Naldrett, A. J. (1994). A numerical model for the compositional variations of Sudbury sulfide ores and its application to exploration. *Economic Geology, 89*, 1599–1607.

Li, C., Barnes, S.-J., Makovicky, E., Rose-Hansen, J., & Makovicky, M. (1996). Partitioning of nickel, copper, iridium, rhenium, platinum, and palladium between monosulfide solid solution and sulfide liquid: Effects of composition and temperature. *Geochimica et Cosmochimica Acta., 60*, 1231- 1238.

Li, C., Naldrett, A. J., Coats, C. J., & Johannessen, P. (1992). Platinum, palladium, gold and copper-rich stringers at Strathcona Mine, Sudbury: Their enrichment by fractionation of a sulfide liquid. *Economic Geology, 87*, 1584–1596.

Maier, W. D. (1991). *Geochemical and petrological trends in the UG2-Merensky interval of the Upper Critical Zone in the Western Bushveld Complex.* PhD Thesis. 118p.

Maier, W. D., & Eales, H. V. (1994). Plagioclase inclusions in orthopyroxene and olivine of the UG2-Merensky Reef interval: regional trends in the western Bushveld Complex. *South African Journal of Geology, 97*, 408-14.

Maier, W. D., & Eales, H. V. (1997). *Correlation within the UG2-Merensky Reef interval of the Western Bushveld Complex, based on geochemical, mineralogical and petrological data.* (Bulletin (Geological Survey (South Africa)), 120 ed.). Geological Survey of South Africa, Council for Geoscience.

Maier, W. D., Arndt, N. T., & Curl, E. A. (2000). Progressive crustal contamination of the Bushveld Complex: evidence from Nd isotopic analyses of cumulate rocks. *Contribution to Mineral Petrology, 140*, 316-327.

Makovicky, M., Makovicky, E., & Rose-Hansen, J. (1986). Experimental studies on the solubility and distribution of platinum group elements in base metal sulfides in platinum deposits. In M. J. Gallagher, R. A. Ixer, C. R. Neary, & H. M. Prichard (Eds.), *Metallogeny of Basic and Ultrabasic Rocks.* Institution of Mining and Metallurgy, London, U.K.

Mathez, E. A. (1995). Magmatic metasomatism and formation of the Merensky reef, Bushveld Complex. *Contributions to Mineralogy and Petrology, 119*, 277-286.

Mathison, C. J. (1987). Pyroxene oikocrysts in troctolitic cumulates – evidence for supercooled crystallisation and postcumulus modification. *Contributions to Mineralogy and Petrology, 97*, 228–236.

Mitchell, A. A., Eales, H. V., & Kruger, F. J. (1998). Magma replenishment and the significance of poikilitic textures in the Lower Main Zone of the western Bushveld Complex, South Africa. *Mineralogical Magazine, 62*, 435-450.

Mondal, S. K., & Mathez, E. A. (2007). Origin of the UG2 chromitite layer, Bushveld Complex. *Journal of Petrology, 48*, 495-510.

Mungall, J. E., Andrews, D. R., Cabri, L. J., Sylvester, P. J., & Tubrett, M. (2005). Partitioning of Cu, Ni, Au, and platinum-group elements between monosulfide solid solution and sulfide melt under controlled oxygen and sulfur fugacities. *Geochimica et Cosmochimica Acta, 69*, 4349-4360.

Naldrett, A. J. (1989). *Magmatic Sulfide Deposits.* Oxford: Oxford University Press.

Naldrett, A. J., Asif, M., Gorbachev, N. S., Kunilov, V. Y., Stekhin, A. I., Fedorenko, V. A., & Lightfoot, P. C. (1994). The composition of the Ni-Cu ores of the Oktyabr'sky Deposit, Noril'sk Region. *Ontario Geological Survey Special, 5*, 357–371.

Naldrett, A. J., Wilson, A., Kinnaird, J., Yudovskaya, M., & Chunnett, G. (2012). The origin of chromitites and related PGE mineralization in the Bushveld Complex: new mineralogical and petrological constraints. *Mineralium Deposita, 47*, 209–232.

Naldrett, T., Kinnaird, J., Wilson, A., & Chunnett, G. (2008). Concentration of PGE in the Earth's Crust with Special Reference to the Bushveld Complex . *Earth Science Frontiers, 15*(5), 264–297.

Penberthy, C. J., & Merkle, R. K. (1999). Lateral variations in the platinum-group element content and mineralogy of the UG2 chromitite layer, Bushveld Complex. *South African Journal of Geology, 102*, 240-250.

Peregoedova, A. V. (1998). The Experimental Study of the Pt-Pd-Partitioning between Monosulfide Solid Solution and Cu-Ni-Sulfide Melt at 900-840°C. *The 8th International Platinum Symposium. Symposium Series S18*, pp. 325-373. Rustenburg: The Southern African Institute of Mining and Metallurgy.

Peregoedova, A. V. (1999). *Physical-chemical behaviour of Pt and Pd in the proces of crystallization of Fe-Ni-Cu containing sulfide liquids and under the subsequent subsolidus transformations (from experimental data).* Institute of Mineralogy and Petrography, Siberian Branch of the Russian Academy of Science, Novosibirsk.

Prevec, S. A., Ashwal, L. D., & Mkaza, M. S. (2005). Mineral disequilibrium in the Merensky Reef, western Bushveld Complex, South Africa: new Sm–Nd isotopic evidence. *Contributions to Mineralogy and Petrology, 149*, 306–315.

Rajamani, V., & Naldrett, A. J. (1978). Partitioning of Fe, Co, Ni and Cu between the sulfide liquid and basaltic melts and the composition of Ni-Cu sulfide deposits. *Economic Geology, 73*, 82-93.

Robb, L. (2005). *Introduction to Ore-Forming Processes.* Blackwell Science Ltd.

Rose, D. H. (2010). *The Merensky Reef at Dwarsriver 372 KT with reference to the mineral chemistry and the platinum group minerals in the Merensky Reef Chromitite Stringers.* Master dissertation, University of Johannesburg. 1, 31, 51, 56-58, 70, 72, 75, 103p.

Rose, D., Viljoen, F., Knoper, M., & Rajesh, H. (2011). Detailed Assessment of Platinum-Group Minerals Associated with Chromitite Stringers in the Merensky Reef of the Eastern Bushveld Complex, South Africa. *The Canadian Mineralogist, 49*, 1385-1396.

Schoenberg, R., Kruger, F. J., Nägler, T. F., Meisel, T., & Kramers, J. D. (1999). PGE enrichment in chromitite layers and the Merensky Reef of the western Bushveld Complex; a Re–Os and Rb–Sr isotope study. *Earth and Planetary Science Letters, 172*, 49-64.

Schouwstra, R. P., Lee, C. A., & Kinloch, E. D. (2000). A short Geological Review of the Bushveld Complex. *Platinum Metals Review., 44*, 33-39.

Schűrmann, L. W. (1993). The geochemistry and petrology of the Upper Critical Zone of Boshoek section of the Western Bushveld Complex. *Bulletin 113 of the Geological Survey of South Africa*.

Seabrook, C. L. (2005). *The Upper Critical and Lower Main Zones of the eastern Bushveld Complex.* PhD Thesis, University of Witwatersrand.

Seabrook, C. L., Cawthorn, R. G., & Kruger, F. J. (2005). The Merensky Reef, Bushveld Complex: Mixing of Minerals Not Mixing of Magmas. *Economic Geology., 100*, 1191–1206.

Sharpe, M. R., & Chadwick, B. (1982). Structures in Transvaal Sequence rocks within and adjacent to the eastern Bushveld Complex. *Geological Society of South Africa Transactions, 85*, 29-41.

Shelembe, R. P. (2006). *The Merensky Unit, Lonplats' Mines, Western Bushveld Complex.* Master thesis, University of Witwatersrand, Johannesburg.

South African Committee for Stratiraphy (SACS). (1980). Stratigraphy of South Africa.Part1. In L. E. Kent, & (Comp) (Eds.), *Lithostratigraphy of the Republic of South Africa, South West Africa/Namibia, and the Republics of Bophuthatswana, Transkei and Venda.* (8 ed.).

Starkey, J. (1968). The geometry of kink bands in crystals-a simple model. *Contributions to Mineralogy and Petrology, 19*, 133-141.

Steele, T. W., Levin, J., & Copelowitz, I. (1975). Preparation and certification of a reference sample of a precious metal ore. *South African National Institute for Metallurgy*(Report No. 1696-1975), 4p.

Tegner, C., & Wilson , J. R. (1995). Textures in a poikilitic olivine gabbro cumulate: evidence for supercooling. *Mineralogy and Petrology, 54*, 161-73.

Teigler, B., & Eales, H. V. (1993). Correlation between chromite composition and PGE mineralization in the Critical Zone of the western Bushveld Complex. *Mineralium Deposita, 28*, 291-302.

Veksler, I. V. (2012). Layered Mafic Intrusions and Ore Systems. *Geo-Future, Inkaba yeAfrica.*

Vermaak, C. F. (1976). The Merensky Reef: thoughts on its environment and genesis. *Economic Geology., 71*, p1270-1298.

Vermaak, C. F. (1995). *The platinum-group metals. A global perspective.* Mintek, Randburg, South Africa.

Viljoen, F., Knoper, M., Rajesh, H., Rose, D., & Greeff, T. (2011). Application of a field emission mineral liberation to the in situ study of platinum-group element mineralisation n the Merensky Reef of the Bushveld Complex, South Africa. In M. Broekmans (Ed.), *10th International Congress for Applied Mineralogy (ICAM)*, (pp. 757-764). Trondheim.

Viljoen, M. J. (1999). *A review of regional variations in facies and grade distribution of the Merensky Reef, western Bushveld Complex, with some mining implications.* Proceedings 15th CMMI Congress, South African Institute of Mining and Metallurgy .

Viljoen, M. J., & Schürmann, L. W. (1998). Platinum Group Metals. In C. R. Anhaeusser, & M. G. Wilson, *The Mineral Resources of South Africa.* (6th ed., pp. 532-568.). Council for Geoscience.

Von Gruenewaldt, G. (1989). Gabbro and Norite. In Bowes (Ed.), *Encyclopedia of Earth Sciences* (Vol. Petrology, pp. 175-178).

von Gruenewaldt, G., & Strydom, J. H. (1985). Geochemical Distribution Patterns Surrounding Tin-Bearing Pipes and the Origin of the Mineralizing Fluids at the Zaaiplaats Tin Mine, Potgietersrus District. *Economic Geology, 80*, 1201-1211.

von Gruenewaldt, G., Hatton, C. J., Merkle, R. R., & Gain, S. B. (1986). Platinum-group element–chromitite associations in cumulates of the Bushveld Complex. *Economic Geology, 81*, 1067–1079.

Wager, L. R., Brown, G. M., & Wadsworth, W. J. (1960). Types of Igneous Cumulates. *Journal of Petrology. Oxford, 1*, 73-85.

Wagner, P. A. (1929). *The platinum deposits and mines of South Africa.*

Williams, E., Boudreau, A. E., & Boorman, S. (2006). Textures of orthopyroxenites from the Burgersfort bulge of the eastern Bushveld Complex, Republic of South Africa. *Contributions to Mineralogy and Petrology, 151*, 480–492.

Wilson, A. H. (1992). The geology of the Great Dyke, Zimbabwe: Crystallization, layering and cumulate formation in the P1 pyroxenite of cyclic unit 1 of the Darwendale Subchamber. *Journal of Petrology, 33*, 611-663.

Wilson, A., & Chunnett, G. (2006). Trace Element and Platinum Group Element Distributions and the Genesis of the Merensky Reef, Western Bushveld Complex, South Africa. *Journal of Petrology, 47*, 2369–2403.

Zientek, M. L. (2012). *Magmatic Ore Deposits in Layered Intrusions—Descriptive Model for Reef-Type PGE and Contact-Type Cu-Ni-PGE Deposits.* Open-file report, U.S. Geological Survey.

Appendix One

A1: Methodology

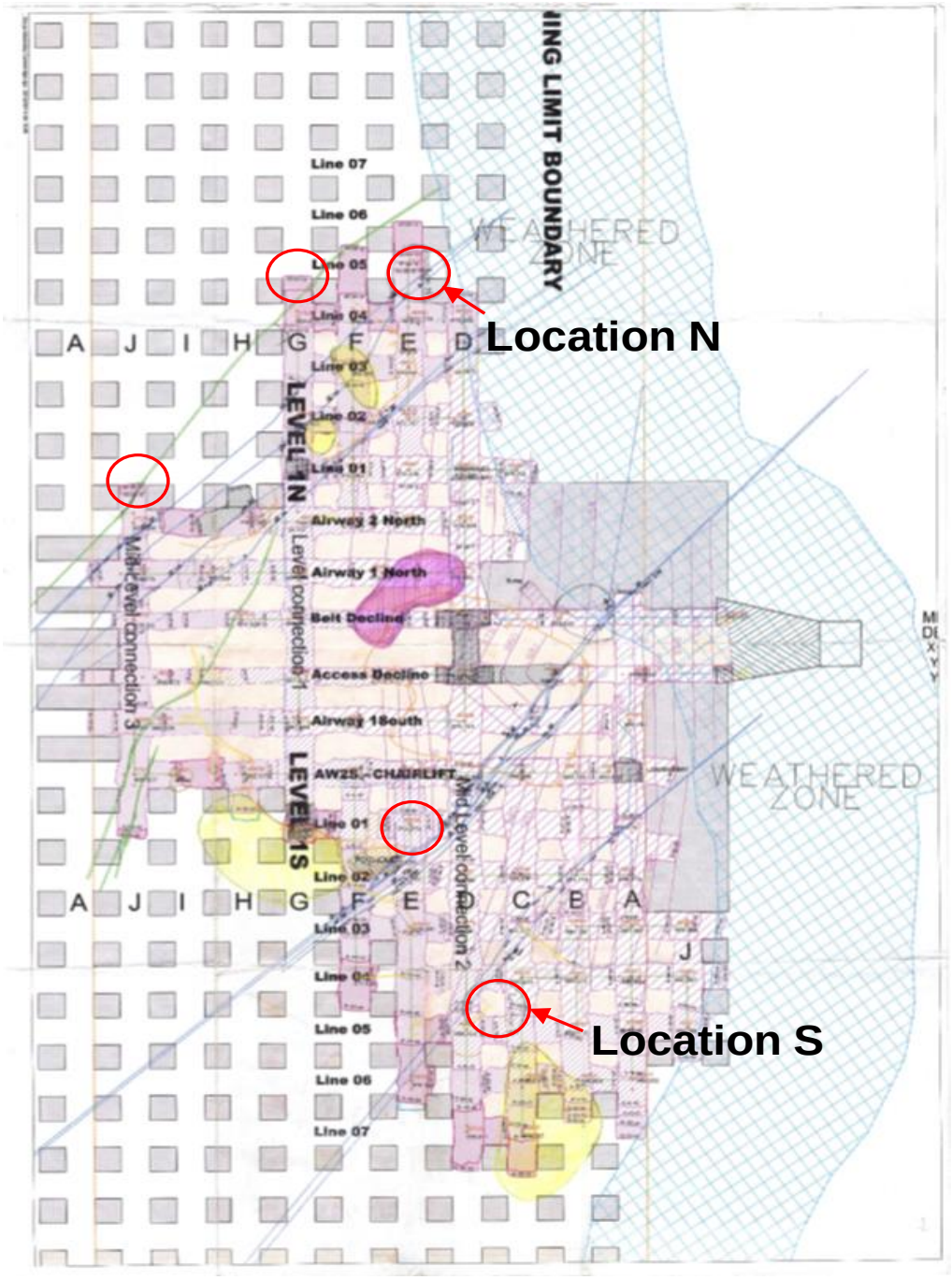

Figure 66: Plan view of the Merensky Reef mine development at TRP in 2012, indicating the areas where underground samples were taken (represented by the red circles)

A1-1 Sampling

A total of 20 samples were collected underground from the Merensky interval in the northern and southern location at a depth of approximately 980m of Two Rivers Platinum (see mine plan attached where sample locations are marked). The thickness of the Merensky pyroxenite ranges from 1.3 m to 2.65 m. A total of 27 drill core samples of the deflection borehole EST013 were collected. These samples were taken at 31m to 170m in depth. However, samples containing the upper and bottom chromite stringers were removed for research at the Berlin University.

Figure 67: Samples taken from MR intervals underground at TRP.

Part of the underground samples from TRP and drill core samples from Eerste Geluk were milled for XRF analyses and the other part were used to make thin sections. A total of 24 and 25 polished sections, of TRP underground samples and EST013 respectively, were made using a Struers LP-30 lapping machine at the preparatory laboratory of the Department of Geology, University of the Free State (UFS). A total of 13 epoxy sections were made of which 2 were from EST013. An additional 5 thin sections were made at the Department of Geology, University of Graz (GU) in an attempt to improve analytical results.

Petrographic studies were carried out on the various lithologies found in the Merensky using a petrographic research microscope Olympus BX-51. Transmitted light microscopy was used for

the silicate phases and reflected light used for the opaque minerals present namely sulphides and oxides. Representation of the different minerals analysed in the form of images were made by the AnalySIS imager software program. The optical Microscope analyses were complimented by SEM EDS/WDS and EPMA analyses.

Figure 68: Petrographic research microscope Olympus

A1-2 SEM EDS/WDS analyses

Optical microscopy has always been an important technique for analysing samples but it does however have its limitations. Optical microscopy was initially followed by SEM-EDS analysis at the Department of geology, UFS. The thin sections were carbon coated using a Carbon Coater Quoram/Q150T and then analysed by a JEOL JSM-6610 SEM. BEC (back scattering) was used and electrons were accelerated to energy of 20 kV. A number of samples were also measured at the University of Graz using a Jeol JSM-6310 Scanning electron microscope with Oxford-Analysis attached (ISIS EDX-System and WDX-600i microspec).

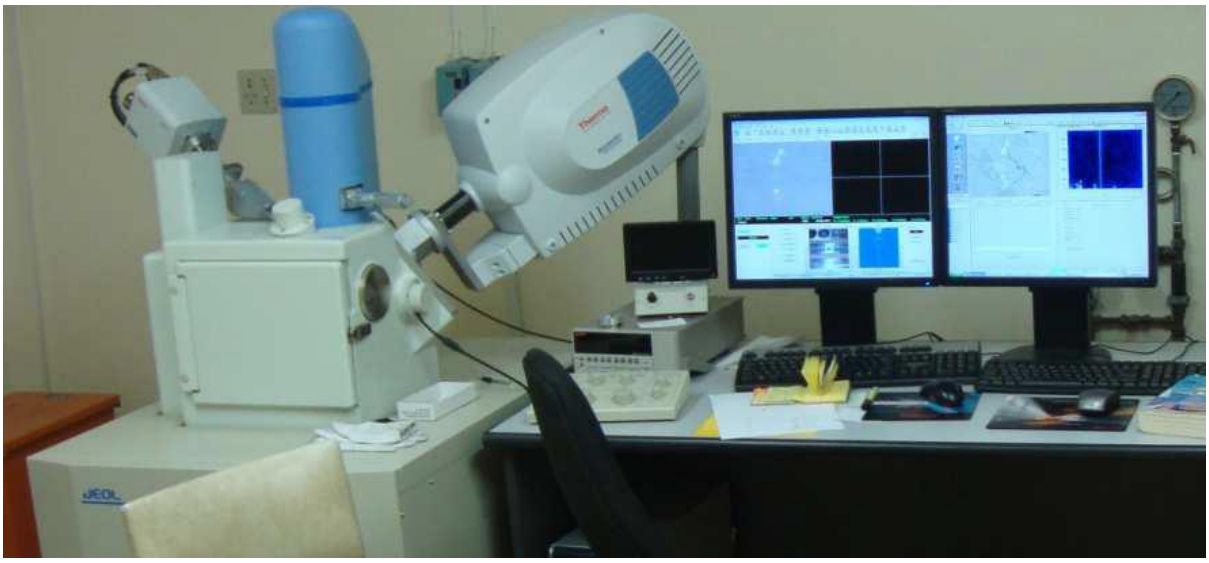

Figure 69: JEOL JSM-6610 SEM with EDX/WDX of Thermofisher at the University of the Free State. (Picture taken by Giebel)

A1-3 EPMA analyses

After optical microscopy and SEM analyses were done, areas of interest were marked on the thin sections. These marked carbon coated thin sections were then analysed using the electron probe micro analyser (EPMA), namely, Jeol JXA 8230 Superprobe, at the Rhodes University, Department of Geology. A total of 16 thin sections were analysed of which 4 were representative of hanging wall rock units of the farms north of the Steelpoort fault, farm Eerste Geluk. The major mineral phases EPMA analyses were done on include orthopyroxene, plagioclase, chromite and sulphide. These minerals were analysed using a spot size of approximately 1 micron. Recalculation of end members of the silicates and oxides was done using the NORM software.

EPMA analyses were also done at the University of Graz using a JEOL JXA-8200 Microprobe located in the Department of Geology in MU Leoben, remote controlled from Graz. Five epoxy sections were analysed focusing mainly on the sulphides and PGMs present. ZAF and Phi-Rho-Z was used for quantification.

A1-4 Mass Spectrometry analyses of plagioclase separates

Mass spectrometry analyses for $^{87}Sr/^{86}Sr$ was done on plagioclase separates of 5 underground samples from HW and FW anorthosite, MR pyroxenite and BSN lense at TRP. Samples were crushed and then sieved at various mesh sizes ranging from 2 mm to 250 µm. Plagioclase was separated manually by hand picking under a binocular microscope. These plagioclase separates of approximately 0.3 g per sample were then sent to the Institut Universitaire Européen de la Mer,

France for isotope analyses. A Mass Spectrometer Thermo-ionization (TI-MS) TRITON Thermo Electron was used for these analyses.

A1-5 Mass Spectrometry analyses of sulphides

Epoxy sections of three samples from borehole TRP-272 were sent to the Geochemistry lab at the University of Cardiff in Wales for LA-ICP-MS analysis of the BMS.

A total of 8 sulphide rich epoxy sections of underground samples at TRP and one from drill core, EST013, were sent to the Laboratory of Radiogenic Isotopes, Czech Geological Survey, Prague, for LA-ICP-MS analyses of base metal sulphides in Merensky reef pyroxenite. In situ analyses of Os, Ir, Ru, Rh, Pd, Pt and Au in sulphides were performed on the epoxy sections using a sector field ICP-MS (Element2, Thermo, Germany) coupled to a NewWave UP 213 laser microprobe (New Wave Research, USA) installed at Institute of Geology AS CR. Optical microscopy was done prior to the analyses to ensure that only fresh sulphide phases were selected and that inclusions were avoided.

A1-6 XRF

X-ray Fluorescence analyses were used to determine the whole rock major and trace element concentrations of the different rock types. Samples were crushed for the preparation of fusion disks and pressed powder pellets for the analyses of major and trace elements respectively. The Panalytical Axios XRF spectrometer at UFS was used to do the XRF analysis using the Super Q analytical software in the Protrace mode for trace element analysis. Samples were analysed for major elements Al_2O_3, CaO, Cr_2O_3, Fe_2O_3, K_2O, MgO, MnO, P_2O_5, TiO_2, Na_2O and SiO and trace elements Ca, Sc, Ti, V, Cr, Fe, Co, Ni, Cu, Zn, Rb, Sr, Y, Zr, Nb, Mo, Ba, Pb, Th and U.

A1-7 X-Ray Computer Tomography (CT Scanner)

CT Scanning was done at the Stellenbosch University, CT Scanner facility, on one of the samples where the TRP MR pyroxenite is in sharp contact with BSN. This method made it possible to investigate and analyse the inside of the sample non-destructively and at high resolution and contrast so that the minerals including sulphides and oxides present in the rock may be viewed in 3D. The use of VGO Studio Max software makes it possible to apply various analyses on the CT data such as defect analysis which allows you to identify voids/pores/cracks present in the rock.

Appendix Two: XRF

A2-1 Major elements: Two Rivers Platinum Mine

Sample	Rock Type	Sum Major	Al_2O_3	CaO	Cr_2O_3	Fe_2O_3	K_2O	MgO	MnO	P_2O_5	TiO_2	Na_2O	SiO_2	Total	FeO	Mg nr
JJB20	PXT	98.98	5.20	4.57	0.83	13.33	0.02	24.55	0.23	0.01	0.28	0.01	50.56	99.54	12.00	0,672
JJB19, 2	MAn	98.28	31.19	15.26	-0.01	0.84	0. 144	0.34	0.02	0.01	0.03	2.37	48.09	98.37	0.76	0,000
JJB19, 1	PXT	96.49	4.65	4.06	0.90	16.62	0.00	21.33	0.08	0.00	0.10	0.01	49.20	97.90	14.96	0,588
JJB18, 2	BSN	99.75	4.10	3.31	0.43	12.17	0.00	28.17	0.22	0.01	0.20	0.01	51.98	100.50	10.95	0,720
JJB18, 1	PXT	99.56	6.20	4.39	0.40	12.61	0.00	23.00	0.08	0.00	0.01	0.01	53.24	99.98	11.35	0,670
JJB17	PXT	97.92	6.03	4.11	0.50	12.56	0.00	23.01	0.07	0.00	0.04	0.01	51.96	98.38	11.30	0,671
JJB16	PXT	100.80	5.75	3.92	0.46	12.37	0.00	23.36	0.08	0.00	0.06	0.71	53.96	100.23	11.13	0,677
JJB15	PXT	98.80	6.83	4.06	1.38	12.14	0.00	22.75	0.06	0.00	0.06	0.01	51.91	99.35	10.92	0,676
JJB14	BSN	100.42	3.72	3.09	0.44	13.18	0.00	26.38	0.10	0.00	0.05	0.01	54.21	100.98	11.86	0,690
JJB13	BSN	100.04	5.87	3.91	0.40	11.15	0.00	26.88	0.20	0.01	0.17	0.01	52.15	100.48	10.04	0,728
JJB12	BSN	101.37	3.01	2.56	0.42	14.76	0.05	26.15	0.12	0.02	0.21	0.01	54.84	101.85	13.28	0,663
JJB11	PXT	97.88	5.51	3.92	0.52	12.59	0.07	22.35	0.08	0.00	0.10	0.01	53.18	98.42	11.33	0,664
JJB10, 2	MAn	99.36	32.58	15.46	0.00	0.71	0.06	0.08	0.00	0.00	0.00	1.49	49.31	99.99	0.64	0,108
JJB10, 1	PXT	96.21	4.33	3.73	0.66	17.56	0.00	21.74	0.07	0.00	0.07	0.01	48.57	97.98	15.80	0,579
JJB9, 2	BSN	100.59	5.32	4.25	0.41	12.57	0.00	24.12	0.09	0.00	0.04	0.01	54.22	100.78	11.31	0,681
JJB9, 1	PXT	97.93	6.75	4.23	0.49	11.50	0.00	23.07	0.06	0.00	0.00	0.01	52.32	98.48	10.34	0,690
JJB8	San	98.22	22.70	10.91	0.09	4.60	0.17	6.68	0.00	0.00	0.00	1.51	51.63	98.65	4.13	0,618
JJB7	PXT	99.05	7.36	4.81	0.37	11.42	0.08	23.55	0.19	0.01	0.19	0.01	51.45	99.52	10.27	0,696
JJB6	PXT	99.46	6.35	4.72	0.94	11.97	0.04	22.19	0.06	0.00	0.10	0.01	53.33	100.01	10.77	0,673
JJB5, 1	MAn	98.91	5.28	4.18	0.96	13.18	0.15	22.49	0.08	0.00	0.14	0.01	52.76	99.43	11.86	0,655
JJB5	PXT	99.32	29.25	15.06	1.24	3.58	0.10	2.06	0.00	0.01	0.07	1.30	47.24	100.21	3.22	0,390
JJB4, 2	PXT	95.45	5.54	4.25	0.33	14.05	0.00	21.25	0.09	0.00	0.04	0.01	50.32	95.91	12.64	0,627
JJB4, 1	PPXT	90.44	3.81	4.47	0.38	14.98	0.00	21.07	0.09	0.00	0.07	0.01	46.09	91.14	13.48	0,610
JJB3	PXT	92.09	4.39	3.62	0.43	14.91	0.00	21.34	0.09	0.05	0.12	0.01	47.44	92.43	13.41	0,614
JJB2	PXT	94.23	3.82	3.32	0.37	15.66	0.00	22.82	0.09	0.00	0.09	0.01	48.47	94.92	14.09	0,618
JJB1	SA-LN	99.61	22.36	11.07	0.11	5.63	0.06	7.94	0.00	0.00	0.00	1.09	51.45	99.82	5.07	0,611

A2-2 Major elements: Eerste Geluk

Sample	Depth	Rock type	SiO_2	TiO_2	Al_2O_3	Fe_2O_3	MgO	MnO	CaO	Na_2O	K_2O	P_2O_5	Cr_2O_3	NiO	Total	FeO	Mg nr
EST13-04	31.76	LN	51.08	0.08	21.59	4.91	10.02	0.09	11.24	1.27	0.09	0.01	0.14	0.03	100.56	4.42	0.69
EST13-05	38.61	MAN	48.17	0.05	29.91	1.31	1.33	0.03	15.51	2.25	0.17	0.01	0.02	0.01	98.78	1.18	0.53
EST13-06	40.91	SAN-MsN	49.66	0.07	25.22	4.25	5.81	0.07	12.74	1.63	0.12	0.01	0.04	0.04	99.65	3.83	0.60
EST13-07	41.07	MsN	49.34	0.06	27.57	2.85	3.39	0.05	14.29	1.73	0.13	0.01	0.03	0.04	99.50	2.57	0.57
EST13-10	41.41	MsN	50.28	0.09	20.84	5.50	8.31	0.10	13.15	1.26	0.09	0.01	0.11	0.06	99.80	4.95	0.63
EST13-11	41.56	MsN	49.86	0.08	24.13	4.34	6.23	0.07	13.31	1.65	0.11	0.01	0.08	0.05	99.91	3.91	0.61
EST13-12	41.77	MLN+CRS	51.19	0.17	6.14	12.69	22.18	0.19	4.87	0.00	0.03	0.01	0.27	0.37	98.08	11.42	0.66
EST13-14	42.23	MLN	53.70	0.19	5.61	12.34	24.56	0.19	3.98	0.29	0.03	0.01	0.49	0.09	101.47	11.10	0.69
EST13-15	42.40	MLN	52.35	0.16	6.17	11.21	23.15	0.18	4.67	0.31	0.04	0.01	0.37	0.08	98.68	10.09	0.70
EST13-16	42.55	MLN	52.86	0.23	5.11	12.92	23.71	0.21	4.06	0.27	0.08	0.05	0.32	0.11	99.93	11.63	0.67
EST13-17	42.75	MLN	52.87	0.15	6.58	11.02	23.21	0.18	4.96	0.15	0.05	0.01	0.35	0.08	99.60	9.92	0.70
EST13-18	42.95	MLN	53.71	0.24	5.14	12.90	24.25	0.21	3.86	0.25	0.10	0.01	0.43	0.08	101.18	11.61	0.68
EST13-20	43.28	MLN	52.76	0.30	3.70	13.68	24.33	0.20	3.76	1.15	0.17	0.02	0.52	0.08	100.67	12.31	0.66
EST13-21	43.48	MLN	50.47	0.17	6.76	11.15	22.32	0.16	4.68	0.38	0.07	0.01	0.62	0.07	96.85	10.03	0.69
EST13-22	43.68	MLN	55.44	0.41	5.19	12.42	21.14	0.15	3.31	0.58	0.89	0.07	0.81	0.08	100.49	11.17	0.65
EST13-23	43.89	PXP-MLN	53.47	0.25	4.00	13.03	25.71	0.22	3.38	0.53	0.07	0.04	0.24	0.09	101.03	11.72	0.69
EST13-24	44.13	fw MLN	53.13	0.30	2.25	13.54	26.94	0.23	2.64	0.03	0.11	0.03	0.27	0.09	99.55	12.18	0.69
EST13-27	44.50	fw MLN	54.08	0.25	4.85	12.08	24.61	0.21	4.56	0.12	0.14	0.01	0.27	0.08	101.27	10.87	0.69
EST13-28	44.66	fw MLN	52.52	0.23	5.06	11.85	24.00	0.20	5.14	0.13	0.07	0.01	0.26	0.08	99.55	10.66	0.69
EST13-29	44.82	fw MLN	53.07	0.23	3.96	13.17	25.43	0.22	3.82	0.00	0.04	0.01	0.26	0.09	100.18	11.85	0.68
EST13-30	44.96	fw MLN	50.52	0.18	5.44	13.64	26.30	0.21	3.56	0.03	0.07	0.01	0.15	0.14	100.26	12.28	0.68
EST13-31	45.14	fw MLN	52.50	0.22	4.26	12.79	25.40	0.22	3.70	0.00	0.04	0.01	0.22	0.09	99.31	11.51	0.69
EST13-32	45.37	fw MLN	53.35	0.24	5.02	12.38	24.72	0.22	3.69	0.15	0.13	0.01	0.23	0.08	100.21	11.14	0.69
EST13-33	45.58	fw MLN	53.52	0.25	4.92	11.94	23.89	0.21	4.85	0.20	0.12	0.02	0.21	0.08	100.19	10.74	0.69
EST13-34	45.78	fw MLN	51.13	0.23	4.93	12.14	23.03	0.22	4.88	0.17	0.12	0.01	0.19	0.07	97.12	10.92	0.68
EST13-35	55.55	GN	52.34	0.09	14.35	7.06	15.35	0.13	10.40	0.88	0.03	0.01	0.16	0.05	100.85	6.35	0.71
EST13-36	170.28	LN	50.95	0.13	19.36	5.92	10.43	0.10	10.98	1.27	0.15	0.02	0.13	0.03	99.46	5.32	0.66

A2-3 Trace elements: Two Rivers Platinum Mine

Sample	Rock Type	Sum Trace	Ca	Sc	Ti	V	Cr	Fe	Co	Ni	Cu	Zn	Rb	Sr	Y	Zr	Nb	Mo	Ba	Pb	Th	U
JJB20	PXT	19.37	44348	34.49	2938	148.67	5286	139165	106.51	1154	311	80.46	2.55	71.22	5.49	10.49	0.23	0.14	22.59	1.56	0.05	1.04
JJB19, 2	MAn	16.42	154258	16.47	400	6.86	58	8819	4.19	29	9	0.35	3.22	448.81	1.41	3.63	0.04	0.68	153.93	0.88	0.52	3.20
JJB19, 1	PXT	23.38	40505	31.31	3064	163.71	6407	171422	306.27	8826	2866	70.65	2.42	59.02	4.65	8.42	0.78	1.72	34.96	1.50	0.50	2.09
JJB18, 2	BSN	16.63	32209	25.94	1927	102.75	2914	126901	119.32	1246	697	64.67	0.84	51.41	3.01	4.43	0.40	0.36	56.46	1.42	1.31	1.39
JJB18, 1	PXT	18.09	44567	26.42	2088	104.18	2930	128948	117.60	1371	514	66.82	2.51	83.97	4.73	9.31	0.45	0.91	63.95	6.82	1.34	1.61
JJB17	PXT	17.62	41553	29.87	2435	115.69	3653	126582	110.15	1149	351	70.09	3.51	83.02	4.11	9.52	0.45	1.07	49.64	2.80	1.33	0.76
JJB16	PXT	16.91	36959	26.08	2506	111.60	3315	125202	93.49	601	99	69.26	6.44	74.51	4.69	18.19	1.24	0.48	41.40	2.27	0.30	1.65
JJB15	PXT	17.62	42281	28.52	2503	166.30	9063	120892	100.49	720	197	74.74	3.19	90.62	3.38	18.28	0.00	0.31	44.09	1.49	0.48	0.83
JJB14	BSN	17.02	29548	27.92	2370	118.45	3151	133348	114.71	894	436	74.23	0.65	41.91	4.34	4.23	0.08	0.31	27.62	2.20	1.33	1.51
JJB13	BSN	16.32	37452	25.33	1775	103.71	2954	119994	98.82	481	112	65.30	1.58	78.62	3.03	3.50	0.39	0.84	63.27	1.00	1.30	0.79
JJB12	BSN	17.98	24664	28.63	4132	140.93	3000	147108	102.77	494	39	91.79	7.24	34.10	6.66	31.06	1.37	0.45	1.56	0.05	1.36	1.01
JJB11	PXT	17.29	37459	27.11	2924	129.18	3636	127795	97.00	554	104	73.77	6.75	72.12	5.78	26.61	1.11	0.13	25.86	0.32	0.27	1.16
JJB10, 2	MAn	16.11	151696	14.29	358	3.74	8	8337	2.80	45	26	0.35	2.99	446.75	0.75	3.13	0.35	0.27	149.78	0.88	0.19	1.87
JJB10, 1	PXT	25.77	38900	26.84	2723	146.43	5223	191063	309.02	13881	5193	57.75	1.29	57.64	5.04	7.74	0.21	1.22	60.19	3.37	0.46	0.21
JJB9, 2	BSN	17.05	40704	27.00	2309	115.18	2749	123456	98.26	696	161	70.50	1.97	68.40	3.75	6.10	0.17	0.96	36.03	0.37	0.44	0.69
JJB9, 1	PXT	16.25	43888	25.74	1592	98.66	3479	112150	92.79	672	230	61.39	1.96	92.33	2.98	5.11	0.39	0.65	81.05	1.24	1.01	1.12
JJB8	San	15.58	105413	20.63	1501	42.93	717	46220	40.32	692	607	17.05	5.38	372.86	3.58	20.80	0.50	0.43	139.76	4.83	0.95	2.70
JJB7	PXT	17.74	47416	26.52	2023	99.29	2742	121755	111.28	1977	948	64.10	5.53	107.30	4.61	14.96	0.35	0.55	76.93	3.36	1.33	1.86
JJB6	PXT	17.79	46039	27.98	3043	157.08	6153	121438	96.58	678	93	71.54	6.68	80.14	5.84	22.31	2.06	1.24	25.04	0.91	1.06	1.17
JJB5	MAn	16.73	147423	19.71	584	17.25	222	18031	12.36	262	137	0.36	3.02	421.36	1.53	3.42	0.36	0.18	139.07	0.90	0.29	2.08
JJB4, 2	PPXT	19.95	42574	29.73	2392	125.07	2650	145618	139.00	3818	1969	72.58	3.32	75.42	5.19	13.21	0.69	1.05	46.46	6.46	0.44	1.03
JJB4, 1	PXT	22.30	46528	31.37	2775	147.99	3029	162010	168.98	5561	2586	76.36	3.06	54.54	6.83	20.57	0.34	0.40	30.48	7.88	1.44	1.11
JJB3	PXT	20.96	37996	28.41	3418	145.38	3560	156359	163.85	5204	2534	73.95	6.78	64.46	6.66	23.72	1.37	0.90	19.95	5.28	1.44	1.95
JJB2	PXT	21.46	33562	29.68	3030	140.09	2964	164972	207.13	6924	2634	74.84	1.82	48.24	5.63	13.59	0.23	1.34	25.33	3.98	1.43	0.83
JJB1	SA-LN	16.85	110604	21.12	1167	48.78	736	53893	47.89	878	620	20.00	2.39	327.27	2.85	5.11	0.37	0.96	128.25	0.78	1.67	1.47

A2-4 Trace elements: Eerste Geluk

Sample	Sum Trace	Ca	Sc	Ti	V	Cr	Fe^{3+}	Co	Ni	Cu	Zn	Rb	Sr	Y	Zr	Nb	Mo	Ba	Pb	Th	U
EST013_04	16.69	113088	21.07	901	43.37	1109	51085	36.93	211	23.97	22.09	2.61	260.39	1.54	3.43	0.38	0.27	128.39	0.94	1.26	1.41
EST013_05	82.79	755487	91.62	2782	116.55	835	65237	32.44	434	288.92	-6.64	12.92	1851.42	8.49	86.68	0.37	0.28	691.39	0.95	1.25	11.46
EST013_06	17.83	132221	22.74	744	37.19	466	43882	32.02	273	123.66	16.76	2.55	352.03	1.28	3.99	0.37	0.35	129.67	0.95	0.47	0.92
EST013_07	17.12	140143	18.10	620	31.37	322	29157	22.18	249	95.42	5.84	3.09	369.66	1.53	4.15	0.37	0.63	163.29	0.01	1.24	0.53
EST013_10	19.12	132652	30.74	935	72.59	970	55299	43.70	458	290.16	20.02	1.89	285.87	2.88	3.74	0.37	0.03	113.90	0.55	1.24	1.85
EST013_11	18.24	135584	19.87	782	50.09	625	44284	34.49	336	161.89	16.36	2.71	336.01	1.87	3.54	0.37	0.29	139.71	0.93	0.13	1.24
EST013_12	89.45	228649	146.35	8115	588.33	13175	620768	690.11	14939	6272.32	304.20	10.71	395.90	17.28	49.36	1.32	1.71	400.77	13.16	1.32	0.81
EST013_14	78.85	175988	123.14	8640	630.69	20289	577760	489.30	3262	244.69	330.64	3.35	353.83	13.33	30.62	1.62	2.70	325.56	9.86	1.51	3.56
EST013_15	80.36	172557	136.44	11382	638.29	16658	597429	479.30	2955	351.59	342.27	16.51	320.79	20.90	112.85	4.21	4.15	234.40	5.30	1.32	3.50
EST013_16	79.05	170143	123.82	10356	595.40	13880	588987	491.62	4012	894.76	330.26	10.72	305.62	25.31	54.42	3.05	1.49	253.09	0.42	2.28	2.36
EST013_17	77.91	225388	116.25	7016	515.92	14858	526740	443.00	2691	193.58	279.24	7.95	426.89	12.64	34.45	0.40	0.57	404.89	1.02	1.32	1.64
EST013_18	78.05	166402	131.17	11102	594.62	16315	581280	466.17	2891	341.50	332.69	15.78	312.33	22.39	81.06	2.78	2.72	235.29	6.72	1.32	7.15
EST013_20	85.56	164147	136.35	15035	834.37	23213	647766	496.67	2956	247.04	380.34	19.60	202.94	28.20	84.68	0.85	1.41	39.51	1.02	1.32	5.24
EST013_21	78.86	220724	120.88	8605	648.38	28939	525031	449.43	2644	264.81	296.61	10.03	451.65	13.34	57.77	3.75	2.32	335.25	1.02	1.32	0.81
EST013_22	79.17	147454	121.55	21970	954.56	33903	582109	466.99	3014	597.79	325.61	180.96	241.42	34.63	178.22	18.32	4.02	44.25	20.98	9.43	9.35
EST013_23	78.51	149520	119.32	11677	572.60	11065	607241	517.65	3290	211.72	341.04	10.10	256.34	25.26	54.29	1.85	3.41	169.41	4.54	1.32	2.76
EST013_24	79.23	111799	131.97	14597	660.04	12238	648333	538.01	3271	107.77	361.62	21.85	97.56	27.77	68.64	0.40	1.81	20.43	1.02	1.32	9.49
EST013_27	80.89	200006	128.81	12024	619.89	12048	579589	478.80	2894	156.78	318.18	24.78	288.25	24.20	76.97	1.80	0.71	176.31	5.41	1.32	8.27
EST013_28	81.70	229085	129.06	11177	618.75	11846	559830	475.36	2811	109.50	290.72	12.48	321.14	23.83	63.07	0.81	1.77	197.37	1.02	1.32	0.81
EST013_29	81.90	168402	130.39	10919	653.06	11726	622516	507.58	3087	154.38	354.25	8.03	225.94	21.08	47.80	1.30	4.15	201.31	4.65	1.32	6.73
EST013_30	81.74	156898	105.80	8040	421.53	6218	638086	629.79	5202	626.41	345.61	18.86	349.72	13.60	47.32	2.30	2.21	344.80	2.15	1.32	9.55
EST013_31	79.87	170614	124.98	10274	604.70	10176	601923	523.72	3327	176.97	331.83	7.79	258.21	20.57	50.06	3.45	3.63	224.09	4.78	2.84	9.86
EST013_32	77.77	165170	124.29	11784	597.84	9137	586279	505.81	2970	132.40	317.62	27.28	308.19	21.10	85.02	5.12	5.00	210.85	7.66	3.70	3.70
EST013_33	80.79	214244	131.88	12229	658.30	9582	566750	477.48	2702	153.88	314.26	21.36	297.46	24.70	91.57	1.66	0.09	194.69	7.07	1.32	4.70
EST013_34	17.54	47053	29.77	2409	137.22	1893	123007	98.81	579	29.69	68.73	5.06	67.30	5.11	13.96	0.40	0.44	42.27	0.08	1.32	0.63
EST013_35	17.83	103515	30.15	876	91.96	1279	71712	57.16	350	9.97	31.27	1.20	200.30	1.61	3.03	0.18	0.89	103.83	0.95	1.02	0.81
EST013_36	17.52	110910	25.05	1344	61.47	1181	60977	46.07	242	12.71	25.08	5.19	281.74	2.56	13.39	0.38	0.30	103.47	0.11	0.52	1.98

Appendix Three: Mineral Chemistry

A3-1.1 Orthopyroxene Compositions (EPMA-Rhodes University)

Sample	Lithology	SiO_2	CaO	K_2O	MgO	Al_2O_3	FeO	MnO	TiO_2	NiO	Na_2O	$Cr2O_3$	Total
JJB19	PXT-MR-CHR	53.9	0.31	0.05	29.27	1.36	12.30	0.00	0.02	0.12	0.00	0.37	97.68
JJB19	PXT-MR-CHR	54.7	0.53	0.00	29.81	1.49	12.00	0.03	0.01	0.10	0.00	0.49	99.14
JJB19	PXT-MR-CHR	58.8	0.26	0.12	33.89	1.25	8.10	0.04	0.02	0.07	0.02	0.86	103.46
JJB19	PXT-MR-CHR	54.6	1.57	0.02	30.58	1.40	9.21	0.02	0.01	0.07	0.02	0.35	97.86
JJB19	PXT-MR-CHR	53.4	3.67	0.01	26.56	1.28	12.68	0.02	0.01	0.07	0.05	0.45	98.20
JJB19	PXT-MR-CHR	53.7	2.54	0.01	27.15	1.25	13.50	0.04	0.00	0.11	0.01	0.39	98.68
JJB19	PXT-MR-CHR	54.1	0.36	0.03	29.76	0.69	12.25	0.03	0.01	0.04	0.00	0.14	97.40
JJB13	PXT-MR	55.1	1.20	0.01	30.45	1.21	11.45	0.04	0.01	0.07	0.04	0.50	100.06
JJB13	BSN-MR	54.4	1.77	0.02	28.54	1.27	13.35	0.06	0.02	0.07	0.01	0.39	99.94
JJB13	BSN-MR	59.2	0.06	0.04	24.92	0.13	9.51	0.00	0.01	0.05	0.01	0.02	93.91
JJB13	BSN-MR	56.1	0.43	0.00	29.26	0.88	13.71	0.05	0.01	0.04	0.00	0.30	100.78
JJB13	BSN-MR	56.0	0.48	0.01	28.25	0.48	14.64	0.04	0.01	0.04	0.01	0.01	99.95
JJB13	BSN-MR	54.8	0.65	0.03	28.30	1.38	14.40	0.03	0.01	0.06	0.02	0.42	100.14
JJB11	PXT-MR	55.5	0.74	0.04	28.05	0.82	14.72	0.07	0.02	0.06	0.02	0.24	100.24
JJB11	PXT-MR	55.8	0.69	0.01	28.51	0.87	15.36	0.02	0.02	0.03	0.01	0.23	101.54
JJB11	PXT-MR	54.4	2.05	0.02	27.88	1.30	13.02	0.02	0.02	0.08	0.04	0.50	99.29
JJB11	PXT-MR	54.6	2.08	0.00	28.13	1.28	13.39	0.03	0.02	0.06	0.02	0.49	100.05
JJB11	PXT-MR	54.6	1.79	0.03	28.27	1.29	13.18	0.01	0.00	0.03	0.05	0.46	99.72
JJB11	PXT-MR	55.0	1.06	0.01	29.03	1.13	13.34	0.05	0.02	0.07	0.00	0.49	100.24
JJB11	PXT-MR	54.9	1.36	0.01	28.91	1.19	12.93	0.05	0.02	0.06	0.00	0.42	99.89
JJB11	PXT-MR	55.1	1.39	0.01	28.93	1.18	12.60	0.02	0.03	0.08	0.02	0.42	99.79
JJB11	PXT-MR	54.5	1.14	0.01	28.92	1.18	12.98	0.04	0.02	0.05	0.02	0.47	99.34
JJB16	PXT-MR	55.9	0.43	0.03	30.57	0.85	11.90	0.02	0.00	0.07	0.01	0.20	99.97
JJB16	PXT-MR	55.3	0.57	0.01	30.43	0.87	11.44	0.02	0.01	0.05	0.02	0.35	99.05
JJB16	PXT-MR	55.5	1.58	0.05	30.19	1.56	10.65	0.03	0.01	0.05	0.02	0.52	100.16
JJB16	PXT-MR	54.4	0.61	0.02	30.37	1.54	11.31	0.07	0.01	0.06	0.00	0.55	98.95
JJB16	PXT-MR	50.2	2.26	0.03	26.05	1.26	8.15	0.03	0.02	0.03	0.06	0.33	88.41
JJB16	PXT-MR	54.2	1.07	0.02	28.71	1.33	13.24	0.06	0.02	0.09	0.03	0.43	99.23
JJB16	PXT-MR	54.4	1.15	0.02	28.90	1.20	13.09	0.09	0.00	0.07	0.03	0.40	99.30
JJB16	PXT-MR	54.6	0.46	0.02	29.50	0.92	13.45	0.01	0.03	0.02	0.00	0.32	99.34
JJB16	PXT-MR	53.8	1.19	0.02	28.33	1.00	12.77	0.03	0.03	0.05	0.01	0.31	97.57
JJB18	BSN-HW	55.9	0.90	0.01	30.15	1.27	11.36	0.02	0.03	0.07	0.01	0.42	100.10
JJB18	BSN-HW	55.5	0.86	0.00	30.02	1.24	11.37	0.02	0.01	0.04	0.02	0.42	99.51
JJB18	BSN-HW	55.8	0.66	0.02	30.19	1.22	11.72	0.03	0.05	0.06	0.00	0.48	100.19
JJB18	BSN-HW	56.2	0.69	0.02	29.99	1.21	11.24	0.05	0.02	0.09	0.02	0.43	100.00
JJB18	BSN-HW	55.1	1.60	0.00	29.83	1.32	11.52	0.05	0.01	0.05	0.03	0.50	100.03
JJB18	BSN-HW	54.5	1.20	0.02	29.87	1.32	11.54	0.06	0.03	0.08	0.02	0.47	99.16
JJB18	BSN-HW	55.0	0.80	0.01	29.95	1.23	11.53	0.04	0.00	0.04	0.01	0.51	99.08
JJB18	BSN-HW	55.1	0.52	0.01	30.09	1.19	12.32	0.03	0.02	0.06	0.02	0.42	99.82
JJB18	BSN-HW	55.4	0.44	0.01	30.17	1.07	11.71	0.00	0.04	0.03	0.00	0.37	99.22
JJB18	BSN-HW	56.0	0.66	0.04	30.24	1.29	11.94	0.01	0.00	0.06	0.03	0.47	100.71
JJB18	BSN-HW	55.8	0.62	0.00	30.23	1.24	12.07	0.04	0.01	0.05	0.05	0.47	100.56
JJB18	BSN-HW	55.4	0.45	0.00	30.33	1.17	11.53	0.00	0.02	0.05	0.03	0.47	99.44
JJB18	BSN-HW	55.9	0.69	0.01	30.64	1.23	11.57	0.07	0.03	0.05	0.03	0.52	100.75
JJB18	BSN-HW	55.2	1.71	0.01	29.84	1.18	12.06	0.03	0.03	0.04	0.02	0.51	100.64
JJB18	BSN-HW	55.2	1.05	0.02	30.37	1.12	11.74	0.05	0.03	0.06	0.03	0.48	100.11
JJB18	BSN-HW	55.4	0.57	0.03	30.05	1.25	11.66	0.03	0.03	0.09	0.02	0.51	99.58
JJB18	BSN-HW	55.3	0.56	0.02	30.34	1.20	12.22	0.06	0.03	0.06	0.02	0.53	100.39
JJB18	BSN-HW	55.3	1.13	0.02	29.43	1.33	12.16	0.10	0.03	0.07	0.02	0.54	100.18
JJB17	PXT-HW	55.1	1.59	0.01	28.85	1.37	11.74	0.06	0.00	0.08	0.02	0.56	99.37
JJB17	PXT-HW	54.7	0.66	0.02	29.10	1.29	12.78	0.02	0.05	0.06	0.01	0.45	99.09
JJB17	PXT-HW	54.6	2.00	0.02	28.73	1.29	12.78	0.00	0.03	0.07	0.01	0.51	99.98
JJB17	PXT-HW	54.0	0.36	0.03	28.36	0.90	13.63	0.04	0.03	0.05	0.02	0.28	97.73
JJB17	PXT-HW	53.9	0.57	0.01	28.24	0.79	14.18	0.05	0.05	0.07	0.03	0.23	98.06
JJB17	PXT-HW	54.0	2.03	0.02	28.94	1.35	11.99	0.06	0.03	0.07	0.03	0.48	99.03

Sample	Lithology	SiO_2	CaO	K_2O	MgO	Al_2O_3	FeO	MnO	TiO_2	NiO	Na_2O	$Cr2O_3$	Total
JJB9	BSN-MR	54.5	1.35	0.02	29.63	1.48	11.10	0.05	0.03	0.09	0.02	0.60	98.85
JJB9	BSN-MR	54.7	0.70	0.00	30.31	1.28	12.05	0.08	0.02	0.13	0.01	0.53	99.78
JJB9	BSN-MR	54.6	1.83	0.02	29.33	1.36	10.93	0.07	0.01	0.10	0.01	0.54	98.78
JJB9	BSN-MR	54.8	0.62	0.01	30.37	1.38	11.71	0.05	0.01	0.06	0.02	0.50	99.51
JJB9	BSN-MR	54.7	1.60	0.00	29.56	1.17	12.41	0.07	0.01	0.09	0.02	0.45	100.06
JJB9	BSN-MR	54.4	0.80	0.02	29.34	1.28	12.26	0.00	0.01	0.10	0.03	0.56	98.77
JJB9	PXT-MR	54.4	0.59	0.03	29.02	0.97	13.77	0.09	0.02	0.11	0.02	0.33	99.38
JJB9	PXT-MR	54.6	2.12	0.03	28.81	1.23	12.01	0.06	0.03	0.10	0.05	0.53	99.61
JJB9	PXT-MR	54.6	0.67	0.04	29.61	1.29	11.97	0.06	0.02	0.11	0.02	0.53	98.94
JJB14	BSN-MR	55.3	0.46	0.04	30.51	1.04	11.98	0.03	0.04	0.00	0.01	0.42	99.78
JJB14	BSN-MR	54.7	0.65	0.01	29.71	1.38	12.13	0.03	0.03	0.06	0.01	0.52	99.23
JJB14	BSN-MR	54.3	0.98	0.02	29.84	1.32	11.85	0.05	0.02	0.06	0.02	0.50	98.95
JJB14	BSN-MR	55.9	0.62	0.00	30.32	1.14	11.60	0.05	0.03	0.00	0.00	0.46	100.10
JJB14	BSN-MR	55.7	0.73	0.01	30.30	1.39	11.26	0.06	0.01	0.00	0.01	0.58	100.09
JJB14	BSN-MR	55.6	0.56	0.03	30.55	1.30	11.35	0.02	0.00	0.00	0.01	0.52	99.94
JJB14	BSN-MR	55.9	0.66	0.02	30.25	1.15	11.67	0.00	0.01	0.00	0.00	0.46	100.10
JJB14	BSN-MR	54.8	1.01	0.01	30.20	1.07	12.00	0.07	0.03	0.07	0.00	0.33	99.63
JJB10	PXT-MR-CHR	55.4	0.55	0.05	31.80	1.34	9.48	0.04	0.02	0.07	0.00	0.31	99.08
JJB10	PXT-MR-CHR	54.9	0.60	0.01	29.69	1.28	12.02	0.00	0.03	0.09	0.01	0.44	99.04
JJB10	PXT-MR-CHR	56.5	0.43	0.04	23.79	1.76	9.03	0.05	0.01	0.03	0.13	0.21	91.94
JJB10	PXT-MR-CHR	55.0	1.12	0.03	29.79	1.29	12.43	0.03	0.01	0.10	0.00	0.37	100.19
TRP-AL7906	An-NOR-PXT HW	53.6	1.69	0.02	25.99	1.28	17.20	0.02	0.01	0.12	0.01	0.36	100.33
TRP-AL7906	An-NOR-PXT HW	53.8	0.46	0.02	26.57	0.86	17.53	0.05	0.03	0.08	0.02	0.25	99.64
TRP-AL7906	An-NOR-PXT HW	53.4	0.51	0.02	25.55	0.83	19.26	0.09	0.00	0.07	0.01	0.19	99.97
TRP-AL7906	An-NOR-PXT HW	54.3	0.56	0.04	26.01	1.02	17.72	0.07	0.01	0.09	0.00	0.29	100.10
TRP-AL7906	An-NOR-PXT HW	53.6	2.06	0.03	25.33	1.00	16.70	0.05	0.01	0.09	0.02	0.23	99.11
TRP-AL7907B	PXT-MR	57.9	0.32	0.02	26.04	1.02	12.79	0.03	0.01	0.13	0.11	0.19	98.60
TRP-AL7907B	PXT-MR	53.9	0.40	0.01	28.48	1.41	14.66	0.07	0.00	0.11	0.01	0.48	99.54
TRP-AL7907B	PXT-MR	54.9	1.24	0.02	28.71	1.52	12.53	0.03	0.02	0.08	0.04	0.49	99.61
TRP-AL7908	PXT-MR	54.0	1.33	0.03	28.33	0.98	13.82	0.06	0.02	0.09	0.01	0.26	98.94
TRP-AL7908	PXT-MR	54.2	0.51	0.02	28.73	0.81	14.14	0.09	0.03	0.12	0.01	0.28	98.98
TRP-AL7908	PXT-MR	54.3	0.42	0.01	29.10	0.68	14.16	0.06	0.03	0.04	0.01	0.23	99.01
TRP-AL7908	PXT-MR	54.6	0.63	0.02	29.07	0.80	14.10	0.09	0.01	0.09	0.02	0.22	99.66
TRP-AL7908	PXT-MR	55.4	0.69	0.00	28.47	0.85	13.84	0.02	0.00	0.12	0.00	0.22	99.62
TRP-AL7908	PXT-MR	54.6	0.53	0.03	28.25	1.04	14.53	0.04	0.03	0.10	0.00	0.27	99.42
TRP-AL7908	PXT-MR	57.9	0.75	0.02	26.10	0.74	12.40	0.03	0.01	0.10	0.08	0.10	98.22
TRP-AL7908	PXT-MR	54.8	0.42	0.03	28.79	0.71	13.50	0.04	0.04	0.11	0.00	0.22	98.61
EST013-11	MsN-HW	56.4	1.68	0.01	27.53	1.17	14.64	0.05	0.01	0.00	0.04	0.40	101.88
EST013-11	MsN-HW	56.4	1.59	0.00	27.48	0.91	15.42	0.06	0.01	0.00	0.02	0.27	102.18
EST013-11	MsN-HW	55.6	0.59	0.02	26.82	0.98	14.66	0.07	0.02	0.00	0.03	0.35	99.10
EST013-11	MsN-HW	55.7	0.69	0.01	27.57	0.87	16.16	0.04	0.01	0.00	0.03	0.27	101.36
EST013-10	MsN-HW	55.8	0.63	0.04	27.56	0.91	15.24	0.07	0.01	0.00	0.00	0.29	100.52
EST013-10	MsN-HW	56.0	1.15	0.00	27.19	1.00	15.67	0.04	0.01	0.00	0.01	0.30	101.39
EST013-10	MsN-HW	55.4	4.94	0.02	25.60	1.13	13.12	0.05	0.00	0.00	0.06	0.37	100.68
EST013-10	MsN-HW	56.6	1.17	0.00	28.10	0.97	14.88	0.04	0.01	0.00	0.01	0.29	102.04
EST013-10	MsN-HW	55.6	0.65	0.01	27.35	1.05	15.25	0.08	0.01	0.00	0.00	0.33	100.29
EST013-10	MsN-HW	55.6	0.65	0.01	27.35	1.05	15.25	0.08	0.01	0.00	0.00	0.33	100.29
EST013-10	MsN-HW	56.0	0.37	0.00	28.00	0.69	15.41	0.06	0.02	0.00	0.02	0.20	100.74

A3-1.2 Cations per 6 oxygens

Sample	Lithology	Si	Ca	K	Mg	Al	Fe	Mn	Ti	Ni	Na	Cr	Total
JJB19	PXT-MR-CHR	1.96	0.01	0.00	1.59	0.06	0.37	0.00	0.00	0.00	0.00	0.01	4.01
JJB19	PXT-MR-CHR	1.96	0.02	0.00	1.59	0.06	0.36	0.00	0.00	0.00	0.00	0.01	4.00
JJB19	PXT-MR-CHR	1.98	0.01	0.01	1.70	0.05	0.23	0.00	0.00	0.00	0.00	0.02	3.99
JJB19	PXT-MR-CHR	1.96	0.06	0.00	1.64	0.06	0.28	0.00	0.00	0.00	0.00	0.01	4.01
JJB19	PXT-MR-CHR	1.96	0.14	0.00	1.45	0.06	0.39	0.00	0.00	0.00	0.00	0.01	4.01
JJB19	PXT-MR-CHR	1.96	0.10	0.00	1.47	0.05	0.41	0.00	0.00	0.00	0.00	0.01	4.01
JJB19	PXT-MR-CHR	1.97	0.01	0.00	1.62	0.03	0.37	0.00	0.00	0.00	0.00	0.00	4.01
JJB13	PXT-MR	1.95	0.05	0.00	1.61	0.05	0.34	0.00	0.00	0.00	0.00	0.01	4.02
JJB13	BSN-MR	1.95	0.07	0.00	1.53	0.05	0.40	0.00	0.00	0.00	0.00	0.01	4.02
JJB13	BSN-MR	2.17	0.00	0.00	1.36	0.01	0.29	0.00	0.00	0.00	0.00	0.00	3.83
JJB13	BSN-MR	1.98	0.02	0.00	1.54	0.04	0.41	0.00	0.00	0.00	0.00	0.01	3.99
JJB13	BSN-MR	2.00	0.02	0.00	1.51	0.02	0.44	0.00	0.00	0.00	0.00	0.00	3.99
JJB13	BSN-MR	1.96	0.02	0.00	1.51	0.06	0.43	0.00	0.00	0.00	0.00	0.01	4.00
JJB11	PXT-MR	1.98	0.03	0.00	1.49	0.03	0.44	0.00	0.00	0.00	0.00	0.01	4.00
JJB11	PXT-MR	1.97	0.03	0.00	1.50	0.04	0.45	0.00	0.00	0.00	0.00	0.01	4.00
JJB11	PXT-MR	1.96	0.08	0.00	1.50	0.06	0.39	0.00	0.00	0.00	0.00	0.01	4.01
JJB11	PXT-MR	1.96	0.08	0.00	1.50	0.05	0.40	0.00	0.00	0.00	0.00	0.01	4.01
JJB11	PXT-MR	1.96	0.07	0.00	1.51	0.05	0.40	0.00	0.00	0.00	0.00	0.01	4.01
JJB11	PXT-MR	1.96	0.04	0.00	1.54	0.05	0.40	0.00	0.00	0.00	0.00	0.01	4.01
JJB11	PXT-MR	1.96	0.05	0.00	1.54	0.05	0.39	0.00	0.00	0.00	0.00	0.01	4.01
JJB11	PXT-MR	1.97	0.05	0.00	1.54	0.05	0.38	0.00	0.00	0.00	0.00	0.01	4.00
JJB11	PXT-MR	1.96	0.04	0.00	1.55	0.05	0.39	0.00	0.00	0.00	0.00	0.01	4.01
JJB16	PXT-MR	1.98	0.02	0.00	1.61	0.04	0.35	0.00	0.00	0.00	0.00	0.01	4.00
JJB16	PXT-MR	1.97	0.02	0.00	1.62	0.04	0.34	0.00	0.00	0.00	0.00	0.01	4.00
JJB16	PXT-MR	1.96	0.06	0.00	1.59	0.06	0.31	0.00	0.00	0.00	0.00	0.01	4.00
JJB16	PXT-MR	1.95	0.02	0.00	1.62	0.06	0.34	0.00	0.00	0.00	0.00	0.02	4.01
JJB16	PXT-MR	1.99	0.10	0.00	1.54	0.06	0.27	0.00	0.00	0.00	0.00	0.01	3.98
JJB16	PXT-MR	1.95	0.04	0.00	1.54	0.06	0.40	0.00	0.00	0.00	0.00	0.01	4.01
JJB16	PXT-MR	1.96	0.04	0.00	1.55	0.05	0.39	0.00	0.00	0.00	0.00	0.01	4.01
JJB16	PXT-MR	1.96	0.02	0.00	1.58	0.04	0.40	0.00	0.00	0.00	0.00	0.01	4.01
JJB16	PXT-MR	1.97	0.05	0.00	1.54	0.04	0.39	0.00	0.00	0.00	0.00	0.01	4.01
JJB18	BSN-HW	1.97	0.03	0.00	1.59	0.05	0.34	0.00	0.00	0.00	0.00	0.01	3.99
JJB18	BSN-HW	1.97	0.03	0.00	1.59	0.05	0.34	0.00	0.00	0.00	0.00	0.01	4.00
JJB18	BSN-HW	1.97	0.02	0.00	1.59	0.05	0.35	0.00	0.00	0.00	0.00	0.01	4.00
JJB18	BSN-HW	1.98	0.03	0.00	1.58	0.05	0.33	0.00	0.00	0.00	0.00	0.01	3.99
JJB18	BSN-HW	1.96	0.06	0.00	1.58	0.06	0.34	0.00	0.00	0.00	0.00	0.01	4.01
JJB18	BSN-HW	1.95	0.05	0.00	1.59	0.06	0.35	0.00	0.00	0.00	0.00	0.01	4.01
JJB18	BSN-HW	1.96	0.03	0.00	1.59	0.05	0.34	0.00	0.00	0.00	0.00	0.01	4.00
JJB18	BSN-HW	1.96	0.02	0.00	1.60	0.05	0.37	0.00	0.00	0.00	0.00	0.01	4.01
JJB18	BSN-HW	1.97	0.02	0.00	1.60	0.04	0.35	0.00	0.00	0.00	0.00	0.01	4.00
JJB18	BSN-HW	1.97	0.02	0.00	1.58	0.05	0.35	0.00	0.00	0.00	0.00	0.01	4.00
JJB18	BSN-HW	1.97	0.02	0.00	1.59	0.05	0.36	0.00	0.00	0.00	0.00	0.01	4.00
JJB18	BSN-HW	1.97	0.02	0.00	1.61	0.05	0.34	0.00	0.00	0.00	0.00	0.01	4.00
JJB18	BSN-HW	1.96	0.03	0.00	1.60	0.05	0.34	0.00	0.00	0.00	0.00	0.01	4.00
JJB18	BSN-HW	1.95	0.06	0.00	1.57	0.05	0.36	0.00	0.00	0.00	0.00	0.01	4.02
JJB18	BSN-HW	1.96	0.04	0.00	1.60	0.05	0.35	0.00	0.00	0.00	0.00	0.01	4.01
JJB18	BSN-HW	1.97	0.02	0.00	1.59	0.05	0.35	0.00	0.00	0.00	0.00	0.01	4.00
JJB18	BSN-HW	1.96	0.02	0.00	1.60	0.05	0.36	0.00	0.00	0.00	0.00	0.01	4.01
JJB18	BSN-HW	1.96	0.04	0.00	1.56	0.06	0.36	0.00	0.00	0.00	0.00	0.02	4.00
JJB17	PXT-HW	1.97	0.06	0.00	1.54	0.06	0.35	0.00	0.00	0.00	0.00	0.02	3.99
JJB17	PXT-HW	1.96	0.03	0.00	1.56	0.05	0.38	0.00	0.00	0.00	0.00	0.01	4.00
JJB17	PXT-HW	1.95	0.08	0.00	1.53	0.05	0.38	0.00	0.00	0.00	0.00	0.01	4.01
JJB17	PXT-HW	1.97	0.01	0.00	1.55	0.04	0.42	0.00	0.00	0.00	0.00	0.01	4.00
JJB17	PXT-HW	1.97	0.02	0.00	1.54	0.03	0.43	0.00	0.00	0.00	0.00	0.01	4.01
JJB17	PXT-HW	1.95	0.08	0.00	1.55	0.06	0.36	0.00	0.00	0.00	0.00	0.01	4.02

Sample	Lithology	Si	Ca	K	Mg	Al	Fe	Mn	Ti	Ni	Na	Cr	Total
JJB9	BSN-MR	1.95	0.05	0.00	1.58	0.06	0.33	0.00	0.00	0.00	0.00	0.02	4.01
JJB9	BSN-MR	1.95	0.03	0.00	1.61	0.05	0.36	0.00	0.00	0.00	0.00	0.01	4.02
JJB9	BSN-MR	1.96	0.07	0.00	1.57	0.06	0.33	0.00	0.00	0.00	0.00	0.02	4.00
JJB9	BSN-MR	1.95	0.02	0.00	1.61	0.06	0.35	0.00	0.00	0.00	0.00	0.01	4.01
JJB9	BSN-MR	1.95	0.06	0.00	1.57	0.05	0.37	0.00	0.00	0.00	0.00	0.01	4.02
JJB9	BSN-MR	1.96	0.03	0.00	1.57	0.05	0.37	0.00	0.00	0.00	0.00	0.02	4.01
JJB9	PXT-MR	1.96	0.02	0.00	1.56	0.04	0.42	0.00	0.00	0.00	0.00	0.01	4.01
JJB9	PXT-MR	1.96	0.08	0.00	1.54	0.05	0.36	0.00	0.00	0.00	0.00	0.02	4.01
JJB9	PXT-MR	1.96	0.03	0.00	1.58	0.05	0.36	0.00	0.00	0.00	0.00	0.02	4.01
JJB14	BSN-MR	1.96	0.02	0.00	1.61	0.04	0.36	0.00	0.00	0.00	0.00	0.01	4.01
JJB14	BSN-MR	1.96	0.02	0.00	1.58	0.06	0.36	0.00	0.00	0.00	0.00	0.01	4.01
JJB14	BSN-MR	1.95	0.04	0.00	1.60	0.06	0.36	0.00	0.00	0.00	0.00	0.01	4.02
JJB14	BSN-MR	1.97	0.02	0.00	1.59	0.05	0.34	0.00	0.00	0.00	0.00	0.01	4.00
JJB14	BSN-MR	1.97	0.03	0.00	1.59	0.06	0.33	0.00	0.00	0.00	0.00	0.02	4.00
JJB14	BSN-MR	1.96	0.02	0.00	1.61	0.05	0.34	0.00	0.00	0.00	0.00	0.01	4.00
JJB14	BSN-MR	1.97	0.02	0.00	1.59	0.05	0.34	0.00	0.00	0.00	0.00	0.01	4.00
JJB14	BSN-MR	1.96	0.04	0.00	1.61	0.05	0.36	0.00	0.00	0.00	0.00	0.01	4.02
JJB10	PXT-MR-CHR	1.96	0.02	0.00	1.68	0.06	0.28	0.00	0.00	0.00	0.00	0.01	4.01
JJB10	PXT-MR-CHR	1.97	0.02	0.00	1.58	0.05	0.36	0.00	0.00	0.00	0.00	0.01	4.00
JJB10	PXT-MR-CHR	2.12	0.02	0.00	1.33	0.08	0.28	0.00	0.00	0.00	0.01	0.01	3.85
JJB10	PXT-MR-CHR	1.96	0.04	0.00	1.58	0.05	0.37	0.00	0.00	0.00	0.00	0.01	4.01
TRP-AL7906	An-NOR-PXT HW	1.95	0.07	0.00	1.41	0.05	0.52	0.00	0.00	0.00	0.00	0.01	4.02
TRP-AL7906	An-NOR-PXT HW	1.96	0.02	0.00	1.45	0.04	0.54	0.00	0.00	0.00	0.00	0.01	4.01
TRP-AL7906	An-NOR-PXT HW	1.96	0.02	0.00	1.40	0.04	0.59	0.00	0.00	0.00	0.00	0.01	4.02
TRP-AL7906	An-NOR-PXT HW	1.97	0.02	0.00	1.41	0.04	0.54	0.00	0.00	0.00	0.00	0.01	4.00
TRP-AL7906	An-NOR-PXT HW	1.97	0.08	0.00	1.39	0.04	0.51	0.00	0.00	0.00	0.00	0.01	4.01
TRP-AL7907B	PXT-MR	2.07	0.01	0.00	1.39	0.04	0.38	0.00	0.00	0.00	0.01	0.01	3.91
TRP-AL7907B	PXT-MR	1.95	0.02	0.00	1.53	0.06	0.44	0.00	0.00	0.00	0.00	0.01	4.02
TRP-AL7907B	PXT-MR	1.96	0.05	0.00	1.53	0.06	0.37	0.00	0.00	0.00	0.00	0.01	4.00
TRP-AL7908	PXT-MR	1.96	0.05	0.00	1.53	0.04	0.42	0.00	0.00	0.00	0.00	0.01	4.02
TRP-AL7908	PXT-MR	1.96	0.02	0.00	1.55	0.03	0.43	0.00	0.00	0.00	0.00	0.01	4.01
TRP-AL7908	PXT-MR	1.96	0.02	0.00	1.57	0.03	0.43	0.00	0.00	0.00	0.00	0.01	4.02
TRP-AL7908	PXT-MR	1.96	0.02	0.00	1.56	0.03	0.42	0.00	0.00	0.00	0.00	0.01	4.02
TRP-AL7908	PXT-MR	1.99	0.03	0.00	1.52	0.04	0.42	0.00	0.00	0.00	0.00	0.01	3.99
TRP-AL7908	PXT-MR	1.97	0.02	0.00	1.52	0.04	0.44	0.00	0.00	0.00	0.00	0.01	4.00
TRP-AL7908	PXT-MR	2.07	0.03	0.00	1.39	0.03	0.37	0.00	0.00	0.00	0.01	0.00	3.91
TRP-AL7908	PXT-MR	1.98	0.02	0.00	1.55	0.03	0.41	0.00	0.00	0.00	0.00	0.01	4.00
EST013-11	MsN-HW	1.98	0.06	0.00	1.44	0.05	0.43	0.00	0.00	0.00	0.00	0.01	3.99
EST013-11	MsN-HW	1.99	0.06	0.00	1.44	0.04	0.45	0.00	0.00	0.00	0.00	0.01	3.99
EST013-11	MsN-HW	2.01	0.02	0.00	1.44	0.04	0.44	0.00	0.00	0.00	0.00	0.01	3.97
EST013-11	MsN-HW	1.98	0.03	0.00	1.46	0.04	0.48	0.00	0.00	0.00	0.00	0.01	4.00
EST013-10	MsN-HW	1.99	0.02	0.00	1.47	0.04	0.45	0.00	0.00	0.00	0.00	0.01	3.99
EST013-10	MsN-HW	1.99	0.04	0.00	1.44	0.04	0.47	0.00	0.00	0.00	0.00	0.01	3.99
EST013-10	MsN-HW	1.98	0.19	0.00	1.36	0.05	0.39	0.00	0.00	0.00	0.00	0.01	3.99
EST013-10	MsN-HW	1.99	0.04	0.00	1.47	0.04	0.44	0.00	0.00	0.00	0.00	0.01	3.99
EST013-10	MsN-HW	1.99	0.02	0.00	1.46	0.04	0.46	0.00	0.00	0.00	0.00	0.01	3.98
EST013-10	MsN-HW	1.99	0.02	0.00	1.46	0.04	0.46	0.00	0.00	0.00	0.00	0.01	3.98
EST013-10	MsN-HW	1.99	0.01	0.00	1.49	0.03	0.46	0.00	0.00	0.00	0.00	0.01	3.99

A3-2.1 Orthopyroxene Compositions (SEM)

Sample	Lithology	MgO	Al_2O_3	SiO_2	CaO	TiO_2	Cr_2O_3	FeO	MnO	Na_2O	Total	Analytical facility
JJB15	PXT-MR	27.54	1.11	55.7	1.69	0	0.48	10.66	0.3		97.48	SEMEdx-UFS
JJB15	PXT-MR	28.23	1	55.71	0.81	0	0.36	10.99	0.33		97.43	SEMEdx-UFS
JJB15	PXT-MR	28.27	1.55	55.97	1.38	0	0.54	9.94	0		97.65	SEMEdx-UFS
JJB15	PXT-MR	27.83	1.17	55.75	0.6	0	0.69	11.29	0		97.33	SEMEdx-UFS
JJB15	PXT-MR	27.6	1.09	56.12	1.61	0	0.47	10.61	0		97.50	SEMEdx-UFS

Sample	Lithology	SiO_2	CaO	K_2O	MgO	Al_2O_3	FeO	MnO	TiO_2	Na_2O	$Cr2O_3$	Total	Analytical Facility
EST013_14	MLN-MR	55.34	0.49	0.00	29.22	1.15	13.73	0.22	0.22	0.00	0.31	100.67	SEMEdxWdx-Graz
EST013_14	MLN-MR	56.09	1.83	0.01	28.78	0.74	12.63	0.21	0.23	0.01	0.38	100.93	SEMEdxWdx-Graz
EST013_14	MLN-MR	56.37	0.59	0.00	31.52	0.85	13.55	0.15	0.30	0.00	0.39	103.73	SEMEdxWdx-Graz
EST013_14	MLN-MR	55.94	0.64	0.00	30.44	0.59	13.79	0.34	0.22	0.03	0.18	102.16	SEMEdxWdx-Graz
EST013_14	MLN-MR	56.05	0.48	0.01	30.24	0.76	13.71	0.34	0.18	0.00	0.37	102.14	SEMEdxWdx-Graz
EST013_14	MLN-MR	56.33	0.67	0.02	30.86	0.74	13.80	0.27	0.27	0.00	0.12	103.08	SEMEdxWdx-Graz
EST013_14	MLN-MR	56.01	0.95	0.04	29.85	1.00	13.55	0.22	0.22	0.00	0.35	102.18	SEMEdxWdx-Graz
EST013_14	MLN-MR	56.07	2.78	0.00	29.02	1.00	12.50	0.23	0.23	0.03	0.31	102.18	SEMEdxWdx-Graz
EST013_14	MLN-MR	54.79	0.81	0.04	29.93	0.76	13.59	0.27	0.22	0.01	0.23	100.64	SEMEdxWdx-Graz
EST013_14	MLN-MR	56.50	0.71	0.01	30.11	0.68	14.06	0.27	0.15	0.00	0.22	102.72	SEMEdxWdx-Graz
EST013_14	MLN-MR	56.50	0.70	0.04	30.87	0.74	13.70	0.28	0.10	0.00	0.22	103.15	SEMEdxWdx-Graz
EST013_14	MLN-MR	55.81	1.67	0.00	29.51	0.87	12.52	0.27	0.15	0.00	0.56	101.36	SEMEdxWdx-Graz
EST013_14	MLN-MR	56.43	0.57	0.00	31.50	1.10	12.67	0.23	0.22	0.00	0.51	103.24	SEMEdxWdx-Graz
EST013_16	MLN-MR	55.88	1.47	0.01	29.45	1.30	13.59	0.31	0.17	0.00	0.45	102.63	SEMEdxWdx-Graz
EST013_16	MLN-MR	55.71	2.18	0.04	28.44	1.13	13.21	0.26	0.23	0.00	0.41	101.61	SEMEdxWdx-Graz
EST013_16	MLN-MR	56.37	0.74	0.00	29.88	0.77	13.78	0.25	0.17	0.00	0.25	102.20	SEMEdxWdx-Graz
EST013_16	MLN-MR	55.24	1.57	0.04	28.64	0.87	13.77	0.25	0.15	0.00	0.44	100.94	SEMEdxWdx-Graz
EST013_16	MLN-MR	56.22	0.69	0.00	30.06	0.42	14.65	0.28	0.17	0.00	0.20	102.69	SEMEdxWdx-Graz
EST013_16	MLN-MR	55.62	0.49	0.00	30.26	1.21	13.77	0.23	0.18	0.00	0.48	102.24	SEMEdxWdx-Graz
EST013_16	MLN-MR	55.94	0.49	0.00	30.29	1.17	13.86	0.30	0.10	0.00	0.53	102.68	SEMEdxWdx-Graz
EST013_16	MLN-MR	55.75	0.43	0.02	30.23	0.85	14.16	0.19	0.05	0.00	0.31	102.00	SEMEdxWdx-Graz
EST013_16	MLN-MR	55.99	0.88	0.04	31.27	1.36	12.76	0.26	0.18	0.00	0.50	103.24	SEMEdxWdx-Graz
EST013_22	MLN-MR	55.32	0.62	0.02	30.33	0.62	14.11	0.35	0.15	0.00	0.31	101.83	SEMEdxWdx-Graz
EST013_22	MLN-MR	56.07	0.57	0.02	30.38	0.38	14.24	0.36	0.12	0.00	0.13	102.27	SEMEdxWdx-Graz
EST013_22	MLN-MR	55.69	0.78	0.00	29.65	0.66	14.18	0.31	0.27	0.03	0.34	101.89	SEMEdxWdx-Graz
EST013_22	MLN-MR	54.87	0.63	0.00	29.25	1.30	13.51	0.30	0.15	0.00	0.50	100.51	SEMEdxWdx-Graz
EST013_22	MLN-MR	54.55	2.34	0.00	28.17	1.28	12.61	0.30	0.22	0.07	0.57	100.10	SEMEdxWdx-Graz
EST013_22	MLN-MR	55.56	0.77	0.01	30.09	0.70	14.52	0.35	0.23	0.00	0.37	102.61	SEMEdxWdx-Graz
EST013_22	MLN-MR	56.39	0.46	0.00	30.46	0.64	14.36	0.26	0.10	0.01	0.16	102.85	SEMEdxWdx-Graz
EST013_22	MLN-MR	54.38	6.17	0.00	25.82	1.53	10.86	0.32	0.22	0.18	0.50	99.97	SEMEdxWdx-Graz
EST013_22	MLN-MR	54.74	0.55	0.00	29.65	0.60	14.42	0.21	0.18	0.00	0.23	100.59	SEMEdxWdx-Graz
EST013_22	MLN-MR	55.64	0.71	0.01	30.23	0.60	14.34	0.23	0.25	0.00	0.25	102.28	SEMEdxWdx-Graz
EST013_22	MLN-MR	54.87	0.55	0.00	29.38	0.74	13.83	0.32	0.22	0.05	0.35	100.31	SEMEdxWdx-Graz
EST013_22	MLN-MR	55.69	0.62	0.01	30.34	1.04	13.95	0.30	0.17	0.00	0.42	102.53	SEMEdxWdx-Graz
EST013_23	MLN-MR	55.04	4.41	0.00	28.10	1.21	11.53	0.22	0.17	0.03	0.35	101.06	SEMEdxWdx-Graz
EST013_23	MLN-MR	54.98	0.71	0.04	29.27	0.98	13.14	0.25	0.18	0.00	0.38	99.92	SEMEdxWdx-Graz
EST013_23	MLN-MR	55.15	0.80	0.00	31.35	1.23	12.83	0.22	0.18	0.00	0.45	102.21	SEMEdxWdx-Graz
EST013_23	MLN-MR	56.31	0.95	0.00	31.26	1.28	11.93	0.25	0.22	0.00	0.37	102.55	SEMEdxWdx-Graz
EST013_23	MLN-MR	55.00	2.14	0.00	30.34	1.47	11.33	0.27	0.25	0.01	0.37	101.19	SEMEdxWdx-Graz
EST013_23	MLN-MR	55.15	3.44	0.01	29.45	1.51	10.99	0.21	0.27	0.00	0.44	101.46	SEMEdxWdx-Graz
EST013_23	MLN-MR	55.99	2.18	0.01	29.90	1.53	11.64	0.22	0.15	0.00	0.42	102.04	SEMEdxWdx-Graz
EST013_23	MLN-MR	55.22	0.50	0.00	30.81	1.76	12.74	0.25	0.08	0.03	0.39	101.77	SEMEdxWdx-Graz
EST013_23	MLN-MR	55.84	0.73	0.01	30.04	1.00	13.14	0.18	0.27	0.01	0.32	101.54	SEMEdxWdx-Graz

Sample	Lithology	SiO_2	CaO	K_2O	MgO	Al_2O_3	FeO	MnO	TiO_2	Na_2O	$Cr2O_3$	Total	Analysis Facility
TRP-PPXT	PPXT-MR	54.53	0.74	0.00	27.56	1.06	13.87	0.34	0.18	0.00	0.38	98.66	SEMEdxWdx-Graz
TRP-PPXT	PPXT-MR	55.43	0.62	0.00	28.45	0.55	14.01	0.30	0.15	0.00	0.23	99.74	SEMEdxWdx-Graz
TRP-PPXT	PPXT-MR	55.00	0.63	0.04	27.76	0.76	14.49	0.23	0.35	0.03	0.31	99.58	SEMEdxWdx-Graz
TRP-PPXT	PPXT-MR	54.55	4.67	0.00	25.00	1.51	12.23	0.23	0.23	0.04	0.54	99.02	SEMEdxWdx-Graz
TRP-PPXT	PPXT-MR	54.72	0.83	0.00	28.27	0.85	13.69	0.25	0.25	0.00	0.42	99.28	SEMEdxWdx-Graz
TRP-PPXT	PPXT-MR	54.98	0.71	0.04	28.57	0.81	14.06	0.34	0.28	0.00	0.41	100.20	SEMEdxWdx-Graz
TRP-PPXT	PPXT-MR	54.98	0.67	0.01	28.30	1.11	14.15	0.18	0.10	0.00	0.54	100.06	SEMEdxWdx-Graz
TRP006	PXT-MR	54.36	2.97	0.01	27.18	1.23	13.17	0.28	0.18	0.01	0.54	99.94	SEMEdxWdx-Graz
TRP006	PXT-MR	52.11	2.94	0.29	23.86	3.89	11.81	0.27	0.33	0.08	0.37	95.95	SEMEdxWdx-Graz
TRP006	PXT-MR	55.04	0.69	0.00	27.79	0.93	15.23	0.30	0.38	0.01	0.23	100.61	SEMEdxWdx-Graz
TRP006	PXT-MR	54.08	0.63	0.02	27.91	0.76	14.90	0.32	0.28	0.00	0.34	99.24	SEMEdxWdx-Graz
TRP006	PXT-MR	55.56	1.96	0.00	27.59	1.45	13.29	0.28	0.10	0.03	0.44	100.70	SEMEdxWdx-Graz
TRP006	PXT-MR	55.66	0.69	0.00	28.52	1.08	14.11	0.28	0.30	0.00	0.42	101.07	SEMEdxWdx-Graz
TRP006	PXT-MR	54.94	1.85	0.00	27.71	1.15	13.65	0.22	0.18	0.04	0.50	100.23	SEMEdxWdx-Graz
TRP006	PXT-MR	54.53	1.83	0.00	27.69	0.91	13.34	0.27	1.12	0.00	0.41	100.10	SEMEdxWdx-Graz
TRP006	PXT-MR	55.54	0.76	0.00	27.79	1.02	14.31	0.34	0.25	0.00	0.39	100.39	SEMEdxWdx-Graz
JJB13	BSN-MR	53.78	0.64	0.00	28.64	0.77	13.96	0.25	0.15	0.00	0.61	98.80	SEMEdxWdx-Graz
JJB13	BSN-MR	55.71	0.64	0.00	28.60	0.77	13.97	0.25	0.15	0.00	0.61	100.71	SEMEdxWdx-Graz
JJB13	BSN-MR	55.73	0.60	0.00	28.24	0.77	14.01	0.23	0.12	0.00	0.45	100.15	SEMEdxWdx-Graz
JJB13	BSN-MR	56.11	0.77	0.00	28.59	1.04	13.56	0.28	0.23	0.00	0.41	100.99	SEMEdxWdx-Graz
JJB13	BSN-MR	55.79	0.50	0.01	28.57	0.94	13.57	0.30	0.28	0.00	0.42	100.40	SEMEdxWdx-Graz
JJB13	BSN-MR	56.07	0.59	0.04	29.10	0.68	13.44	0.28	0.22	0.00	0.32	100.74	SEMEdxWdx-Graz
JJB13	BSN-MR	56.09	1.39	0.00	28.50	0.83	13.69	0.25	0.25	0.00	0.39	101.39	SEMEdxWdx-Graz
JJB13	BSN-MR	56.09	0.81	0.04	28.44	1.08	13.62	0.32	0.18	0.00	0.58	101.17	SEMEdxWdx-Graz
JJB13	BSN-MR	56.07	0.64	0.00	28.22	0.87	14.65	0.31	0.18	0.00	0.44	101.39	SEMEdxWdx-Graz
JJB13	BSN-MR	56.56	0.83	0.02	28.98	0.72	13.20	0.26	0.17	0.01	0.44	101.19	SEMEdxWdx-Graz
JJB13	BSN-MR	56.01	2.80	0.01	26.73	1.15	11.80	0.31	0.17	0.07	0.57	99.61	SEMEdxWdx-Graz
JJB14	BSN-MR	54.34	0.83	0.08	29.48	1.15	13.17	0.25	0.30	0.01	0.42	100.04	SEMEdxWdx-Graz
JJB14	BSN-MR	55.37	0.50	0.04	30.23	0.93	12.27	0.34	0.22	0.03	0.51	100.42	SEMEdxWdx-Graz
JJB14	BSN-MR	54.79	0.81	0.11	29.91	0.98	12.07	0.19	0.15	0.03	0.54	99.58	SEMEdxWdx-Graz
JJB14	BSN-MR	54.45	0.69	0.11	29.88	1.02	11.98	0.30	0.25	0.23	0.44	99.33	SEMEdxWdx-Graz
JJB14	BSN-MR	55.34	1.13	0.00	30.26	1.17	11.89	0.22	0.18	0.05	0.51	100.76	SEMEdxWdx-Graz
JJB14	BSN-MR	54.85	0.69	0.05	29.61	0.91	12.38	0.27	0.15	0.08	0.53	99.51	SEMEdxWdx-Graz
JJB14	BSN-MR	54.92	0.53	0.45	30.06	1.00	12.32	0.21	0.27	0.04	0.45	100.25	SEMEdxWdx-Graz
JJB14	BSN-MR	54.70	0.69	0.04	29.27	1.08	12.49	0.26	0.20	0.05	0.53	99.30	SEMEdxWdx-Graz
JJB14	BSN-MR	55.90	0.53	0.00	31.01	1.44	11.67	0.18	0.10	0.00	0.53	101.35	SEMEdxWdx-Graz
JJB14	BSN-MR	56.22	2.10	0.00	29.50	1.17	10.74	0.14	0.08	0.03	0.61	100.60	SEMEdxWdx-Graz
JJB14	BSN-MR	55.86	1.09	0.00	30.59	1.32	11.45	0.28	0.12	0.03	0.58	101.33	SEMEdxWdx-Graz
JJB14	BSN-MR	56.39	0.78	0.00	31.72	1.08	11.37	0.25	0.20	0.00	0.53	102.32	SEMEdxWdx-Graz
JJB14	BSN-MR	54.62	0.90	0.00	31.07	1.30	11.39	0.26	0.17	0.03	0.66	100.38	SEMEdxWdx-Graz
JJB14	BSN-MR	55.02	0.84	0.00	31.27	1.08	11.35	0.21	0.13	0.00	0.50	100.39	SEMEdxWdx-Graz
JJB18	BSN-HW	55.94	0.81	0.00	29.73	0.79	12.30	0.28	0.27	0.04	0.57	100.74	SEMEdxWdx-Graz
JJB18	BSN-HW	56.18	0.73	0.00	29.70	0.91	12.14	0.27	0.15	0.00	0.41	100.48	SEMEdxWdx-Graz
JJB18	BSN-HW	56.48	0.90	0.00	29.28	0.91	12.44	0.30	0.17	0.03	0.58	101.08	SEMEdxWdx-Graz
JJB18	BSN-HW	56.05	0.64	0.05	29.68	0.64	12.05	0.31	0.32	0.05	0.48	100.28	SEMEdxWdx-Graz
JJB18	BSN-HW	55.99	0.63	0.04	29.73	0.93	12.61	0.25	0.25	0.00	0.51	100.92	SEMEdxWdx-Graz
JJB18	BSN-HW	56.52	0.55	0.00	29.63	0.89	12.45	0.28	0.28	0.00	0.54	101.15	SEMEdxWdx-Graz
JJB18	BSN-HW	56.50	0.63	0.06	29.27	0.85	12.30	0.19	0.28	0.00	0.50	100.58	SEMEdxWdx-Graz
JJB18	BSN-HW	56.35	0.66	0.02	29.15	0.74	12.31	0.32	0.18	0.00	0.38	100.12	SEMEdxWdx-Graz
JJB18	BSN-HW	56.88	0.84	0.02	29.10	0.94	12.38	0.23	0.22	0.00	0.57	101.19	SEMEdxWdx-Graz

A3-2.2 Cations per 6 oxygens

Sample	Lithology	Si	Ca	Mg	Al	Fe	Mn	Total
JJB15	PXT-MR	2.02	0.07	1.49	0.05	0.32	0.01	3.96
JJB15	PXT-MR	2.02	0.03	1.52	0.04	0.33	0.01	3.96
JJB15	PXT-MR	2.02	0.05	1.52	0.07	0.30	0.00	3.95
JJB15	PXT-MR	2.03	0.02	1.51	0.05	0.34	0.00	3.95
JJB15	PXT-MR	2.03	0.06	1.49	0.05	0.32	0.00	3.95

Sample	Lithology	Si	Ca	K	Mg	Al	Fe	Mn	Ti	Ni	Na	Cr	Total
EST013_14	MLN-MR	1.96	0.02	0.00	1.54	0.05	0.41	0.01	0.01	0.00	0.02	0.01	4.02
EST013_14	MLN-MR	1.98	0.07	0.00	1.51	0.03	0.37	0.01	0.01	0.00	0.03	0.01	4.01
EST013_14	MLN-MR	1.94	0.02	0.00	1.61	0.03	0.39	0.00	0.01	0.00	0.03	0.01	4.05
EST013_14	MLN-MR	1.96	0.02	0.00	1.59	0.02	0.40	0.01	0.01	0.00	0.01	0.00	4.03
EST013_14	MLN-MR	1.96	0.02	0.00	1.57	0.03	0.40	0.01	0.00	0.00	0.03	0.01	4.03
EST013_14	MLN-MR	1.95	0.02	0.00	1.59	0.03	0.40	0.01	0.01	0.00	0.01	0.00	4.03
EST013_14	MLN-MR	1.95	0.04	0.00	1.55	0.04	0.40	0.01	0.01	0.00	0.02	0.01	4.03
EST013_14	MLN-MR	1.96	0.10	0.00	1.51	0.04	0.37	0.01	0.01	0.00	0.02	0.01	4.02
EST013_14	MLN-MR	1.95	0.03	0.00	1.58	0.03	0.40	0.01	0.01	0.00	0.02	0.01	4.04
EST013_14	MLN-MR	1.96	0.03	0.00	1.56	0.03	0.41	0.01	0.00	0.00	0.01	0.01	4.02
EST013_14	MLN-MR	1.95	0.03	0.00	1.59	0.03	0.40	0.01	0.00	0.00	0.01	0.01	4.03
EST013_14	MLN-MR	1.96	0.06	0.00	1.54	0.04	0.37	0.01	0.00	0.00	0.04	0.02	4.03
EST013_14	MLN-MR	1.94	0.02	0.00	1.61	0.04	0.36	0.01	0.01	0.00	0.03	0.01	4.04
EST013_16	MLN-MR	1.94	0.05	0.00	1.53	0.05	0.40	0.01	0.00	0.00	0.03	0.01	4.03
EST013_16	MLN-MR	1.96	0.08	0.00	1.49	0.05	0.39	0.01	0.01	0.00	0.03	0.01	4.02
EST013_16	MLN-MR	1.97	0.03	0.00	1.55	0.03	0.40	0.01	0.00	0.00	0.02	0.01	4.02
EST013_16	MLN-MR	1.96	0.06	0.00	1.51	0.04	0.41	0.01	0.00	0.00	0.03	0.01	4.03
EST013_16	MLN-MR	1.96	0.03	0.00	1.56	0.02	0.43	0.01	0.00	0.00	0.01	0.01	4.03
EST013_16	MLN-MR	1.94	0.02	0.00	1.57	0.05	0.40	0.01	0.00	0.00	0.03	0.01	4.04
EST013_16	MLN-MR	1.94	0.02	0.00	1.57	0.05	0.40	0.01	0.00	0.00	0.04	0.01	4.04
EST013_16	MLN-MR	1.95	0.02	0.00	1.58	0.04	0.41	0.01	0.00	0.00	0.02	0.01	4.03
EST013_16	MLN-MR	1.93	0.03	0.00	1.61	0.06	0.37	0.01	0.00	0.00	0.03	0.01	4.05
EST013_22	MLN-MR	1.95	0.02	0.00	1.59	0.03	0.42	0.01	0.00	0.00	0.02	0.01	4.04
EST013_22	MLN-MR	1.96	0.02	0.00	1.59	0.02	0.42	0.01	0.00	0.00	0.01	0.00	4.03
EST013_22	MLN-MR	1.96	0.03	0.00	1.55	0.03	0.42	0.01	0.01	0.00	0.02	0.01	4.03
EST013_22	MLN-MR	1.95	0.02	0.00	1.55	0.05	0.40	0.01	0.00	0.00	0.03	0.01	4.03
EST013_22	MLN-MR	1.94	0.09	0.00	1.50	0.05	0.38	0.01	0.01	0.00	0.04	0.02	4.03
EST013_22	MLN-MR	1.94	0.03	0.00	1.57	0.03	0.42	0.01	0.01	0.00	0.03	0.01	4.04
EST013_22	MLN-MR	1.96	0.02	0.00	1.58	0.03	0.42	0.01	0.00	0.00	0.01	0.00	4.03
EST013_22	MLN-MR	1.95	0.24	0.00	1.38	0.06	0.33	0.01	0.01	0.01	0.03	0.01	4.02
EST013_22	MLN-MR	1.95	0.02	0.00	1.58	0.03	0.43	0.01	0.00	0.00	0.02	0.01	4.04
EST013_22	MLN-MR	1.95	0.03	0.00	1.58	0.02	0.42	0.01	0.01	0.00	0.02	0.01	4.04
EST013_22	MLN-MR	1.96	0.02	0.00	1.56	0.03	0.41	0.01	0.01	0.00	0.02	0.01	4.03
EST013_22	MLN-MR	1.94	0.02	0.00	1.58	0.04	0.41	0.01	0.00	0.00	0.03	0.01	4.04
EST013_23	MLN-MR	1.95	0.17	0.00	1.48	0.05	0.34	0.01	0.00	0.00	0.02	0.01	4.03
EST013_23	MLN-MR	1.96	0.03	0.00	1.55	0.04	0.39	0.01	0.00	0.00	0.03	0.01	4.02
EST013_23	MLN-MR	1.92	0.03	0.00	1.63	0.05	0.37	0.01	0.00	0.00	0.03	0.01	4.06
EST013_23	MLN-MR	1.94	0.04	0.00	1.61	0.05	0.34	0.01	0.01	0.00	0.02	0.01	4.03
EST013_23	MLN-MR	1.93	0.08	0.00	1.59	0.06	0.33	0.01	0.01	0.00	0.03	0.01	4.04
EST013_23	MLN-MR	1.93	0.13	0.00	1.54	0.06	0.32	0.01	0.01	0.00	0.03	0.01	4.04
EST013_23	MLN-MR	1.95	0.08	0.00	1.55	0.06	0.34	0.01	0.00	0.00	0.03	0.01	4.03
EST013_23	MLN-MR	1.93	0.02	0.00	1.60	0.07	0.37	0.01	0.00	0.00	0.03	0.01	4.04
EST013_23	MLN-MR	1.96	0.03	0.00	1.57	0.04	0.39	0.01	0.01	0.00	0.02	0.01	4.02

Sample	Lithology	Si	Ca	K	Mg	Al	Fe	Mn	Ti	Na	Cr	Total
TRP-PPXT	PPXT-MR	1.98	0.03	0.00	1.49	0.05	0.42	0.01	0.01	0.00	0.01	3.99
TRP-PPXT	PPXT-MR	1.99	0.02	0.00	1.52	0.02	0.42	0.01	0.00	0.00	0.01	3.99
TRP-PPXT	PPXT-MR	1.98	0.02	0.00	1.49	0.03	0.44	0.01	0.01	0.00	0.01	3.99
TRP-PPXT	PPXT-MR	1.98	0.18	0.00	1.35	0.06	0.37	0.01	0.01	0.00	0.02	3.98
TRP-PPXT	PPXT-MR	1.97	0.03	0.00	1.52	0.04	0.41	0.01	0.01	0.00	0.01	4.00
TRP-PPXT	PPXT-MR	1.97	0.03	0.00	1.52	0.03	0.42	0.01	0.01	0.00	0.01	4.00
TRP-PPXT	PPXT-MR	1.97	0.03	0.00	1.51	0.05	0.42	0.01	0.00	0.00	0.02	4.00
TRP006	PXT-MR	1.95	0.11	0.00	1.46	0.05	0.40	0.01	0.00	0.00	0.02	4.01
TRP006	PXT-MR	1.94	0.12	0.01	1.32	0.17	0.37	0.01	0.01	0.01	0.01	3.97
TRP006	PXT-MR	1.97	0.03	0.00	1.48	0.04	0.46	0.01	0.01	0.00	0.01	4.00
TRP006	PXT-MR	1.96	0.02	0.00	1.51	0.03	0.45	0.01	0.01	0.00	0.01	4.01
TRP006	PXT-MR	1.97	0.07	0.00	1.46	0.06	0.39	0.01	0.00	0.00	0.01	3.99
TRP006	PXT-MR	1.97	0.03	0.00	1.50	0.04	0.42	0.01	0.01	0.00	0.01	3.99
TRP006	PXT-MR	1.96	0.07	0.00	1.48	0.05	0.41	0.01	0.00	0.00	0.01	4.00
TRP006	PXT-MR	1.95	0.07	0.00	1.48	0.04	0.40	0.01	0.03	0.00	0.01	3.99
TRP006	PXT-MR	1.98	0.03	0.00	1.48	0.04	0.43	0.01	0.01	0.00	0.01	3.99
JJB13	BSN-MR	1.95	0.03	0.00	1.55	0.03	0.42	0.01	0.00	0.00	0.02	4.02
JJB13	BSN-MR	1.98	0.02	0.00	1.51	0.03	0.41	0.01	0.00	0.00	0.02	3.99
JJB13	BSN-MR	1.99	0.02	0.00	1.50	0.03	0.42	0.01	0.00	0.00	0.01	3.99
JJB13	BSN-MR	1.98	0.03	0.00	1.50	0.04	0.40	0.01	0.01	0.00	0.01	3.99
JJB13	BSN-MR	1.98	0.02	0.00	1.51	0.04	0.40	0.01	0.01	0.00	0.01	3.99
JJB13	BSN-MR	1.98	0.02	0.00	1.53	0.03	0.40	0.01	0.01	0.00	0.01	3.99
JJB13	BSN-MR	1.98	0.05	0.00	1.50	0.03	0.40	0.01	0.01	0.00	0.01	3.99
JJB13	BSN-MR	1.98	0.03	0.00	1.50	0.04	0.40	0.01	0.00	0.00	0.02	3.99
JJB13	BSN-MR	1.98	0.02	0.00	1.49	0.04	0.43	0.01	0.00	0.00	0.01	3.99
JJB13	BSN-MR	1.99	0.03	0.00	1.52	0.03	0.39	0.01	0.00	0.00	0.01	3.99
JJB13	BSN-MR	2.00	0.11	0.00	1.42	0.05	0.35	0.01	0.00	0.00	0.02	3.97
JJB14	BSN-MR	1.94	0.03	0.00	1.57	0.05	0.39	0.01	0.01	0.00	0.01	4.02
JJB14	BSN-MR	1.96	0.02	0.00	1.59	0.04	0.36	0.01	0.01	0.00	0.01	4.01
JJB14	BSN-MR	1.96	0.03	0.00	1.59	0.04	0.36	0.01	0.00	0.00	0.02	4.01
JJB14	BSN-MR	1.95	0.03	0.00	1.60	0.04	0.36	0.01	0.01	0.02	0.01	4.03
JJB14	BSN-MR	1.95	0.04	0.00	1.59	0.05	0.35	0.01	0.00	0.00	0.01	4.01
JJB14	BSN-MR	1.96	0.03	0.00	1.58	0.04	0.37	0.01	0.00	0.01	0.01	4.01
JJB14	BSN-MR	1.95	0.02	0.02	1.59	0.04	0.37	0.01	0.01	0.00	0.01	4.02
JJB14	BSN-MR	1.96	0.03	0.00	1.56	0.05	0.37	0.01	0.01	0.00	0.01	4.01
JJB14	BSN-MR	1.95	0.02	0.00	1.61	0.06	0.34	0.01	0.00	0.00	0.01	4.01
JJB14	BSN-MR	1.98	0.08	0.00	1.54	0.05	0.32	0.00	0.00	0.00	0.02	3.99
JJB14	BSN-MR	1.95	0.04	0.00	1.59	0.05	0.33	0.01	0.00	0.00	0.02	4.01
JJB14	BSN-MR	1.95	0.03	0.00	1.63	0.04	0.33	0.01	0.01	0.00	0.01	4.02
JJB14	BSN-MR	1.93	0.03	0.00	1.64	0.05	0.34	0.01	0.00	0.00	0.02	4.03
JJB14	BSN-MR	1.94	0.03	0.00	1.65	0.04	0.33	0.01	0.00	0.00	0.01	4.02
JJB18	BSN-HW	1.97	0.03	0.00	1.56	0.03	0.36	0.01	0.01	0.00	0.02	4.00
JJB18	BSN-HW	1.98	0.03	0.00	1.56	0.04	0.36	0.01	0.00	0.00	0.01	3.99
JJB18	BSN-HW	1.98	0.03	0.00	1.53	0.04	0.37	0.01	0.00	0.00	0.02	3.99
JJB18	BSN-HW	1.98	0.02	0.00	1.56	0.03	0.36	0.01	0.01	0.00	0.01	3.99
JJB18	BSN-HW	1.97	0.02	0.00	1.56	0.04	0.37	0.01	0.01	0.00	0.01	4.00
JJB18	BSN-HW	1.98	0.02	0.00	1.55	0.04	0.37	0.01	0.01	0.00	0.01	3.99
JJB18	BSN-HW	1.99	0.02	0.00	1.54	0.04	0.36	0.01	0.01	0.00	0.01	3.98
JJB18	BSN-HW	1.99	0.02	0.00	1.54	0.03	0.36	0.01	0.00	0.00	0.01	3.98
JJB18	BSN-HW	1.99	0.03	0.00	1.52	0.04	0.36	0.01	0.01	0.00	0.02	3.98

End Member Recalculation of orthopyroxene in hanging wall pyroxenite and MsN

TRP_Pxt		En	Wo	Fs
(n=6)	Min	78.48	0.72	15.78
	Max	80.06	4.16	20.80
	Mean	78.79	2.07	18.14
	Std. Dev.	3.68	5.15	1.85
TRP272_Pxt				
(n=5)	Min	70.79	0.94	25.16
	Max	73.90	4.16	25.05
	Mean	72.08	2.16	25.76
	Std. Dev.	1.18	1.55	1.47
TRP_BSN		En	Wo	Fs
(n=28)	Min	79.65	0.93	15.51
	Max	82.38	3.38	18.06
	Mean	81.34	1.67	16.99
	Std. Dev.	0.61	0.73	0.78
EST013_MsN		En	Wo	Fs
(n=10)	Min	70.04	0.12	11.49
	Max	88.39	9.81	24.39
	Mean	75.92	2.16	21.93
	Std. Dev.	4.70	2.76	3.85

End Member recalculation of orthopyroxene in pyroxenite vs pegmatoidal pyroxenite

TRP_PXT		En	Wo	Fs
(n=9)	Min	73.12	1.24	19.41
	Max	77.25	6.61	23.23
	Mean	75.67	3.23	21.10
	Std. Dev.	1.26	2.06	1.14
TRP_PPXT		En	Wo	Fs
(n=7)	Min	70.96	1.22	19.50
	Max	77.56	9.54	22.38
	Mean	76.21	2.56	21.23
	Std. Dev.	2.35	3.08	0.90

End Member Recalculation of orthopyroxene in Merensky Reef pyroxenite

TRP_Pxt		En	Wo	Fs
(n=33)	Min	74.26	0.52	11.77
	Max	87.71	7.60	22.42
	Mean	79.84	2.41	17.75
	Std. Dev.	2.89	1.56	2.31
TRP272_Pxt		En	Wo	Fs
(n=15)	Min	77.41	0.66	13.10
	Max	85.85	2.73	21.55
	Mean	79.54	1.35	19.11
	Std. Dev.	2.17	0.64	2.18
TRP_BSN		En	Wo	Fs
(n=48)	Min	75.55	0.12	13.10
	Max	85.07	5.69	22.34
	Mean	80.33	1.61	18.06
	Std. Dev.	2.30	0.89	2.27
EST013_MLN		En	Wo	Fs
(n=42)	Min	76.08	0.83	13.50
	Max	84.75	8.78	20.48
	Mean	80.35	2.17	17.48
	Std. Dev.	2.00	1.77	1.71

A3-3.1 Clinopyroxene Compositions (EPMA-Rhodes University)

Sample	Lithology	SiO_2	CaO	K2O	MgO	Al_2O_3	FeO	MnO	TiO_2	NiO	Na_2O	Cr_2O_3	Total
JJB18	BSN-HW	52.37	23.31	0.01	16.28	1.87	3.33	0.04	0.04	0.04	0.30	0.90	98.48
JJB18	BSN-HW	53.13	20.61	0.14	17.97	2.44	3.84	0.02	0.02	0.06	0.28	0.75	99.26
JJB18	BSN-HW	52.88	22.76	0.02	16.50	1.94	3.88	0.03	0.05	0.05	0.37	0.94	99.41
JJB9	BSN-MR	52.59	23.84	0.02	16.55	1.48	3.06	0.04	0.01	0.07	0.30	0.89	98.85
JJB9	BSN-MR	52.19	23.17	0.03	15.99	1.79	3.11	0.00	0.03	0.06	0.29	0.98	97.64
JJB9	BSN-MR	52.75	22.91	0.00	16.49	1.55	3.27	0.00	0.01	0.03	0.28	0.85	98.15
JJB9	PXT-MR	53.51	22.42	0.01	16.29	1.92	4.06	0.00	0.03	0.00	0.35	0.87	99.46
JJB14	BSN-MR	52.28	22.60	0.02	16.39	1.90	4.45	0.00	0.03	0.04	0.37	0.95	99.04
JJB14	BSN-MR	53.40	22.35	0.02	16.43	1.94	4.30	0.01	0.02	0.00	0.35	0.99	99.81
JJB14	BSN-MR	53.43	23.34	0.01	16.56	1.35	3.39	0.00	0.05	0.00	0.28	0.52	98.94
JJB10	PXT-MR-CHR	53.14	23.16	0.02	16.15	2.01	3.91	0.02	0.02	0.06	0.27	0.91	99.67
JJB10	PXT-MR-CHR	52.98	23.82	0.00	16.23	1.57	3.09	0.02	0.04	0.09	0.23	0.77	98.83
JJB10	PXT-MR-CHR	52.91	23.32	0.02	16.33	1.32	4.78	0.04	0.06	0.06	0.20	0.20	99.23
JJB10	PXT-MR-CHR	53.30	24.12	0.01	16.07	1.01	3.94	0.04	0.04	0.07	0.16	0.20	98.96
TRP-AL7906	An-NOR-PXT HW	50.38	12.07	0.34	17.50	7.04	7.79	0.01	0.08	0.08	0.55	1.03	96.86
EST013-11	MsN-HW	53.96	23.94	0.03	15.68	1.15	4.73	0.01	0.03	0.00	0.24	0.30	100.06
EST013-11	MsN-HW	54.60	23.50	0.02	15.45	1.42	4.98	0.07	0.04	0.00	0.25	0.45	100.78
EST013-10	MsN-HW	54.39	23.12	0.03	16.01	1.51	5.29	0.06	0.06	0.00	0.31	0.37	101.15
EST013-10	MsN-HW	55.17	23.62	0.02	16.28	0.86	4.51	0.05	0.02	0.00	0.24	0.23	101.01
EST013-10	MsN-HW	54.62	23.92	0.01	15.87	1.28	4.86	0.00	0.04	0.00	0.29	0.37	101.26

A3-3.2 Cations per 6 oxygens

Sample	Lithology	Si	Ca	K	Mg	Al	Fe	Mn	Ti	Ni	Na	Cr	Total
JJB18	BSN-HW	1.93	0.92	0.00	0.90	0.08	0.10	0.00	0.00	0.01	0.06	0.03	4.04
JJB18	BSN-HW	1.94	0.80	0.01	0.98	0.10	0.12	0.00	0.00	0.01	0.05	0.02	4.03
JJB18	BSN-HW	1.94	0.89	0.00	0.90	0.08	0.12	0.00	0.00	0.01	0.07	0.03	4.04
JJB9	BSN-MR	1.94	0.94	0.00	0.91	0.06	0.09	0.00	0.00	0.01	0.06	0.03	4.05
JJB9	BSN-MR	1.94	0.92	0.00	0.89	0.08	0.10	0.00	0.00	0.01	0.07	0.03	4.04
JJB9	BSN-MR	1.95	0.91	0.00	0.91	0.07	0.10	0.00	0.00	0.01	0.06	0.02	4.03
JJB9	PXT-MR	1.95	0.88	0.00	0.89	0.08	0.12	0.00	0.00	0.01	0.06	0.03	4.02
JJB14	BSN-MR	1.93	0.89	0.00	0.90	0.08	0.14	0.00	0.00	0.01	0.07	0.03	4.05
JJB14	BSN-MR	1.94	0.87	0.00	0.89	0.08	0.13	0.00	0.00	0.01	0.07	0.03	4.03
JJB14	BSN-MR	1.96	0.92	0.00	0.91	0.06	0.10	0.00	0.00	0.01	0.04	0.02	4.02
JJB10	PXT-MR-CHR	1.94	0.91	0.00	0.88	0.09	0.12	0.00	0.00	0.01	0.06	0.03	4.03
JJB10	PXT-MR-CHR	1.95	0.94	0.00	0.89	0.07	0.10	0.00	0.00	0.01	0.05	0.02	4.03
JJB10	PXT-MR-CHR	1.96	0.92	0.00	0.90	0.06	0.15	0.00	0.00	0.01	0.01	0.01	4.02
JJB10	PXT-MR-CHR	1.97	0.96	0.00	0.89	0.04	0.12	0.00	0.00	0.01	0.01	0.01	4.01
TRP-AL7906	An-NOR-PXT HW	1.87	0.48	0.02	0.97	0.31	0.24	0.00	0.00	0.02	0.07	0.03	4.01
EST013-11	MsN-HW	1.98	0.94	0.00	0.86	0.05	0.14	0.00	0.00	0.01	0.02	0.01	4.01
EST013-11	MsN-HW	1.98	0.91	0.00	0.84	0.06	0.15	0.00	0.00	0.01	0.03	0.01	4.00
EST013-10	MsN-HW	1.97	0.90	0.00	0.86	0.06	0.16	0.00	0.00	0.01	0.03	0.01	4.01
EST013-10	MsN-HW	1.99	0.91	0.00	0.88	0.04	0.14	0.00	0.00	0.01	0.02	0.01	3.99
EST013-10	MsN-HW	1.97	0.93	0.00	0.85	0.05	0.15	0.00	0.00	0.01	0.03	0.01	4.01

A3-4.1 Clinopyroxene Compositions (SEM)

Sample	Lithology	MgO	Al_2O_3	SiO_2	CaO	TiO_2	V_2O_5	Cr_2O_3	MnO	FeO	NiO	Total	Analytical Facility
TRP-AL7907	PXT-MR	13.64	1.68	53.23	24.4	0.27	0.23	0.94	0.16	4.90	0.00	99.45	SEMEdx-UFS
TRP-AL7908	PXT-MR	15.02	1.68	53.42	22.83	0.47	0.21	0.23	0.28	4.95	0.36	99.45	SEMEdx-UFS
TRP-AL7908	PXT-MR	14.35	1.52	52.97	24.57	0.61	0.00	0.64	0.24	4.58	0.00	99.48	SEMEdx-UFS
TRP-AL7908	PXT-MR	14.56	1.59	53.67	23.81	0.48	0.00	0.6	0.39	4.42	0.00	99.52	SEMEdx-UFS
TRP-AL7908	PXT-MR	14.15	0.98	53.74	24.44	0.58	0.00	0.5	0.00	5.04	0.00	99.43	SEMEdx-UFS
TRP-AL7908	PXT-MR	13.88	1.38	52.6	24.92	0.37	0.6	0.48	0.00	4.99	0.21	99.43	SEMEdx-UFS
JJB11	PXT-MR	14.92	1.12	53.43	24.2	0.00	0.00	1.25	0.00	4.11	0.00	0.00	SEMEdx-UFS
JJB11	PXT-MR	14.97	1.13	53.56	23.16	0.00	0.00	0	0.00	5.81	0.00	0.00	SEMEdx-UFS
JJB11	PXT-MR	14.97	1.14	52.79	22.69	0.22	0.00	0.64	0.00	5.68	0.30	0.23	SEMEdx-UFS
JJB11	PXT-MR	14.39	1.79	52.31	24.39	0.29	0.00	1.21	0.00	4.19	0.00	0.43	SEMEdx-UFS
JJB15	PXT-MR	14.25	2.21	52.29	24.41	0.00	0.00	1.19	0.00	4.15	0.00	0.52	SEMEdx-UFS

Sample	Lithology	SiO_2	CaO	K_2O	MgO	Al_2O_3	FeO	MnO	TiO_2	Na_2O	$Cr2O_3$	Total	Analytical Facility
EST013_14	MLN-MR	53.16	21.83	0.00	16.40	1.87	4.89	0.12	0.40	0.47	0.98	100.11	SEMEdxWdx-Graz
EST013_14	MLN-MR	53.29	21.86	0.00	16.56	1.47	4.89	0.14	0.57	0.34	0.64	99.76	SEMEdxWdx-Graz
EST013_14	MLN-MR	57.68	12.12	0.07	23.55	0.81	4.68	0.12	0.12	0.12	0.25	99.51	SEMEdxWdx-Graz
EST013_14	MLN-MR	53.63	22.26	0.00	16.83	1.21	4.77	0.15	0.47	0.32	0.57	100.22	SEMEdxWdx-Graz
EST013_14	MLN-MR	52.86	21.97	0.00	16.20	1.55	5.03	0.15	0.55	0.39	0.80	99.51	SEMEdxWdx-Graz
EST013_14	MLN-MR	53.72	20.96	0.00	17.14	2.04	4.90	0.08	0.28	0.42	1.08	100.63	SEMEdxWdx-Graz
EST013_14	MLN-MR	53.05	22.23	0.00	16.33	1.93	4.55	0.14	0.47	0.46	0.88	100.05	SEMEdxWdx-Graz
EST013_16	MLN-MR	53.40	22.02	0.00	15.97	2.10	4.64	0.08	0.27	0.49	1.02	99.98	SEMEdxWdx-Graz
EST013_16	MLN-MR	53.38	22.04	0.00	16.37	2.21	4.58	0.13	0.30	0.47	0.86	100.33	SEMEdxWdx-Graz
EST013_16	MLN-MR	54.45	22.18	0.00	17.41	1.21	4.75	0.21	0.30	0.30	0.41	101.20	SEMEdxWdx-Graz
EST013_16	MLN-MR	53.50	21.83	0.00	16.90	1.59	5.22	0.13	0.43	0.36	0.54	100.51	SEMEdxWdx-Graz
EST013_16	MLN-MR	53.48	22.14	0.00	16.22	1.51	5.07	0.10	0.53	0.40	0.57	100.03	SEMEdxWdx-Graz
EST013_16	MLN-MR	53.44	22.14	0.00	16.95	1.74	4.80	0.12	0.57	0.36	0.64	100.75	SEMEdxWdx-Graz
EST013_16	MLN-MR	53.87	21.76	0.00	17.18	1.72	5.13	0.13	0.63	0.35	0.70	101.47	SEMEdxWdx-Graz
EST013_16	MLN-MR	53.40	21.93	0.00	16.28	2.02	4.95	0.13	0.52	0.34	0.76	100.32	SEMEdxWdx-Graz
EST013_16	MLN-MR	53.63	22.39	0.00	16.73	1.10	4.36	0.13	0.22	0.34	0.61	99.50	SEMEdxWdx-Graz
EST013_16	MLN-MR	53.78	22.37	0.00	16.61	1.51	4.84	0.19	0.35	0.36	0.70	100.73	SEMEdxWdx-Graz
EST013_16	MLN-MR	53.29	22.08	0.00	16.38	1.83	4.45	0.10	0.30	0.40	0.99	99.84	SEMEdxWdx-Graz
EST013_16	MLN-MR	53.61	22.43	0.00	16.76	1.87	3.95	0.18	0.43	0.35	0.92	100.51	SEMEdxWdx-Graz
EST013_22	MLN-MR	52.54	21.00	0.02	16.42	1.70	5.11	0.13	0.62	0.46	0.72	98.71	SEMEdxWdx-Graz
EST013_22	MLN-MR	53.46	21.81	0.00	16.43	1.64	4.89	0.19	0.40	0.38	0.63	99.84	SEMEdxWdx-Graz
EST013_22	MLN-MR	53.12	21.53	0.00	16.27	1.45	4.72	0.13	0.47	0.39	0.58	98.67	SEMEdxWdx-Graz
EST013_23	MLN-MR	53.16	22.11	0.00	16.45	1.74	4.49	0.12	0.28	0.34	0.70	99.38	SEMEdxWdx-Graz
EST013_23	MLN-MR	52.52	21.84	0.02	16.12	1.81	4.61	0.12	0.42	0.39	0.63	98.47	SEMEdxWdx-Graz
EST013_23	MLN-MR	52.82	21.52	0.00	16.35	1.45	4.66	0.17	0.30	0.36	0.45	98.09	SEMEdxWdx-Graz
EST013_23	MLN-MR	53.40	22.57	0.01	17.49	0.87	3.81	0.05	0.15	0.12	0.12	98.59	SEMEdxWdx-Graz
EST013_23	MLN-MR	53.38	22.08	0.00	17.24	1.64	4.00	0.13	0.42	0.38	0.79	100.06	SEMEdxWdx-Graz
EST013_23	MLN-MR	52.95	21.77	0.00	16.83	1.59	4.75	0.13	0.48	0.31	0.82	99.62	SEMEdxWdx-Graz

Sample	Lithology	SiO_2	CaO	K_2O	MgO	Al_2O_3	FeO	MnO	TiO_2	Na_2O	$Cr2O_3$	Total	Analysis Facility
TRP-PPXT	PPXT-MR	51.90	21.24	0.00	14.92	1.87	5.57	0.14	0.57	0.36	0.77	97.35	SEMEdxWdx-Graz
TRP-PPXT	PPXT-MR	53.57	21.18	0.00	15.97	1.00	5.35	0.05	0.33	0.28	0.44	98.18	SEMEdxWdx-Graz
TRP-PPXT	PPXT-MR	52.90	21.52	0.00	15.82	1.53	5.16	0.18	0.55	0.31	0.76	98.73	SEMEdxWdx-Graz
TRP-PPXT	PPXT-MR	52.84	22.01	0.00	15.85	1.76	4.67	0.10	0.43	0.30	0.80	98.77	SEMEdxWdx-Graz
TRP-PPXT	PPXT-MR	52.35	21.35	0.00	14.91	2.53	5.04	0.13	0.62	0.46	0.86	98.25	SEMEdxWdx-Graz
TRP-PPXT	PPXT-MR	52.69	21.60	0.00	15.70	1.81	4.72	0.14	0.47	0.30	0.86	98.30	SEMEdxWdx-Graz
TRP006	PXT-MR	52.69	20.23	0.00	15.95	1.78	5.97	0.14	0.58	0.34	0.66	98.34	SEMEdxWdx-Graz
TRP006	PXT-MR	53.27	21.72	0.00	15.50	1.25	5.02	0.09	0.32	0.32	0.47	97.95	SEMEdxWdx-Graz
TRP006	PXT-MR	53.42	22.09	0.00	15.90	1.13	4.43	0.03	0.37	0.32	0.77	98.46	SEMEdxWdx-Graz
TRP006	PXT-MR	53.29	21.51	0.00	15.82	1.68	5.00	0.06	0.53	0.40	0.79	99.09	SEMEdxWdx-Graz
TRP006	PXT-MR	52.41	21.83	0.01	15.07	2.82	4.49	0.08	0.40	0.40	1.32	98.83	SEMEdxWdx-Graz
TRP006	PXT-MR	52.65	22.00	0.00	15.20	2.15	4.53	0.05	0.23	0.42	1.05	98.29	SEMEdxWdx-Graz
TRP006	PXT-MR	53.42	21.84	0.00	15.20	2.25	4.53	0.06	0.30	0.42	0.75	98.77	SEMEdxWdx-Graz
TRP006	PXT-MR	52.52	21.55	0.00	15.52	1.57	4.73	0.10	0.42	0.34	0.70	97.45	SEMEdxWdx-Graz
TRP006	PXT-MR	52.46	21.42	0.00	15.75	1.42	5.26	0.10	0.58	0.30	0.56	97.85	SEMEdxWdx-Graz
JJB17	PXT-HW	57.08	21.90	0.02	18.37	1.64	4.37	0.10	0.35	0.27	0.58	104.70	SEMEdxWdx-Graz
JJB17	PXT-HW	56.95	21.84	0.04	18.75	1.79	4.08	0.17	0.32	0.26	0.91	105.10	SEMEdxWdx-Graz
JJB17	PXT-HW	56.61	22.23	0.00	18.95	1.62	4.25	0.10	0.23	0.22	0.57	104.78	SEMEdxWdx-Graz
JJB17	PXT-HW	57.23	22.14	0.01	19.32	1.36	3.96	0.12	0.28	0.19	0.48	105.08	SEMEdxWdx-Graz
JJB13	BSN-MR	52.95	22.05	0.00	15.24	1.44	4.54	0.14	0.45	0.39	0.99	98.19	SEMEdxWdx-Graz
JJB13	BSN-MR	53.89	22.35	0.00	15.74	1.17	4.18	0.09	0.27	0.30	0.77	98.75	SEMEdxWdx-Graz
JJB13	BSN-MR	53.61	22.64	0.00	15.79	1.10	4.07	0.15	0.28	0.36	0.73	98.73	SEMEdxWdx-Graz
JJB13	BSN-MR	52.82	22.02	0.01	15.12	1.89	4.95	0.13	0.63	0.31	0.82	98.71	SEMEdxWdx-Graz
JJB13	BSN-MR	53.23	22.32	0.00	15.30	1.13	4.55	0.14	0.35	0.34	0.63	97.99	SEMEdxWdx-Graz
JJB13	BSN-MR	53.76	22.43	0.00	15.17	0.74	4.25	0.12	0.12	0.31	0.56	97.44	SEMEdxWdx-Graz
JJB13	BSN-MR	53.53	20.48	0.00	16.61	1.72	6.01	0.17	0.60	0.40	0.79	100.31	SEMEdxWdx-Graz
JJB13	BSN-MR	54.15	23.20	0.00	15.22	1.34	4.17	0.01	0.37	0.26	0.69	99.40	SEMEdxWdx-Graz
JJB14	BSN-MR	52.67	21.28	0.01	15.98	1.83	4.91	0.06	0.48	0.43	0.98	98.65	SEMEdxWdx-Graz
JJB14	BSN-MR	52.90	22.12	0.00	16.08	1.87	4.14	0.06	0.42	0.50	0.95	99.05	SEMEdxWdx-Graz
JJB14	BSN-MR	53.44	15.04	0.00	20.25	1.78	7.90	0.19	0.37	0.40	0.91	100.27	SEMEdxWdx-Graz
JJB14	BSN-MR	52.50	22.36	0.00	16.65	1.59	3.90	0.12	0.27	0.47	0.92	98.77	SEMEdxWdx-Graz
JJB14	BSN-MR	52.24	21.94	0.00	16.00	1.72	4.25	0.13	0.37	0.46	0.99	98.10	SEMEdxWdx-Graz
JJB14	BSN-MR	52.69	21.97	0.01	16.12	1.85	4.41	0.15	0.33	0.40	0.95	98.89	SEMEdxWdx-Graz
JJB14	BSN-MR	52.52	22.65	0.00	16.46	1.81	4.04	0.05	0.45	0.38	0.99	99.36	SEMEdxWdx-Graz
JJB14	BSN-MR	52.95	22.26	0.02	16.30	1.78	3.69	0.21	0.18	0.38	0.96	98.73	SEMEdxWdx-Graz
JJB14	BSN-MR	53.20	22.88	0.00	16.78	1.34	3.51	0.13	0.22	0.31	0.79	99.16	SEMEdxWdx-Graz
JJB14	BSN-MR	53.10	22.35	0.02	16.50	1.76	3.91	0.17	0.32	0.32	0.95	99.39	SEMEdxWdx-Graz
JJB14	BSN-MR	52.90	22.19	0.00	15.98	1.89	4.27	0.13	0.25	0.43	0.96	99.02	SEMEdxWdx-Graz
JJB14	BSN-MR	52.69	22.42	0.00	16.25	1.96	3.94	0.13	0.22	0.44	0.95	99.00	SEMEdxWdx-Graz
JJB18	BSN-HW	53.44	22.36	0.00	16.12	1.36	4.28	0.09	0.50	0.44	0.86	99.46	SEMEdxWdx-Graz
JJB18	BSN-HW	54.53	23.02	0.01	15.98	1.27	3.47	0.09	0.40	0.40	0.92	100.10	SEMEdxWdx-Graz
JJB18	BSN-HW	53.57	22.32	0.00	15.49	1.61	4.32	0.14	0.52	0.43	0.96	99.36	SEMEdxWdx-Graz
JJB18	BSN-HW	53.63	22.39	0.01	15.80	1.17	4.43	0.13	0.47	0.44	0.91	99.38	SEMEdxWdx-Graz
JJB18	BSN-HW	53.44	22.43	0.00	15.29	1.74	4.01	0.08	0.42	0.42	1.02	98.84	SEMEdxWdx-Graz
JJB18	BSN-HW	54.08	22.09	0.00	16.08	1.42	4.26	0.09	0.37	0.42	0.89	99.70	SEMEdxWdx-Graz
JJB18	BSN-HW	53.53	21.32	0.00	16.32	1.49	4.79	0.09	0.47	0.42	0.92	99.34	SEMEdxWdx-Graz
JJB18	BSN-HW	54.27	22.57	0.00	15.92	1.53	3.87	0.21	0.55	0.36	0.94	100.22	SEMEdxWdx-Graz
JJB18	BSN-HW	54.06	22.30	0.00	16.22	1.45	4.18	0.06	0.52	0.35	0.89	100.04	SEMEdxWdx-Graz
JJB18	BSN-HW	54.34	22.36	0.00	15.74	1.15	3.89	0.13	0.23	0.35	0.88	99.06	SEMEdxWdx-Graz
JJB18	BSN-HW	54.08	22.16	0.00	16.32	1.36	4.41	0.10	0.35	0.35	0.94	100.07	SEMEdxWdx-Graz
JJB18	BSN-HW	54.42	22.39	0.00	16.33	1.11	4.16	0.08	0.33	0.34	0.82	99.98	SEMEdxWdx-Graz
JJB18	BSN-HW	54.79	22.30	0.00	16.25	1.45	3.92	0.06	0.33	0.35	0.94	100.40	SEMEdxWdx-Graz
JJB18	BSN-HW	54.32	22.25	0.00	15.77	1.64	4.27	0.17	0.42	0.38	0.82	100.03	SEMEdxWdx-Graz
JJB18	BSN-HW	53.97	22.28	0.02	16.05	1.62	4.32	0.09	0.48	0.35	0.82	100.02	SEMEdxWdx-Graz
JJB18	BSN-HW	54.12	22.57	0.00	15.75	1.62	4.16	0.17	0.58	0.40	0.85	100.23	SEMEdxWdx-Graz

A3-4.2 Cations per 6 oxygens

Sample	Lithology	Si	Ca	K	Mg	Al	Fe	Mn	Ti	Ni	Na	Cr	Total
TRP-AL7907	PXT-MR	1.96	0.96	0.00	0.75	0.07	0.15	0.01	0.01	0.00	0.07	0.03	4.01
TRP-AL7908	PXT-MR	1.98	0.90	0.00	0.83	0.07	0.15	0.01	0.01	0.00	0.02	0.01	3.98
TRP-AL7908	PXT-MR	1.95	0.97	0.00	0.79	0.07	0.14	0.01	0.02	0.00	0.05	0.02	4.01
TRP-AL7908	PXT-MR	1.97	0.94	0.00	0.80	0.07	0.14	0.01	0.01	0.00	0.04	0.02	3.99
TRP-AL7908	PXT-MR	1.98	0.97	0.00	0.78	0.04	0.16	0.00	0.02	0.00	0.04	0.01	3.99
TRP-AL7908	PXT-MR	1.96	1.00	0.00	0.77	0.06	0.16	0.00	0.01	0.00	0.03	0.01	4.01
JJB11	PXT-MR	1.97	0.95	0.00	0.82	0.05	0.13	0.00	0.00	0.00	0.09	0.04	4.04
JJB11	PXT-MR	1.99	0.92	0.00	0.83	0.05	0.18	0.00	0.00	0.00	0.00	0.00	3.98
JJB11	PXT-MR	1.97	0.91	0.00	0.83	0.05	0.18	0.00	0.01	0.00	0.05	0.02	4.01
JJB11	PXT-MR	1.94	0.97	0.00	0.79	0.08	0.13	0.00	0.01	0.00	0.09	0.04	4.04
JJB15	PXT-MR	1.94	0.97	0.00	0.79	0.10	0.13	0.00	0.00	0.00	0.09	0.03	4.04

Sample	Lithology	Si	Ca	K	Mg	Al	Fe	Mn	Ti	Ni	Na	Cr	Total
EST013_14	MLN-MR	1.95	0.86	0.00	0.89	0.08	0.15	0.00	0.01	0.00	0.03	0.03	4.00
EST013_14	MLN-MR	1.96	0.86	0.00	0.91	0.06	0.15	0.00	0.02	0.00	0.02	0.02	4.00
EST013_14	MLN-MR	2.04	0.46	0.00	1.24	0.03	0.14	0.00	0.00	0.00	0.01	0.01	3.94
EST013_14	MLN-MR	1.96	0.87	0.00	0.92	0.05	0.15	0.00	0.01	0.00	0.02	0.02	4.00
EST013_14	MLN-MR	1.95	0.87	0.00	0.89	0.07	0.16	0.00	0.02	0.00	0.03	0.02	4.00
EST013_14	MLN-MR	1.95	0.82	0.00	0.93	0.09	0.15	0.00	0.01	0.00	0.03	0.03	4.00
EST013_14	MLN-MR	1.94	0.87	0.00	0.89	0.08	0.14	0.00	0.01	0.00	0.03	0.03	4.01
EST013_16	MLN-MR	1.95	0.86	0.00	0.87	0.09	0.14	0.00	0.01	0.00	0.03	0.03	4.00
EST013_16	MLN-MR	1.95	0.86	0.00	0.89	0.10	0.14	0.00	0.01	0.00	0.03	0.02	4.00
EST013_16	MLN-MR	1.97	0.86	0.00	0.94	0.05	0.14	0.01	0.01	0.00	0.02	0.01	4.00
EST013_16	MLN-MR	1.95	0.85	0.00	0.92	0.07	0.16	0.00	0.01	0.00	0.03	0.02	4.01
EST013_16	MLN-MR	1.96	0.87	0.00	0.89	0.07	0.16	0.00	0.01	0.00	0.03	0.02	4.00
EST013_16	MLN-MR	1.94	0.86	0.00	0.92	0.07	0.15	0.00	0.02	0.00	0.03	0.02	4.01
EST013_16	MLN-MR	1.94	0.84	0.00	0.92	0.07	0.15	0.00	0.02	0.00	0.02	0.02	4.00
EST013_16	MLN-MR	1.95	0.86	0.00	0.89	0.09	0.15	0.00	0.01	0.00	0.02	0.02	3.99
EST013_16	MLN-MR	1.97	0.88	0.00	0.92	0.05	0.13	0.00	0.01	0.00	0.02	0.02	4.00
EST013_16	MLN-MR	1.96	0.87	0.00	0.90	0.06	0.15	0.01	0.01	0.00	0.03	0.02	4.00
EST013_16	MLN-MR	1.95	0.87	0.00	0.89	0.08	0.14	0.00	0.01	0.00	0.03	0.03	4.00
EST013_16	MLN-MR	1.95	0.87	0.00	0.91	0.08	0.12	0.01	0.01	0.00	0.02	0.03	4.00
EST013_22	MLN-MR	1.95	0.84	0.00	0.91	0.07	0.16	0.00	0.02	0.00	0.03	0.02	4.00
EST013_22	MLN-MR	1.96	0.86	0.00	0.90	0.07	0.15	0.01	0.01	0.00	0.03	0.02	4.00
EST013_22	MLN-MR	1.97	0.85	0.00	0.90	0.06	0.15	0.00	0.01	0.00	0.03	0.02	3.99
EST013_23	MLN-MR	1.96	0.87	0.00	0.90	0.08	0.14	0.00	0.01	0.00	0.02	0.02	4.00
EST013_23	MLN-MR	1.95	0.87	0.00	0.89	0.08	0.14	0.00	0.01	0.00	0.03	0.02	4.00
EST013_23	MLN-MR	1.97	0.86	0.00	0.91	0.06	0.15	0.01	0.01	0.00	0.03	0.01	4.00
EST013_23	MLN-MR	1.97	0.89	0.00	0.96	0.04	0.12	0.00	0.00	0.00	0.01	0.00	4.01
EST013_23	MLN-MR	1.95	0.86	0.00	0.94	0.07	0.12	0.00	0.01	0.00	0.03	0.02	4.01
EST013_23	MLN-MR	1.95	0.86	0.00	0.92	0.07	0.15	0.00	0.01	0.00	0.02	0.02	4.00

Sample	Lithology	Si	Ca	K	Mg	Al	Fe	Mn	Ti	Na	Cr	Total
TRP-PPXT	PPXT-MR	1.96	0.86	0.00	0.84	0.08	0.18	0.00	0.02	0.03	0.02	3.99
TRP-PPXT	PPXT-MR	1.99	0.84	0.00	0.89	0.04	0.17	0.00	0.01	0.02	0.01	3.98
TRP-PPXT	PPXT-MR	1.96	0.86	0.00	0.88	0.07	0.16	0.01	0.02	0.02	0.02	3.99
TRP-PPXT	PPXT-MR	1.96	0.87	0.00	0.88	0.08	0.14	0.00	0.01	0.02	0.02	3.99
TRP-PPXT	PPXT-MR	1.95	0.85	0.00	0.83	0.11	0.16	0.00	0.02	0.03	0.03	3.98
TRP-PPXT	PPXT-MR	1.96	0.86	0.00	0.87	0.08	0.15	0.00	0.01	0.02	0.03	3.98
TRP006	PXT-MR	1.96	0.81	0.00	0.89	0.08	0.19	0.00	0.02	0.02	0.02	3.98
TRP006	PXT-MR	1.99	0.87	0.00	0.86	0.06	0.16	0.00	0.01	0.02	0.01	3.98
TRP006	PXT-MR	1.98	0.88	0.00	0.88	0.05	0.14	0.00	0.01	0.02	0.02	3.98
TRP006	PXT-MR	1.97	0.85	0.00	0.87	0.07	0.15	0.00	0.01	0.03	0.02	3.98
TRP006	PXT-MR	1.94	0.87	0.00	0.83	0.12	0.14	0.00	0.01	0.03	0.04	3.98
TRP006	PXT-MR	1.96	0.88	0.00	0.84	0.09	0.14	0.00	0.01	0.03	0.03	3.99
TRP006	PXT-MR	1.97	0.86	0.00	0.84	0.10	0.14	0.00	0.01	0.03	0.02	3.97
TRP006	PXT-MR	1.97	0.87	0.00	0.87	0.07	0.15	0.00	0.01	0.02	0.02	3.98
TRP006	PXT-MR	1.97	0.86	0.00	0.88	0.06	0.16	0.00	0.02	0.02	0.02	3.99
JJB17	PXT-HW	1.98	0.81	0.00	0.95	0.07	0.13	0.00	0.01	0.02	0.02	3.98
JJB17	PXT-HW	1.97	0.81	0.00	0.96	0.07	0.12	0.00	0.01	0.02	0.02	3.99
JJB17	PXT-HW	1.96	0.83	0.00	0.98	0.07	0.12	0.00	0.01	0.01	0.02	4.00
JJB17	PXT-HW	1.97	0.82	0.00	0.99	0.06	0.11	0.00	0.01	0.01	0.01	3.99
JJB13	BSN-MR	1.97	0.88	0.00	0.85	0.06	0.14	0.00	0.01	0.03	0.03	3.98
JJB13	BSN-MR	1.99	0.88	0.00	0.87	0.05	0.13	0.00	0.01	0.02	0.02	3.98
JJB13	BSN-MR	1.98	0.90	0.00	0.87	0.05	0.13	0.00	0.01	0.03	0.02	3.99
JJB13	BSN-MR	1.96	0.88	0.00	0.84	0.08	0.15	0.00	0.02	0.02	0.02	3.98
JJB13	BSN-MR	1.99	0.89	0.00	0.85	0.05	0.14	0.00	0.01	0.02	0.02	3.98
JJB13	BSN-MR	2.01	0.90	0.00	0.85	0.03	0.13	0.00	0.00	0.02	0.02	3.97
JJB13	BSN-MR	1.96	0.80	0.00	0.90	0.07	0.18	0.01	0.02	0.03	0.02	3.99
JJB13	BSN-MR	1.99	0.91	0.00	0.83	0.06	0.13	0.00	0.01	0.02	0.02	3.97
JJB14	BSN-MR	1.95	0.85	0.00	0.88	0.08	0.15	0.00	0.01	0.03	0.03	3.99
JJB14	BSN-MR	1.95	0.87	0.00	0.88	0.08	0.13	0.00	0.01	0.07	0.03	4.02
JJB14	BSN-MR	1.94	0.58	0.00	1.09	0.08	0.24	0.01	0.01	0.06	0.03	4.03
JJB14	BSN-MR	1.94	0.89	0.00	0.92	0.07	0.12	0.00	0.01	0.07	0.03	4.04
JJB14	BSN-MR	1.94	0.87	0.00	0.89	0.08	0.13	0.00	0.01	0.07	0.03	4.03
JJB14	BSN-MR	1.94	0.87	0.00	0.89	0.08	0.14	0.00	0.01	0.07	0.03	4.03
JJB14	BSN-MR	1.93	0.89	0.00	0.90	0.08	0.12	0.00	0.01	0.07	0.03	4.04
JJB14	BSN-MR	1.95	0.88	0.00	0.90	0.08	0.11	0.01	0.00	0.07	0.03	4.03
JJB14	BSN-MR	1.95	0.90	0.00	0.92	0.06	0.11	0.00	0.01	0.06	0.02	4.03
JJB14	BSN-MR	1.94	0.88	0.00	0.90	0.08	0.12	0.01	0.01	0.07	0.03	4.03
JJB14	BSN-MR	1.95	0.88	0.00	0.88	0.08	0.13	0.00	0.01	0.07	0.03	4.02
JJB14	BSN-MR	1.94	0.88	0.00	0.89	0.09	0.12	0.00	0.01	0.07	0.03	4.03
JJB18	BSN-HW	1.96	0.88	0.00	0.88	0.06	0.13	0.00	0.01	0.06	0.02	4.01
JJB18	BSN-HW	1.98	0.90	0.00	0.86	0.05	0.11	0.00	0.01	0.06	0.03	4.00
JJB18	BSN-HW	1.97	0.88	0.00	0.85	0.07	0.13	0.00	0.01	0.07	0.03	4.01
JJB18	BSN-HW	1.97	0.88	0.00	0.86	0.05	0.14	0.00	0.01	0.06	0.03	4.01
JJB18	BSN-HW	1.97	0.89	0.00	0.84	0.08	0.12	0.00	0.01	0.03	0.03	3.98
JJB18	BSN-HW	1.98	0.87	0.00	0.88	0.06	0.13	0.00	0.01	0.03	0.03	3.98
JJB18	BSN-HW	1.97	0.84	0.00	0.89	0.06	0.15	0.00	0.01	0.03	0.03	3.99
JJB18	BSN-HW	1.98	0.88	0.00	0.86	0.07	0.12	0.01	0.02	0.03	0.03	3.98
JJB18	BSN-HW	1.97	0.87	0.00	0.88	0.06	0.13	0.00	0.01	0.02	0.03	3.98
JJB18	BSN-HW	2.00	0.88	0.00	0.86	0.05	0.12	0.00	0.01	0.02	0.03	3.97
JJB18	BSN-HW	1.97	0.87	0.00	0.89	0.06	0.13	0.00	0.01	0.02	0.03	3.99
JJB18	BSN-HW	1.99	0.88	0.00	0.89	0.05	0.13	0.00	0.01	0.02	0.02	3.98
JJB18	BSN-HW	1.99	0.87	0.00	0.88	0.06	0.12	0.00	0.01	0.02	0.03	3.97
JJB18	BSN-HW	1.98	0.87	0.00	0.86	0.07	0.13	0.01	0.01	0.03	0.02	3.97
JJB18	BSN-HW	1.97	0.87	0.00	0.87	0.07	0.13	0.00	0.01	0.02	0.02	3.98
JJB18	BSN-HW	1.97	0.88	0.00	0.86	0.07	0.13	0.01	0.02	0.03	0.02	3.98

End Member Recalculation of clinopyroxene in hanging wall pyroxenite

TRP_Pxt		En	Wo	Fs
(n=5)	Min	45,65	41,85	3,50
	Max	52,14	50,85	6,76
	Mean	50,32	43,87	5,81
	Std. Dev.	2,68	3,92	1,32
TRP272_Pxt		En	Wo	Fs
(n=4)	Min	41.38	50.56	7.32
	Max	42.12	49.22	9.18
	Mean	41.79	49.92	8.29
	Std. Dev.	0.35	0.69	1.02
TRP_BSN		En	Wo	Fs
(n=19)	Min	45.58	40.87	3.81
	Max	53.55	47.92	7.89
	Mean	47.28	46.20	6.51
	Std. Dev.	1.80	1.54	0.96
EST013_MsN		En	Wo	Fs
(n=5)	Min	44.12	46.00	7.03
	Max	45.58	47.90	8.42
	Mean	44.91	47.34	7.75
	Std. Dev.	0.62	0.77	0.51

End Member Recalculation of clinopyroxene in Merensky Reef pyroxenite

TRP_Pxt		En	Wo	Fs
(n=9)	Min	42.56	45.92	4.57
	Max	48.03	50.33	10.36
	Mean	45.14	47.98	6.88
	Std. Dev.	2.19	1.63	2.08
TRP272_Pxt		En	Wo	Fs
(n=10)	Min	40.32	46.29	4.57
	Max	48.03	51.53	8.22
	Mean	44.01	49.11	6.88
	Std. Dev.	3.13	2.00	1.39
TRP_BSN		En	Wo	Fs
(n=46)	Min	44.44	41.65	4.07
	Max	50.33	48.68	9.85
	Mean	46.91	46.22	6.87
	Std. Dev.	1.46	1.45	1.11
EST013_MLN		En	Wo	Fs
(n=27)	Min	46.98	41.71	5.27
	Max	50.43	45.11	8.27
	Mean	48.44	44.20	7.37
	Std. Dev.	0.84	0.74	0.73

End Member recalculation of clinopyroxene in pyroxenite vs pegmatoidal pyroxenite

TRP_PXT		En	Wo	Fs
(n=9)	Min	45.66	42.52	7.28
	Max	47.54	46.75	9.94
	Mean	46.35	45.47	8.18
	Std. Dev.	0.58	1.28	0.80
TRP_BSN		En	Wo	Fs
(n=6)	Min	45.22	44.55	7.78
	Max	46.80	45.72	9.45
	Mean	46.29	45.19	8.52
	Std. Dev.	0.69	0.42	0.61

A3-5.1 Plagioclase Compositions (EPMA-Rhodes University)

Sample	Lithology	SiO_2	CaO	K_2O	MgO	Al_2O_3	FeO	MnO	TiO_2	NiO	Na_2O	Cr_2O_3	Total
JJB19	PXT-MR-CHR	50.56	13.44	0.06	0.03	31.40	0.49	0.01	0.02	0.00	3.67	0.00	99.68
JJB19	PXT-MR-CHR	51.31	13.59	0.05	0.00	31.75	0.06	0.00	0.00	0.00	3.78	0.00	100.55
JJB19	PXT-MR-CHR	44.95	18.04	0.03	0.01	36.07	0.21	0.00	0.00	0.00	1.03	0.23	100.56
JJB19	PXT-MR-CHR	54.61	1.57	0.02	30.58	1.40	9.21	0.02	0.01	0.07	0.02	0.35	97.86
JJB19	PXT-MR-CHR	44.85	17.68	0.02	0.02	35.72	0.34	0.00	0.00	0.00	1.38	0.30	100.29
JJB19	PXT-MR-CHR	49.61	14.38	0.08	0.00	32.48	0.17	0.02	0.00	0.01	3.38	0.01	100.13
JJB11	PXT-MR	56.06	10.08	0.13	0.01	28.49	0.07	0.00	0.01	0.01	5.88	0.02	100.76
JJB11	PXT-MR	50.74	13.91	0.11	0.01	31.22	0.17	0.01	0.00	0.01	3.55	0.00	99.73
JJB16	PXT-MR	51.38	13.58	0.07	0.00	31.54	0.16	0.00	0.01	0.00	3.70	0.02	100.47
JJB16	PXT-MR	51.21	13.19	0.09	0.01	31.60	0.09	0.00	0.00	0.01	3.82	0.00	100.01
JJB16	PXT-MR	48.09	15.75	0.06	0.01	32.81	0.07	0.03	0.00	0.02	2.73	0.02	99.57
JJB16	PXT-MR	49.20	15.15	0.04	0.01	32.59	0.03	0.00	0.00	0.00	3.08	0.00	100.11
JJB16	PXT-MR	48.35	15.62	0.05	0.00	33.23	0.00	0.00	0.03	0.01	2.61	0.01	99.90
JJB16	PXT-MR	48.98	14.24	0.18	0.03	32.14	0.30	0.04	0.00	0.01	3.03	0.02	98.97
JJB16	PXT-MR	51.88	13.11	0.12	0.01	31.16	0.13	0.00	0.00	0.05	4.08	0.00	100.53
JJB16	PXT-MR	54.20	12.06	0.10	0.02	30.23	0.14	0.00	0.00	0.02	4.90	0.00	101.68
JJB16	PXT-MR	51.98	12.85	0.11	0.03	30.96	0.07	0.00	0.00	0.02	4.31	0.00	100.32
JJB18	BSN-HW	51.08	13.79	0.16	0.01	31.78	0.18	0.00	0.00	0.00	3.63	0.01	100.63
JJB18	BSN-HW	51.51	13.82	0.15	0.01	31.85	0.22	0.01	0.00	0.01	3.75	0.05	101.38
JJB18	BSN-HW	51.32	12.70	0.16	0.04	31.00	0.48	0.00	0.00	0.00	3.98	0.00	99.68
JJB18	BSN-HW	52.42	12.48	0.18	0.03	30.67	0.07	0.02	0.01	0.01	4.29	0.01	100.19
JJB18	BSN-HW	51.54	13.48	0.14	0.04	31.33	0.30	0.00	0.00	0.01	3.84	0.02	100.70
JJB9	BSN-MR	47.63	16.02	0.06	0.00	33.83	0.21	0.00	0.00	0.00	2.26	0.00	100.02
JJB9	BSN-MR	48.73	15.01	0.13	0.03	32.78	0.19	0.01	0.02	0.00	2.99	0.02	99.91
JJB9	BSN-MR	49.63	14.69	0.13	0.01	32.56	0.20	0.02	0.02	0.00	3.20	0.03	100.48
JJB9	BSN-MR	49.49	14.86	0.11	0.02	32.59	0.14	0.00	0.00	0.00	2.96	0.00	100.17
JJB9	PXT-MR	50.99	13.76	0.17	0.01	31.10	0.19	0.00	0.00	0.01	3.69	0.01	99.92
JJB14	BSN-MR	51.08	13.76	0.23	0.00	31.39	0.23	0.03	0.00	0.01	3.69	0.00	100.40
JJB14	BSN-MR	50.33	14.18	0.15	0.02	31.67	0.00	0.01	0.00	0.01	3.50	0.00	99.87
JJB14	BSN-MR	46.94	13.50	0.14	0.02	31.60	3.91	0.03	0.00	0.00	2.67	0.01	98.81
JJB10	PXT-MR-CHR	49.74	15.27	0.13	0.02	32.57	0.29	0.00	0.00	0.01	2.74	0.04	100.82
JJB10	PXT-MR-CHR	47.03	16.98	0.08	0.03	33.71	0.16	0.02	0.00	0.02	1.83	0.02	99.88
JJB10	PXT-MR-CHR	47.18	16.05	0.05	0.03	33.40	0.09	0.00	0.03	0.00	2.33	0.00	99.17
JJB10	PXT-MR-CHR	49.08	14.82	0.15	0.02	32.26	0.18	0.00	0.01	0.00	3.05	0.00	99.57
JJB10	PXT-MR-CHR	48.48	15.15	0.13	0.02	32.21	0.23	0.02	0.00	0.02	2.80	0.00	99.06
JJB10	PXT-MR-CHR	48.53	14.99	0.15	0.01	32.57	0.25	0.01	0.02	0.00	2.83	0.00	99.35
TRP-Al7906	An-NOR-PXT HW	48.05	15.67	0.09	0.01	33.45	0.12	0.02	0.01	0.00	2.70	0.01	100.14
TRP-Al7906	An-NOR-PXT HW	48.79	15.70	0.08	0.01	33.25	0.22	0.03	0.00	0.00	2.75	0.03	100.84
TRP-Al7906	An-NOR-PXT HW	49.37	15.32	0.09	0.02	32.96	0.11	0.01	0.00	0.02	3.01	0.00	100.91
TRP-Al7906	An-NOR-PXT HW	48.61	15.54	0.06	0.01	33.06	0.11	0.00	0.00	0.00	2.79	0.02	100.19
TRP-Al7906	An-NOR-PXT HW	48.58	15.43	0.09	0.02	32.85	0.14	0.02	0.01	0.00	2.73	0.03	99.89
TRP-Al7906	An-NOR-PXT HW	48.35	15.48	0.10	0.00	33.11	0.13	0.00	0.00	0.02	2.68	0.01	99.88
TRP-Al7907B	PXT-MR	56.26	9.69	0.04	0.00	28.39	0.13	0.03	0.00	0.00	6.16	0.00	100.71
TRP-Al7907B	PXT-MR	55.91	9.59	0.02	0.02	28.18	0.20	0.01	0.01	0.02	6.32	0.00	100.27
TRP-AL7908	PXT-MR	54.52	10.41	0.06	0.02	28.63	0.18	0.00	0.00	0.01	6.05	0.01	99.89

Sample	Lithology	SiO_2	CaO	K_2O	MgO	Al_2O_3	FeO	MnO	TiO_2	NiO	Na_2O	Cr_2O_3	Total
EST013-11	MsN-HW	48.26	15.59	0.13	0.00	32.99	0.32	0.00	0.00	0	2.72	0.01	100.01
EST013-11	MsN-HW	48.36	16.10	0.14	0.00	33.30	0.29	0.00	0.01	0	2.64	0.02	100.87
EST013-11	MsN-HW	48.99	15.43	0.16	0.01	33.12	0.17	0.00	0.00	0	2.78	0.03	100.68
EST013-11	MsN-HW	47.81	16.15	0.09	0.01	33.64	0.10	0.00	0.02	0	2.34	0.01	100.17
EST013-11	MsN-HW	47.70	16.51	0.10	0.00	33.52	0.24	0.02	0.00	0	2.36	0.01	100.46
EST013-11	MsN-HW	48.27	15.79	0.14	0.01	33.37	0.28	0.00	0.00	0	2.58	0.00	100.44
EST013-11	MsN-HW	48.71	15.45	0.14	0.01	32.94	0.00	0.03	0.01	0	2.80	0.00	100.08
EST013-11	MsN-HW	48.64	15.57	0.16	0.03	33.17	0.24	0.03	0.00	0	2.62	0.02	100.48
EST013-11	MsN-HW	48.34	15.60	0.16	0.02	33.19	0.22	0.01	0.00	0	2.42	0.02	99.99
EST013-11	MsN-HW	48.64	15.59	0.15	0.00	33.09	0.23	0.02	0.01	0	2.70	0.04	100.46
EST013-10	MsN-HW	48.63	15.73	0.13	0.01	32.88	0.21	0.00	0.00	0	2.82	0.00	100.41
EST013-10	MsN-HW	48.18	15.78	0.11	0.03	33.17	0.10	0.00	0.00	0	2.63	0.00	100.00
EST013-10	MsN-HW	49.26	15.08	0.18	0.00	32.67	0.19	0.02	0.01	0	2.93	0.01	100.37
EST013-10	MsN-HW	48.67	15.43	0.14	0.02	33.44	0.31	0.00	0.00	0	2.73	0.00	100.73
EST013-10	MsN-HW	49.07	15.74	0.13	0.00	33.50	0.07	0.00	0.00	0	2.63	0.01	101.14
EST013-10	MsN-HW	48.09	16.45	0.08	0.02	33.49	0.20	0.00	0.01	0	2.29	0.01	100.64
EST013-10	MsN-HW	48.48	15.73	0.12	0.01	33.36	0.24	0.00	0.00	0	2.70	0.00	100.64
EST013-10	MsN-HW	48.43	15.81	0.11	0.01	33.52	0.19	0.00	0.02	0	2.69	0.02	100.82
EST013-10	MsN-HW	48.26	15.60	0.11	0.00	33.26	0.19	0.02	0.00	0	2.77	0.01	100.22
EST013-10	MsN-HW	48.43	15.92	0.11	0.02	33.57	0.14	0.02	0.02	0	2.58	0.00	100.78

A3-5.2 Cations per 8 oxygens

Sample	Lithology	Si	Ca	K	Mg	Al	Fe	Mn	Ti	Ni	Na	Cr	Total
JJB19	PXT-MR-CHR	2.31	0.66	0.00	0.00	1.69	0.02	0.00	0.00	0.00	0.33	0.00	5.01
JJB19	PXT-MR-CHR	2.32	0.66	0.00	0.00	1.69	0.00	0.00	0.00	0.00	0.33	0.00	5.00
JJB19	PXT-MR-CHR	2.06	0.89	0.00	0.00	1.95	0.01	0.00	0.00	0.00	0.09	0.01	5.01
JJB19	PXT-MR-CHR	2.61	0.08	0.00	2.18	0.08	0.37	0.00	0.00	0.00	0.00	0.01	5.34
JJB19	PXT-MR-CHR	2.06	0.87	0.00	0.00	1.94	0.01	0.00	0.00	0.00	0.12	0.01	5.02
JJB19	PXT-MR-CHR	2.26	0.70	0.00	0.00	1.74	0.01	0.00	0.00	0.00	0.30	0.00	5.02
JJB11	PXT-MR	2.50	0.48	0.01	0.00	1.50	0.00	0.00	0.00	0.00	0.51	0.00	5.01
JJB11	PXT-MR	2.32	0.68	0.01	0.00	1.68	0.01	0.00	0.00	0.00	0.31	0.00	5.00
JJB16	PXT-MR	2.32	0.66	0.00	0.00	1.68	0.01	0.00	0.00	0.00	0.32	0.00	5.00
JJB16	PXT-MR	2.32	0.64	0.01	0.00	1.69	0.00	0.00	0.00	0.00	0.34	0.00	5.00
JJB16	PXT-MR	2.21	0.78	0.00	0.00	1.78	0.00	0.00	0.00	0.00	0.24	0.00	5.02
JJB16	PXT-MR	2.25	0.74	0.00	0.00	1.75	0.00	0.00	0.00	0.00	0.27	0.00	5.02
JJB16	PXT-MR	2.21	0.77	0.00	0.00	1.79	0.00	0.00	0.00	0.00	0.23	0.00	5.01
JJB16	PXT-MR	2.26	0.70	0.01	0.00	1.75	0.01	0.00	0.00	0.00	0.27	0.00	5.01
JJB16	PXT-MR	2.34	0.63	0.01	0.00	1.66	0.00	0.00	0.00	0.00	0.36	0.00	5.01
JJB16	PXT-MR	2.41	0.58	0.01	0.00	1.59	0.01	0.00	0.00	0.00	0.42	0.00	5.01
JJB16	PXT-MR	2.35	0.62	0.01	0.00	1.65	0.00	0.00	0.00	0.00	0.38	0.00	5.02
JJB18	BSN-HW	2.31	0.67	0.01	0.00	1.69	0.01	0.00	0.00	0.00	0.32	0.00	5.01
JJB18	BSN-HW	2.31	0.66	0.01	0.00	1.69	0.01	0.00	0.00	0.00	0.33	0.00	5.01
JJB18	BSN-HW	2.34	0.62	0.01	0.00	1.67	0.02	0.00	0.00	0.00	0.35	0.00	5.01
JJB18	BSN-HW	2.37	0.60	0.01	0.00	1.64	0.00	0.00	0.00	0.00	0.38	0.00	5.00
JJB18	BSN-HW	2.33	0.65	0.01	0.00	1.67	0.01	0.00	0.00	0.00	0.34	0.00	5.01
JJB9	BSN-MR	2.18	0.79	0.00	0.00	1.83	0.01	0.00	0.00	0.00	0.20	0.00	5.01
JJB9	BSN-MR	2.23	0.74	0.01	0.00	1.77	0.01	0.00	0.00	0.00	0.27	0.00	5.02
JJB9	BSN-MR	2.26	0.72	0.01	0.00	1.74	0.01	0.00	0.00	0.00	0.28	0.00	5.02
JJB9	BSN-MR	2.25	0.73	0.01	0.00	1.75	0.01	0.00	0.00	0.00	0.26	0.00	5.00
JJB9	PXT-MR	2.32	0.67	0.01	0.00	1.67	0.01	0.00	0.00	0.00	0.33	0.00	5.01
JJB14	BSN-MR	2.32	0.67	0.01	0.00	1.68	0.01	0.00	0.00	0.00	0.32	0.00	5.01
JJB14	BSN-MR	2.34	0.71	0.01	0.00	1.74	0.00	0.00	0.00	0.00	0.00	0.00	4.80
JJB14	BSN-MR	2.24	0.69	0.01	0.00	1.78	0.16	0.00	0.00	0.00	0.00	0.00	4.88
JJB10	PXT-MR-CHR	2.29	0.75	0.01	0.00	1.77	0.01	0.00	0.00	0.00	0.00	0.00	4.83
JJB10	PXT-MR-CHR	2.19	0.85	0.00	0.00	1.85	0.01	0.00	0.00	0.00	0.00	0.00	4.89
JJB10	PXT-MR-CHR	2.21	0.81	0.00	0.00	1.84	0.00	0.00	0.00	0.00	0.00	0.00	4.87
JJB10	PXT-MR-CHR	2.29	0.74	0.01	0.00	1.78	0.01	0.00	0.00	0.00	0.00	0.00	4.83
JJB10	PXT-MR-CHR	2.27	0.76	0.01	0.00	1.78	0.01	0.00	0.00	0.00	0.00	0.00	4.84
JJB10	PXT-MR-CHR	2.27	0.75	0.01	0.00	1.80	0.01	0.00	0.00	0.00	0.00	0.00	4.84
TRP-Al7906	An-NOR-PXT HW	2.23	0.78	0.01	0.00	1.83	0.00	0.00	0.00	0.00	0.00	0.00	4.86
TRP-Al7906	An-NOR-PXT HW	2.25	0.78	0.00	0.00	1.81	0.01	0.00	0.00	0.00	0.00	0.00	4.85
TRP-Al7906	An-NOR-PXT HW	2.27	0.76	0.01	0.00	1.79	0.00	0.00	0.00	0.00	0.00	0.00	4.83
TRP-Al7906	An-NOR-PXT HW	2.25	0.77	0.00	0.00	1.81	0.00	0.00	0.00	0.00	0.00	0.00	4.84
TRP-Al7906	An-NOR-PXT HW	2.26	0.77	0.01	0.00	1.80	0.01	0.00	0.00	0.00	0.00	0.00	4.84
TRP-Al7906	An-NOR-PXT HW	2.25	0.77	0.01	0.00	1.81	0.01	0.00	0.00	0.00	0.00	0.00	4.85
TRP-Al7907B	PXT-MR	2.60	0.48	0.00	0.00	1.55	0.01	0.00	0.00	0.00	0.00	0.00	4.63
TRP-Al7907B	PXT-MR	2.51	0.46	0.00	0.00	1.49	0.01	0.00	0.00	0.00	0.55	0.00	5.02
TRP-AL7908	PXT-MR	2.47	0.50	0.00	0.00	1.53	0.01	0.00	0.00	0.00	0.53	0.00	5.04

Sample	Lithology	Si	Ca	K	Mg	Al	Fe	Mn	Ti	Ni	Na	Cr	Total
EST013-11	MsN-HW	2.21	0.77	0.01	0.00	1.78	0.01	0.00	0.00	0.00	0.24	0.00	5.02
EST013-11	MsN-HW	2.20	0.79	0.01	0.00	1.79	0.01	0.00	0.00	0.00	0.23	0.00	5.03
EST013-11	MsN-HW	2.23	0.75	0.01	0.00	1.77	0.01	0.00	0.00	0.00	0.24	0.00	5.01
EST013-11	MsN-HW	2.19	0.79	0.01	0.00	1.81	0.00	0.00	0.00	0.00	0.21	0.00	5.01
EST013-11	MsN-HW	2.18	0.81	0.01	0.00	1.81	0.01	0.00	0.00	0.00	0.21	0.00	5.02
EST013-11	MsN-HW	2.20	0.77	0.01	0.00	1.80	0.01	0.00	0.00	0.00	0.23	0.00	5.02
EST013-11	MsN-HW	2.23	0.76	0.01	0.00	1.77	0.00	0.00	0.00	0.00	0.25	0.00	5.01
EST013-11	MsN-HW	2.22	0.76	0.01	0.00	1.78	0.01	0.00	0.00	0.00	0.23	0.00	5.01
EST013-11	MsN-HW	2.21	0.77	0.01	0.00	1.79	0.01	0.00	0.00	0.00	0.21	0.00	5.00
EST013-11	MsN-HW	2.22	0.76	0.01	0.00	1.78	0.01	0.00	0.00	0.00	0.24	0.00	5.02
EST013-10	MsN-HW	2.22	0.77	0.01	0.00	1.77	0.01	0.00	0.00	0.00	0.25	0.00	5.02
EST013-10	MsN-HW	2.21	0.77	0.01	0.00	1.79	0.00	0.00	0.00	0.00	0.23	0.00	5.02
EST013-10	MsN-HW	2.24	0.74	0.01	0.00	1.75	0.01	0.00	0.00	0.00	0.26	0.00	5.01
EST013-10	MsN-HW	2.21	0.75	0.01	0.00	1.79	0.01	0.00	0.00	0.00	0.24	0.00	5.02
EST013-10	MsN-HW	2.22	0.76	0.01	0.00	1.79	0.00	0.00	0.00	0.00	0.23	0.00	5.01
EST013-10	MsN-HW	2.19	0.80	0.00	0.00	1.80	0.01	0.00	0.00	0.00	0.20	0.00	5.01
EST013-10	MsN-HW	2.21	0.77	0.01	0.00	1.79	0.01	0.00	0.00	0.00	0.24	0.00	5.02
EST013-10	MsN-HW	2.20	0.77	0.01	0.00	1.80	0.01	0.00	0.00	0.00	0.24	0.00	5.02
EST013-10	MsN-HW	2.21	0.76	0.01	0.00	1.79	0.01	0.00	0.00	0.00	0.25	0.00	5.02
EST013-10	MsN-HW	2.20	0.78	0.01	0.00	1.80	0.01	0.00	0.00	0.00	0.23	0.00	5.02

A3-6.1 Plagioclase Compositions (SEM)

Sample	Lithology	Na_2O	Al_2O_3	SiO2	CaO	SrO	FeO	K_2O	Total	Analytical Facility
JJB11	PXT-MR	4.54	29.83	50.87	13.67	0.94	0.00	0.14	99.99	SEMEdx-UFS
JJB11	PXT-MR	4.48	30.21	50.52	14.8	0.00	0.00	0.00	100.01	SEMEdx-UFS
JJB11	PXT-MR	3.78	31.76	48.06	15.58	0.83	0.00	0.00	100.01	SEMEdx-UFS
JJB11	PXT-MR	4.49	29.81	50.24	14.44	1.03	0.00	0.00	100.01	SEMEdx-UFS
JJB11	PXT-MR	5.03	28.95	51.42	13.32	1.01	0.00	0.27	100.00	SEMEdx-UFS
JJB11	PXT-MR	5.98	28.25	53.58	11.33	0.00	0.71	0.16	100.01	SEMEdx-UFS
JJB11	PXT-MR	5.05	29.06	52.13	13.47	0.00	0.00	0.29	100.00	SEMEdx-UFS
JJB15	PXT-MR	3.72	31.29	48.56	16.43	0.00	0.00	0.00	100.00	SEMEdx-UFS
JJB15	PXT-MR	3.86	30.94	49.43	14.99	0.64	0.00	0.14	100.00	SEMEdx-UFS
JJB15	PXT-MR	3.55	31.27	48.65	15.68	0.85	0.00	0.00	100.00	SEMEdx-UFS
JJB15	PXT-MR	3.56	31.59	48.50	15.94	0.41	0.00	0.00	100.00	SEMEdx-UFS
JJB17	PXT-HW	4.10	30.64	49.60	14.86	0.80	0.00	0.00	100.00	SEMEdx-UFS
JJB17	PXT-HW	3.00	32.23	47.10	16.58	1.09	0.00	0.00	100.00	SEMEdx-UFS
JJB17	PXT-HW	4.02	30.38	49.44	15.23	0.94	0.00	0.00	100.01	SEMEdx-UFS
JJB17	PXT-HW	3.23	31.48	48.02	16.23	1.05	0.00	0.00	100.01	SEMEdx-UFS
JJB17	PXT-HW	5.35	28.94	51.89	13.16	0.66	0.00	0.00	100.00	SEMEdx-UFS
JJB17	PXT-HW	5.28	29.01	52.17	12.71	0.83	0.00	0.00	100.00	SEMEdx-UFS
JJB17	PXT-HW	3.71	30.99	49.09	15.34	0.87	0.00	0.00	100.00	SEMEdx-UFS
JJB17	PXT-HW	2.72	32.23	47.81	16.98	0.26	0.00	0.00	100.00	SEMEdx-UFS
JJB17	PXT-HW	4.41	30.72	49.96	14.19	0.73	0.00	0.00	100.01	SEMEdx-UFS

Sample	Lithology	SiO_2	CaO	K_2O	MgO	Al_2O_3	FeO	MnO	TiO_2	Na_2O	$Cr2O_3$	Total	Analytical Facility
EST013_14	MLN-MR	55.99	10.68	0.23	0.20	29.19	0.10	0.04	0.10	5.47	0.00	102.00	SEMEdxWdx-Graz
EST013_14	MLN-MR	55.19	10.87	0.08	0.03	29.15	0.33	0.00	0.05	5.55	0.01	101.29	SEMEdxWdx-Graz
EST013_14	MLN-MR	46.98	17.22	0.01	0.05	34.56	0.21	0.00	0.00	1.56	0.01	100.61	SEMEdxWdx-Graz
EST013_14	MLN-MR	52.39	13.47	0.02	0.17	31.14	0.18	0.00	0.00	3.92	0.00	101.30	SEMEdxWdx-Graz
EST013_14	MLN-MR	48.54	15.73	0.00	0.15	33.18	0.22	0.00	0.00	2.49	0.00	100.31	SEMEdxWdx-Graz
EST013_14	MLN-MR	49.63	15.06	0.00	0.00	32.10	0.22	0.05	0.03	2.90	0.03	100.02	SEMEdxWdx-Graz
EST013_14	MLN-MR	52.99	12.80	0.20	0.07	30.57	0.14	0.00	0.03	4.17	0.00	100.97	SEMEdxWdx-Graz
EST013_14	MLN-MR	52.76	12.84	0.25	0.00	30.61	0.17	0.00	0.07	4.08	0.01	100.79	SEMEdxWdx-Graz
EST013_16	MLN-MR	53.82	12.13	0.16	0.18	29.63	0.19	0.00	0.07	4.61	0.00	100.79	SEMEdxWdx-Graz
EST013_16	MLN-MR	51.96	13.67	0.14	0.03	31.16	0.15	0.06	0.07	3.71	0.03	100.99	SEMEdxWdx-Graz
EST013_16	MLN-MR	53.59	12.47	0.16	0.00	30.32	0.14	0.00	0.00	4.31	0.04	101.04	SEMEdxWdx-Graz
EST013_16	MLN-MR	49.44	15.28	0.01	0.00	32.86	0.33	0.00	0.05	2.68	0.03	100.68	SEMEdxWdx-Graz
EST013_16	MLN-MR	53.12	12.91	0.25	0.00	30.53	0.21	0.00	0.00	4.02	0.07	101.12	SEMEdxWdx-Graz
EST013_16	MLN-MR	53.53	12.63	0.19	0.00	30.46	0.18	0.04	0.05	4.03	0.00	101.11	SEMEdxWdx-Graz
EST013_22	MLN-MR	60.93	6.65	0.16	0.00	25.09	0.08	0.03	0.10	8.02	0.00	101.05	SEMEdxWdx-Graz
EST013_22	MLN-MR	55.37	10.52	0.23	0.00	28.47	0.17	0.00	0.08	5.57	0.00	100.41	SEMEdxWdx-Graz
EST013_22	MLN-MR	55.26	10.31	0.11	0.12	28.44	0.21	0.00	0.08	5.99	0.01	100.52	SEMEdxWdx-Graz
EST013_22	MLN-MR	55.94	10.37	0.23	0.00	28.61	0.09	0.01	0.00	5.86	0.00	101.11	SEMEdxWdx-Graz
EST013_22	MLN-MR	54.79	10.33	0.14	0.00	28.17	0.17	0.00	0.00	5.58	0.01	99.19	SEMEdxWdx-Graz
EST013_23	MLN-MR	54.12	11.68	0.24	0.13	29.64	0.12	0.00	0.00	4.45	0.00	100.39	SEMEdxWdx-Graz
EST013_23	MLN-MR	52.97	12.30	0.22	0.00	29.89	0.06	0.00	0.02	4.45	0.00	99.90	SEMEdxWdx-Graz
EST013_23	MLN-MR	50.10	14.45	0.10	0.03	31.80	0.28	0.04	0.02	3.01	0.03	99.86	SEMEdxWdx-Graz
EST013_23	MLN-MR	44.60	18.48	0.00	0.13	34.94	0.22	0.00	0.02	0.62	0.06	99.07	SEMEdxWdx-Graz
EST013_23	MLN-MR	44.30	18.61	0.01	0.10	35.37	0.21	0.00	0.00	0.57	0.00	99.17	SEMEdxWdx-Graz
EST013_23	MLN-MR	44.56	18.36	0.04	0.00	34.78	0.32	0.00	0.07	0.67	0.06	98.86	SEMEdxWdx-Graz
EST013_23	MLN-MR	52.73	12.41	0.20	0.00	30.29	0.23	0.00	0.00	4.27	0.00	100.14	SEMEdxWdx-Graz
EST013_23	MLN-MR	51.98	12.73	0.20	0.00	30.31	0.13	0.00	0.10	4.06	0.07	99.59	SEMEdxWdx-Graz

Sample	Lithology	SiO_2	CaO	K_2O	MgO	Al_2O_3	FeO	MnO	TiO_2	Na_2O	$Cr2O_3$	Total	Analysis Facility
TRP-PPXT	PPXT-MR	51.41	13.15	0.11	0.00	31.01	0.17	0.05	0.00	3.72	0.00	99.61	SEMEdxWdx-Graz
TRP-PPXT	PPXT-MR	51.49	13.17	0.25	0.28	30.80	0.27	0.05	0.00	3.65	0.00	99.97	SEMEdxWdx-Graz
TRP-PPXT	PPXT-MR	52.37	12.62	0.25	0.00	30.10	0.32	0.00	0.02	3.83	0.00	99.51	SEMEdxWdx-Graz
TRP-PPXT	PPXT-MR	50.06	14.03	0.18	0.02	31.91	0.55	0.06	0.02	3.06	0.00	99.90	SEMEdxWdx-Graz
TRP-PPXT	PPXT-MR	50.64	13.92	0.20	0.03	31.06	0.27	0.00	0.00	3.29	0.01	99.43	SEMEdxWdx-Graz
TRP-PPXT	PPXT-MR	51.36	13.59	0.23	0.00	30.85	0.26	0.04	0.13	3.52	0.00	99.98	SEMEdxWdx-Graz
TRP006	PXT-MR	53.87	11.89	0.22	0.18	29.91	0.13	0.06	0.02	4.70	0.01	101.00	SEMEdxWdx-Graz
TRP006	PXT-MR	57.65	8.94	0.39	0.00	27.19	0.09	0.00	0.00	6.58	0.00	100.84	SEMEdxWdx-Graz
TRP006	PXT-MR	54.02	11.64	0.19	0.25	30.29	0.26	0.00	0.02	4.68	0.07	101.41	SEMEdxWdx-Graz
TRP006	PXT-MR	54.19	11.54	0.24	0.08	29.59	0.18	0.01	0.08	4.70	0.00	100.62	SEMEdxWdx-Graz
JJB13	BSN-MR	49.12	15.20	0.00	0.00	29.81	0.19	0.00	0.00	2.62	0.04	96.98	SEMEdxWdx-Graz
JJB13	BSN-MR	51.07	13.71	0.08	0.15	28.68	0.06	0.00	0.00	3.38	0.03	97.17	SEMEdxWdx-Graz
JJB13	BSN-MR	52.58	13.04	0.10	0.00	29.06	0.14	0.00	0.00	4.29	0.00	99.21	SEMEdxWdx-Graz
JJB13	BSN-MR	52.05	13.75	0.06	0.00	30.17	0.28	0.00	0.00	3.86	0.00	100.18	SEMEdxWdx-Graz
JJB13	BSN-MR	52.58	12.97	0.06	0.00	29.19	0.18	0.00	0.00	4.26	0.00	99.25	SEMEdxWdx-Graz
JJB13	BSN-MR	49.18	16.02	-0.01	0.00	32.04	0.10	0.00	0.00	2.37	0.00	99.71	SEMEdxWdx-Graz
JJB13	BSN-MR	53.76	12.45	0.06	0.00	28.81	0.22	0.00	0.00	4.68	0.00	99.98	SEMEdxWdx-Graz
JJB13	BSN-MR	53.72	12.65	0.06	0.00	29.27	0.21	0.00	0.00	4.57	0.00	100.47	SEMEdxWdx-Graz
JJB13	BSN-MR	50.49	14.43	0.02	0.00	29.97	0.27	0.00	0.00	3.38	0.00	98.56	SEMEdxWdx-Graz
JJB13	BSN-MR	55.04	11.63	0.13	0.00	28.27	0.18	0.00	0.00	4.99	0.00	100.24	SEMEdxWdx-Graz
JJB13	BSN-MR	58.04	9.68	0.14	0.00	26.75	0.13	0.00	0.00	6.55	0.00	101.30	SEMEdxWdx-Graz
JJB13	BSN-MR	56.03	10.70	0.06	0.00	27.09	0.08	0.00	0.00	5.61	0.00	99.57	SEMEdxWdx-Graz
JJB13	BSN-MR	57.70	9.65	0.10	0.00	26.81	0.19	0.00	0.00	6.24	0.00	100.69	SEMEdxWdx-Graz
JJB13	BSN-MR	52.50	13.71	0.07	0.08	29.80	0.10	0.05	0.12	3.94	0.00	100.37	SEMEdxWdx-Graz
JJB13	BSN-MR	53.55	12.51	0.04	0.00	28.51	0.24	0.08	0.00	4.76	0.00	99.68	SEMEdxWdx-Graz
JJB14	BSN-MR	50.36	13.77	0.00	0.00	32.42	0.14	0.05	0.00	3.57	0.00	100.31	SEMEdxWdx-Graz
JJB14	BSN-MR	49.95	13.77	0.00	0.00	32.38	0.37	0.04	0.00	3.44	0.00	99.95	SEMEdxWdx-Graz
JJB14	BSN-MR	50.57	13.46	0.00	0.00	32.25	0.05	0.00	0.00	3.59	0.00	99.92	SEMEdxWdx-Graz
JJB14	BSN-MR	49.20	14.59	0.00	0.00	33.86	0.12	0.00	0.00	2.97	0.00	100.74	SEMEdxWdx-Graz
JJB14	BSN-MR	49.48	14.05	0.00	0.00	33.06	0.17	0.09	0.00	3.26	0.00	100.11	SEMEdxWdx-Graz
JJB14	BSN-MR	48.56	14.85	0.00	0.00	33.61	0.28	0.01	0.00	2.84	0.00	100.16	SEMEdxWdx-Graz
JJB14	BSN-MR	50.79	13.56	0.00	0.00	32.57	0.14	0.05	0.00	3.56	0.00	100.67	SEMEdxWdx-Graz
JJB14	BSN-MR	50.10	13.66	0.00	0.00	32.59	0.17	0.00	0.00	3.59	0.00	100.10	SEMEdxWdx-Graz
JJB14	BSN-MR	50.94	13.26	0.00	0.00	31.84	0.35	0.00	0.00	3.86	0.00	100.24	SEMEdxWdx-Graz
JJB14	BSN-MR	49.08	14.45	0.00	0.00	33.01	0.15	0.01	0.00	3.19	0.00	99.90	SEMEdxWdx-Graz
JJB14	BSN-MR	50.23	13.19	0.00	0.00	31.53	0.19	0.03	0.00	3.81	0.00	98.99	SEMEdxWdx-Graz
JJB14	BSN-MR	50.06	13.68	0.00	0.00	32.61	0.33	0.05	0.00	3.48	0.00	100.22	SEMEdxWdx-Graz
JJB14	BSN-MR	50.34	13.71	0.00	0.00	33.22	0.26	0.01	0.00	3.56	0.00	101.09	SEMEdxWdx-Graz
JJB14	BSN-MR	48.18	14.82	0.00	0.00	32.82	0.45	0.00	0.00	3.24	0.00	99.50	SEMEdxWdx-Graz
JJB14	BSN-MR	50.29	13.59	0.00	0.00	31.97	0.15	0.05	0.00	3.68	0.00	99.74	SEMEdxWdx-Graz
JJB14	BSN-MR	50.42	13.35	0.00	0.00	31.95	0.32	0.00	0.00	3.81	0.00	99.86	SEMEdxWdx-Graz
JJB14	BSN-MR	47.68	15.31	0.00	0.00	33.46	0.39	0.01	0.00	2.62	0.00	99.47	SEMEdxWdx-Graz
JJB14	BSN-MR	48.99	14.90	0.00	0.00	33.42	0.31	0.00	0.00	2.97	0.00	100.59	SEMEdxWdx-Graz
JJB14	BSN-MR	50.29	13.50	0.00	0.00	31.89	0.09	0.00	0.00	3.94	0.00	99.72	SEMEdxWdx-Graz
JJB14	BSN-MR	50.68	13.52	0.00	0.00	32.59	0.32	0.00	0.00	3.71	0.00	100.82	SEMEdxWdx-Graz
JJB18	BSN-HW	52.54	13.12	0.19	0.00	28.91	0.22	0.08	0.00	4.06	0.00	99.12	SEMEdxWdx-Graz
JJB18	BSN-HW	52.39	12.52	0.20	0.00	28.06	0.21	0.03	0.07	4.39	0.00	97.87	SEMEdxWdx-Graz
JJB18	BSN-HW	53.70	12.62	0.19	0.18	28.89	0.21	0.04	0.08	4.34	0.00	100.25	SEMEdxWdx-Graz
JJB18	BSN-HW	54.57	14.52	0.00	0.00	29.83	0.26	0.00	0.00	3.21	0.03	102.43	SEMEdxWdx-Graz
JJB18	BSN-HW	51.41	13.82	0.17	0.00	29.97	0.57	0.00	0.02	3.55	0.09	99.58	SEMEdxWdx-Graz
JJB18	BSN-HW	51.58	13.84	0.20	0.00	29.44	0.10	0.00	0.07	3.60	0.03	98.86	SEMEdxWdx-Graz
JJB18	BSN-HW	53.33	12.91	0.24	0.03	29.19	0.48	0.00	0.05	4.17	0.06	100.46	SEMEdxWdx-Graz
JJB18	BSN-HW	54.19	12.65	0.19	0.00	28.96	0.28	0.03	0.02	4.38	0.00	100.70	SEMEdxWdx-Graz
JJB18	BSN-HW	53.20	12.59	0.18	0.00	29.25	0.24	0.00	0.05	4.29	0.06	99.87	SEMEdxWdx-Graz
JJB18	BSN-HW	53.97	12.16	0.20	0.00	28.64	0.19	0.00	0.02	4.62	0.00	99.81	SEMEdxWdx-Graz

A3-6.2 Cations per 8 oxygens

Sample	Lithology	Si	Ca	K	Mg	Al	Fe	Mn	Ti	Ni	Na	Cr	Total
JJB11	PXT-MR	2.34	0.67	0.01	0.00	1.62	0.00	0.00	0.00	0.00	0.41	0.00	5.05
JJB11	PXT-MR	2.31	0.73	0.00	0.00	1.63	0.00	0.00	0.00	0.00	0.40	0.00	5.07
JJB11	PXT-MR	2.23	0.77	0.00	0.00	1.74	0.00	0.00	0.00	0.00	0.34	0.00	5.08
JJB11	PXT-MR	2.32	0.72	0.00	0.00	1.62	0.00	0.00	0.00	0.00	0.40	0.00	5.07
JJB11	PXT-MR	2.37	0.66	0.02	0.00	1.58	0.00	0.00	0.00	0.00	0.45	0.00	5.07
JJB11	PXT-MR	2.44	0.55	0.01	0.00	1.52	0.03	0.00	0.00	0.00	0.53	0.00	5.07
JJB11	PXT-MR	2.38	0.66	0.02	0.00	1.56	0.00	0.00	0.00	0.00	0.45	0.00	5.07
JJB15	PXT-MR	2.24	0.81	0.00	0.00	1.70	0.00	0.00	0.00	0.00	0.33	0.00	5.08
JJB15	PXT-MR	2.28	0.74	0.01	0.00	1.68	0.00	0.00	0.00	0.00	0.35	0.00	5.06
JJB15	PXT-MR	2.25	0.78	0.00	0.00	1.71	0.00	0.00	0.00	0.00	0.32	0.00	5.05
JJB15	PXT-MR	2.24	0.79	0.00	0.00	1.72	0.00	0.00	0.00	0.00	0.32	0.00	5.06
JJB17	PXT-HW	2.29	0.74	0.00	0.00	1.67	0.00	0.00	0.00	0.00	0.37	0.00	5.06
JJB17	PXT-HW	2.19	0.83	0.00	0.00	1.77	0.00	0.00	0.00	0.00	0.27	0.00	5.06
JJB17	PXT-HW	2.29	0.76	0.00	0.00	1.66	0.00	0.00	0.00	0.00	0.36	0.00	5.06
JJB17	PXT-HW	2.23	0.81	0.00	0.00	1.72	0.00	0.00	0.00	0.00	0.29	0.00	5.05
JJB17	PXT-HW	2.38	0.65	0.00	0.00	1.57	0.00	0.00	0.00	0.00	0.48	0.00	5.07
JJB17	PXT-HW	2.39	0.62	0.00	0.00	1.57	0.00	0.00	0.00	0.00	0.47	0.00	5.06
JJB17	PXT-HW	2.27	0.76	0.00	0.00	1.69	0.00	0.00	0.00	0.00	0.33	0.00	5.05
JJB17	PXT-HW	2.21	0.84	0.00	0.00	1.75	0.00	0.00	0.00	0.00	0.24	0.00	5.04
JJB17	PXT-HW	2.30	0.70	0.00	0.00	1.67	0.00	0.00	0.00	0.00	0.39	0.00	5.06

Sample	Lithology	Si	Ca	K	Mg	Al	Fe	Mn	Ti	Ni	Na	Cr	Total
EST013_14	MLN-MR	2.47	0.51	0.01	0.01	1.52	0.00	0.00	0.00	0.00	0.47	0.00	5.00
EST013_14	MLN-MR	2.46	0.52	0.00	0.00	1.53	0.01	0.00	0.00	0.00	0.48	0.00	5.01
EST013_14	MLN-MR	2.14	0.84	0.00	0.00	1.86	0.01	0.00	0.00	0.00	0.14	0.00	5.00
EST013_14	MLN-MR	2.35	0.65	0.00	0.01	1.65	0.01	0.00	0.00	0.00	0.34	0.00	5.00
EST013_14	MLN-MR	2.21	0.77	0.00	0.01	1.78	0.01	0.00	0.00	0.00	0.22	0.00	5.00
EST013_14	MLN-MR	2.27	0.74	0.00	0.00	1.73	0.01	0.00	0.00	0.00	0.26	0.00	5.00
EST013_14	MLN-MR	2.38	0.62	0.01	0.00	1.62	0.01	0.00	0.00	0.00	0.36	0.00	5.00
EST013_14	MLN-MR	2.37	0.62	0.01	0.00	1.62	0.01	0.00	0.00	0.00	0.36	0.00	5.00
EST013_16	MLN-MR	2.42	0.58	0.01	0.01	1.57	0.01	0.00	0.00	0.00	0.40	0.00	5.00
EST013_16	MLN-MR	2.34	0.66	0.01	0.00	1.65	0.01	0.00	0.00	0.00	0.32	0.00	5.00
EST013_16	MLN-MR	2.40	0.60	0.01	0.00	1.60	0.01	0.00	0.00	0.00	0.37	0.00	4.99
EST013_16	MLN-MR	2.24	0.74	0.00	0.00	1.76	0.01	0.00	0.00	0.00	0.24	0.00	4.99
EST013_16	MLN-MR	2.38	0.62	0.01	0.00	1.61	0.01	0.00	0.00	0.00	0.35	0.00	4.99
EST013_16	MLN-MR	2.40	0.61	0.01	0.00	1.61	0.01	0.00	0.00	0.00	0.35	0.00	4.98
EST013_22	MLN-MR	2.69	0.31	0.01	0.00	1.30	0.00	0.00	0.00	0.00	0.69	0.00	5.01
EST013_22	MLN-MR	2.49	0.51	0.01	0.00	1.51	0.01	0.00	0.00	0.00	0.48	0.00	5.01
EST013_22	MLN-MR	2.48	0.50	0.01	0.01	1.51	0.01	0.00	0.00	0.00	0.52	0.00	5.03
EST013_22	MLN-MR	2.49	0.50	0.01	0.00	1.50	0.00	0.00	0.00	0.00	0.51	0.00	5.01
EST013_22	MLN-MR	2.49	0.50	0.01	0.00	1.51	0.01	0.00	0.00	0.00	0.49	0.00	5.01
EST013_23	MLN-MR	2.43	0.56	0.01	0.01	1.57	0.00	0.00	0.00	0.00	0.39	0.00	4.98
EST013_23	MLN-MR	2.40	0.60	0.01	0.00	1.60	0.00	0.00	0.00	0.00	0.39	0.00	5.00
EST013_23	MLN-MR	2.29	0.71	0.01	0.00	1.71	0.01	0.00	0.00	0.00	0.27	0.00	4.99
EST013_23	MLN-MR	2.08	0.92	0.00	0.01	1.92	0.01	0.00	0.00	0.00	0.06	0.00	4.99
EST013_23	MLN-MR	2.06	0.93	0.00	0.01	1.94	0.01	0.00	0.00	0.00	0.05	0.00	5.00
EST013_23	MLN-MR	2.08	0.92	0.00	0.00	1.91	0.01	0.00	0.00	0.00	0.06	0.00	4.99
EST013_23	MLN-MR	2.39	0.60	0.01	0.00	1.62	0.01	0.00	0.00	0.00	0.37	0.00	5.00
EST013_23	MLN-MR	2.37	0.62	0.01	0.00	1.63	0.00	0.00	0.00	0.00	0.36	0.00	5.00

Sample	Lithology	Si	Ca	K	Mg	Al	Fe	Mn	Ti	Na	Cr	Total
TRP-PPXT	PPXT-MR	2.34	0.64	0.01	0.00	1.67	0.01	0.00	0.00	0.33	0.00	4.99
TRP-PPXT	PPXT-MR	2.34	0.64	0.01	0.02	1.65	0.01	0.00	0.00	0.32	0.00	5.00
TRP-PPXT	PPXT-MR	2.39	0.62	0.01	0.00	1.62	0.01	0.00	0.00	0.34	0.00	4.98
TRP-PPXT	PPXT-MR	2.29	0.69	0.01	0.00	1.72	0.02	0.00	0.00	0.27	0.00	5.00
TRP-PPXT	PPXT-MR	2.32	0.68	0.01	0.00	1.68	0.01	0.00	0.00	0.29	0.00	4.99
TRP-PPXT	PPXT-MR	2.34	0.66	0.01	0.00	1.65	0.01	0.00	0.00	0.31	0.00	4.99
TRP006	PXT-MR	2.41	0.57	0.01	0.01	1.58	0.00	0.00	0.00	0.41	0.00	5.01
TRP006	PXT-MR	2.57	0.43	0.02	0.00	1.43	0.00	0.00	0.00	0.57	0.00	5.01
TRP006	PXT-MR	2.41	0.56	0.01	0.02	1.59	0.01	0.00	0.00	0.40	0.00	5.00
TRP006	PXT-MR	2.43	0.56	0.01	0.01	1.57	0.01	0.00	0.00	0.41	0.00	4.99
JJB13	BSN-MR	2.31	0.77	0.00	0.00	1.65	0.01	0.00	0.00	0.24	0.00	4.98
JJB13	BSN-MR	2.39	0.69	0.00	0.01	1.58	0.00	0.00	0.00	0.31	0.00	4.98
JJB13	BSN-MR	2.41	0.64	0.01	0.00	1.57	0.01	0.00	0.00	0.38	0.00	5.00
JJB13	BSN-MR	2.36	0.67	0.00	0.00	1.61	0.01	0.00	0.00	0.34	0.00	5.00
JJB13	BSN-MR	2.40	0.64	0.00	0.00	1.57	0.01	0.00	0.00	0.38	0.00	5.00
JJB13	BSN-MR	2.25	0.79	0.00	0.00	1.73	0.00	0.00	0.00	0.21	0.00	4.99
JJB13	BSN-MR	2.44	0.60	0.00	0.00	1.54	0.01	0.00	0.00	0.41	0.00	5.00
JJB13	BSN-MR	2.42	0.61	0.00	0.00	1.56	0.01	0.00	0.00	0.40	0.00	5.00
JJB13	BSN-MR	2.34	0.72	0.00	0.00	1.63	0.01	0.00	0.00	0.30	0.00	5.00
JJB13	BSN-MR	2.48	0.56	0.01	0.00	1.50	0.01	0.00	0.00	0.44	0.00	4.99
JJB13	BSN-MR	2.58	0.46	0.01	0.00	1.40	0.00	0.00	0.00	0.56	0.00	5.01
JJB13	BSN-MR	2.53	0.52	0.00	0.00	1.44	0.00	0.00	0.00	0.49	0.00	4.99
JJB13	BSN-MR	2.57	0.46	0.01	0.00	1.41	0.01	0.00	0.00	0.54	0.00	5.00
JJB13	BSN-MR	2.38	0.67	0.00	0.01	1.59	0.00	0.00	0.00	0.35	0.00	5.00
JJB13	BSN-MR	2.44	0.61	0.00	0.00	1.53	0.01	0.00	0.00	0.42	0.00	5.01
JJB14	BSN-MR	2.28	0.67	0.00	0.00	1.73	0.01	0.00	0.00	0.31	0.00	5.01
JJB14	BSN-MR	2.28	0.67	0.00	0.00	1.74	0.01	0.00	0.00	0.30	0.00	5.01
JJB14	BSN-MR	2.30	0.66	0.00	0.00	1.73	0.00	0.00	0.00	0.32	0.00	5.00
JJB14	BSN-MR	2.26	0.72	0.00	0.00	1.84	0.00	0.00	0.00	0.00	0.00	4.82
JJB14	BSN-MR	2.29	0.70	0.00	0.00	1.81	0.01	0.00	0.00	0.00	0.00	4.81
JJB14	BSN-MR	2.25	0.74	0.00	0.00	1.84	0.01	0.00	0.00	0.00	0.00	4.83
JJB14	BSN-MR	2.34	0.67	0.00	0.00	1.77	0.01	0.00	0.00	0.00	0.00	4.78
JJB14	BSN-MR	2.32	0.68	0.00	0.00	1.78	0.01	0.00	0.00	0.00	0.00	4.79
JJB14	BSN-MR	2.36	0.66	0.00	0.00	1.74	0.01	0.00	0.00	0.00	0.00	4.77
JJB14	BSN-MR	2.28	0.72	0.00	0.00	1.81	0.01	0.00	0.00	0.00	0.00	4.81
JJB14	BSN-MR	2.36	0.66	0.00	0.00	1.74	0.01	0.00	0.00	0.00	0.00	4.77
JJB14	BSN-MR	2.32	0.68	0.00	0.00	1.78	0.01	0.00	0.00	0.00	0.00	4.79
JJB14	BSN-MR	2.31	0.67	0.00	0.00	1.80	0.01	0.00	0.00	0.00	0.00	4.79
JJB14	BSN-MR	2.26	0.74	0.00	0.00	1.81	0.02	0.00	0.00	0.00	0.00	4.83
JJB14	BSN-MR	2.34	0.68	0.00	0.00	1.75	0.01	0.00	0.00	0.00	0.00	4.78
JJB14	BSN-MR	2.35	0.67	0.00	0.00	1.75	0.01	0.00	0.00	0.00	0.00	4.78
JJB14	BSN-MR	2.23	0.77	0.00	0.00	1.84	0.02	0.00	0.00	0.00	0.00	4.85
JJB14	BSN-MR	2.26	0.74	0.00	0.00	1.82	0.01	0.00	0.00	0.00	0.00	4.83
JJB14	BSN-MR	2.29	0.66	0.00	0.00	1.72	0.00	0.00	0.00	0.35	0.00	5.02
JJB14	BSN-MR	2.29	0.65	0.00	0.00	1.73	0.01	0.00	0.00	0.32	0.00	5.01
JJB18	BSN-HW	2.41	0.64	0.01	0.00	1.56	0.01	0.00	0.00	0.36	0.00	5.00
JJB18	BSN-HW	2.43	0.62	0.01	0.00	1.53	0.01	0.00	0.00	0.39	0.00	5.00
JJB18	BSN-HW	2.43	0.61	0.01	0.01	1.54	0.01	0.00	0.00	0.38	0.00	5.00
JJB18	BSN-HW	2.41	0.69	0.00	0.00	1.56	0.01	0.00	0.00	0.28	0.00	4.94
JJB18	BSN-HW	2.35	0.68	0.01	0.00	1.62	0.02	0.00	0.00	0.32	0.00	5.00
JJB18	BSN-HW	2.37	0.68	0.01	0.00	1.60	0.00	0.00	0.00	0.32	0.00	4.99
JJB18	BSN-HW	2.41	0.63	0.01	0.00	1.56	0.02	0.00	0.00	0.37	0.00	5.00
JJB18	BSN-HW	2.44	0.61	0.01	0.00	1.54	0.01	0.00	0.00	0.38	0.00	4.99
JJB18	BSN-HW	2.41	0.61	0.01	0.00	1.57	0.01	0.00	0.00	0.38	0.00	4.99
JJB18	BSN-HW	2.45	0.59	0.01	0.00	1.53	0.01	0.00	0.00	0.41	0.00	5.00

End Member Recalculation of plagioclase in hanging wall pyroxenite and mesonorite

TRP_Pxt		Ab	Or	An
(n=9)	Min	22.5	0.00	57.1
	Max	42.9	0.00	77.5
	Mean	32.33	0.00	67.67
	Std. Dev.	7.25	0.00	7.25
TRP272_Pxt		Ab	Or	An
(n=6)	Min	23.60	0.30	73.40
	Max	26.20	0.60	75.80
	Mean	24.35	0.52	75.17
	Std. Dev.	0.95	0.12	0.90
TRP_BSN		Ab	Or	An
(n=15)	Min	28.60	0.00	58.50
	Max	40.30	1.40	71.40
	Mean	35.19	1.01	63.81
	Std. Dev.	3.36	0.32	3.58
EST013_MsN		Ab	Or	An
(n=20)	Min	20.00	0.50	73.20
	Max	25.70	1.00	79.50
	Mean	23.06	0.74	76.19
	Std. Dev.	1.45	0.15	1.54

End Member recalculation of plagioclase in pyroxenite vs pegmatoidal pyroxenite

TRP_PXT		Ab	Or	An
(n=3)	Min	41.20	1.20	56.80
	Max	41.80	1.40	57.60
	Mean	41.53	1.27	57.20
	Std. Dev.	0.31	0.12	0.40
TRP_PPXT		En	Wo	Fs
(n=6)	Min	28.00	0.70	65.60
	Max	34.90	1.50	70.90
	Mean	31.77	1.23	67.05
	Std. Dev.	2.59	0.31	2.65

End Member Recalculation of plagioclase in Merensky Reef pyroxenite

TRP_Pxt		Ab	Or	An
(n=32)	Min	12.3	0.00	48.30
	Max	51.00	1.50	87.60
	Mean	31.22	0.51	68.27
	Std. Dev.	8.27	0.39	8.41
TRP272_Pxt		Ab	Or	An
(n=9)	Min	16.30	0.10	45.50
	Max	54.30	0.80	83.30
	Mean	33.03	0.50	66.47
	Std. Dev.	15.26	0.30	15.10
TRP_BSN		Ab	Or	An
(n=48)	Min	21.10	0.00	44.60
	Max	54.60	1.40	78.90
	Mean	33.94	0.40	65.66
	Std. Dev.	6.79	0.48	7.00
EST013_MLN		Ab	Or	An
(n=23)	Min	14.10	0.00	48.50
	Max	50.90	1.50	85.80
	Mean	36.96	0.87	62.18
	Std. Dev.	9.64	0.51	9.95

A3-7 Chromite Compositions (EPMA-Rhodes University)

Sample	Lithology	SiO	CaO	K_2O	MgO	Al_2O_3	FeO	MnO	TiO_2	NiO	Na_2O	Cr_2O_3	Total
JJB19	PXT-MR-CHR	0.06	0.00	0.04	7.23	15.86	31.51	0.08	0.14	0.16	0.00	41.52	96,60
JJB19	PXT-MR-CHR	0.04	0.01	0.05	7.16	16.52	31.12	0.10	0.12	0.17	0.00	40.61	95,88
JJB19	PXT-MR-CHR	0.09	0.00	0.02	7.12	15.79	33.57	0.09	0.14	0.18	0.00	40.05	97,07
JJB19	PXT-MR-CHR	0.06	0.00	0.02	7.22	15.72	33.48	0.09	1.29	0.16	0.00	40.05	98,09
JJB19	PXT-MR-CHR	0.40	0.03	0.02	5.05	12.16	32.55	0.04	1.17	0.19	0.00	38.69	90,31
JJB19	PXT-MR-CHR	0.07	0.00	0.02	7.14	15.63	33.78	0.05	1.30	0.25	0.00	39.28	97,51
JJB19	PXT-MR-CHR	0.01	0.00	0.02	3.27	9.38	42.40	0.12	2.00	0.25	0.00	38.15	95,58
JJB19	PXT-MR-CHR	0.06	0.01	0.02	3.29	9.41	42.09	0.09	2.06	0.30	0.00	38.05	95,39
JJB11	PXT-MR	0.05	0.00	0.03	2.78	7.67	42.00	0.07	1.37	0.14	0.00	44.84	98,94
JJB11	PXT-MR	0.19	0.03	0.02	0.44	8.36	41.95	0.04	1.64	0.17	0.00	42.57	95,40
JJB16	PXT-MR	0.03	0.00	0.01	0.45	8.71	41.45	0.10	0.02	0.06	0.00	45.45	96,28
JJB16	PXT-MR	0.13	0.16	0.07	0.24	5.58	48.99	0.06	0.16	0.09	0.00	38.31	93,79
JJB18	BSN-HW	2.33	1.12	0.04	4.00	6.92	37.51	0.07	1.08	0.10	0.03	43.85	97,05
JJB18	BSN-HW	0.07	0.02	0.04	2.81	10.61	33.63	0.09	0.27	0.01	0.01	49.55	97,09
JJB18	BSN-HW	0.55	0.05	0.04	3.29	10.91	32.52	0.10	0.04	0.04	0.02	49.29	96,84
JJB18	BSN-HW	0.04	0.02	0.00	2.54	7.16	39.18	0.11	0.09	0.11	0.00	46.73	95,97
JJB17	PXT-HW	0.06	0.00	0.03	2.89	8.54	41.73	0.09	1.31	0.19	0.02	40.72	95,57
JJB17	PXT-HW	0.05	0.01	0.02	3.07	8.16	39.71	0.13	1.23	0.13	0.00	44.20	96,72
JJB17	PXT-HW	0.03	0.02	0.01	3.18	7.76	41.01	0.10	1.20	0.09	0.00	43.24	96,63
JJB17	PXT-HW	0.07	0.02	0.01	0.42	5.78	44.40	0.14	0.65	0.05	0.01	42.78	94,33
JJB17	PXT-HW	0.04	0.00	0.04	3.25	9.34	40.49	0.14	0.16	0.16	0.00	42.08	95,70
JJB17	PXT-HW	0.01	0.00	0.04	4.50	11.87	35.69	0.09	0.53	0.10	0.02	45.29	98,13
JJB14	BSN-MR	0.04	0.01	0.03	3.61	9.99	34.32	0.11	0.53	0.01	0.00	49.78	98,44
JJB14	BSN-MR	0.07	0.01	0.02	3.52	10.11	36.43	0.12	0.79	0.05	0.01	48.04	99,17
JJB10	PXT-MR-CHR	0.05	0.00	0.02	7.32	14.81	33.36	0.08	1.41	0.22	0.01	41.12	98,40
JJB10	PXT-MR-CHR	0.01	0.00	0.01	7.31	14.77	34.19	0.09	1.11	0.20	0.00	41.67	99,35
JJB10	PXT-MR-CHR	0.03	0.01	0.04	7.16	13.38	33.87	0.08	1.45	0.20	0.00	42.77	98,98
JJB10	PXT-MR-CHR	0.02	0.00	0.03	5.25	10.63	36.88	0.07	0.20	0.28	0.01	42.76	96,12
TRP-AL7908	PXT-MR	0.05	0.00	0.01	0.53	8.10	33.16	0.12	0.07	0.04	0.00	54.58	96,66

A3-8 Chromite Compositions (SEM)

Sample	Lithology	SiO_2	CaO	MgO	Al_2O_3	Fe_2O_3	MnO	TiO_2	V_2O_5	Na_2O	Cr_2O_3	Total	Analytical facility
JJB12	BSN-MR	0.00	0.00	1.53	6.09	52.38	0.42	1.18	1.46	0.00	36.93	99.99	SEMEdx-UFS
JJB12	BSN-MR	0.00	0.00	1.79	5.36	50.20	0.07	1.65	0.00	0.00	40.94	100.01	SEMEdx-UFS
JJB12	BSN-MR	0.00	0.00	1.77	4.69	52.29	0.00	2.43	0.00	0.00	38.82	100.00	SEMEdx-UFS
JJB12	BSN-MR	0.00	0.00	1.27	3.73	49.62	0.00	1.34	1.39	0.00	42.64	99.99	SEMEdx-UFS
JJB12	BSN-MR	0.00	0.00	1.21	6.38	50.86	0.00	1.70	1.14	0.00	38.71	100.00	SEMEdx-UFS
JJB12	BSN-MR	0.00	0.00	1.37	6.35	49.19	0.27	1.30	2.04	0.00	39.49	100.01	SEMEdx-UFS
JJB13	BSN-MR	0.92	0.00	1.29	3.12	59.89	0.00	1.10	1.11	0.00	32.55	99.98	SEMEdx-UFS
JJB13	BSN-MR	1.26	0.00	2.02	4.69	50.92	0.00	1.05	1.33	0.00	38.73	100.00	SEMEdx-UFS
JJB13	BSN-MR	0.00	0.00	1.44	3.66	62.22	0.54	3.43	0.00	0.00	28.72	100.01	SEMEdx-UFS
JJB13	BSN-MR	0.00	0.00	1.56	3.51	62.12	0.47	3.40	0.00	0.00	28.93	99.99	SEMEdx-UFS
JJB13	BSN-MR	0.72	0.00	0.81	2.44	57.82	0.47	2.72	0.00	0.00	35.03	100.01	SEMEdx-UFS
JJB13	BSN-MR	13.58	0.00	7.68	2.76	47.60	0.00	1.93	0.00	0.00	26.45	100.00	SEMEdx-UFS
JJB13	BSN-MR	0.32	0.00	1.33	4.02	54.04	0.31	2.20	0.00	0.00	37.78	100.00	SEMEdx-UFS
JJB15	PXT-MR	0.00	0.00	3.36	8.74	40.32	0.00	1.39	0.00	0.00	46.18	99.99	SEMEdx-UFS
JJB15	PXT-MR	0.00	0.00	3.51	8.67	40.91	0.00	1.33	0.00	0.00	45.57	99.99	SEMEdx-UFS
JJB15	PXT-MR	0.00	0.00	3.16	7.70	42.07	0.01	0.98	0.65	0.00	45.43	100.00	SEMEdx-UFS
JJB15	PXT-MR	0.00	0.00	3.06	7.69	41.24	0.00	1.05	0.00	0.00	46.95	99.99	SEMEdx-UFS
JJB15	PXT-MR	0.00	0.00	3.36	7.33	40.72	0.00	1.44	0.00	0.00	47.14	99.99	SEMEdx-UFS
JJB15	PXT-MR	0.00	3.24	0.57	1.11	37.21	0.00	1.30	0.00	0.00	56.57	100.00	SEMEdx-UFS
JJB15	PXT-MR	0.00	0.00	3.09	6.98	41.00	0.00	1.21	0.71	0.00	47.01	100.00	SEMEdx-UFS
JJB15	PXT-MR	0.00	0.00	3.16	8.89	39.72	0.26	0.95	0.00	0.00	47.02	100.00	SEMEdx-UFS
JJB15	PXT-MR	0.00	0.00	1.86	6.06	40.52	0.21	1.04	0.00	0.00	50.31	100.00	SEMEdx-UFS
JJB16	PXT-MR	0.00	0.00	0.91	3.33	55.01	0.19	1.68	0.00	0.00	38.87	99.99	SEMEdx-UFS
JJB16	PXT-MR	6.13	0.00	4.02	1.88	43.44	0.50	1.42	0.00	0.00	42.61	100.00	SEMEdx-UFS
JJB16	PXT-MR	0.00	0.00	1.87	6.01	45.83	0.30	0.99	0.63	0.00	44.38	100.01	SEMEdx-UFS
JJB16	PXT-MR	0.00	0.00	2.02	6.61	46.60	0.00	1.26	0.68	0.00	42.84	100.01	SEMEdx-UFS
JJB16	PXT-MR	0.00	0.00	1.58	7.35	45.00	0.36	1.02	0.51	0.00	44.18	100.00	SEMEdx-UFS
JJB16	PXT-MR	0.00	0.00	2.64	6.96	39.52	0.29	0.63	0.00	0.00	49.97	100.01	SEMEdx-UFS
JJB16	PXT-MR	0.00	0.00	3.16	10.16	38.11		0.68	0.00	0.00	47.89	100.00	SEMEdx-UFS
JJB16	PXT-MR	0.00	0.00	3.00	9.38	39.46	0.06	0.58	0.68	0.00	46.84	100.00	SEMEdx-UFS

Sample	Lithology	SiO_2	CaO	MgO	Al_2O_3	Fe_2O_3	MnO	TiO_2	V_2O_5	Cr_2O_3	Cu_2O	Ta_2O_5	ZnO	Total	Analytical facility
EST13-14	MLN-MR	0.00	0.00	0.51	5.21	50.92	0.00	1.02	0.88	41.46	0.00	0.00	0.00	100.00	SEMEdx-UFS
EST13-14	MLN-MR	0.00	0.00	0.78	4.32	51.77	0.00	1.51	1.00	40.62	0.00	0.00	0.00	100.00	SEMEdx-UFS
EST13-14	MLN-MR	0.00	0.00	0.78	4.41	52.14	0.72	1.14	0.97	39.84	0.00	0.00	0.00	100.00	SEMEdx-UFS
EST13-14	MLN-MR	0.23	0.00	0.82	4.80	52.25	0.00	1.60	0.87	39.20	0.23	0.00	0.00	99.77	SEMEdx-UFS
EST13-14	MLN-MR	0.48	0.00	0.86	4.93	52.70	0.00	1.12	1.13	38.78	0.00	0.00	0.00	99.52	SEMEdx-UFS
EST13-14	MLN-MR	0.00	0.00	0.72	4.65	53.08	0.00	1.23	1.45	38.87	0.00	0.00	0.00	100.00	SEMEdx-UFS
EST13-14	MLN-MR	0.00	0.00	1.06	4.70	50.31	0.00	2.05	0.00	41.88	0.00	0.00	0.00	100.00	SEMEdx-UFS
EST13-14	MLN-MR	0.00	0.00	0.75	4.89	50.64	0.00	1.82	1.02	40.87	0.00	0.00	0.00	99.99	SEMEdx-UFS
EST13-14	MLN-MR	0.00	0.00	0.70	4.76	52.35	0.00	1.42	0.95	39.82	0.00	0.00	0.00	100.00	SEMEdx-UFS
EST13-14	MLN-MR	4.97	0.98	3.82	4.74	48.32	0.26	1.05	0.86	35.00	0.00	0.00	0.00	94.05	SEMEdx-UFS
EST13-16	MLN-MR	0.00	0.00	1.44	1.47	44.20	0.48	0.00	1.23	51.17	0.00	0.00	0.00	99.99	SEMEdx-UFS
EST13-16	MLN-MR	0.00	0.00	1.44	1.47	44.20	0.48	0.00	1.23	51.17	0.00	0.00	0.00	99.99	SEMEdx-UFS
EST13-16	MLN-MR	0.00	0.00	1.26	5.44	48.33	0.00	1.49	1.27	42.22	0.00	0.00	0.00	100.01	SEMEdx-UFS
EST13-16	MLN-MR	0.00	0.00	1.17	5.02	48.89	0.00	1.23	1.20	42.50	0.00	0.00	0.00	100.01	SEMEdx-UFS
EST13-16	MLN-MR	0.00	0.00	1.61	5.63	45.63	0.00	1.13	1.58	44.43	0.00	0.00	0.00	100.01	SEMEdx-UFS
EST13-16	MLN-MR	0.00	0.00	1.37	5.41	44.95	0.00	0.77	1.18	46.31	0.00	0.00	0.00	99.99	SEMEdx-UFS
EST13-16	MLN-MR	0.00	0.00	14.79	6.65	43.56	0.32	0.82	0.94	32.93	0.00	0.00	0.00	100.01	SEMEdx-UFS
EST13-16	MLN-MR	0.00	0.00	1.35	5.17	48.00	0.00	1.16	1.17	43.15	0.00	0.00	0.00	100.00	SEMEdx-UFS
EST13-16	MLN-MR	0.00	0.00	1.57	5.62	46.86	0.00	1.14	1.02	43.77	0.00	0.00	0.00	99.98	SEMEdx-UFS
EST13-18	MLN-MR	0.00	0.00	3.42	8.22	39.48	0.31	1.34	0.58	46.64	0.00	0.00	0.00	99.99	SEMEdx-UFS
EST13-18	MLN-MR	0.00	0.00	3.28	8.17	39.65	0.00	1.42	0.00	47.47	0.00	0.00	0.00	99.99	SEMEdx-UFS
EST13-18	MLN-MR	0.00	0.00	2.28	5.27	41.39	0.46	1.85	0.00	48.75	0.00	0.00	0.00	100.00	SEMEdx-UFS
EST13-18	MLN-MR	0.00	0.00	1.72	5.10	44.77	0.00	0.98	1.04	46.39	0.00	0.00	0.00	100.00	SEMEdx-UFS
EST13-18	MLN-MR	0.00	0.00	1.97	5.96	48.83	0.29	1.44	1.25	40.26	0.00	0.00	0.00	100.00	SEMEdx-UFS
EST13-18	MLN-MR	0.00	0.00	1.23	5.41	50.05	0.00	1.89	0.00	40.73	0.00	0.00	0.68	99.99	SEMEdx-UFS
EST13-20	MLN-MR	0.00	0.00	0.85	3.54	53.21	0.00	1.44	1.29	39.66	0.00	0.00	0.00	99.99	SEMEdx-UFS
EST13-20	MLN-MR	0.00	0.00	0.78	3.84	52.67	0.00	1.05	1.50	40.16	0.00	0.00	0.00	100.00	SEMEdx-UFS
EST13-20	MLN-MR	0.00	0.00	1.74	4.73	48.74	0.00	1.38	1.04	42.36	0.00	0.00	0.00	99.99	SEMEdx-UFS
EST13-20	MLN-MR	0.00	0.00	1.50	5.34	47.44	0.00	1.34	1.06	42.81	0.00	0.51	0.00	100.00	SEMEdx-UFS
EST13-20	MLN-MR	0.00	0.00	1.00	5.12	51.36	0.00	1.33	1.03	40.16	0.00	0.00	0.00	100.00	SEMEdx-UFS
EST13-20	MLN-MR	0.00	0.00	0.69	4.39	52.22	0.00	1.24	0.98	40.48	0.00	0.00	0.00	100.00	SEMEdx-UFS
EST13-20	MLN-MR	0.00	0.00	0.78	4.21	50.08	0.25	1.03	1.24	42.41	0.00	0.00	0.00	100.00	SEMEdx-UFS
EST13-22	MLN-MR	0.00	0.00	1.17	5.70	48.42	0.20	0.00	0.47	44.04	0.00	0.00	0.00	100.00	SEMEdx-UFS
EST13-22	MLN-MR	0.00	0.00	1.37	5.10	48.09	0.57	0.00	0.53	44.34	0.00	0.00	0.00	100.00	SEMEdx-UFS
EST13-22	MLN-MR	0.00	0.00	1.16	5.14	48.46	0.50	0.00	0.77	43.98	0.00	0.00	0.00	100.01	SEMEdx-UFS
EST13-22	MLN-MR	0.00	0.00	1.11	4.58	48.81	0.00	0.00	0.73	44.78	0.00	0.00	0.00	100.01	SEMEdx-UFS
EST13-22	MLN-MR	0.00	0.00	1.17	4.85	47.70	0.00	0.35	0.67	45.26	0.00	0.00	0.00	100.00	SEMEdx-UFS
EST13-22	MLN-MR	0.00	0.00	1.16	5.03	48.61	0.00	0.00	0.86	44.35	0.00	0.00	0.00	100.01	SEMEdx-UFS
EST13-22	MLN-MR	0.00	0.00	0.85	4.09	48.44	0.00	0.52	0.67	45.43	0.00	0.00	0.00	100.00	SEMEdx-UFS
EST13-22	MLN-MR	0.00	0.00	1.09	3.96	49.96	0.00	1.19	0.00	43.80	0.00	0.00	0.00	100.00	SEMEdx-UFS
EST13-22	MLN-MR	0.00	0.00	1.15	4.00	48.99	0.29	0.61	0.68	44.28	0.00	0.00	0.00	100.00	SEMEdx-UFS
EST13-22	MLN-MR	0.00	0.00	1.36	4.35	48.73	0.00	0.60	0.93	44.03	0.00	0.00	0.00	100.00	SEMEdx-UFS

A3-9 Sulphide Compositions (EPMA- Rhodes University)

	EPMA: Rhodes University										
Sample Name	Rock Type	Sulphide	S	Cu	Fe	Ni	Zn	Co	As	Pb	Total
JJB19.1	PXT	Pyrrhotite	38.52	0.00	60.08	0.21	0.00	0.23	0.05	0.00	99.10
JJB19.1	PXT	Chalcopyrite	34.17	34.70	30.91	0.03	0.00	0.03	0.00	0.00	99.84
JJB19.1	PXT	Pyrrhotite	39.04	0.00	59.90	0.19	0.01	0.01	0.03	0.00	99.16
JJB19.1	PXT	Pyrrhotite	38.19	0.00	61.80	0.15	0.00	0.05	0.04	0.00	100.23
JJB19.1	PXT	Pentlandite	32.82	0.00	31.73	35.07	0.00	0.18	0.03	0.00	99.84
JJB11	PXT	Pyrite	51.38	2.04	46.05	0.00	0.00	0.24	0.03	0.00	99.74
JJB17	PXT	Chalcopyrite	33.65	34.91	30.71	0.00	0.00	0.02	0.00	0.00	99.29
JJB17	PXT	Pyrrhotite	37.90	0.00	60.64	0.05	0.00	0.03	0.00	0.00	98.62
JJB17	PXT	Pyrrhotite	38.15	0.06	61.01	0.12	0.00	0.02	0.02	0.00	99.38
JJB9	PXT	Chalcopyrite	35.08	36.10	30.76	0.00	0.00	0.03	0.01	0.00	101.97
JJB9	PXT	Chalcopyrite	34.11	35.13	31.81	0.00	0.00	0.05	0.00	0.00	101.10
JJB9	BSN	Chalcopyrite	34.83	35.82	30.84	0.00	0.00	0.01	0.00	0.00	101.51
JJB9	BSN	Chalcopyrite	34.60	35.06	30.67	0.00	0.00	0.02	0.02	0.00	100.37
JJB14	BSN	Pyrrhotite	38.88	0.11	62.05	0.05	0.04	0.05	0.01	0.00	101.19
JJB14	BSN	Pyrrhotite	38.26	0.00	62.58	0.15	0.00	0.05	0.03	0.00	101.07
JJB14	BSN	Chalcopyrite	34.29	35.92	32.22	0.00	0.00	0.01	0.03	0.00	102.47
JJB14	BSN	Chalcopyrite	34.38	36.62	30.89	0.00	0.00	0.01	0.01	0.00	101.92
JJB10.1	PXT	Pyrite	52.12	0.00	47.43	0.01	0.00	0.02	0.00	0.00	99.58
JJB10.1	PXT	Pyrite	52.76	0.13	47.59	0.03	0.00	0.05	0.01	0.00	100.58
JJB10.1	PXT	Chalcopyrite	34.16	33.28	30.70	0.00	0.00	0.02	0.00	0.00	98.15
JJB10.1	PXT	Pyrite	52.54	0.14	46.49	0.00	0.04	0.05	0.01	0.00	99.27
JJB10.1	PXT	Pyrite	53.10	0.06	47.26	0.00	0.01	0.04	0.00	0.00	100.47
AL7906	PXT	Pyrrhotite	38.93	0.00	59.91	0.07	0.00	0.05	0.03	0.00	99.00
AL7906	PXT	Chalcopyrite	34.26	32.04	30.62	0.19	0.00	0.03	0.00	0.00	97.13
AL7906	PXT	Chalcopyrite	34.02	35.36	30.06	0.12	0.00	0.04	0.00	0.00	99.60
AL7906	PXT	Pyrite	53.22	0.01	47.18	0.00	0.04	0.05	0.00	0.00	100.50
AL7907	PXT	Chalcopyrite	35.00	33.85	31.68	0.24	0.00	0.00	0.00	0.00	100.78
AL7907	PXT	Pyrrhotite	37.97	0.22	61.84	0.00	0.00	0.01	0.04	0.00	100.09
AL7907	PXT	Pyrrhotite	38.49	0.02	60.58	0.00	0.00	0.06	0.04	0.00	99.19
AL7907	PXT	Chalcopyrite	34.78	33.94	29.65	0.05	0.00	0.00	0.00	0.00	98.42
AL7907	PXT	Pentlandite	33.97	0.00	35.43	32.98	0.00	0.09	0.03	0.00	102.49
AL7908	PXT	Pyrrhotite	38.52	0.00	62.13	0.12	0.00	0.03	0.03	0.00	100.83
AL7908	PXT	Pyrrhotite	38.90	0.00	63.16	0.10	0.00	0.05	0.04	0.00	102.25
AL7908	PXT	Pyrrhotite	37.44	0.07	62.78	0.12	0.00	0.02	0.02	0.00	100.46
AL7908	PXT	Pyrrhotite	38.40	0.00	61.58	0.15	0.00	0.04	0.05	0.00	100.22
AL7908	PXT	Pentlandite	33.31	0.00	34.74	32.57	0.00	0.14	0.00	0.00	100.76
AL7908	PXT	Pyrrhotite	38.39	0.00	58.62	0.00	0.00	0.03	0.01	0.00	97.05
AL7908	PXT	Chalcopyrite	35.06	33.79	31.25	0.01	0.00	0.00	0.00	0.00	100.10
AL7908	PXT	Chalcopyrite	34.06	31.55	30.75	0.04	0.00	0.01	0.02	0.00	96.43
AL7908	PXT	Pyrrhotite	35.60	0.13	60.30	0.00	0.04	0.03	0.02	0.00	96.12
AL7908	PXT	Pyrrhotite	38.40	0.02	62.59	0.00	0.00	0.02	0.04	0.00	101.07
EST013-11	MsN	Pyrrhotite	37.66	0.15	59.96	0.92	0.01	0.05	0.02	0.00	98.77
EST013-11	MsN	Chalcopyrite	34.00	32.96	30.34	0.04	0.00	0.00	0.00	0.00	97.33
EST013-11	MsN	Chalcopyrite	33.98	33.39	30.80	0.06	0.00	0.02	0.02	0.00	98.26
EST013-11	MsN	Pyrrhotite	38.81	0.03	59.08	0.80	0.05	0.04	0.00	0.00	98.81
EST013-11	MsN	Pyrrhotite	39.09	0.00	60.84	0.89	0.00	0.03	0.00	0.00	100.84
EST013-11	MsN	Pyrrhotite	37.78	0.00	59.04	0.83	0.00	0.02	0.05	0.00	97.72
EST013-11	MsN	Pyrrhotite	38.92	0.11	60.83	0.67	0.00	0.04	0.03	0.00	100.59
EST013-11	MsN	Pyrrhotite	38.57	0.00	61.14	0.75	0.04	0.01	0.03	0.00	100.54
EST013-11	MsN	Pyrrhotite	38.87	0.00	59.43	1.15	0.00	0.04	0.05	0.00	99.53
EST013-11	MsN	Pentlandite	32.52	0.00	30.02	37.83	0.03	0.23	0.07	0.00	100.70
EST013-11	MsN	Pyrrhotite	39.36	0.02	60.34	0.76	0.00	0.03	0.00	0.00	100.50
EST013-11	MsN	Pentlandite	34.55	0.00	37.16	29.43	0.00	0.10	0.00	0.00	101.23
EST013-11	MsN	Pyrrhotite	38.83	0.00	60.20	0.59	0.00	0.04	0.03	0.00	99.70

A3-10 Sulphide Compositions (EPMA- University of Leoben)

EMPA: University of Leoben

Sample	Rocktype	Sulphide	As	Pt	S	Cu	Fe	Rh	Bi	Zn	Ni	Te	Ir	Pd	Ru	Total
JJB3	PXT	Pentlandite	0.00	0.00	32.85	0.00	30.93	0.00	0.00	0.00	35.79	0.00	0.00	0.00	0.00	99.57
JJB3	PXT	Pyrrhotite	0.00	0.00	38.19	0.03	59.00	0.00	0.00	0.01	0.66	0.00	0.00	0.00	0.00	97.89
JJB3	PXT	Pyrite	0.00	0.00	51.86	0.03	45.58	0.00	0.00	0.00	0.05	0.00	0.00	0.00	0.00	97.52
JJB3	PXT	Pyrrhotite	0.00	0.00	38.66	0.00	59.52	0.00	0.00	0.02	0.30	0.00	0.00	0.00	0.00	98.50
JJB3	PXT	Pyrrhotite	0.00	0.00	38.81	0.03	59.75	0.00	0.00	0.00	0.33	0.00	0.00	0.00	0.00	98.92
JJB10	PXT	Pyrrhotite	0.00	0.00	37.83	0.00	59.51	0.00	0.00	0.02	0.60	0.00	0.00	0.00	0.00	97.96
JJB10	PXT	Pyrrhotite	0.04	0.00	40.09	0.01	60.85	0.01	0.17	0.02	0.63	0.02	0.02	0.00	0.00	101.86
JJB10	PXT	Pyrrhotite	0.00	0.00	39.01	0.01	60.31	0.00	0.14	0.00	0.59	0.01	0.00	0.00	0.00	100.06
JJB10	PXT	Pyrrhotite	0.02	0.00	39.68	0.01	60.77	0.00	0.12	0.02	0.36	0.00	0.00	0.00	0.00	100.99
JJB10	PXT	Pyrrhotite	0.00	0.01	40.15	0.00	60.57	0.03	0.12	0.01	0.32	0.00	0.00	0.00	0.00	101.20
JJB10	PXT	Pentlandite	0.00	0.00	33.55	0.17	30.67	0.00	0.01	0.03	34.94	0.00	0.00	0.00	0.00	99.37
JJB10	PXT	Pentlandite	0.00	0.03	34.01	0.00	31.43	0.00	0.13	0.00	35.43	0.00	0.00	0.00	0.00	101.02
JJB10	PXT	Pyrrhotite	0.00	0.03	40.01	0.08	60.14	0.02	0.12	0.02	0.42	0.02	0.03	0.00	0.00	100.90
JJB10	PXT	Pentlandite	0.00	0.00	33.75	0.24	31.18	0.08	0.06	0.00	35.05	0.06	0.00	0.00	0.00	100.42
JJB10	PXT	Chalcopyrite	0.01	0.04	35.44	32.94	31.30	0.00	0.10	0.05	1.94	0.00	0.06	0.00	0.00	101.88
JJB10	PXT	Pentlandite	0.03	0.00	32.87	0.00	31.26	0.01	0.12	0.00	34.89	0.00	0.00	0.00	0.00	99.17
JJB10	PXT	Pyrrhotite	0.02	0.00	39.74	0.13	60.22	0.00	0.17	0.02	0.27	0.00	0.00	0.00	0.00	100.55
JJB10	PXT	Chalcopyrite	0.00	0.00	35.45	35.05	31.23	0.00	0.15	0.07	0.04	0.02	0.00	0.00	0.00	102.02
JJB18	BSN	Pyrrhotite	0.00	0.00	38.86	0.00	59.92	0.00	0.00	0.00	0.45	0.00	0.00	0.00	0.00	99.23
JJB18	BSN	Pentlandite	0.00	0.00	33.74	0.00	31.53	0.00	0.00	0.00	33.28	0.00	0.00	0.00	0.00	98.55
JJB18	BSN	Pentlandite	0.00	0.00	33.64	0.00	31.59	0.00	0.00	0.00	33.62	0.00	0.00	0.00	0.00	98.84
JJB18	BSN	Pentlandite	0.00	0.00	33.41	0.00	31.29	0.00	0.00	0.00	34.09	0.00	0.00	0.00	0.00	98.79
JJB18	BSN	Pyrrhotite	0.00	0.00	38.37	0.01	59.99	0.00	0.00	0.00	0.73	0.00	0.00	0.00	0.00	99.10
JJB18	BSN	Pyrrhotite	0.00	0.00	38.93	0.00	60.30	0.00	0.00	0.00	0.42	0.00	0.00	0.00	0.00	99.65
JJB18	BSN	Chalcopyrite	0.00	0.00	36.60	31.30	29.78	0.00	0.00	0.02	0.00	0.00	0.00	0.00	0.00	97.70
JJB18	BSN	Pyrrhotite	0.00	0.00	39.06	0.01	61.05	0.00	0.00	0.00	0.31	0.00	0.00	0.00	0.00	100.43
JJB18	BSN	Pentlandite	0.00	0.00	33.29	0.00	31.41	0.00	0.00	0.00	33.91	0.00	0.00	0.00	0.00	98.60
JJB18	BSN	Pentlandite	0.00	0.00	33.78	0.00	31.44	0.00	0.00	0.03	33.72	0.00	0.00	0.00	0.00	98.97
JJB18	BSN	Pyrrhotite	0.00	0.00	38.06	0.20	59.23	0.00	0.00	0.00	0.58	0.00	0.00	0.00	0.00	98.08
JJB18	BSN	Chalcopyrite	0.00	0.00	34.60	33.94	30.42	0.00	0.00	0.05	0.25	0.00	0.00	0.00	0.00	99.27
JJB18	BSN	Pyrrhotite	0.00	0.00	39.28	0.03	60.28	0.00	0.00	0.00	0.34	0.00	0.00	0.00	0.00	99.94
JJB18	BSN	Chalcopyrite	0.00	0.00	34.18	32.76	30.10	0.00	0.00	0.06	0.66	0.00	0.00	0.00	0.00	97.76
JJB18	BSN	Pentlandite	0.00	0.00	34.14	0.00	32.78	0.00	0.10	0.00	33.06	0.02	0.02	0.00	0.00	100.11
JJB20	PXT	Pyrrhotite	0.00	0.00	37.87	0.00	59.61	0.00	0.00	0.01	0.61	0.00	0.00	0.00	0.00	98.10
JJB20	PXT	Pyrrhotite	0.00	0.00	37.41	0.00	59.42	0.00	0.00	0.02	0.64	0.00	0.00	0.00	0.00	97.48
JJB20	PXT	Pentlandite	0.00	0.00	33.01	0.00	30.91	0.00	0.00	0.01	34.57	0.00	0.00	0.00	0.00	98.50
JJB20	PXT	Pyrite	0.00	0.00	52.17	0.06	46.93	0.00	0.00	0.00	0.01	0.00	0.00	0.00	0.00	99.16
JJB20	PXT	Pentlandite	0.00	0.00	32.98	0.14	31.48	0.00	0.00	0.02	34.76	0.00	0.00	0.00	0.00	99.38
JJB20	PXT	Pentlandite	0.00	0.00	34.10	0.00	32.40	0.00	0.13	0.00	34.36	0.03	0.00	0.00	0.00	101.02
JJB20	PXT	Chalcopyrite	0.04	0.02	35.40	33.96	30.49	0.00	0.10	0.04	0.07	0.00	0.00	0.00	0.00	100.11
JJB20	PXT	Arsenopyrite	29.69	30.81	12.37	1.65	1.74	6.00	0.00	0.00	0.16	0.00	27.33	0.00	0.00	109.74
JJB20	PXT	Pentlandite	0.00	0.00	33.71	0.00	31.73	0.00	0.10	0.00	34.65	0.03	0.02	0.00	0.00	100.24

A3-11 PGM Compositions (EPMA- University of Leoben)

Sample	As	Pt	S	Cu	Fe	Rh	Bi	Zn	Ni	Te	Ir	Pd	Ru	Total
JJB20	0.01	36.93	0.07	0.07	1.24	0.03	19.50	0.05	0.94	41.40	0.00	0.00	0.00	100.25
JJB20	0.04	37.76	0.08	0.10	1.72	0.00	19.04	0.00	1.55	40.80	0.00	0.00	0.00	101.08
JJB20	27.64	35.12	12.12	1.58	2.21	4.18	0.00	0.00	0.23	0.01	27.18	0.00	0.00	110.26
JJB20	28.05	34.52	12.83	1.67	1.64	4.18	0.00	0.00	0.22	0.01	29.19	0.00	0.00	112.31
JJB20	0.04	33.34	0.13	0.00	1.71	1.36	6.65	0.00	1.49	54.42	0.05	0.00	0.00	99.18
JJB20	0.01	33.06	0.13	0.00	1.61	1.36	6.61	0.00	1.35	54.31	0.16	3.43	0.00	102.03
JJB18	44.49	48.63	1.96	0.00	3.02	0.60	0.00	0.00	1.06	0.03	0.00	0.00	0.21	100.00
JJB18	17.19	64.26	4.75	0.01	8.85	1.03	0.00	0.00	3.24	0.00	0.00	0.18	0.49	100.00
JJB18	36.80	42.17	8.08	0.00	8.64	0.25	0.00	0.00	3.88	0.02	0.13	0.00	0.04	100.00
JJB3	0.02	40.12	0.06	0.43	0.78	0.08	14.90	0.00	0.04	43.93	0.00	0.02	0.03	100.42
JJB3	0.00	40.21	0.13	0.09	1.65	0.07	12.04	0.02	0.03	44.79	0.00	0.00	0.07	99.08
JJB3	0.00	41.11	0.06	0.23	0.37	0.17	9.41	0.00	0.02	48.76	0.00	0.05	0.03	100.20
JJB3	0.01	41.58	0.06	0.46	0.58	0.07	8.73	0.00	0.02	49.72	0.00	0.01	0.02	101.24
JJB3	0.04	39.49	0.08	0.32	1.27	0.07	15.77	0.04	0.08	42.84	0.00	0.00	0.01	100.00
JJB10	0.02	36.58	0.11	0.00	2.34	2.85	8.78	0.01	0.29	51.60	0.00	0.00	0.00	102.57
JJB10	0.00	36.16	0.09	0.00	1.42	2.39	10.02	0.00	0.09	50.23	0.00	0.00	0.00	100.39
JJB10	0.00	33.00	0.17	0.00	2.72	2.37	8.20	0.05	0.05	52.33	0.02	0.00	0.00	98.91
JJB10	0.02	33.71	0.43	0.00	3.22	4.75	2.83	0.03	0.04	55.03	0.00	0.00	0.00	100.07
JJB10	0.02	37.03	0.61	0.01	1.99	1.48	8.92	0.02	0.97	45.58	0.00	0.00	0.00	96.62
JJB10	0.00	40.23	0.06	0.00	0.69	0.11	11.56	0.02	0.12	47.10	0.00	0.00	0.00	99.90
JJB10	0.02	39.79	0.09	0.00	1.39	0.10	13.18	0.01	0.09	46.02	0.00	0.00	0.00	100.67
JJB10	0.04	40.14	0.12	0.00	1.98	0.19	9.57	0.00	0.05	49.02	0.00	0.00	0.00	101.11
JJB10	0.00	38.95	0.08	0.06	0.85	0.86	8.97	0.03	0.05	51.39	0.00	0.00	0.00	101.24
JJB10	0.00	37.41	0.13	0.26	1.11	0.80	10.52	0.01	0.10	47.48	0.00	0.00	0.00	97.80
JJB10	0.00	38.42	0.09	0.08	0.83	0.97	8.15	0.03	0.05	51.07	0.00	0.00	0.00	99.69
JJB10	0.00	39.47	0.06	0.29	1.09	0.08	14.77	0.00	0.36	44.70	0.00	0.00	0.00	100.81
JJB10	0.00	36.53	0.11	0.27	1.09	0.09	10.08	0.00	0.04	48.87	0.01	0.00	0.00	97.08
JJB10	0.08	0.08	43.55	0.11	18.51	1.42	0.00	0.00	0.75	0.00	1.67	0.10	31.70	97.97
JJB10	0.40	0.64	40.84	0.05	13.23	1.84	0.00	0.00	0.83	0.00	2.17	0.15	37.46	97.61
JJB10	0.59	1.23	41.10	0.09	12.98	1.76	0.00	0.00	0.85	0.00	2.69	0.06	36.31	97.65
JJB10	0.03	38.33	0.39	0.79	1.85	0.07	8.24	0.05	0.07	32.82	0.01	0.00	0.00	82.65
JJB10	0.02	40.26	0.02	0.46	0.74	0.10	10.49	0.02	0.04	48.23	0.00	0.00	0.00	100.38
JJB10	0.00	40.20	0.03	0.46	0.89	0.13	10.02	0.03	0.05	48.39	0.00	0.00	0.00	100.20
JJB10	0.00	40.37	0.05	0.14	1.19	0.05	7.64	0.05	0.06	46.69	0.06	0.00	0.00	96.30
JJB10	0.03	0.00	35.26	34.98	31.17	0.00	0.13	0.05	0.01	0.00	0.00	0.00	0.00	101.63
JJB10	0.02	38.22	0.14	0.03	1.04	0.08	10.61	0.02	0.90	42.60	0.00	0.00	0.00	93.68
JJB10	2.21	2.35	29.61	2.05	6.96	1.17	0.00	0.00	0.12	0.04	6.89	0.00	28.08	79.49
JJB10	1.55	1.15	31.89	0.59	10.23	1.05	0.00	0.00	0.10	0.00	8.47	0.02	28.76	83.79

Standards used by EPMA-Rhodes University

SILICATES:

	Element	Standard name	Mass(%)	ZAF Fac.	Z	A	F
1	SiO2	Olivine_SPI	41.5800	2.8511	4.4023	0.6476	1.0000
2	CaO	Cr_Diopside_SPI	25.5000	0.8676	0.9360	0.9265	1.0005
3	K2O	Orthoclase_SPI	15.9600	1.0761	1.2041	0.8936	1.0002
4	MgO	Olivine_SPI	50.4300	4.8491	7.8682	0.6144	1.0032
5	Al2O3	Kyanite_SPI	62.9200	4.4417	5.8542	0.7537	1.0066
6	FeO	Almandine_SPI	23.2700	0.1990	0.2024	0.9830	1.0000
7	MnO	Rhodonite_SPI	42.3000	0.2677	0.2737	0.9782	1.0000
8	TiO2	Rutile_SPI	99.9834	0.5904	0.6060	0.9742	1.0000
9	NiO	Nickel_Silicide_SPI	102.6928	0.1222	0.1238	0.9874	1.0000
10	Na2O	Albite_SPI	11.5900	5.5020	10.7239	0.5109	1.0041
11	Cr2O3	Chromium_Oxide_SPI	100.0131	0.3636	0.3706	0.9811	1.0000

SULPHIDES:

	Element	Standard name	Mass(%)	ZAF Fac.	Z	A	F
1	S	Chalcopyrite_AGAR	34.9300	2.1550	2.8515	0.7555	1.0003
2	Cu	Chalcopyrite_AGAR	34.4400	0.0876	0.0900	0.9734	1.0000
3	Fe	Pyrite_Agar	46.4000	0.2107	0.2168	0.9718	1.0000
4	Ni	Pentlandite_SPI	36.0000	0.1187	0.1228	0.9659	1.0000
5	Zn	Sphalerite_SPI	67.0700	0.0633	0.0640	0.9904	1.0000
6	Co	Cobaltite_Agar	19.1600	0.1709	0.1748	0.9779	1.0000
7	As	Arsenopyrite_SPI	46.6400	4.4028	8.8708	0.4963	1.0000
8	Pb	Galena_SPI	86.6000	2.7233	3.4515	0.7890	1.0000

Standards used by EPMA-University of Leoben

SULPHIDES & PGM:

	Element	Standard name	Mass(%)	ZAF Fac.	Z	A	F
1	As	P3_07_PtAs2L	43.4400	6.1809	14.7721	0.4184	1.0000
2	Rh	P3_04_Rh_mKE	100.0000	2.7135	3.5152	0.7719	1.0000
3	S	P3_24_NiS_KE	35.3200	2.8108	4.3648	0.6436	1.0005
4	Cu	P3_21_CuFeS2KE	34.6200	0.2352	0.2486	0.9465	1.0000
5	Fe	P3_21_CuFeS2KE	30.4300	0.4891	0.4902	0.9522	1.0480
6	Pd	S3_03_Pd_KE	100.0000	2.3426	2.9027	0.8070	1.0000
7	Bi	P3_18_Bi2Te3KE	52.3200	3.2940	5.0720	0.6494	1.0000
8	Zn	P3_25_sphalKE	60.3000	0.1917	0.1968	0.9745	1.0000
9	Ni	P3_24_NiS_KE	64.6800	0.2978	0.3071	0.9698	1.0000
10	Ru	S3_02_Ru_KE	100.0000	2.9681	3.9104	0.7590	1.0000
11	Te	P3_18_BiTeKE3	47.6800	1.3058	1.9189	0.6805	1.0000
12	Pt	P3_07_PtAs2L	56.5600	0.1183	0.1218	0.9714	1.0000
13	Ir	P3_05_Ir_L	100.0000	0.1445	0.1506	0.9596	1.0000

Appendix Four: LA ICP-MS

A4-1 LA ICP-MS studies at Cardiff University, Wales

Region	Assumed Internal Std S	S/Se	57Fe	59Co	61Ni	65Cu	66Zn	75As	82Se	101Ru*	103Rh*	106Pd*	108Pd*	109Ag	111Cd	121Sb	125Te	185Re	189Os	193Ir	195Pt	197Au	209Bi
	%		%	ppm	%	%	ppm	ppm	ppm	ppm	ppm	ppm	ppm	ppm	ppm	ppm	ppm	ppm	ppm	ppm	ppm	ppm	ppm
AL7909A a1Po	38.5	3639	60.18	45	0.26	<0.03	<15	<9	106	<0.05	<0.1	<0.15	<0.2	<0.1	<0.8	<0.9	<0.9	<0.02	<0.02	<0.02	<0.02	<0.01	<0.05
AL7909A a1Cp	34.5	2025	34.60	<5	<0.05	22.29	19150	<9	170	<0.05	<0.1	<0.15	<0.2	16.5	12.1	<0.9	<0.9	0.07	<0.02	<0.02	<0.02	0.16	<0.05
AL7909A a2Po2	38.5	2560	59.92	9	0.10	<0.03	<15	<9	150	45.6	0.22	0.30	0.33	0.29	<0.8	<0.9	<0.9	0.34	4.10	4.51	0.44	<0.01	<0.05
AL7909A a2Pn1	34	1897	36.43	5684	29.83	<0.03	<15	<9	179	13.0	5.80	359	364	18.3	<0.8	<0.9	<0.9	0.23	2.88	2.85	0.74	0.16	<0.05
AL7909A a2Po2	38.5	2194	55.70	9	0.12	<0.03	<15	<9	176	0.79	<0.1	<0.15	<0.2	<0.1	<0.8	<0.9	<0.9	0.69	0.51	0.30	0.10	0.03	<0.05
A7909A a2Pn2	34	2493	32.42	6167	33.29	<0.03	<15	<9	136	9.39	7.25	397	403	2.82	<0.8	<0.9	<0.9	0.29	3.71	3.49	0.98	<0.01	<0.05
A7909A a2Pn3	34	1902	33.32	6169	33.54	<0.03	<15	<9	179	94.2	6.30	399	390	4.86	<0.8	<0.9	<0.9	0.19	6.57	2.12	1.00	0.03	<0.05
A7909A a2Cp (+Pn)	34.5	2662	28.11	364	1.63	27.90	1850	<9	130	1.42	0.20	18.6	17.8	2.13	<0.8	<0.9	<0.9	<0.02	0.17	0.08	<0.02	0.34	<0.05
AL7909A a2Cp2	34.5	2309	27.28	<5	<0.05	27.15	2755	<9	149	16.1	<0.1	<0.15	<0.2	3.14	2.41	<0.9	<0.9	0.22	4.80	3.38	1.14	0.44	0.13
AL7909A a2 Pn4	34	1722	35.11	6661	32.63	<0.03	<15	<9	198	22.1	4.80	402	419	2.63	<0.8	<0.9	<0.9	0.25	5.09	3.67	0.69	0.08	<0.05
AL7909A a2Po3	38.5	2348	56.41	45	0.30	<0.03	<15	<9	164	13.7	0.13	4.02	3.57	0.35	<0.8	<0.9	<0.9	0.21	2.07	1.68	0.07	<0.01	<0.05
AL7909A a2Cp3 (+Pn)	34.5	2123	29.21	908	4.47	24.19	7783	<9	163	11.0	1.76	64.6	68.8	7.41	5.91	<0.9	<0.9	1.46	3.75	0.68	3.19	0.06	0.38
A7909A a3Po1	38.5	3419	59.06	33	0.23	0.12	<15	<9	113	0.74	<0.1	0.73	0.73	0.40	<0.8	<0.9	<0.9	1.57	1.43	0.60	0.60	<0.01	<0.05
A7909A a3Cp	35	2832	38.44	249	1.60	17.95	5712	<9	124	4.63	<0.1	5.19	5.22	4.74	1.45	<0.9	<0.9	0.18	1.90	2.13	3.11	0.79	0.18
AL7909A a3Cp2	34.5	2679	28.71	<5	<0.05	25.57	2699	<9	129	0.15	<0.1	<0.15	<0.2	3.11	6.90	<0.9	1.85	0.04	<0.02	0.03	0.14	1.08	<0.05
AL7909A a3Po2	38.5	2652	57.89	7	0.11	0.96	101	<9	145	0.77	<0.1	<0.15	<0.2	0.19	<0.8	<0.9	<0.9	0.20	1.15	0.78	0.45	0.04	<0.05
AL7916 a1Pn1	34	1681	34.01	5615	34.31	<0.03	<15	<9	202	48.0	252	229	228	1.03	<0.8	<0.9	2.52	0.33	8.10	12.3	2.34	<0.01	<0.05
AL7916 a1Cp1	34.5	2740	26.77	<5	<0.05	27.15	1950	<9	126	<0.05	<0.1	<0.15	<0.2	3.03	2.82	<0.9	<0.9	<0.02	<0.02	<0.02	<0.02	0.04	<0.05
AL7916 a2Po	38.5	2325	57.39	16	0.17	<0.03	<15	<9	166	47.5	0.14	<0.15	<0.2	0.18	<0.8	<0.9	<0.9	0.52	5.85	4.66	2.45	<0.01	<0.05
AL7916 a2Pn	34	2017	37.22	2965	16.20	1.75	1716	<9	169	55.0	27.2	117	118	6.06	1.13	<0.9	1.29	<0.02	2.88	3.16	1.89	0.19	<0.05
AL7916 a3Cp	35	2545	27.83	29	0.15	26.19	1860	<9	138	0.10	<0.1	1.26	1.48	3.93	2.26	<0.9	<0.9	<0.02	0.08	0.18	0.16	0.16	<0.05
AL7916 a4Po1	38.5	2381	58.44	14	0.25	<0.03	<15	<9	162	20.5	<0.1	<0.15	<0.2	0.26	<0.8	<0.9	<0.9	0.49	5.39	2.89	2.16	<0.01	<0.05
AL7916 a4Pn1	34	1929	38.80	2658	19.35	1.10	156	<9	176	16.2	8.19	106	106	5.38	0.88	<0.9	<0.9	0.16	2.52	2.16	3.11	0.06	<0.05
AL7916 a4Pn2	34	1787	29.50	3877	25.54	5.54	537	<9	190	24.5	18.5	224	220	37.35	<0.8	<0.9	1.81	0.21	4.94	3.80	2.23	0.35	<0.05
AL7916 a4Cp1 (+Pn)	34.5	2424	26.60	523	3.27	21.77	1601	<9	142	4.11	2.19	32.1	31.5	13.10	4.06	<0.9	<0.9	0.06	0.19	0.54	0.64	2.05	<0.05
AL7916 a4Po2	38.5	2374	60.85	44	0.45	<0.03	24	<9	162	2.64	0.20	1.82	2.01	0.32	<0.8	<0.9	<0.9	0.03	1.02	0.39	0.33	0.02	<0.05
AL7916 a4Pn2	34	1959	29.49	4549	27.79	<0.03	<15	<9	174	62.6	42.2	209	206	0.43	<0.8	<0.9	<0.9	0.28	6.86	5.45	2.85	0.03	<0.05
AL7916 a4 mixPo-Pn	36	2211	43.68	2958	19.50	<0.03	<15	<9	163	24.2	25.5	153	151	1.07	<0.8	<0.9	<0.9	0.18	3.10	3.40	2.63	0.06	<0.05
AL7916 a5 Pn1	34	3340	33.76	3904	23.34	<0.03	55	<9	102	8.67	5.69	190	189	2.50	<0.8	1.33	<0.9	<0.02	1.29	2.07	0.54	0.04	<0.05
AL7916 a5Po1	38.5	2338	56.41	232	1.43	<0.03	62	<9	165	3.13	0.35	11.4	10.9	0.50	<0.8	<0.9	<0.9	0.05	1.28	1.50	<0.02	<0.01	<0.05
AL7916 a5 Po2	38.5	3490	58.89	13	0.20	<0.03	<15	<9	110	19.2	<0.1	<0.15	<0.2	0.39	<0.8	<0.9	<0.9	0.16	1.39	1.31	0.15	<0.01	<0.05
AL7916 a5 Pn	34	2607	33.56	5926	33.84	<0.03	29	<9	130	16.5	93.3	203	205	1.97	<0.8	<0.9	<0.9	0.25	2.56	4.62	0.69	0.03	<0.05
AL7916 a5 Po	38.5	3861	54.60	123	0.99	<0.03	<15	<9	100	0.98	0.90	4.05	3.85	0.54	<0.8	<0.9	<0.9	0.25	0.99	0.38	0.13	<0.01	<0.05
A7916 a6Pn1	34	2118	35.06	6277	36.30	<0.03	<15	<9	161	13.6	26.7	225	230	0.93	<0.8	<0.9	<0.9	0.08	2.25	2.80	0.73	<0.01	<0.05
A7916 a6Po1	38.5	2923	56.18	123	0.85	<0.03	<15	<9	132	3.80	0.49	4.41	4.57	0.90	<0.8	<0.9	<0.9	0.03	1.95	0.82	0.06	<0.01	<0.05
AL7916 a6Po2	38.5	2536	60.72	12	0.23	<0.03	<15	<9	152	7.23	<0.1	<0.15	<0.2	0.12	<0.8	<0.9	<0.9	0.26	3.09	2.06	0.22	0.03	<0.05
AL7916 a6Pn2	34	2393	29.18	5700	32.67	<0.03	<15	<9	142	25.2	31.4	197	196	1.33	<0.8	<0.9	<0.9	0.19	3.74	3.02	0.35	0.06	<0.05
AL7916 a6 Pn3	34	2319	31.08	5563	32.46	<0.03	<15	<9	147	28.6	37.7	207	208	1.41	<0.8	<0.9	<0.9	0.21	4.08	2.88	0.43	<0.01	<0.05
AL7916 a7Po1	38.5	2441	53.80	10	0.20	<0.03	<15	<9	158	2.79	<0.1	<0.15	<0.2	<0.1	<0.8	<0.9	<0.9	0.24	2.39	1.06	0.58	<0.01	<0.05
AL7916 a7Pn1	34	1817	36.89	5272	24.00	<0.03	40	<9	187	54.4	46.7	131	131	3.00	<0.8	<0.9	<0.9	<0.02	5.67	3.28	0.23	<0.01	<0.05
AL7916 a7Po2	38.5	2017	57.83	17	0.26	<0.03	<15	<9	191	3.48	<0.1	<0.15	<0.2	<0.1	<0.8	<0.9	<0.9	0.14	2.08	1.55	0.56	<0.01	<0.05
AL7916 a7Po3	38.5	2266	55.48	17	0.29	<0.03	<15	<9	170	4.62	0.12	<0.15	<0.2	0.56	<0.8	<0.9	<0.9	0.26	2.43	1.34	0.60	0.02	<0.05

Region	Assumed Internal Std S	S/Se	57Fe	59Co	61Ni	65Cu	66Zn	75As	82Se	101Ru*	103Rh*	106Pd*	108Pd*	109Ag	111Cd	121Sb	125Te	185Re	189Os	193Ir	195Pt	197Au	209Bi
	%		%	ppm	%	%	ppm	ppm	ppm	ppm	ppm	ppm	ppm	ppm	ppm	ppm	ppm	ppm	ppm	ppm	ppm	ppm	ppm
AL7909B a1L1 Pn1	34.0	1944	38.16	5704	32.99	<0.03	43	<9	175	12.1	8.64	218	209	3.01	<0.8	<0.9	<0.9	0.03	2.11	3.55	0.26	<0.01	<0.05
AL7909B a1L1 Po1	38.5	2628	60.31	247	1.29	<0.03	<15	<9	147	0.34	0.19	7.48	6.62	0.47	<0.8	<0.9	<0.9	<0.02	0.17	0.13	<0.02	0.02	<0.05
AL7909B a1L2 Po2	38.5	1984	61.35	80	0.37	<0.03	63	<9	194	28.0	0.19	2.03	2.17	0.72	<0.8	<0.9	2.34	0.43	3.96	4.27	0.31	<0.01	<0.05
AL7909B a1L2 Pn2	34.0	2185	41.82	5002	33.69	<0.03	17	<9	156	43.3	5.59	196	197	3.15	<0.8	<0.9	<0.9	0.23	3.84	5.70	0.73	<0.01	0.05
AL7909B a1L3 Po3	38.5	2594	63.96	9	0.12	<0.03	34	<9	148	3.80	<0.1	<0.15	<0.2	0.72	<0.8	<0.9	<0.9	0.26	2.31	1.05	0.17	<0.01	<0.05
AL7909B a1L4 Po4	38.5	2941	64.46	5	0.11	<0.03	26	<9	131	0.26	<0.1	<0.15	<0.2	0.34	<0.8	<0.9	<0.9	1.98	2.96	0.39	1.07	0.02	<0.05
AL7909B a2L1 Pn1	34.0	1803	38.24	4828	36.22	<0.03	70	<9	189	53.0	30.1	245	244	13.5	<0.8	<0.9	2.28	0.37	7.14	6.38	<0.02	<0.01	<0.05
AL7909B a2L1 Cp+Pn	34.5	2902	31.31	1011	7.86	29.09	1770	<9	119	10.5	4.60	53.1	56.9	18.0	1.19	<0.9	0.98	0.15	0.79	1.07	<0.02	0.17	<0.05
AL7079B a2L2 Pn2	34.0	2023	39.29	4987	36.59	<0.03	64	<9	168	79.0	22.3	242	244	10.6	<0.8	<0.9	5.05	0.58	12.36	10.78	0.18	0.03	<0.05
AL7079B a2L2 Po2	38.5	2947	63.25	410	2.64	<0.03	31	<9	131	4.78	1.73	21.0	19.3	1.23	<0.8	<0.9	<0.9	0.13	0.84	1.41	0.28	<0.01	<0.05
AL7079B a2L3 Pn3	34.0	2077	38.54	4923	35.26	<0.03	40	<9	164	11.4	9.98	269	271	12.6	<0.8	<0.9	<0.9	0.09	2.70	4.03	0.06	<0.01	<0.05
AL7079B a2L3 Po+Cp	37.0	3719	53.46	63	0.41	4.64	1108	<9	100	<0.05	<0.1	3.62	3.22	2.66	1.63	<0.9	1.61	0.03	<0.02	<0.02	<0.02	<0.01	<0.05
AL7909B a2L4 Pn	34.0	2173	35.63	4367	32.76	1.63	428	<9	157	11.3	8.77	249	255	37.5	<0.8	<0.9	1.44	0.23	2.96	3.94	0.15	0.09	0.09
AL7079B a3L1 Po1	38.5	3360	65.14	6	0.12	<0.03	<15	<9	115	4.02	<0.1	<0.15	<0.2	0.31	<0.8	<0.9	<0.9	0.34	1.60	1.57	0.83	<0.01	<0.05
AL7079B a3L2 Po+Pn	38.0	3643	56.46	455	2.74	<0.03	42	<9	104	16.2	<0.1	16.3	16.4	3.11	<0.8	<0.9	<0.9	0.32	2.41	1.48	0.65	<0.01	<0.05
AL7079B a3L3 Po+Pn	37.0	3678	47.93	1447	9.97	<0.03	<15	<9	101	10.1	3.69	54.8	54.7	1.57	<0.8	<0.9	<0.9	<0.02	2.04	1.13	0.13	<0.01	<0.05
AL7079B a3L3 Po	38.5	3496	54.82	64	0.50	<0.03	<15	<9	110	0.70	0.17	2.28	2.87	0.50	<0.8	<0.9	<0.9	0.16	0.42	0.18	<0.02	<0.01	<0.05
AL7079B a3L4 Pn	34.0	3074	52.41	2210	14.33	<0.03	27	<9	111	0.60	0.81	102	103	4.58	<0.8	<0.9	1.65	0.14	<0.02	0.32	0.22	<0.01	<0.05
AL79079 a3L4 Po	38.5	2804	62.47	81	0.61	<0.03	22	<9	137	<0.05	<0.1	4.01	4.27	0.72	<0.8	<0.9	<0.9	0.26	0.30	0.20	0.21	<0.01	<0.05
AL7909B a4L1 Po1	38.5	4957	61.96	74	0.86	<0.03	50	<9	78	<0.05	<0.1	3.86	4.50	0.65	<0.8	<0.9	<0.9	0.07	0.22	0.07	<0.02	<0.01	<0.05
AL7909B a4L1 Pn1	34.0	2665	36.74	4770	30.76	<0.03	29	<9	128	11.1	1.22	177	179	3.21	<0.8	<0.9	<0.9	0.09	2.54	1.66	0.10	<0.01	<0.05
AL7909B a4L2 Po2 (+Pn)	37.0	4624	52.17	1285	9.27	<0.03	<15	<9	80	0.56	0.41	52.9	53.7	1.60	<0.8	<0.9	<0.9	0.12	0.39	0.35	<0.02	0.03	<0.05
AL7909B a4L2 Pn2	34.0	2222	39.45	4839	33.85	<0.03	<15	<9	153	15.2	3.15	198	201	16.5	<0.8	<0.9	<0.9	0.07	2.61	2.03	0.06	0.05	<0.05
AL7909B a4L3 pn3	34.0	2330	36.60	5278	33.74	1.02	60	<9	146	15.4	8.62	227	232	3.91	<0.8	<0.9	1.18	0.27	1.60	2.45	0.29	<0.01	<0.05
AL7909B a4L4 Po3	38.5	5513	60.18	5	0.09	<0.03	<15	<9	70	<0.05	<0.1	<0.15	<0.2	0.34	<0.8	<0.9	<0.9	<0.02	<0.02	<0.02	<0.02	<0.01	<0.05
AL7909B a4L5 Pn4	34.0	2660	42.43	4932	33.76	<0.03	65	<9	128	44.4	16.5	199	204	1.74	<0.8	<0.9	0.97	0.27	4.48	4.12	<0.02	<0.01	<0.05
AL7909B a4L6 Po4	38.5	3336	59.82	76	0.48	1.40	161	<9	115	36.1	0.48	3.41	3.31	2.19	<0.8	<0.9	1.12	0.14	5.17	4.07	0.11	0.07	<0.05
AL7909B A4L6 Cp1	35.0	2802	38.54	332	2.08	26.78	4900	<9	125	0.13	<0.1	29.9	29.1	87.7	2.81	<0.9	<0.9	<0.02	<0.02	<0.02	<0.02	0.33	<0.05
AL7909B a5L1 Po1	38.5	4302	63.38	5	0.09	<0.03	<15	<9	90	0.16	<0.1	<0.15	<0.2	0.41	<0.8	<0.9	<0.9	0.08	0.41	0.15	0.05	<0.01	<0.05
AL7909B a5L2 Pn1	34.0	2556	36.49	5078	33.83	0.15	651	<9	133	6.20	7.20	217	224	12.4	0.86	<0.9	<0.9	<0.02	1.14	1.44	<0.02	<0.01	<0.05
AL7909B a5L2 Cp1 (+Pn)	35.0	5385	35.21	1068	7.97	21.68	41800	<9	65	0.15	0.67	48.2	48.3	4.94	21.84	<0.9	<0.9	<0.02	0.06	0.19	<0.02	0.09	<0.05
AL7909B a5L3 Pn2	34.0	1689	36.37	5107	33.00	1.04	19	<9	201	91.5	19.8	207	213	43.3	<0.8	<0.9	1.92	0.16	12.29	8.63	0.18	<0.01	<0.05
AL7909B a5L4 Pn3	34.0	2838	36.67	4846	31.86	0.61	49	<9	120	20.4	13.7	209	205	4.41	<0.8	<0.9	<0.9	0.13	2.70	3.66	0.22	<0.01	<0.05
AL7909B a5L4 Cp1 (+Pn)	35.0	3963	29.16	1861	12.18	25.68	957	<9	88	10.7	5.63	81.9	81.9	6.00	1.61	<0.9	1.49	<0.02	0.51	1.39	0.16	0.07	<0.05
AL7909B a6L1 Pn1	34.0	2231	33.74	4432	31.75	-0.03	909	<9	152	35.5	6.88	122	125	2.83	0.94	<0.9	<0.9	0.03	3.50	3.46	2.45	<0.01	<0.05
AL7909B a6L1 Cp1 (+Pn)	35.0	4268	29.55	858	6.21	34.25	7886	<9	82	4.31	0.92	22.7	22.6	2.33	4.33	<0.9	<0.9	0.04	0.57	0.79	0.36	0.05	<0.05
AL7909B a6L2 Pn2	34.0	2738	36.96	4107	29.82	<0.03	<15	<9	124	33.6	7.35	125	124	1.95	<0.8	<0.9	<0.9	0.22	4.36	2.86	6.29	0.02	<0.05
AL7909B a6L3 Po1	38.5	3434	57.39	8	0.14	<0.03	16	<9	112	47.9	0.23	<0.15	<0.2	0.45	<0.8	<0.9	<0.9	0.05	3.44	5.23	1.11	<0.01	<0.05
AL7909B a6L4 Po2	38.5	3325	61.15	24	0.21	<0.03	<15	<9	116	43.2	<0.1	0.44	0.38	0.49	<0.8	<0.9	<0.9	1.19	6.43	4.62	3.92	0.03	<0.05
AL7909B a6L4 Pn3	34.0	3085	38.08	4351	31.26	<0.03	<15	<9	110	24.9	2.30	135	136	8.56	<0.8	<0.9	<0.9	0.35	5.45	3.17	3.06	0.04	<0.05
AL7909B a6L5 Pn4	34.0	2621	40.03	4843	33.84	<0.03	132	<9	130	59.6	4.60	140	140	11.5	<0.8	<0.9	1.71	0.68	5.69	6.40	4.17	0.03	<0.05
AL7909B a6L6 Pn5	34.0	2698	36.63	4804	34.28	<0.03	26	<9	126	11.4	11.3	151	152	5.22	<0.8	<0.9	<0.9	0.23	2.95	4.58	2.95	<0.01	<0.05
AL7909B a7L1 Pn1	34.0	2845	34.05	4311	29.75	<0.03	<15	<9	120	4.99	8.02	149	144	3.29	<0.8	<0.9	<0.9	0.38	2.05	3.33	1.49	<0.01	<0.05
AL7909B a7L1 Po1	38.5	3277	60.05	98	0.74	<0.03	<15	<9	118	6.91	<0.1	2.85	2.79	0.30	<0.8	<0.9	<0.9	0.33	3.62	2.80	1.92	<0.01	<0.05
AL7909B a7L2 Po2	38.5	2966	60.11	9	0.17	<0.03	<15	<9	130	16.2	<0.1	<0.15	<0.2	0.10	<0.8	<0.9	<0.9	0.38	4.64	3.01	1.56	<0.01	<0.05
AL7909B a7L3 Pn2	34.0	2808	40.77	3243	22.53	3.27	137	<9	121	25.7	18.1	111	112	5.81	<0.8	<0.9	2.47	0.12	3.81	3.64	0.76	<0.01	<0.05
AL7909B a7L3 Cp(+Pn)	35.0	3933	28.49	673	4.24	29.48	2402	<9	89	2.78	4.07	25.7	27.9	7.96	<0.8	<0.9	<0.9	<0.02	0.57	0.79	0.28	0.15	<0.05
AL7909B a7L4 Pn3	34.0	2373	30.39	5464	34.42	<0.03	84	<9	143	46.9	27.7	157	156	6.22	<0.8	<0.9	3.35	0.18	8.34	5.73	1.16	<0.01	<0.05
AL7909B a7L4 Po3	38.0	3185	58.67	124	1.00	0.06	1038	<9	119	2.92	0.61	3.77	3.93	0.51	0.95	<0.9	<0.9	0.10	1.41	0.68	0.18	<0.01	<0.05

A4-2 LA ICP-MS analyses at the Laboratory of Radiogenic Isotopes, Czech Geological Survey, Prague

Sample name	Sulphide	Ru99	Ru101	Rh103	Pd105	Pd106	Pd108	Re185 pres Pt	Re pres faktor	Os189	Ir193	Pt195	Au197
spots 80um	*IDL max*	*0,240*	*0,113*	*0,0297*	*2,85*	*0,413*	*0,846*	*0,041*		*0,0273*	*0,0169*	*0,0216*	*0,0367*
JJB 4a	chalc	<0.3	<0.1	Cu63Ar40	Cu65Ar40	<0.4	<0.8	<0.04		<0.03	<0.02	<0.02	<0.04
JJB 4a	chalc	<0.3	<0.1	Cu63Ar40	Cu65Ar40	<0.4	<0.8	<0.04		<0.03	<0.02	<0.02	<0.04
JJB 4a	chalc	<0.3	<0.1	Cu63Ar40	Cu65Ar40	<0.4	<0.8	<0.04		<0.03	<0.02	<0.02	<0.04
JJB 4a	chalc	<0.3	<0.1	Cu63Ar40	Cu65Ar40	<0.4	<0.8	<0.04		<0.03	<0.02	<0.02	<0.04
JJB 4a	chalc	<0.3	<0.1	Cu63Ar40	Cu65Ar40	<0.4	<0.8	<0.04		<0.03	<0.02	<0.02	<0.04
JJB 4a	chalc	<0.3	<0.1	Cu63Ar40	Cu65Ar40	<0.4	<0.8	<0.04		<0.03	<0.02	<0.02	<0.04
JJB 4a	pyrr	1.41	1.05	<0.03	<3	<0.4	<0.8	not calib	0.25	0.45	0.38	<0.02	<0.04
JJB 4a	pyrr	0.68	0.81	<0.03	<3	<0.4	<0.8	not calib	0.08	0.33	0.28	<0.02	<0.04
JJB 4a	pyrr	2.14	1.96	<0.03	<3	<0.4	<0.8	0.28	0.29	0.50	0.52	0.25	<0.04
JJB 4a	pyrr	2.27	2.17	<0.03	<3	<0.4	<0.8	not calib	0.08	0.41	0.43	<0.02	<0.04
JJB 4a	pyrr	2.73	2.63	<0.03	<3	<0.4	<0.8	0.24	0.34	0.61	0.79	0.97	<0.04
JJB 4a	pyrr	0.61	0.59	<0.03	<3	<0.4	<0.8	0.16	0.16	0.27	0.28	0.10	<0.04
JJB 4a	FeCoS	2.07	2.00	<0.03	<3	<0.4	<0.8	0.12	0.12	0.29	0.30	0.07	<0.04
JJB 4a	pent	1.50	1.42	0.64	39.2	37.0	37.1	not calib	0.06	0.14	0.38	0.15	<0.04
JJB 4a	FeCoS	1.94	1.89	<0.03	<3	<0.4	<0.8	0.25	0.30	0.40	0.39	0.11	<0.04
JJB 4a	pyrr	1.39	1.32	<0.03	<3	<0.4	<0.8	0.16	0.17	0.22	0.23	0.09	<0.04
JJB 4a	pent	2.93	3.24	2.30	26.3	26.4	25.6	0.13	0.17	0.44	0.59	0.03	<0.04
JJB 4a	pent	5.40	5.51	1.97	31.1	29.9	28.7	not calib	0.13	0.83	0.63	<0.02	<0.04
JJB 4a	pent	0.95	0.94	0.86	47.4	45.4	49.7	not calib	0.17	<0.03	0.29	<0.02	<0.04
JJB 4a	pent	6.88	6.89	4.29	37.1	37.2	36.0	not calib	0.25	0.95	0.90	<0.02	<0.04
JJB 4a	pent	2.15	2.10	1.13	49.2	47.9	47.1	not calib	0.07	0.15	0.33	<0.02	<0.04
JJB 10	chalc	<0.3	<0.1	Cu63Ar40	Cu65Ar40	<0.4	<0.8	<0.04		<0.03	<0.02	<0.02	<0.04
JJB 10	chalc	<0.3	<0.1	Cu63Ar40	Cu65Ar40	<0.4	<0.8	<0.04		<0.03	<0.02	0.10	<0.04
JJB 10	chalc	<0.3	<0.1	Cu63Ar40	Cu65Ar40	<0.4	<0.8	<0.04		<0.03	<0.02	0.04	<0.04
JJB 10	chalc	<0.3	<0.1	Cu63Ar40	Cu65Ar40	<0.4	<0.8	<0.04		<0.03	<0.02	0.09	<0.04
JJB 10	chalc	1.62	1.18	Cu63Ar40	Cu65Ar40	<0.4	<0.8	<0.04		2.30	1.35	0.43	<0.04
JJB 10	chalc	<0.3	<0.1	Cu63Ar40	Cu65Ar40	<0.4	<0.8	<0.04		<0.03	<0.02	0.05	<0.04
JJB 10	pent	1.59	1.60	33.07	281	270	265	<0.04		0.09	0.80	7.03	<0.04
JJB 10	pyrr	4.29	4.53	0.10	<3	<0.4	<0.8	0.23	0.22	6.90	4.69	0.88	<0.04
JJB 10	pyrr	1.27	1.20	0.06	<3	<0.4	<0.8	0.08	0.09	2.89	1.00	0.19	<0.04
JJB 10	pent	18.74	17.76	165.20	262	256	262	0.07	0.08	5.91	3.82	6.97	<0.04
JJB 10	pent	1.39	0.99	1.87	341	337	344	0.22	0.24	0.95	1.08	8.66	<0.04
JJB 10	pyrr	2.78	2.82	2.24	<3	<0.4	<0.8	0.05	0.05	3.44	1.86	0.22	<0.04
JJB 10	pyrr	6.14	6.61	0.19	<3	<0.4	<0.8	0.57	0.55	6.29	4.84	1.95	<0.04
JJB 10	pyrr	7.36	7.08	0.09	<3	<0.4	<0.8	0.12	0.12	6.89	4.59	0.47	<0.04
JJB 10	pyrr	6.81	6.83	0.13	<3	<0.4	<0.8	0.16	0.16	5.15	3.88	1.03	<0.04
JJB 10	pyrr	5.10	5.18	0.06	<3	<0.4	<0.8	0.23	0.22	5.60	3.70	0.79	<0.04
JJB 10	pyrr	8.22	8.00	0.10	<3	<0.4	<0.8	0.11	0.10	6.78	3.53	0.44	<0.04
JJB 10	pyrr	42.68	42.05	2.72	<3	<0.4	<0.8	0.14	0.13	5.95	3.83	0.40	<0.04
JJB 10	pent	16.3	15.5	25.6	434	428	434	0.12	0.12	4.54	3.07	7.10	<0.04
JJB 10	pent	9.63	9.43	41.9	360	369	384	0.21	0.21	3.13	1.57	6.59	<0.04
JJB 10	pent	15.5	16.2	94.8	230	236	242	0.23	0.23	2.81	4.10	4.94	<0.04

Sample name	Sulphide	Ru99	Ru101	Rh103	Pd105	Pd106	Pd108	Re185 pres Pt	Re pres faktor	Os189	Ir193	Pt195	Au197
spots 55um	*IDL max*	*0,436*	*0,203*	*0,0638*	*4,95*	*0,872*	*1,51*	*0,029*		*0,0511*	*0,0409*	*0,0429*	*0,0981*
JJB 19.1	pyrr	<0.4	0.20	<0.06	<5	<0.8	<1.5	<0.03		0.25	0.21	0.24	<0.1
JJB 19.1	chalc	<0.4	<0.2	Cu63Ar40	Cu65Ar40	<0.8	<1.5	<0.03		<0.05	<0.04	0.10	<0.1
JJB 19.1	CoS	Co59Ar40	9.76	38.19	<5	<0.8	<1.5	0.032		0.79	1.06	3.64	<0.1
JJB 19.1	chalc	<0.4	<0.2	Cu63Ar40	Cu65Ar40	<0.8	<1.5	<0.03		<0.05	<0.04	<0.04	<0.1
JJB 19.1	pent	67.0	58.5	78.28	252	230	325	<0.03		9.65	7.60	4.92	<0.1
JJB 19.1	chalc	<0.4	<0.2	Cu63Ar40	Cu65Ar40	0.52	<1.5	<0.03		<0.05	<0.04	<0.04	<0.1
JJB 19.1	chalc	<0.4	<0.2	Cu63Ar40	Cu65Ar40	<0.8	<1.5	<0.03		<0.05	<0.04	0.07	<0.1
JJB 19.1	pent	18.2	18.9	0.24	95	103	89	<0.03		3.61	2.27	3.27	<0.1
JJB 19.1	pyrr	1.97	2.08	0.20	<5	<0.8	<1.5	<0.03		2.14	0.42	1.37	<0.1
JJB 19.1	pyrr	3.94	3.78	0.97	<5	<0.8	<1.5	0.230		2.59	0.58	8.67	<0.1
JJB 19.1	pent	1.32	1.67	0.06	176	186	183	0.315		0.18	0.34	0.63	<0.1
JJB 19.1	chalc	<0.4	<0.2	Cu63Ar40	Cu65Ar40	<0.8	<1.5	<0.03		<0.05	0.03	<0.04	<0.1
JJB 19.1	CoS	109	108	825	<5	<0.8	<1.5	0.299		6.02	7.69	2.73	<0.1
JJB 19.1	CoS	8.92	6.42	11.26	<5	3.38	3.51	0.072		1.26	1.65	21.3	<0.1
JJB 19.1	pent	2.25	2.39	1.65	120	162	128	0.139		1.68	0.12	3.90	<0.1
JJB 19.1	chalc	<0.4	<0.2	Cu63Ar40	Cu65Ar40	<0.8	<1.5	<0.03		<0.05	<0.04	0.05	<0.1
EST 013 16904	pyrr	<0.4	<0.2	3.11	<5	<0.8	<1.5	1.28		0.31	0.34	2.17	<0.1
EST 013 16904	pyrr	<0.4	<0.2	1.39	<5	<0.8	<1.5	<0.03		<0.05	0.05	0.15	<0.1
EST 013 16904	pyrr	<0.4	<0.2	0.61	<5	<0.8	0	0.25		0.37	0.19	0.35	<0.1
EST 013 16904	chalc	<0.4	<0.2	Cu63Ar40	Cu65Ar40	<0.8	<1.5	<0.03		<0.05	0.05	<0.04	<0.1
EST 013 16904	pent	19.9	20.7	46.35	508	296	361	0.37		7.89	6.25	25.3	<0.1
EST 013 16904	pyrr	0.80	0.59	0.21	<5	<0.8	<1.5	0.20		1.19	0.46	0.22	<0.1
EST 013 16904	pent	7.68	7.76	17.58	407	255	256	0.13		3.22	1.63	16.3	<0.1
EST 013 16904	chalc	<0.4	<0.2	Cu63Ar40	Cu65Ar40	<0.8	<1.5	<0.03		<0.05	<0.04	0.11	<0.1
EST 013 16904	pent	3.28	2.61	20.45	217	216	205	0.14		0.53	1.27	6.72	<0.1
EST 013 16904	chalc	<0.4	<0.2	Cu63Ar40	Cu65Ar40	<0.8	<1.5	<0.03		<0.05	<0.04	<0.04	<0.1
EST 013 16904	pyrr	0.78	0.48	0.52	<5	<0.8	<1.5	0.13		1.43	0.54	0.67	<0.1
EST 013 16904	pyrr	0.40	0.49	3.97	<5	<0.8	<1.5	0.04		0.98	0.38	0.20	<0.1
EST 013 16904	pyrr	<0.4	1.69	0.93	<5	<0.8	<1.5	0.06		0.10	0.05	0.30	<0.1
EST 013 16904	pyrr	0.54	0.58	0.11	<5	<0.8	<1.5	0.04		0.83	0.42	0.08	<0.1
EST 013 16904	pent	16.3	16.7	22.45	233	218	241	<0.03		5.98	3.96	8.30	<0.1
EST 013 16904	pent	4.18	3.50	24.96	365	323	389	<0.03		1.03	4.42	8.72	<0.1
EST 013 16904	pent	2.27	1.69	4.93	169	177	172	<0.03		1.10	1.42	12.12	<0.1
EST 013 16904	chalc	<0.4	<0.2	Cu63Ar40	Cu65Ar40	<0.8	<1.5	<0.03		<0.05	<0.04	0.37	<0.1
EST 013 16904	chalc	<0.4	<0.2	Cu63Ar40	Cu65Ar40	<0.8	<1.5	<0.03		<0.05	<0.04	0.12	<0.1
EST 013 16904	pent	6.38	5.71	0.17	180	178	177	<0.03		1.19	0.41	4.98	<0.1
EST 013 16904	chalc	<0.4	<0.2	Cu63Ar40	Cu65Ar40	<0.8	<1.5	<0.03		<0.05	<0.04	<0.04	<0.1
EST 013 16904	chalc	<0.4	<0.2	Cu63Ar40	Cu65Ar40	<0.8	<1.5	<0.03		<0.05	<0.04	<0.04	<0.1
EST 013 16904	pent	3.12	2.67	5.00	157	177	156	<0.03		1.04	1.03	7.00	<0.1
spots 80um	*IDL max*	*0,205*	*0,0967*	*0,0288*	*2,21*	*0,354*	*0,547*	*0,0049*		*0,0335*	*0,0206*	*0,0205*	*0,0324*
JJB 18a	pyrr	4.02	4.25	<0.03	<2	<0.3	<0.5	0.369		1.69	0.52	0.15	<0.03
JJB 18a	pyrr	3.54	3.73	<0.03	<2	<0.3	<0.5	0.451		1.59	0.49	0.22	<0.03
JJB 18a	pyrr	1.88	1.98	<0.03	<2	<0.3	<0.5	0.472		0.95	0.38	0.36	<0.03
JJB 18a	pyrr	0.65	0.70	<0.03	<2	<0.3	<0.5	0.096		0.45	0.05	0.14	<0.03
JJB 18a	pyrr	0.87	0.93	<0.03	<2	<0.3	<0.5	0.253		0.76	0.16	0.37	<0.03
JJB 18a	pyrr	2.30	2.32	<0.03	<2	<0.3	<0.5	0.297		1.51	0.68	0.34	<0.03
JJB 18a	chalc	0.30	0.13	Cu63Ar40	Cu65Ar40	<0.3	<0.5	<0.01		<0.03	<0.02	<0.02	<0.03
JJB 18a	chalc	0.46	0.13	Cu63Ar40	Cu65Ar40	<0.3	<0.5	<0.01		<0.03	<0.02	<0.02	<0.03
JJB 18a	chalc	0.51	0.16	Cu63Ar40	Cu65Ar40	<0.3	<0.5	<0.01		<0.03	<0.02	<0.02	<0.03
JJB 18a	pent	4.13	1.35	4.35	163	166	166	<0.01		0.09	0.28	<0.02	<0.03
JJB 18a	pent	3.27	1.36	1.26	166	167	173	0.035		0.25	0.13	0.05	<0.03
JJB 18a	pent	3.35	1.50	0.24	179	186	183	<0.01		<0.03	<0.02	0.03	<0.03
JJB 18a	pent	3.08	1.25	0.78	180	186	183	<0.01		0.02	<0.02	0.05	<0.03
JJB 18a	pent	6.93	4.28	4.60	234	237	233	0.08		1.00	0.46	0.20	<0.03
JJB 18a	pent	6.91	4.13	6.15	247	251	242	0.09		1.24	0.53	0.25	<0.03
JJB 18a	chalc	0.29	0.12	Cu63Ar40	Cu65Ar40	<0.3	<0.5	<0.01		<0.03	<0.02	<0.02	<0.03
JJB 18a	chalc	0.31	0.14	Cu63Ar40	Cu65Ar40	<0.3	<0.5	<0.01		<0.03	<0.02	<0.02	<0.03
JJB 18c	pyrr	3.50	3.43	<0.03	<2	<0.3	<0.5	0.26		1.49	0.56	0.25	<0.03
JJB 18c	pyrr	3.00	3.35	<0.03	<2	<0.3	<0.5	0.08		1.00	0.64	0.34	<0.03
JJB 18c	pyrr	4.16	4.20	<0.03	<2	<0.3	<0.5	0.23		1.33	0.59	0.24	<0.03
JJB 18c	pyrr	4.87	4.94	<0.03	<2	<0.3	<0.5	1.27		2.30	0.70	2.00	<0.03
JJB 18c	pyrr	3.33	3.35	<0.03	<2	<0.3	<0.5	0.02		1.30	0.43	0.05	<0.03
JJB 18c	pyrr	4.94	4.83	<0.03	<2	<0.3	<0.5	0.16		1.32	0.49	0.10	<0.03

Sample name	Sulphide	Ru99	Ru101	Rh103	Pd105	Pd106	Pd108	Re185 pres Pt	Re pres faktor	Os189	Ir193	Pt195	Au197
JJB 18c	chalc	0.24	0.15	Cu63Ar40	Cu65Ar40	<0.3	<0.5	<0.01		<0.03	<0.02	<0.02	<0.03
JJB 18c	chalc	0.29	0.15	Cu63Ar40	Cu65Ar40	<0.3	<0.5	<0.01		<0.03	<0.02	<0.02	<0.03
JJB 18c	chalc	0.30	0.13	Cu63Ar40	Cu65Ar40	<0.3	<0.5	<0.01		<0.03	<0.02	<0.02	<0.03
JJB 18c	pent	9.10	6.84	0.50	206	212	210	0.08		2.01	1.06	0.14	<0.03
JJB 18c	pent	4.54	2.95	2.21	190	191	194	0.04		0.72	0.30	0.21	<0.03
JJB 18c	pent	6.20	4.45	5.17	191	194	195	0.51		1.26	1.46	1.13	<0.03
JJB 18c	pent	11.02	7.42	5.98	178	180	178	0.09		1.33	0.73	7.41	<0.03
JJB 18c	pent	6.70	4.97	2.24	191	190	191	0.36		1.24	0.44	0.66	<0.03
JJB 18c	pent	4.99	3.48	2.11	175	178	179	0.07		0.79	0.39	0.26	<0.03
JJB 18c	chalc	0.38	0.19	Cu63Ar40	Cu65Ar40	<0.3	<0.5	<0.01		<0.03	<0.02	<0.02	<0.03
JJB 18c	chalc	0.32	0.15	Cu63Ar40	Cu65Ar40	<0.3	<0.5	<0.01		<0.03	<0.02	<0.02	<0.03
JJB 18c	chalc	<0.2	<0.1	Cu63Ar40	Cu65Ar40	<0.3	<0.5	<0.01		<0.03	<0.02	<0.02	<0.03
spots 80um	***IDL max***	***0.134***	***0.069***	***0.019***	***1.65***	***0.272***	***0.472***	***0.0078***		***0.016***	***0.0117***	***0.0131***	***0.0291***
JJB 3	pyrr	0.51	0.56	0.09	<2	<0.3	<0.5	0.43		1.89	2.19	1.68	<0.03
JJB 3	pyrr	2.98	3.28	0.03	<2	<0.3	<0.5	0.04		2.04	1.34	0.28	<0.03
JJB 3	pyrr	0.68	0.69	0.09	<2	<0.3	<0.5	0.23		1.84	1.89	1.63	<0.03
JJB 3	pyrr	2.24	2.37	<0.02	<2	<0.3	<0.5	<0.01		1.41	0.63	<0.02	<0.03
JJB 3	pyrr	<0.2	<0.1	<0.02	<2	<0.3	<0.5	<0.01		<0.02	<0.01	<0.02	<0.03
JJB 3	pyrr	2.28	2.50	0.15	<2	<0.3	<0.5	0.46		2.05	2.72	1.34	<0.03
JJB 3	pent	32.70	32.83	12.70	105	92	89	0.09		3.78	1.16	1.97	<0.03
JJB 3	pent	9.86	9.34	17.35	131	123	179	0.04		1.54	1.62	4.02	<0.03
JJB 3	pent	48.60	48.39	25.08	178	176	179	0.23		7.04	4.72	7.18	<0.03
JJB 3	faze x FeCoS	91.32	105.09	6.40	<2	<0.3	<0.5	0.09		3.93	4.51	1.68	<0.03
JJB 3	faze x FeCoS	17.18	19.76	0.14	<2	<0.3	<0.5	<0.01		2.72	2.98	0.28	<0.03
JJB 3	pent	13.63	13.97	19.82	168	166	173	<0.01		1.66	1.26	1.96	<0.03
JJB 3	faze x CoFeCoS	Co59Ar40	3.42	0.68	<2	<0.3	<0.5	0.06		4.92	3.09	51.45	<0.03
JJB 3	chalc	<0.2	<0.1	Cu63Ar40	Cu65Ar40	<0.3	<0.5	<0.01		<0.02	<0.01	0.22	<0.03
JJB 3	chalc	<0.2	<0.1	Cu63Ar40	Cu65Ar40	<0.3	<0.5	<0.01		<0.02	<0.01	0.05	<0.03
JJB 3	chalc	<0.2	<0.1	Cu63Ar40	Cu65Ar40	<0.3	<0.5	<0.01		<0.02	<0.01	<0.02	<0.03
JJB 3	chalc	<0.2	<0.1	Cu63Ar40	Cu65Ar40	<0.3	<0.5	<0.01		<0.02	<0.01	<0.02	<0.03
JJB 3	chalc	<0.2	<0.1	Cu63Ar40	Cu65Ar40	<0.3	<0.5	<0.01		<0.02	<0.01	<0.02	<0.03
JJB 3	chalc	0.42	0.20	Cu63Ar40	Cu65Ar40	0.196	<0.34	<0.01		<0.02	<0.01	0.03	<0.03
JJB 3	faze x FeCoS	27.57	32.10	0.14	<2	<0.3	<0.5	0.09		3.23	2.99	1.31	<0.03
JJB 7	pent	51.96	51.32	16.07	131	128	134	0.03		2.21	4.01	7.18	<0.03
JJB 7	pent	57.19	51.47	1.93	129	127	127	0.11		3.26	4.13	6.60	<0.03
JJB 7	pent	3.50	3.29	2.79	152	149	154	0.03		2.47	1.77	5.17	<0.03
JJB 7	faze x FeCoS	119.11	120.34	1.39	<2	<0.3	<0.5	0.48		7.39	10.19	4.28	<0.03
JJB 7	pent	34.31	34.04	19.33	144	141	145	0.06		5.80	2.92	8.96	<0.03
JJB 7	pyrr	3.34	3.72	0.03	<2	<0.3	<0.5	0.09		3.21	2.02	0.52	<0.03
JJB 7	pyrr	2.48	2.46	0.07	<2	<0.3	<0.5	0.44		3.08	4.12	1.60	<0.03
JJB 7	pyrr	3.12	3.67	<0.02	<2	<0.3	<0.5	0.04		3.07	2.18	0.99	<0.03
JJB 7	pyrr	<0.2	0.16	2.08	<2	<0.3	<0.5	<0.01		<0.02	<0.01	<0.02	<0.03
JJB 7	pyrr	3.31	3.58	2.32	<2	<0.3	<0.5	0.40		2.10	3.60	2.32	<0.03
JJB 7	pyrr	2.12	2.12	2.67	<2	<0.3	<0.5	<0.01		5.65	9.75	0.75	<0.03
JJB 7	chalc	5.15	3.39	Cu63Ar40	Cu65Ar40	<0.3	<0.5	<0.01		0.17	0.32	0.70	<0.03
JJB 7	chalc	<0.2	<0.1	Cu63Ar40	Cu65Ar40	<0.3	<0.5	<0.01		<0.02	<0.01	0.06	<0.03
JJB 7	chalc	<0.2	0.14	Cu63Ar40	Cu65Ar40	<0.3	<0.5	<0.01		<0.02	<0.01	0.13	<0.03
JJB 7	chalc	<0.2	<0.1	Cu63Ar40	Cu65Ar40	<0.3	<0.5	<0.01		0.14	0.11	0.25	<0.03
JJB 7	chalc	<0.2	0.19	Cu63Ar40	Cu65Ar40	1.14	1.17	<0.01		0.12	0.11	0.63	<0.03
JJB 7	chalc	<0.2	0.15	Cu63Ar40	Cu65Ar40	<0.3	<0.5	<0.01		<0.02	<0.01	<0.02	<0.03
		0.203	0.082	0.027	2.340	0.336	0.559	0.005		0.015	0.017	0.019	0.030
JJB 20	pyrr	4.21	4.29	0.05				0.11		3.49	3.18	3.22	<0.03
JJB 20	pent	Co59Ar40	Ni61Ar40	105.79	78.3	80.8	81.8	0.06		0.67	0.33	0.12	<0.03
JJB 20	pent	Co59Ar40	Ni61Ar40	3.38	77.2	78.0	77.6	0.26		0.37	0.11	0.05	<0.03
JJB 20	pent	Co59Ar40	Ni61Ar40	22.00	76.5	77.0	78.3	0.17		2.33	0.87	<0.02	<0.03
JJB 20	pyrr	0.85	0.84	0.18	<2.5	0.4	<0.6	0.30		1.49	0.26	0.05	<0.03
JJB 20	pent	Co59Ar40	Ni61Ar40	1.83	93.3	91.1	92.8	0.16		0.50	0.15	0.03	<0.03
JJB 20	pyrr	0.21	0.23	<0.05	<2.5	<0.4	<0.6	<0.01		<0.02	0.02	0.02	<0.03
JJB 20	pyrr	<0.2	0.16	0.16	<2.5	<0.4	<0.6	0.11		0.41	0.07	0.02	<0.03
JJB 20	pyrr	0.66	0.68	0.10	<2.5	<0.4	<0.6	0.14		0.91	0.21	0.04	<0.03
JJB 20	pyrr	0.35	0.36	<0.05	<2.5	<0.4	<0.6	0.10		0.64	0.13	<0.02	<0.03
JJB 20	pyrr	0.88	0.93	3.20	<2.5	<0.4	<0.6	0.19		1.45	0.26	0.04	<0.03
JJB 20	pyrr	0.41	0.40	<0.05	<2.5	<0.4	<0.6	0.20		1.02	0.20	0.04	<0.03
JJB 20	chalk	<0.2	<0.1	Cu63Ar40	Cu65Ar40	<0.4	<0.6	<0.01		<0.02	<0.02	<0.02	<0.03
JJB 20	chalk	<0.2	<0.1	Cu63Ar40	Cu65Ar40	<0.4	<0.6	<0.01		<0.02	<0.02	<0.02	<0.03
JJB 20	chalk	<0.2	<0.1	Cu63Ar40	Cu65Ar40	<0.4	<0.6	<0.01		<0.02	<0.02	<0.02	<0.03
JJB 20	chalk	<0.2	<0.1	Cu63Ar40	Cu65Ar40	<0.4	<0.6	<0.01		<0.02	<0.02	0.04	<0.03
JJB 20	chalk	<0.2	<0.1	Cu63Ar40	Cu65Ar40	<0.4	<0.6	<0.01		<0.02	<0.02	<0.02	<0.03
JJB 20	chalk	<0.2	<0.1	Cu63Ar40	Cu65Ar40	<0.4	<0.6	<0.01		<0.02	<0.02	<0.02	<0.03